

TH 1733

EVOLUTION OF THE FLAVRIAN PLUTON AND ITS ASSOCIATION WITH THE VHMS DEPOSITS AND GRANITOID-HOSTED GOLD DEPOSITS OF THE NORANDA CAULDRON, ROUYN-NORANDA, QUEBEC, CANADA

Documents complémentaires

Additional Files



Licence



License

Cette première page a été ajoutée
au document et ne fait pas partie du
rapport tel que soumis par les auteurs.

Énergie et Ressources
naturelles

Québec 

TH 1733

Université de Montréal

**Evolution of the Flavrian Pluton and its Association with the VHMS Deposits
and Granitoid-Hosted Gold Deposits of the Noranda Cauldron, Rouyn-Noranda,
Quebec, Canada**

par

Michel G. Richard

Département de Géologie

Faculté des Arts et Sciences

**Thèse présentée à la Faculté des études supérieures
en vue de l'obtention du grade de
Philosophiæ Doctor (Ph.D.)
en géologie**

Décembre 1998

©Michel G. Richard, 1998





**National Library
of Canada**

**Acquisitions and
Bibliographic Services**

395 Wellington Street
Ottawa ON K1A 0N4
Canada

**Bibliothèque nationale
du Canada**

**Acquisitions et
services bibliographiques**

395, rue Wellington
Ottawa ON K1A 0N4
Canada

Your file Votre référence

Our file Notre référence

The author has granted a non-exclusive licence allowing the National Library of Canada to reproduce, loan, distribute or sell copies of this thesis in microform, paper or electronic formats.

The author retains ownership of the copyright in this thesis. Neither the thesis nor substantial extracts from it may be printed or otherwise reproduced without the author's permission.

L'auteur a accordé une licence non exclusive permettant à la Bibliothèque nationale du Canada de reproduire, prêter, distribuer ou vendre des copies de cette thèse sous la forme de microfiche/film, de reproduction sur papier ou sur format électronique.

L'auteur conserve la propriété du droit d'auteur qui protège cette thèse. Ni la thèse ni des extraits substantiels de celle-ci ne doivent être imprimés ou autrement reproduits sans son autorisation.

0-612-42273-9

Canada

Université de Montréal
Faculté des études supérieures

Cette thèse intitulée:

**Evolution of the Flavrian Pluton and its Association with the VHMS Deposits
and Granitoid-Hosted Gold Deposits of the Noranda Cauldron, Rouyn-Noranda,
Quebec, Canada**

présentée par:

Michel G. Richard

a été évaluée par un jury composé des personnes suivantes:

M. John Stix:	président-rapporteur
M. Claude Hubert:	directeur de recherche
M. Alex C. Brown:	codirecteur
M. Walter Trzcienski:	membre du jury
M. Gérald Riverin:	examineur externe
M. François Courchesne:	représentant du doyen de la F.E.S.

Thèse acceptée le:

14. 12. 1998

SUMMARY

The Flavrian subvolcanic pluton is composed of the following intrusive phases: (1) Méritens quartz-diorite; (2) homogeneous tonalite; (3) hybrid and heterogeneous tonalite; (4) trondhjemite porphyry; (5) pink trondhjemite; (6) coarse-grained trondhjemite; (7) granophyre and microgranite; (8) Eldrich diorite; and (9) late trondhjemite. Pink trondhjemite, trondhjemite porphyry, coarse-grained trondhjemite and granophyre are sub-phases of the early trondhjemite. Crosscutting relationships indicate that late trondhjemite, which occupies 30% of the pluton's outcropping surface, is the latest felsic intrusive phase within the pluton. A preliminary discordant U-Pb zircon date suggests that late trondhjemite was intruded at 2679 Ma, which is 20 Ma younger than early trondhjemite.

The internal and external contacts of the pluton indicate that it is a composite sill-shaped intrusion that was emplaced at high crustal levels during asymmetric subsidence of a cauldron. The sharp nature of internal contacts indicates that ascending magma was emplaced in fractures and faults, resulting in a dike-fed sill geometry. Evidence of several magmatic pulses during emplacement of individual phases illustrates the episodic nature of emplacement. Episodic magmatic pulses would have caused cyclical internal pressure variations within the pluton. A model involving principal stress vector reversals is presented in order to explain the pressure-controlled geometry of intrusive phases. Evidence of pressure variations during emplacement is recorded in many of the observed textures. The distinct geometry of the numerous dikes and sills, the concordant relation between the pluton and the surrounding volcanic rocks and the observed link between subsidence and intrusion indicate that emplacement occurred in an extensional tectonic regime.

The geochemical evolution of the Flavrian pluton from Méritens quartz-diorite to granophyre is characterized by a general enrichment in SiO_2 , Na_2O , Y, Nb, Zr, Hf, Ta, Th, U and REE and a relative depletion in Al_2O_3 , Fe_2O_3^* , MnO, MgO, CaO, Co,

Sc, V and Sr. La/Yb ratios remained relatively constant and Eu was depleted as the more differentiated phases were introduced into the pluton, with variations occurring in the silica-rich phases. The general negative correlation between Eu/Eu* and Th suggests that feldspar crystallization played an important role in the differentiation process of the pluton.

A broad negative correlation between compatible and incompatible elements and a crude positive correlation between incompatible elements characterize the sequence of intrusion from Méritens quartz-diorite to early coarse-grained trondhjemite. Granophyre is clearly distinguished by its relative enrichment in incompatible elements, and possibly represents a late-stage, high SiO₂, Na₂O and incompatible element enriched differentiate of early trondhjemite. Consequently, Méritens quartz-diorite, tonalite, early trondhjemite and granophyre are genetically linked. Late trondhjemite shows a distinct depletion in incompatible elements compared to other trondhjemite, suggesting that it was derived from a different magmatic source. In addition, chondrite-normalized REE patterns suggest that late trondhjemite is not equivalent to the Lac Dufault granodiorite.

Significant scatter in the geochemical data occurs at specific SiO₂ intervals. Scatter between 64.8 and 68.8% SiO₂ is attributed to interaction between what is now represented by Méritens quartz-diorite and early trondhjemite. Variations in incompatible element concentrations and La/Yb ratios between 75 and 77% SiO₂ for coarse-grained trondhjemite were probably caused by the separation of an aqueous fluid phase from the trondhjemite magma through boiling. In addition, between 77 and 79.2% SiO₂, the sharp increase in incompatible elements is due to the intrusion and crystallization of granophyre.

Crosscutting relationships between various phases of the pluton and volcanic rocks of the Noranda cauldron indicate that development of the Noranda cauldron, and its associated VHMS deposits, is constrained to an interval of time that began

with intrusion of the Méritens quartz-diorite and ended before complete emplacement of the phases that compose the early trondhjemite. The brecciation texture characteristic of early trondhjemite may represent a link between boiling of the intrusive phase and development of the VHMS deposits.

Similar geochemical signatures for the Méritens quartz-diorite and andesites of the Noranda cauldron suggest that quartz-diorite is an intrusive equivalent of andesite. Similar conclusions can be drawn for early trondhjemite and rhyolite from the Noranda cauldron. However, compositional differences between early trondhjemite and Cycle 4 rhyolite suggest that the link between the chamber and the overlying volcanic rocks terminated before or during the onset of Cycle 4 volcanism. The chemical compositions of granophyre, Eldrich diorite and late trondhjemite indicate that these phases did not have extrusive equivalents within the Noranda cauldron.

Economic mineralization at the Pierre Beauchemin gold mine was clearly associated with shears and fractures developed in and near the Eldrich diorite dike in response to a WNW-ESE compression. Shear and vein orientations, along with ore shoot plunges, are controlled by competency contrasts of the host rocks. Gold mineralization is associated with pyritization, albitization, carbonatization and chloritization of the host rocks.

Based on crosscutting relationships and kinematic analysis, the distribution of ore lenses at the Pierre Beauchemin gold mine is interpreted to have been associated with faults that formed in response to a WNW-ESE compression that occurred after 2681 Ma.

RÉSUMÉ

Le pluton subvolcanique de Flavrian, situé dans le camp minier de Rouyn-Noranda, Abitibi, Québec, est associé à plusieurs gisements de cuivre-zinc (Cu-Zn) et gisements d'or (Au). Grâce à cette association, ce type de pluton suscite un intérêt marqué dans l'industrie de l'exploration minière. Le rôle du pluton dans la formation des gisements demeure cependant controversé.

Les gisements de Cu-Zn, localisés dans les roches volcaniques surmontant le pluton, sont reconnus comme étant de type sulfures volcanogènes exhalatifs. La formation de ces gisements serait, selon plusieurs auteurs, synchrone à la mise en place du pluton de Flavrian. Un concept, généralement accepté pour la formation des gisements de ce type, suggère qu'une chambre magmatique localisée sous le plancher océanique aurait fourni la chaleur nécessaire à la formation du système hydrothermal responsable de la production des gisements exhalatifs. La relation directe entre la mise en place du pluton subvolcanique et la production des gisements de sulfures volcanogènes est une interprétation basée sur des datations absolues obtenues par la méthode uranium-plomb (U-Pb), par des relations géochimiques, ainsi que par des corrélations avec les systèmes hydrothermaux sur fonds océaniques modernes. Toutefois, le pluton de Flavrian est "à caractère" composite i.e. formé de plusieurs intrusions. La complexité reliée à cette mise en place composite complique de beaucoup la théorie.

Le travail de recherche comporte deux volets principaux: (1) l'étude de l'évolution du pluton de Flavrian et son rôle dans la genèse des gisements de Cu-Zn du camp minier de Rouyn-Noranda et (2) l'étude de la distribution de l'or à la mine Pierre Beauchemin, située dans le secteur nord-ouest du pluton de Flavrian.

Le but du premier volet est de vérifier les relations spatiales, temporelles et géochimiques entre le pluton subvolcanique de Flavrian et les gisements de Cu-Zn du camp minier de Rouyn-Noranda. L'essentiel des travaux a donc consisté à: (1) répertorier systématiquement les caractéristiques structurales et pétrographiques du

pluton de Flavrian, (2) déterminer la nature des contacts et la séquence de mise en place de chacune de ses phases, (3) caractériser son évolution géochimique, (4) déterminer les relations de recoupement entre les différentes phases du pluton et les roches encaissantes des gisements de Cu-Zn et (5) établir les relations géochimiques entre le pluton de Flavrian et les roches volcaniques du camp minier.

La cartographie du pluton de Flavrian démontre son aspect multiphasé. L'ordre de mise en place des différentes phases du pluton est la suivante: (1) diorite quartzifère de Méritens, tonalite homogène et tonalite hétérogène (roches hybrides), (2) trondhémite porphyrique, (3) trondhémite rose, (4) trondhémite à grain grossier, (5) granophyre et microgranite, (6) diorite Eldrich et (7) trondhémite tardive. Les trondhémite rose, porphyrique et à grain grossier, ainsi que le granophyre sont des phases de la trondhémite précoce.

Les relations de recoupement ainsi que les données géochronologiques préliminaires indiquent que la trondhémite tardive, qui occupe environ 30% de la superficie du pluton, est environ 20 Ma plus jeune que les roches volcaniques du camp minier et n'a donc aucune relation avec la formation des gisements de Cu-Zn.

La géométrie interne du pluton est essentiellement caractérisée par une succession de plusieurs filons-couches. Ces filons-couches sont nourris par des dykes orientés parallèlement aux failles synvolcaniques dans les roches volcaniques surmontant le pluton. Par conséquent, l'orientation de ces failles qui contrôlent la localisation des gisements stratiformes de Cu-Zn peut être déduite par une cartographie détaillée des dykes du pluton. La géométrie particulière que démontrent les dykes et filons-couches nécessite des changements abrupts de pression lors de la mise en place du pluton. Un modèle fondé sur l'inversion des principaux axes de déformation est suggéré ici pour expliquer cette géométrie particulière et caractéristique. Les évidences de variations de pression ainsi que d'inversion des principaux axes de déformation sont ensuite considérées dans l'élaboration d'un modèle de mise en place du pluton.

L'évolution géochimique du pluton de Flavrian, de la diorite quartzifère de Méritens au granophyre, est caractérisée par un enrichissement général en SiO_2 , Na_2O , Y, Nb, Zr, Hf, Ta, Th, U et en terres rares ainsi que par un appauvrissement en Al_2O_3 , Fe_2O_3^* , MnO, MgO, CaO, Co, Sc, V et Sr. Le ratio La/Yb est demeuré relativement constant alors qu'il y a eu appauvrissement en Eu à mesure que les phases plus différenciées ont été introduites dans le pluton. Ces tendances sont toutefois perturbées dans les phases riches en silice. La corrélation négative de Eu/Eu^* vs Th de la séquence intrusive débutant par la diorite quartzifère et se terminant par le granophyre suggère que la cristallisation fractionnée du feldspath a provoqué la différenciation du pluton. Le granophyre est enrichi en SiO_2 , Na_2O et en éléments incompatibles comparé à la trondhémite précoce. Le granophyre représente donc un niveau de différenciation plus élevé que la trondhémite précoce. Ces données démontrent qu'il y a un lien génétique entre la diorite quartzifère, la tonalite, la trondhémite précoce et le granophyre. La géochimie distincte de la trondhémite tardive indique qu'elle représente une phase tardive et distincte qui a probablement été dérivée d'une autre source que la trondhémite précoce. Ceci appuie les observations de terrain ainsi que les données géochronologiques. Les données de terres rares normalisées indiquent que la trondhémite tardive n'est pas équivalente à la granodiorite du Lac Dufault, comme l'a suggéré Kennedy (1984).

Les données géochimiques démontrent que des perturbations dans les tendances géochimiques du pluton sont observées à des intervalles de SiO_2 bien définis. Entre 64.8 et 68.8% SiO_2 , l'interaction entre la diorite quartzifère de Méritens et la trondhémite précoce a causé des perturbations marquées dans les tendances géochimiques de la majorité des éléments, à l'exception du Th, Ta et Nb. L'interaction s'est probablement produite par mélange et assimilation partielle de la diorite quartzifère par la trondhémite. Entre 75 et 77% SiO_2 , la trondhémite précoce montre des variations importantes en éléments incompatibles et en La/Yb. Ces variations sont probablement causées par la séparation d'une phase aqueuse lors de l'ébullition de la trondhémite précoce. L'augmentation marquée en éléments incompatibles, entre 77 and 79.2% SiO_2 , résulte de la mise en place et de la cristallisation du granophyre.

Les relations de recoupement entre le pluton et les roches volcaniques du chaudron de Noranda indiquent que le chaudron, ainsi que les gisements de sulfures volcanogènes qu'il contient, se sont développés pendant la mise en place de la diorite quartzifère de Méritens mais avant la mise en place de toutes les phases appartenant à la trondhémite précoce.

Une comparaison des signatures géochimiques des éléments traces des roches plutoniques et volcaniques suggère que la diorite quartzifère de Méritens représente l'équivalent plutonique des andésites du chaudron. Ces mêmes données indiquent que la trondhémite précoce est l'équivalent des rhyolites du chaudron. Par contre, des différences significatives entre la trondhémite précoce et les rhyolites du Cycle 4 suggèrent que le lien entre le pluton et les roches volcaniques felsiques du chaudron s'est terminé pendant ou avant le Cycle 4.

La texture de brèche caractéristique de la trondhémite précoce, suggère qu'un épisode magmatique-hydrothermal important s'est produit lors de la mise en place de cette phase. Les relations de recoupement démontrent que sa mise en place correspond à l'intervalle de temps pendant lequel les gisements de sulfures volcanogènes ont été formés. Par conséquent, l'épisode de séparation du fluide magmatique-hydrothermal lors de la mise en place de la trondhémite précoce est interprété comme étant associé à la formation des gisements de sulfures volcanogènes.

Les compositions géochimiques du granophyre, de la diorite Eldrich et de la trondhémite tardive indiquent que ces phases plutoniques n'ont pas d'équivalents extrusifs. Cette conclusion est soutenue par les relations de recoupement qui démontrent nettement que ces phases sont tardives.

Les principaux objectifs du deuxième volet sont d'expliquer la distribution des lentilles aurifères à la mine Pierre Beauchemin et de formuler des hypothèses sur l'âge de cette minéralisation. Les zones aurifères, traditionnellement exploitées dans

le pluton de Flavrian, étaient toutes localisées dans des zones de failles ou de fractures associées à des dykes de diorite. La distribution des concentrations économiques à l'intérieur de ces structures représente un intérêt de premier ordre pour l'exploration minière dans cette région.

Une cartographie systématique de sept niveaux de développement souterrain à la mine Pierre Beauchemin, avec une emphase structurale, a permis l'étude de la distribution des lentilles économiques. Les observations ont été complétées par une analyse structurale de l'ensemble du pluton. Les objectifs encourus étaient de: (1) documenter les caractéristiques pétrographiques des unités reprises dans la zone de déformation, (2) décrire et documenter le comportement des fractures en fonction de la rhéologie des roches (en passant de la roche compétente à la roche moins compétente), (3) évaluer l'effet de l'anisotropie primaire sur la distribution géométrique des zones aurifères à des échelles variées et (4) établir un modèle expliquant la concentration et distribution de l'or à l'intérieur de la faille. De plus, les données souterraines obtenues à la mine Pierre Beauchemin ont été comparées aux observations et interprétations acquises lors de la cartographie de surface afin de situer l'évènement aurifère dans le contexte évolutif du pluton.

À la mine Pierre Beauchemin, les travaux démontrent que les concentrations économiques en or sont localisées dans des zones de cisaillement ou de fractures associées aux dykes de diorite recoupant le pluton. Les indicateurs cinématiques démontrent que ces zones se sont développées lors d'une compression WNW-ESE. Localement, la réfraction des zones de cisaillement se produit lorsqu'il y a passage des dykes aux roches granitiques. Il est suggéré que la différence de compétence entre les dykes de diorite et la roche encaissante, de composition granitique, contrôle les relations géométriques entre les vecteurs de glissement et l'orientation des cisaillements.

Différents types de veines sont rencontrés. Leurs textures varient selon la rhéologie des roches. L'orientation des veines et des zones de cisaillement, à l'intérieur des unités incompetentes, est contrôlée par l'orientation générale de l'unité

incompétente. Dans les unités compétentes, les veines aurifères sont réfractées et généralement orientées parallèlement aux courbures dans la zone de faille. Toutes les veines sont localisées dans des endroits ayant subi de la dilatation, principalement par un mouvement sur des surfaces non-planaires des dykes de diorite.

Deux types de cheminées minéralisées sont rencontrés à la mine: (1) les cheminées associées aux dykes de diorite et (2) celles associées aux roches encaissantes, de composition granitique. Ces cheminées peuvent s'anastomoser et se réfracter entre elles. Le type et la localisation d'une cheminée sont contrôlés par le relais dextre des dykes incompetents dans l'encaissant compétent. L'orientation des cheminées est contrôlée par la géométrie des dykes dont les plongées varient en fonction de leur axe de courbure.

Les études pétrographiques démontrent que la minéralisation aurifère est associée à une altération hydrothermale caractérisée par la pyritisation, la carbonatation, l'albitisation et la chloritisation des roches encaissantes

L'analyse structurale de la mine Pierre Beauchemin indique que la distribution des zones aurifères est contrôlée par le développement des failles et fractures lors d'une compression WNW-ESE qui a eu lieu après 2681 Ma.

TABLE OF CONTENTS

JURY IDENTIFICATION	ii
SUMMARY	iii
RÉSUMÉ	vi
TABLE OF CONTENTS	xii
LIST OF FIGURES	xvi
LIST OF TABLES	xxiii
DEDICATION	xxiv
ACKNOWLEDGMENTS	xxv
INTRODUCTION	1
Statement of the Problem.....	2
Methodology.....	4
Structure of Thesis.....	6
Location and Access.....	8
History.....	8
Previous Work.....	10
CHAPTER 1. GENERAL GEOLOGY	14
1.1 Regional Geology.....	15
1.1.1 The Southern Volcanic Zone.....	15
1.1.2 Plutonic rocks of the Southern Volcanic Zone.....	19
1.1.3 Structural framework of the Southern Volcanic Zone.....	20
1.1.4 The Blake River Group.....	22
1.1.5 The Noranda Volcanic Complex.....	25
1.1.6 Metamorphism.....	29
1.1.7 Alteration.....	29
1.1.8 Ore deposits in the Noranda area.....	31
1.2 The Flavrian Pluton.....	37

CHAPTER 2. DESCRIPTION OF INTRUSIVE UNITS, FIELD RELATIONSHIPS AND SEQUENCE OF INTRUSION..	40
2.1 Introduction.....	41
2.2 Description of Intrusive Units.....	41
2.2.1 The Méritens quartz-diorite.....	44
2.2.2 Tonalite.....	48
2.2.3 Hybrid rocks.....	52
2.2.4 Early trondhjemite.....	54
2.2.5 Early trondhjemite matrix breccia.....	64
2.2.6 Eldrich diorite.....	67
2.2.7 Late trondhjemite.....	69
2.2.8 Late trondhjemite matrix breccia.....	69
2.2.9 Late mafic dikes.....	71
2.3 Field Relationships and the Sequence of Intrusive Phases.....	71
2.3.1 Geochronology of Flavrian pluton.....	88
2.4 Geometry of the Flavrian Pluton.....	90
2.4.1 Orientations of contacts between internal phases.....	91
2.4.2 Dike orientations.....	92
2.4.3 Internal deformation.....	100
2.4.4 Shape of the Flavrian pluton and relationship to the host BRG volcanic rocks.....	106
2.5 Summary and Discussion.....	116
 CHAPTER 3. GEOCHEMISTRY OF THE FLAVRIAN PLUTON.....	 130
3.1 Introduction.....	131
3.1.1 Sample preparation, method of analysis and precision....	131
3.2 Description of Geochemical Characteristics of Intrusive Phases.....	133
3.2.1 Méritens quartz-diorite.....	133
3.2.2 Tonalite and hybrid rocks.....	142
3.2.3 Trondhjemite porphyry.....	144

3.2.4	Pink trondhjemite.....	146
3.2.5	Coarse-grained trondhjemite.....	149
3.2.6	Granophyre.....	151
3.2.7	Eldrich diorite.....	154
3.2.8	Late trondhjemite.....	154
3.3	Description of Trends, Breaks and Inflections in the Geochemical Data.....	156
3.3.1	General statement.....	156
3.3.2	The Méritens quartz-diorite / tonalite transition.....	158
3.3.3	Geochemical variations within tonalite.....	160
3.3.4	Geochemical variations within trondhjemite.....	161
3.4	Trace Element and REE Variation Diagrams.....	162
3.5	Discussion.....	168
 CHAPTER 4. RELATIONSHIP BETWEEN THE FLAVRIAN SUBVOLCANIC PLUTON AND VOLCANIC ROCKS OF THE NORANDA CAULDRON.....		 184
4.1	Introduction.....	185
4.2	Field Relationships Between the Flavrian Pluton, the Volcanic Rocks and VHMS Deposits of the Noranda Cauldron.....	186
4.2.1	Timing of intrusion relative to the formation of the Ansil Cu-Zn deposit.....	187
4.2.2	Timing of intrusion relative to the Corbet Cu-Zn deposit...	194
4.3	Geochemical Comparison with Volcanic Rock of the Noranda Cauldron.....	196
4.3.1	Description of selected trace element diagrams.....	196
4.3.2	Interpretation of geochemical data.....	200
4.4	Discussion.....	203
 CHAPTER 5. DISTRIBUTION OF GOLD MINERALIZATION AT THE PIERRE BEAUCHEMIN MINE.....		 209
5.1	Introduction.....	210
5.2	Description of Host Rocks at the Pierre Beauchemin Mine.....	212

5.2.1	General.....	212
5.2.2	The granitoid rocks.....	216
5.2.3	The Eldrich diorite.....	219
5.3	The Eldrich Fault Zone.....	222
5.3.1	Shear orientations.....	223
5.3.2	Slip vectors and fault kinematics.....	225
5.4	Mineralization.....	225
5.4.1	Vein types and their orientations.....	225
5.4.2	Vein mineralogy.....	228
5.4.3	Vein textures.....	234
5.4.4	Vein geochemistry.....	235
5.4.5	Constraints on the sequence of alteration events.....	238
5.4.6	Ore shoots.....	244
5.5	Discussion.....	249
5.5.1	Host-rock competency.....	249
5.5.2	Shear zones.....	249
5.5.3	Mineralization.....	252
GENERAL DISCUSSION AND CONCLUSIONS.....		263
REFERENCES.....		288
APPENDICES.....		i-1
Appendix I	Geological Map of the Flavrian Pluton (1:20 000 Scale) Including Sample Location.....	i-1
Appendix II	Work Completed on Samples.....	ii-1
Appendix III	Mineralogy Table.....	iii-1
Appendix IV	Geochemical Data.....	iv-1
Appendix V	Simplified Geological Maps of Pierre Beauchemin Mine.....	v-1
Appendix VI	Location of Pierre Beauchemin Sample.....	vi-1

LIST OF FIGURES

Figure 1.1.	Simplified geological map of the Abitibi Subprovince.....	16
Figure 1.2.	Simplified geological map of the southeastern part of Superior province.....	17
Figure 1.3.	Simplified geological map of the Southern Volcanic Zone of the Abitibi greenstone belt.....	18
Figure 1.4.	Simplified geological map of the eastern Blake River Group in Quebec.....	24
Figure 1.5.	$\text{Na}_2\text{O}+\text{K}_2\text{O}$ vs $\text{K}_2\text{O} / (\text{K}_2\text{O}+\text{Na}_2\text{O}) \times 100$ graph of the intrusive phases of the Flavrian pluton.....	30
Figure 1.6.	Stratigraphic position of VHMS deposits within the Noranda cauldron.....	33
Figure 1.7.	Normative quartz-alkali feldspar-plagioclase.....	38
Figure 1.8.	AFM diagram for the rocks of the Flavrian pluton.....	39
Figure 1.9.	Yb vs Al_2O_3 diagram for the trondhjemites and tonalites of the Flavrian pluton.....	39
Figure 2.1.	Geology of the Flavrian pluton.....	42
Figure 2.2.	Photograph of Méritens quartz-diorite in the vicinity of Lac Fourcet near the pluton's eastern boundary.....	45
Figure 2.3.	Slabbed samples of Méritens quartz-diorite and homogeneous tonalite showing various textures.....	46
Figure 2.4.	Photomicrographs of intrusive phases of the Flavrian pluton.....	47
Figure 2.5.	Slabbed samples showing various textures of tonalite.....	50
Figure 2.6.	Typical field exposures of homogeneous and "spotted" tonalite.....	51
Figure 2.7.	Photographs of hybrid rocks from levels 6 and 7 at the Pierre Beauchemin gold deposit.....	53
Figure 2.8.	Slabbed samples of trondhjemite porphyry, coarse early trondhjemite, pink trondhjemite and granophyre.....	56

Figure 2.9. Photomicrographs of trondhjemite porphyry, coarse early trondhjemite, pink trondhjemite and granophyre.....	57
Figure 2.10. Photomicrographs of the magmatic brecciation texture within early trondhjemite.....	59
Figure 2.11. Photographs of pegmatite lenses within microgranite and granophyre.....	63
Figure 2.12. Epidote-quartz alteration of microgranite and coarse early trondhjemite.....	65
Figure 2.13. Photograph of early trondhjemite matrix breccia, Flavrian northeast.....	66
Figure 2.14. Slabbed sample and photomicrographs of Eldrich diorite showing typical dioritic texture.....	68
Figure 2.15. Slabbed sample and photomicrograph of late trondhjemite showing coarse granitic texture, and photograph showing numerous inclusions.....	70
Figure 2.16. Sketch from photograph of late trondhjemite matrix breccia.....	71
Figure 2.17. Schematic cross-section of the early trondhjemite-tonalite contact in the northwest part of the Flavrian pluton.....	73
Figure 2.18. Geological map of an area in the northeastern part of the Flavrian pluton showing structural and contact relationships between the early trondhjemite and tonalite.....	75
Figure 2.19. Photograph of contact area between tonalite and early trondhjemite matrix breccia.....	76
Figure 2.20. Schematic cross-section parallel to strike showing contact area between early trondhjemite and tonalite.....	78
Figure 2.21. Geological map of an outcrop within early trondhjemite showing internal contact relationships between various phases of early trondhjemite.....	79
Figure 2.22. Photograph of contact between pink trondhjemite and coarse early trondhjemite.....	80
Figure 2.23. Photograph and sketch showing contact relationships between coarse and microgranitic early trondhjemite.....	82

Figure 2.24. Close-up of contact between coarse and microgranitic early trondhjemite.....	83
Figure 2.25. Sketch from field observations showing intrusive relationships between various phases of early trondhjemite, Flavrian east.....	84
Figure 2.26. Photograph of contact relationships between late trondhjemite and late trondhjemite matrix breccia.....	87
Figure 2.27. $Pb^{207}/^{206}$ isochron diagram for the late trondhjemite of the Flavrian pluton.....	89
Figure 2.28. Lower hemisphere equal-area stereographic projections of trondhjemite veins, epidote-quartz \pm magnetite veins and aplitic dikes within the Flavrian and Powell plutons.....	93
Figure 2.29. Schematic diagram (based from photograph) illustrating the dike-fed sill geometry of early trondhjemite crosscutting tonalite.....	94
Figure 2.30. Sketch from field observations illustrating geometrical relationships between coarse early trondhjemite and two generations of finer-grained sills and dikes.....	96
Figure 2.31. Photograph showing early trondhjemite crosscutting tonalite along two preferred orientations.....	97
Figure 2.32. Photograph of early trondhjemite dike crosscutting tonalite. Level 5, Pierre Beauchemin gold deposit.....	98
Figure 2.33. Photomicrographs of contact between early trondhjemite dike and host tonalite.....	99
Figure 2.34. Detailed geological map showing multiple generations of dikes crosscutting a tonalite; eastern Powell pluton.....	101
Figure 2.35. Photographs of an early trondhjemite dike crosscutting tonalite.....	102
Figure 2.36. Photomicrographs of ZY section view of the (S_1) spaced cleavage transecting early trondhjemite, southern part of the Flavrian.....	104
Figure 2.37. Simplified geology map of the Noranda cauldron area.....	107
Figure 2.38. East-west cross-section through the Corbet massive sulphide deposit.....	109

Figure 2.39. Geological map of the southern contact between the Flavrian pluton and the andesitic volcanic rocks.....	111
Figure 2.40. Photograph of contact between the coarse early trondhjemite and andesitic volcanic rocks of the Eldrich pendant.....	113
Figure 2.41. Schematic diagram depicting the shape of the Flavrian pluton relative to surrounding rocks as interpreted from a 2.5D Bouguer anomaly profile.....	115
Figure 2.42. Schematic explanation for the intrusion of horizontal sills fed by dikes.....	121
Figure 2.43. Composite cross-section of the Noranda cauldron.....	128
Figure 3.1. Major element variation diagrams of the intrusive phases of the Flavrian pluton.....	135
Figure 3.2. Compatible trace element variation diagrams of the intrusive phases of the Flavrian pluton.....	136
Figure 3.3. LILE and incompatible trace element variation diagrams of the intrusive phases of the Flavrian pluton.....	138
Figure 3.4. REE variation diagrams of the intrusive phases of the Flavrian pluton.....	139
Figure 3.5. Chondrite-normalized REE patterns of Méritens quartz-diorite, tonalite and trondhjemite porphyry.....	140
Figure 3.6. La/Yb and Eu/Eu* vs SiO ₂ and Th diagrams of the intrusive phases of the Flavrian pluton.....	141
Figure 3.7. Chondrite-normalized REE patterns of pink and coarse-grained trondhjemite.....	148
Figure 3.8. Chondrite-normalized REE patterns of granophyre, Eldrich diorite late trondhjemite.....	153
Figure 3.9. Compatible vs incompatible trace element diagrams of the intrusive phases of the Flavrian pluton.....	164
Figure 3.10. Incompatible vs incompatible trace element diagrams of the intrusive phases of the Flavrian pluton.....	166

Figure 3.11.	Chondrite-normalized REE patterns of late trondhjemite and Lac Dufault granodiorite.....	178
Figure 4.1.	Composite plan of the Ansil VHMS deposit showing the intruding Flavrian pluton beneath Ansil and geological cross-section 46590 N of Ansil deposit.....	188
Figure 4.2.	Selected geochemical variation diagrams comparing samples from the Flavrian pluton and volcanic rocks from the Noranda cauldron.....	197
Figure 4.3.	Diagram showing interpretation of the evolution of the Flavrian subvolcanic pluton in relation to the volcanic rocks of the Noranda cauldron.....	206
Figure 5.1.	Simplified geological map of the Noranda cauldron showing locations of gold deposits within the Flavrian and Powell plutons...	211
Figure 5.2.	Simplified geological map of the Flavrian pluton showing location of the Pierre Beauchemin gold deposit.....	213
Figure 5.3.	Photographs of primary layering within trondhjemite, level 4 south (8+ 80 N) and undeformed contact between tonalite and diorite, level 4 (13+80 N).....	214
Figure 5.4.	Photographs of small diorite dike crosscutting aplite dike within trondhjemite and en echelon diorite dikes within tonalite, level 6 (11+80 N).....	215
Figure 5.5.	Stereographic polar projections of unstrained granitoid-diorite contact.....	217
Figure 5.6.	Photomicrographs of unstrained trondhjemite, an intersection-type vein and a shear vein.....	218
Figure 5.7.	Photomicrographs of unstrained diorite, highly strained unmineralized diorite and a contact vein.....	220
Figure 5.8.	Sketched from photograph of a shear zone at a granitoid-dike contact, level 6 N (15+10 N).....	221
Figure 5.9.	Lower hemisphere equal-area stereographic polar projections of shear zone orientations measured throughout the mine showing domains I through V.....	224
Figure 5.10.	Lower hemisphere equal-area stereographic representation of slip vector orientations measured from slickenlines on major shear surfaces.....	226

Figure 5.11. Cross-section at azimuth N90°, perpendicular to the main diorite dike of structural domain III.....	229
Figure 5.12. Cross-section at 17+40 N, showing sectional shear refraction and various vein types.....	230
Figure 5.13. Lower hemisphere equal-area stereographic polar projections of economically mineralized veins from domains I through V.....	231
Figure 5.14. Photomicrographs of polished sections from the Pierre Beauchemin deposit.....	233
Figure 5.15. Geology of level 1 showing the antidilational jog (domain IV) between diorite dikes.....	236
Figure 5.16. Average gains and losses in major elements from samples collected within economically mineralized zones at the Pierre Beauchemin gold deposit.....	237
Figure 5.17. Sketch from notes of textural and colour variations of tonalite where approaching a mineralized vein, manway between levels 4 and 5 (15+00 N).....	239
Figure 5.18. Sketch from notes of carbonate vein containing fragment of wall-rock tonalite. The fragment is cut by a specularite veinlet that is in turn cut by chlorite veinlets, level 1 survey station 1-48.....	240
Figure 5.19. Sketch from microscopic observations showing recrystallized quartz-albite matrix transected by carbonate-chlorite-pyrite veinlet.....	242
Figure 5.20. Stockwork carbonate veining within diorite and photomicrograph of carbonate veinlet crosscutting diorite, level 4 (14+20 N).....	243
Figure 5.21. Milky quartz vein containing fragments of wall-rock at contact between trondhjemite and subhorizontal lamprophyre.....	245
Figure 5.22. Lower hemisphere equal-area stereographic representation of the 5 main ore shoots measured from a three-dimensional reconstruction of the deposit.....	246
Figure 5.23. Longitudinal projection of diorite dikes and mineralized zones on a vertical plane oriented N30°.....	247

Figure 5.24. Planar composite projection of refracting ore shoots throughout levels 1 to 10.....	248
Figure 5.25. Lower hemisphere equal-area stereographic projection of main shear plane orientations and their associated slip vectors.....	251
Figure 5.26. Schematic model for the creation of zones of dilation.....	254
Figure 5.27. Lower hemisphere equal-area stereographic projection of main shear-vein orientations, slip vectors and ore-shoot plunges.....	257
Figure 5.28. Three-dimensional representation of the Pierre Beauchemin gold deposit.....	258
Figure 5.29. Conceptual model of the Pierre Beauchemin gold deposit.....	259
Figure D.1. Cartoon depicting the evolution of the Flavrian pluton in relation to the Noranda cauldron.....	266

LIST OF TABLES

Table I.	Comparison of measured structures and deformation events in the Southern Volcanic Zone.....	23
Table II.	Lithostratigraphic subdivisions of the Noranda Volcanic Complex...	26
Table III.	Subsidence cycles and associated volcanic formations in the Noranda cauldron.....	28
Table IV.	Grades, tonnage and stratigraphic positions of VHMS deposits of the Noranda Volcanic Complex.....	32
Table V.	Granitoid-hosted gold deposits within the Noranda Volcanic Complex.....	36
Table VI.	Mineralogical, textural and major-element geochemical features of the various phases of the Flavrian pluton.....	43
Table VII.	Summary of plagioclase compositions and oxygen isotope values for several phases of the Flavrian pluton.....	173
Table VIII.	Selected major element geochemistry of drill core samples from the intrusive border phase of the Flavrian pluton, beneath the Ansil deposit.....	192
Table IX.	Ore shoots and their associated veins.....	227

I dedicate this work to my grand parents, Edward and Françoise Quirk.

ACKNOWLEDGMENTS

I would like to thank my research advisors, Dr. Claude Hubert and Dr. Alex C. Brown for their time and the interest they showed in my research. This project benefited from financial and logistical support from the following companies: Cambior Inc., Cominco Ltd, Inmet Mining Corp., Noranda Ltd and Placer Dome Inc. The project also received financing from NSRC through a strategic grant to Dr. Claude Hubert and Dr. Alex C. Brown.

I would like to thank the following people for their support of the project from its very beginning: André Ouellet, Michel Gilbert and Robin Potvin of Cambior Exploration Inc.; Réjean Sirois, Louis Jalbert, Marc Ruel and Jean Caron from Cambior Mines; Dave Moore from Cominco Ltd; Charles Beaudry from Noranda Ltd; Pierre Bertrand from SOQUEM and Michel Labrie from Inmet Mining Corp. Scott Monroe and Sabri Karahan from Cominco Madencilik in Turkey, as well as Jon Collins from Cominco Ltd showed enormous patience and support.

My sincere thanks to the technical staff at the University of Montreal and École Polytechnique for sharing their experience and their time: Jean-Pierre Bourque, Gaston Gélinas, Jean-Luc Bastien, Amira, Gilles Gauthier, Michel Démidoff, Jean Kiepura and Jean Beaulieu. Special thanks to Michèle, Joanne, Annick, Lyne, Chantal, Marguerite and Chantal for their patience during my 1001 requests.

My interest in Archean tectonics and mineralization is largely due to the numerous discussions with colleagues. Jean-Philippe Desrochers, Louis Gauthier, Abdelay Belkibir, Shirley Péloquin, Pascal Marquis and Paul Bédard helped generate many of the ideas of this manuscript. To François Robert and James M. Franklin, I offer my gratitude for their inspiration.

Thanks to Richard and Carole Dufresne, Jean Gouthier, Philippe Cloutier and Sylvie Caza for their high quality, low cost accommodations in Rouyn-Noranda.

Finally, I offer my deepest and sincere thanks to Chris who is largely responsible for the quality of presentation of this thesis. Her infinite patience, humour and support helped me through the long hours.

INTRODUCTION

INTRODUCTION

Statement of the Problem

The Flavrian pluton is located in the Rouyn-Noranda mining district, one of the most productive copper, zinc and gold districts in the province of Québec. More than fifty deposits have been discovered in the district, with over forty of them having been mined (Lulin, 1990). Thirty-eight polymetallic volcanic-hosted massive sulphide (VHMS) deposits and over twenty vein gold deposits were located within the Noranda Volcanic Complex, the core of which is intruded by the Flavrian pluton. The spatial association between the Flavrian pluton and the VHMS and gold deposits of the Rouyn-Noranda district has long been regarded as evidence of a link between intrusion of the pluton and the formation of the deposits (Goldie, 1976; Gibson and Watkinson, 1990). Evidence from previous studies indicating that the Flavrian pluton and volcanic rocks of the Noranda cauldron are comagmatic and contemporaneous further supports the pluton's association to mineralization (Goldie, 1976; Paradis et al., 1988; Mortensen, 1993).

The Flavrian pluton occurs about 1.5 to 2 km stratigraphically below the majority of VHMS deposits. The pluton is generally regarded to have played a role of "heat-engine" in the generation of the VHMS deposits of the Noranda area (Gibson and Watkinson, 1990; Franklin, 1992). According to this concept, intrusion of the Flavrian pluton induced large-scale hydrothermal activity through heat transfer from the hot magma to the relatively cold surrounding volcanic rocks (Cathles, 1993) and

large-scale convection of seawater into the host volcanic rocks resulted in metal remobilization and redeposition, with a possible contribution of metals from the magma itself (Kennedy, 1984).

However, previous work on the Flavrian intrusion (Goldie, 1976; Kennedy, 1984) indicated that it was composed of several intrusive phases, suggesting a complex emplacement history and raising questions as to what part of the intrusion, if any, was present during the formation of the VHMS deposits. The shape, size, composition, emplacement history and evolution of each of the intrusive phases would have influenced the overall thermal energy and the possible chemical contribution of the pluton to the hydrothermal system.

The intrusive rocks of the Flavrian and associated Powell plutons host several gold deposits and prospects. The deposits commonly present complex distributions of ore lenses and shoots and are generally recognized as being shear-related and formed during late-stage tectonic events (Richard et al., 1990; Richard et al., 1991; Picard, 1990; Carrier, 1994). Our detailed structural study of the Pierre Beauchemin gold deposit enables a description of the distribution of ore veins and ore shoots. In addition, fundamental crosscutting relationships between ore and host rocks are established. The structural data were incorporated into a model explaining the geometry of the ores. Finally, the evolution of the Pierre Beauchemin deposit is incorporated and compared to the emplacement and structural history of the Flavrian pluton, enabling interpretations to be made as to the timing of gold mineralization and the potential role played by the pluton in the gold-mineralizing event. The relatively

good exposure of the Flavrian pluton and more than 7 km of underground access at the Pierre Beauchemin deposit were considered as unique opportunities to study a fossil magma chamber potentially related to several VHMS and gold deposits.

The main objectives of the study are: (1) to define the sequence and mechanism of intrusion of the pluton; (2) to characterize the chemical evolution of the intrusive phases; (3) to compare the pluton's evolution to the volcanic rocks of the Noranda cauldron and their associated VHMS deposits and suggest as to what part of the pluton, if any, played a role in the formation of the deposits; and finally (4) to study the geometrical distribution and structural controls of gold mineralization at the Pierre Beauchemin mine located within the Flavrian pluton and propose a sequence of events that led to gold mineralization.

Methodology

Our work on the Flavrian subvolcanic pluton of the Rouyn-Noranda mining camp consisted of 1:5000-scale mapping of the numerous lithologic phases of the intrusion, as well as detailed (1:500 and 1:250) mapping of crucial areas where the geometric relationships among the various intrusive phases of the pluton were well exposed. Five months of field investigations were conducted to map the pluton at the 1:5000 scale and to isolate areas showing key relationships. Information was compiled at 1:20 000 scale and is presented in Appendix I.

Structural data and samples were gathered during mapping. The relationships between intrusive phases within the pluton and the nature of the contacts between the phases provided a basis for the establishment of a sequence of intrusion and a mechanism of emplacement. The petrographic and geochemical studies of units recognized in the field further characterize each of the phases of the pluton and define the physical and chemical conditions of emplacement. The geochemical data are used to identify processes that led to the differentiation of the pluton. Key crosscutting relationships and the trace element signature of each of the phases allow a comparison with volcanic units of the Noranda cauldron. This comparison is used to establish possible extrusive equivalents of intrusive phases and to constrain the size and composition of the pluton during the formation of VHMS deposits.

In addition to the surface mapping of the pluton, eight months of fieldwork was conducted at the Pierre Beauchemin mine. Over 7 km of underground development was mapped at a scale of 1:250. Data from several drill logs and drill core are also incorporated in the study. Petrographic analyses of phases recognized underground are used to identify the host rocks and to determine their mechanical behavior within the deformed and mineralized zones. All data are combined to establish a detailed three dimensional map of the deposit and a sequence of events leading to gold mineralization.

Structure of Thesis

The INTRODUCTION includes a statement of the problem, a description of the methodology used and a brief summary of the structure of the thesis. Also included is information on the location and access of the study area and a summary of the discovery history of the Rouyn-Noranda mining camp and particularly, the Pierre Beauchemin gold deposit. In addition, a comprehensive list of previous geological studies of the Flavrian pluton is given under "previous work".

CHAPTER 1 summarizes the geology of the Abitibi Subprovince, the Southern Volcanic Zone, the Blake River Group and the Noranda Volcanic Complex. Particular attention is paid to volcanic rocks of the Noranda cauldron and the associated VHMS deposits.

CHAPTER 2 describes each of the intrusive phases of the Flavrian pluton, their sequence of emplacement and the nature of their contacts. The chapter also presents data on the orientation of numerous contacts and dikes. These data are compared to the orientations of syn-volcanic faults that host VHMS deposits within the Noranda cauldron. An emplacement model for the Flavrian pluton is proposed based on information from the intrusion sequence and the nature and orientation of the contacts between intrusive phases.

CHAPTER 3 describes the geochemical signature of each of the intrusive phases and the trends, breaks and inflections in the geochemical data. A discussion of

some of the geochemical features in the data is presented along with a summary of the geochemical evolution of the pluton based on our interpretation of the data.

In CHAPTER 4, several key relationships between phases of the Flavrian pluton and various geological elements studied within the Noranda cauldron are presented. In addition, the Flavrian pluton is compared to volcanic rocks of the Noranda cauldron using trace element data. Data for the volcanic rocks were provided by Shirley Péloquin. These data, along with the key relationships, are used to determine what part of the Flavrian pluton played a role in the development of the VHMS deposits. The basic geochemical data are presented in Appendix IV.

CHAPTER 5 presents a detailed description of the structures and geometry of ore lenses and shoots within the Pierre Beauchemin gold mine. The focus is on structural data, which consist of orientations of numerous shears, slip vectors, veins and ore shoots. Observations are incorporated into a discussion of the mechanical development of the ore deposit and hypotheses are presented for the timing of gold mineralization relative to the emplacement of the pluton.

The section entitled GENERAL DISCUSSION AND CONCLUSIONS summarizes our results and presents a model for the intrusion and evolution of the Flavrian pluton and its relationship to the VHMS and gold deposits of the Noranda cauldron, together with a list of the main conclusions resulting from this study.

Location and Access

The Flavrian pluton is located approximately 10 km northwest of the town of Rouyn-Noranda, in northwestern Québec. The pluton occupies the northern part of Beauchastel Township and the southern part of Duprat Township. The central part of the pluton is easily accessed via a paved road in a northerly direction from the village of Évain. Several gravel roads lead to the southern and western parts of the pluton, and to the Pierre Beauchemin mine located 17 km northwest of Rouyn-Noranda. Access to the northeastern and eastern parts of the pluton is difficult due to large swampy areas. However, several all-terrain-vehicle and cross-country skiing paths cross these areas of the pluton.

History

The Noranda mining district has over 75 years of exploration history (Lulin, 1990). The economic importance of the district was quickly realized with the discovery of the giant Home mine in the early 1920's. The discovery of several gold deposits (e.g., Francoeur and Anglo-Rouyn) followed the excitement generated by the Home discovery. The Amulet A and C, Newbec and Old Waite deposits were all discovered in the mid-1920's, followed by the Amulet F discovery in 1929. During the 1930's, exploration shifted to gold, and a series of deposits were uncovered, including the Elder and Senator Rouyn deposits. The West McDonald-Gallen deposit was discovered in 1944 and the Quemont and East Waite deposits were discovered in 1945 and 1948, respectively. The Eldrich (Pierre Beauchemin) gold deposit was

discovered during the mid-1950's (see details below) and the initial discovery of the Mobrun deposit occurred in 1955. Up until the mid-1950's, the majority of discoveries in the district were attributed to prospecting, since most of the deposits occurred at or near surface. A series of "blind" VHMS discoveries between 1957 and 1974 were attributed to increased knowledge of the geology of the district. Deposits discovered during this period include Vauze, Norbec, Delbridge, Millenbach and Corbet. Successful exploration continued with the discovery of the Ansil deposit over 1000 m below surface in 1981. The latest deposits to be found in the district were the Silidor gold deposit in 1986 and the 1100 lens at Mobrun in 1987.

The first drill holes in the area now occupied by the Pierre Beauchemin gold mine were drilled in 1927. In 1954, the Eldrich property was created by the amalgamation of properties held by Boulder Hill Gold Mines Ltd., Knobhill Gold Mines Ltd., Belfast Mines Ltd. and the "Cook claims" (Honsberger, 1954; Tagliamonte, 1979). In 1955, the deposit contained reserves of 589 670 tonnes grading 6.9 g/t Au. Eldrich Mines Ltd. sunk a 325 m shaft and developed seven levels of drifts. The Eldrich mine operated between 1955 to 1962 and produced 651 045 tonnes of flux-type ore (between 65 and 67% SiO₂) grading 4.78 g/t Au. Following additional exploration, reserves of 1 170 268 tonnes grading 5.49 g/t Au were estimated at the mine and adjacent property during 1986. The property was jointly owned by Sullivan Inc. (50%), SOQUEM (25%) and Ressources Aiguebelle Ltée (25%).

Finally, in 1987, Cambior Inc. bought the mine and renamed it Pierre Beauchemin. Cambior developed the mine to 11 levels (1900 feet), outlining reserves of 1.5 Mt. grading 5.1 g/t Au. Cambior officially closed the mine in 1993.

Previous Work

The first maps completed on various parts of the Flavrian pluton were produced by the following workers: Cooke et al. (1931), Gussow (1937), Robinson (1943), Mackenzie (1941), Kindle (1941), Wilson (1941), L'Espérance (1950, 1951, 1952), Behr et al. (1958), Dugas (1960, 1965) and Hogg (1960).

The first complete systematic map of the pluton was provided by Goldie (1976, 1978, 1979a, 1979b). Goldie studied the emplacement relations, petrographic characteristics and petrogenetic and metamorphic evolution of the Flavrian pluton. Goldie, based mainly on major element geochemical analysis, suggested the genetic link between the Flavrian pluton and the host volcanic rocks of the Noranda area. Paradis (1984) and Paradis et al. (1988) focussed on characterizing the pluton using trace elements. The results presented by Paradis supported Goldie's work, indicating a cogenetic link between the Flavrian pluton and volcanic rocks of the Rouyn-Noranda area. Kennedy (1984) remapped the pluton and conducted a detailed geochemical study of intrusive phases from an alteration perspective. Kennedy was the first to suggest that the central part of the pluton was a late intrusive phase. He also established the relative degree of alteration of the phases using petrographic data, geochemistry, mineral chemistry, oxygen isotopic data, and concluded that interaction

with seawater followed by interaction with meteoric fluids caused the alteration of the pluton. Kennedy also suggested that the metal found in the Central Noranda cauldron area may have come directly from the pluton and that gold deposits were probably related to intrusion of the late "plagiogranite" phase in the central part of the pluton.

Rive et al. (1990), Sutcliffe et al. (1993) and Feng et al. (1993), from a regional geochemical study, placed the Flavrian pluton within the plutonic evolution of the southern volcanic zone Abitibi. These studies, based in part on observations reported by Campbell et al. (1982), demonstrated that VHMS-related subvolcanic plutons could be distinguished from other plutonic suites. VHMS-related plutons are characterized by transitional (tholeiitic to calcalkaline) signatures, dioritic to trondhjemitic compositions, low Al, K, Rb and Sr contents, enhanced TiO_2 , Fe_2O_3 , Nb, Y and Sc contents, flat rare earth element (REE) profiles, and negative Eu anomalies that increase with heavy rare earth element (HREE) abundances. As such, subvolcanic plutons are indirect exploration targets, and consequently Franklin (1992) and Richard et al. (1993) have described the characteristics of VHMS-associated subvolcanic intrusions in considerable detail. The chemical characteristics of VHMS-associated subvolcanic intrusions were also described by Galley (1996) in a short course written from an exploration perspective and focused on the identification of favorable plutons using geochemistry.

Jolly (1980) and Powell et al. (1993) conducted regional studies of metamorphism across the field area. The area has undergone regional subgreenschist

to greenschist facies metamorphism with local areas of amphibolite grade metamorphism (Goldie, 1979b).

Feng and Kerrich (1990) evaluated the pressure conditions during the emplacement of the Flavrian pluton. Their results, based on the aluminum contents of amphiboles, suggest that the pluton solidified at a pressure of ~1 Kb. However, Goldie (1991) questioned their interpretations, noting that the amphiboles studied by Feng and Kerrich (1990) were metamorphic in origin and not igneous.

A high-resolution seismic reflection survey through the northern part of the Central Noranda cauldron was conducted by LITHOPROBE's Abitibi-Grenville project (Verpaelst et al., 1991). Data can be obtained from the geophysical personnel at l'École Polytechnique de Montréal. In the Noranda cauldron area, seismic reflectors are generally shallow-dipping and locally separated by what are interpreted as steeply-dipping discontinuities.

A detailed gravity survey undertaken in the eastern Blake River Group, including lines across the Flavrian and Powell plutons, (Chouteau and Deschamps, 1989) has been reprocessed and reinterpreted by Bellefleur (1992). Results confirm Goldie's interpretation, suggesting that the Flavrian pluton is a sill-like body.

Using oxygen isotopes, Cathles (1993) studied the altered volcanic and plutonic rocks in the Rouyn-Noranda area. He proposed a model of fluid circulation and interaction centred on the Flavrian pluton. The pattern of isotopic alteration presented

by Cathles is dominated by a nearly continuous 2 to 3 km wide ring coincident with the margins of the pluton. Cathles interprets the pattern of isotopic alteration as resulting from a long-lived (~10 Ma) hydrothermal system.

Studies conducted by Méthot (1987) and Trudel et al. (1989) at the Pierre Beauchemin mine, described zones of alteration related to the mineralized bodies. Other studies of gold deposits hosted within the Flavrian and associated Powell plutons include descriptions of the Silidor mine by Picard (1990), Gaulin (1992) and Carrier (1994) and of the Elder mine by Gaulin and Trudel (1990) and Trudel et al. (1991).

CHAPTER 1

CHAPTER 1. GENERAL GEOLOGY

1.1 Regional Geology

The Flavrian subvolcanic pluton intruded the Blake River Group volcanic strata of the Southern Volcanic Zone of the Abitibi Greenstone Belt. The Abitibi Greenstone Belt (Fig. 1.1) is an Archean volcano-plutonic subprovince of the Superior Structural Province within the Canadian Precambrian Shield (Card, 1990). The Abitibi greenstone belt was divided into three lithotectonic domains (Fig. 1.2) by Ludden et al. (1986): a northern domain composed of the oldest volcano-plutonic rocks; a central domain generally composed of intrusive rocks (trondhjemite, tonalite, granodiorite and orthogneiss); and finally, a southern domain dominated by supracrustal volcanic rocks.

1.1.1 The Southern Volcanic Zone

Weakly metamorphosed volcanic terrains dominate the Southern Volcanic Zone (SVZ) of the Abitibi greenstone belt (Fig. 1.3). The terrains are generally bordered by tectonic zones where deformation and metamorphism is accentuated (Hubert et al., 1984). The SVZ is divided into five major groups according to their age and the nature of the rocks (MERQ-OGS, 1984). The Hunter Mine Group is dated at 2730 Ma (Mortensen, 1987) and is composed of bimodal (andesite-rhyolite) calcalkaline volcanic rocks. The Malartic Group and laterally equivalent Stroughton-Roquemaure Group are composed of komatiites, tholeiites and magnesian basalts. A

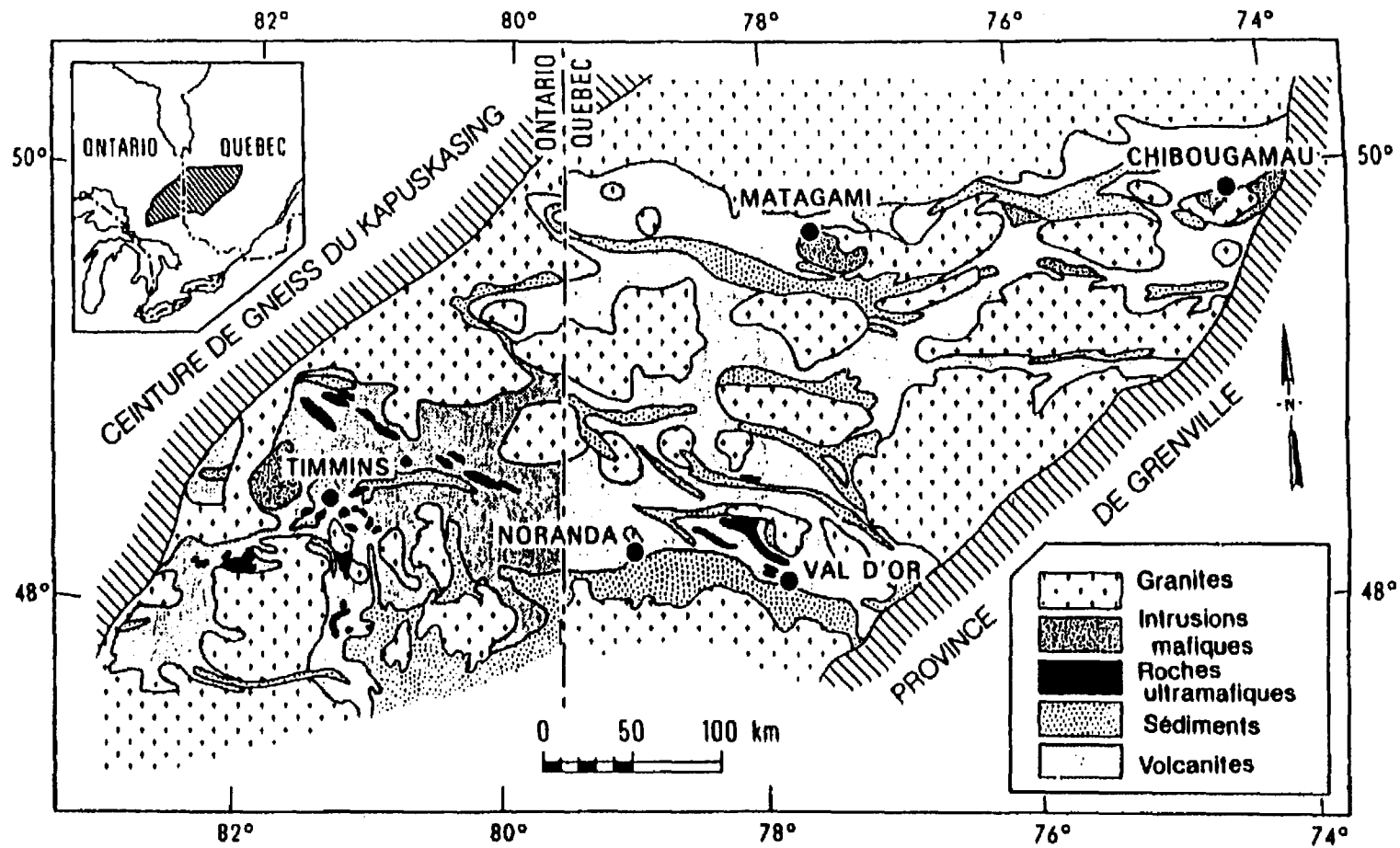


Figure 1.1: Simplified geological map of the Abitibi Subprovince. Modified from Goodwin and Ridler (1970).

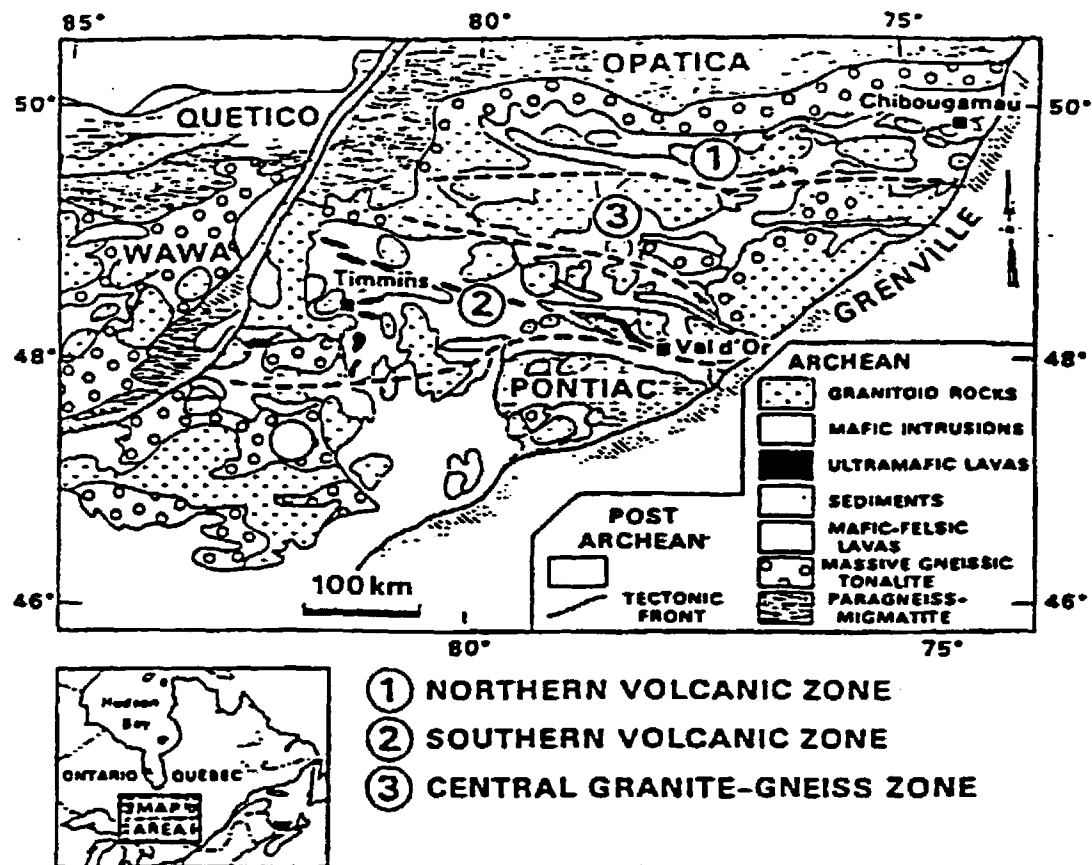


Figure 1.2: Simplified geological map of the southeastern part of Superior Province showing the north, central and southern lithotectonic domains of the Abitibi greenstone belt. From Ludden et al. (1986).

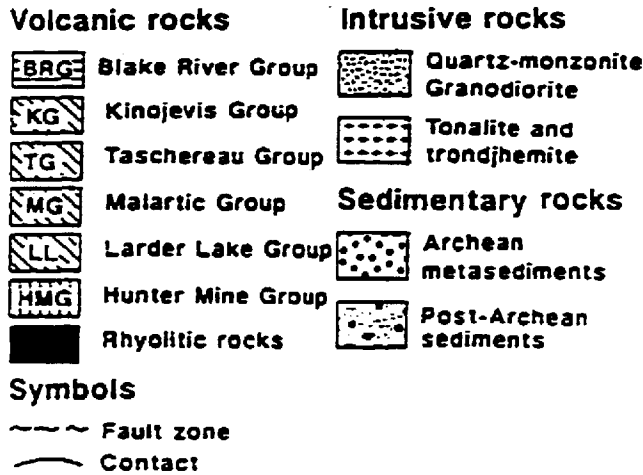
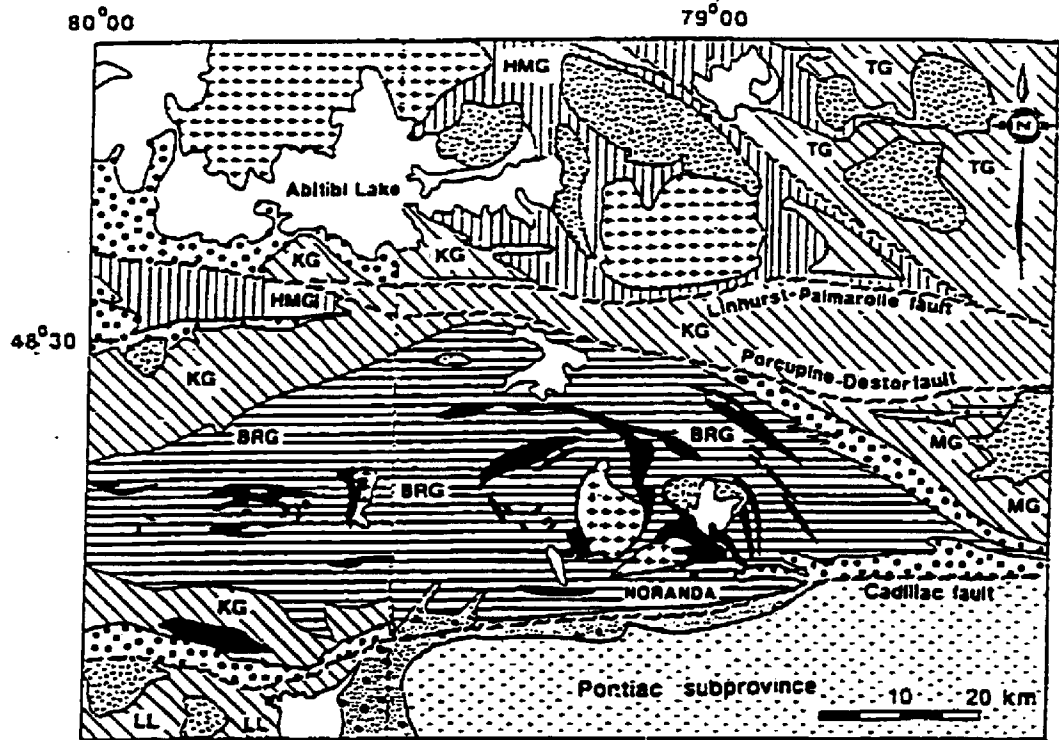


Figure 1.3: Simplified geological map of the Southern Volcanic Zone of the Abitibi greenstone belt. Modified from Laflèche et al. (1992).

rhyolite yielded an age of 2714 Ma (Corfu et al., 1989). Abundant tholeiitic basalts and gabbro sill complexes characterize the Kinojevis Group. The Blake River Group, dated at 2703 and 2698 Ma (Mortensen, 1987; 1993), is composed of both tholeiitic and bimodal calcalkaline volcanic rocks (Gélinas et al., 1984). The Blake River Group is bordered to the north by the Destor-Porcupine Fault and to the south by the Larder Lake-Cadillac Tectonic Zone. The Larder Lake-Cadillac Tectonic Zone separates the Abitibi Subprovince from the Pontiac Subprovince. The Blake River Group is discussed in more detail in Section 1.1.4. Finally, the Timiskaming Group discordantly overlies the Blake River group and marks the end of volcanism in the Abitibi Subprovince. This group is characterized by alkaline volcanic rocks (Ujike, 1985) and fluvial and alluvial sediments (Ojakangas, 1985).

In the Southern Volcanic Zone, volcanism occurred over an interval of approximately 50 Ma, from 2747 Ma for the Pacaud structural complex (Ontario) to 2698 Ma for the Blake River Group (Mortensen, 1993).

1.1.2 Plutonic rocks of the Southern Volcanic Zone

A number of researchers have studied the evolution of the plutonic rocks of the Abitibi greenstone belt (Rive et al., 1990; Feng and Kerrich, 1993; Sutcliffe et al., 1993). These authors have described plutonic suites defined by their relative chronology, mineralogy, geochemistry and metal associations. Five main suites have been identified: (1) syn-volcanic to pre-tectonic (2.72 to 2.70 Ga) layered intrusions of ultramafic to mafic composition and tholeiitic affinity (the Dundonald sill and Kamiskotia complex, western Abitibi) are associated with magmatically derived Ni-

Cu deposits; (2) syn-volcanic layered intrusions (2.75 to 2.96 Ga) with compositions ranging from diorite to trondhjemite are tholeiitic to calcalkaline and are associated with Cu-Zn VHMS deposits and porphyry type Cu-Mo-Au deposits. Examples include the Flavrian pluton (Noranda area), the Bourlamaque pluton (Val d'Or area) and the Cléricy pluton (Cléricy area); (3) tonalitic to trondhjemitic intrusions dated between 2.85 and 2.69 Ga (Round Lake batholith) are syn- to late-tectonic; (4) late- to post-tectonic diorite-monzonite to syenite intrusions yielding ages of 2.80 to 2.67 Ga are associated with alkaline magmatism along major discontinuities and are commonly associated with gold-bearing structures; and (5) late to post-tectonic, two-mica monzodiorite-monzonite, granodiorite intrusions and muscovite-garnet are dated between 2.71 and 2.64 Ga and associated with pegmatitic Mo, Li and Be deposits. The chemical evolution of plutonic rocks within the Abitibi is viewed by many as resulting from accretionary tectonic processes (Feng and Kerrich, 1993; Sutcliffe et al., 1993).

1.1.3 Structural framework of the Southern Volcanic Zone

Most tectonic studies of the SVZ were conducted in the Blake River Group. Wilson (1941) described relations between the main groups and laid the groundwork for following studies. In the Rouyn-Noranda and Cléricy areas, Boivin (1974), Goulet (1978), Trudel (1978), Hubert et al. (1984) and Laflèche (1991) recognized two principal phases of deformation (D_1 and D_2) characterized by P_1 and P_2 folds and associated S_1 and S_2 schistositys. These principal deformation phases were followed by two additional minor phases of deformation that did not seriously affect earlier geometrical relationships. The first phase folds resulting from D_1 are closed, upright,

south. The cauldron's eastern margin is poorly defined and is interpreted to have been buried by post-cauldron volcanic rocks in the vicinity of the Dalembert shear. The western structural margin is interpreted to have been eroded and is estimated to occur near the western edge of the Flavrian pluton, possibly represented by inferred ring fractures defined by the Méritens quartz-diorite (Goldie, 1976; Gibson and Watkinson, 1990).

Cauldron subsidence is interpreted by Gibson and Watkinson (1990) to have occurred during extrusion of the Noranda Cauldron volcanic rocks. Cycle 3 or the "Mine Sequence" developed during two cauldron subsidence cycles separated by a hiatus in volcanic activity. A third phase of subsidence is interpreted to have occurred along the Horne Fault during extrusion of Cycle 4 strata. A summary of the formations and the relative stratigraphy of the Noranda Volcanic Complex is presented in Table III.

The NVC is intruded by three main plutonic suites: (1) syn-volcanic plutons are multi-phase, sill-like intrusions that range in composition from quartz-diorite to trondhjemite and are comagmatic with their host volcanic rocks (examples include the Flavrian (2700 ± 1.6 Ma), Powell and Cléricy ($2696 +1.7/ -1.4$ Ma) subvolcanic plutons); (2) post-volcanic plutons are mainly composed of granodiorite and show well-developed metamorphic aureoles (e.g., the Lac Dufault ($2690 +2.2/ -2.0$ Ma) and Dalembert plutons); and (3) the Aldermac pluton is primarily composed of syenite and is not metamorphosed, suggesting a relatively young age (2680 Ma) (geochronological data from Mortensen, 1993).

EOH (ERA)	CYCLE	FORMATION	MAP SYMBOL	PRINCIPAL LITHOLOGY		
PHANEROZOIC				Sand, gravel, alluvium		
Unconformity						
PROTEROZOIC				Diabase dikes		
Intrusive Contact						
ARCHEAN	INTRUSIONS	Aldermac Syenite Dufault Pluton Dalambert Pluton Newbec Breccia Flavrian Pluton Here Diorite	6	Lamprophyre dikes Syenite plugs, dikes. Composite granodiorite intrusion Granodiorite Metrolithic diatreme breccia Diorite, gabbro sills and dikes Diorite, trondjemite, tonalite intrusions Diorite, gabbro intrusions		
		Intrusive Contact				
			Cycle 5			Rhyolitic and andesitic flows/breccias
			Cycle 4			Rhyolitic and andesitic flows/breccias
			Cycle 3	HUNTER BLOCK		
				Upper North Duprat Andesite	XI UNDA	Massive and pillowed andesitic flows
				Upper North Duprat Rhyolite	VII-X UNDR	Aphyric, feldspar porphyritic and quartz porphyritic rhyolitic flows
				Lower North Duprat Andesite	VII LHDA	Massive and pillowed andesitic flows
				Lower North Duprat Rhyolite	VI LADR	Aphyric, feldspar porphyritic and quartz porphyritic rhyolitic flows
				Hunter Andesite	V N	Massive and pillowed andesitic flows
				FLAVRIAN BLOCK		
				Amulet Andesite	XI A	Massive and pillowed andesitic flows, minor tuff
				Waite/Millenbach Rhyolite	X W/N	Feldspar porphyritic and minor quartz porphyritic rhyolitic flows
				Waite/Millenbach Andesite	IX W/N	Massive and pillowed andesitic flows and minor tuff
				Amulet	VIII A	Silicified andesitic flows, minor rhyolite feldspar and quartz feldspar porphyritic rhyolitic flows and minor breccia (Beecham Breccia) at base of unit
				Amulet Upper Member	VIII AL	
				Amulet Lower Member	VIII AI	
				Rusty Ridge	VII R	Massive and pillowed andesitic flows, minor rhyolitic breccias
			Northwest	VI N	Feldspar phytic rhyolitic flows	
			Cranston Member	VI NC	Quartz feldspar porphyritic rhyolitic flow	
	Flavrian	V F	Massive and pillowed andesitic flows			
	Ansill Member	V FA	Quartz feldspar porphyritic rhyolitic flow			
	POWELL BLOCK					
	Powell Andesite	XI P	Massive and pillowed andesitic flows			
	Quefont Rhyolite	X Q	Aphyric and quartz-feldspar porphyritic rhyolite			
	Joliet Rhyolite	VI J	Feldspar phytic rhyolitic flow			
	Brownlee Rhyolite	VI B	Feldspar phytic rhyolitic flow			
	Cycle 2			Rhyolitic and andesitic flows/breccias		
	Cycle 1			Rhyolitic and andesitic flows/breccias		
	MINE SEQUENCE	HUNTER BLOCK FLAVRIAN BLOCK POWELL BLOCK	NORANDA VOLCANIC COMPLEX			

Roman numeral prefix indicates order of stratigraphic succession
Cycle 5 may be the stratigraphic equivalent of Cycles 2 or 3

Table III: Volcanic cycles and associated volcanic formations in the Noranda cauldron. From Gibson and Watkinson (1990).

Diorite and gabbro dikes occur throughout in the NVC, commonly obscuring stratigraphic relationships. Lagraa (1994) identified five distinct diorite suites ranging in composition from calcalkaline to tholeiitic.

1.1.6 Metamorphism

The Noranda Volcanic Complex was affected by regional metamorphism that occurred as a result of the Kenoran orogeny at about 2680 Ma. Greenschist facies mineral assemblages dominate in the Noranda area with prehnite-pumpellyite assemblages occurring north of the Hunter Creek Fault (Jolly, 1980). Contact metamorphic mineral assemblages occur as aureoles surrounding post-volcanic plutons such as the Lac Dufault and Aldermac plutons. The contact metamorphic aureole surrounding the Lac Dufault pluton has affected cross-strata alteration zones related to the VHMS deposits (de Rosen-Spence, 1969; Riverin and Hodgson, 1980). Amphibolite facies contact metamorphic assemblages also occur around the late trondhjemite phase within the Flavrian pluton (Kennedy, 1984).

1.1.7 Alteration

Na-metasomatism affected all rocks in the NVC. Intense spilitization occurred within the Flavrian pluton and in the surrounding volcanic rocks. Figure 1.5 shows that rocks from the Flavrian pluton are Na-metasomatized. Epidote alteration is common throughout the Flavrian pluton and is manifested in the form of epidote patches, quartz-epidote veins, and quartz-epidote miarolitic cavities and orbicules. Quartz-epidote alteration also overprinted spilitization and silicification in the volcanic rocks of the NVC (Gibson, 1992, personal communication).

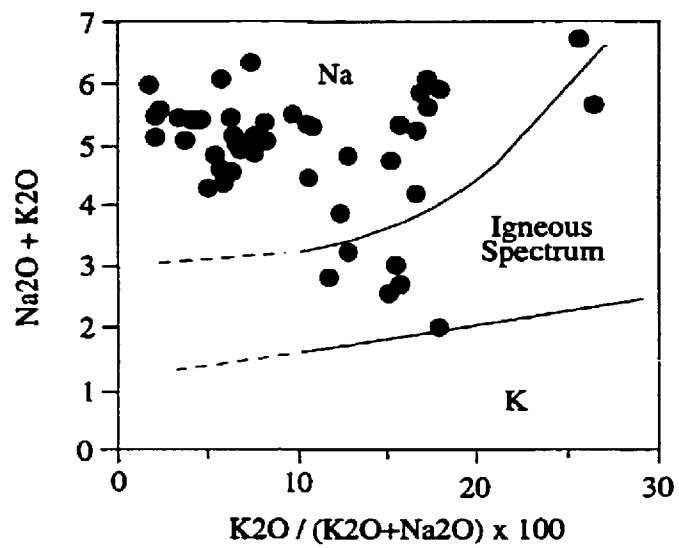


Figure 1.5: $Na_2O + K_2O$ vs $K_2O / (K_2O + Na_2O) \times 100$ graph of intrusive phases of the Flavrian pluton. Note that rocks from the Flavrian pluton plot outside the igneous spectrum, indicating spilitization. Classification from Hughes (1973).

Hematitic alteration is widespread in the Flavrian pluton and occurs mainly in the form of veinlets crosscutting spilitized rocks. Locally, zones containing quartz veinlets, chlorite-carbonate-pyrite veins and breccias and sericite indicate multiple phases of hydrothermal activity.

1.1.8 Ore deposits in the Noranda area

Three main deposit types occur in the Noranda area: (1) polymetallic volcanic-hosted massive sulphide (VHMS) deposits; (2) structurally-controlled vein and disseminated Au deposits; and (3) porphyry Cu-Mo-Au deposits. Most of the deposits occur in the central part of the Noranda volcanic complex, stratigraphically above and within the Flavrian pluton.

VHMS deposits

Thirty-eight volcanic-hosted massive sulphide (VHMS) deposits are known within the Noranda Volcanic Complex (Table IV). The majority of these deposits occur within the Noranda cauldron (Cycle 3) volcanic rocks. However, the gold-rich Home deposit (Kerr and Mason, 1990), the biggest in the NVC (>150 Mt), may be hosted in pre-cauldron volcanic rocks (Kerr and Gibson, 1993). The stratigraphic position of intra-cauldron VHMS deposits is presented in Figure 1.6. Two deposits, Ansil and Corbet, occur within the first cauldron cycle, however, the remainder, i.e., the majority of deposits, occur within the second cauldron cycle, above the "C contact" horizon, which marks a period of quiescence between the two cauldron subsidence cycles (Gibson and Watkinson, 1990). The second cauldron subsidence

Stratigraphic Position	Deposit	Massive Sulphide	Stringer Sulphide	Multiple Lenses	M/Tons	% Cu	% Zn	oz. Ag	oz. Au	Cu-Zn Ratio
1st Cycle	Four Corners		X							-
	Inmont		X							-
	Yvanex	X								Zn-rich
3rd Cycle	Ansil (1)	X	X		2.1	7.18	0.57	0.60	0.06	92
Mine	Vauze (2)	X	X	X	0.37	2.94	1.00	0.80	0.02	74
Sequence	Norbec (3)	X	X		4.35	2.77	4.50	1.40	0.02	38
	D-Zone (4)	INCLUDED WITH NORBEC (3)								
	East Waite (5)	X	X		1.65	4.10	3.25	0.91	0.05	56
	Old Waite (6)	X	X	X	1.24	4.70	2.98	0.63	0.03	61
	F-Shaft (7)	X	X		0.3	1.40	8.60	1.35	0.01	28
	C Deposits (8)	X	X	X	0.62	2.20	8.50	2.53	0.01	20
	Lower A (9)	X	X		5.17	5.10	5.20	1.29	0.04	49
	Upper A (9)	X	X		0.20	2.30	6.10	1.35	0.06	28
	#11 (9)	X	X		0.49	3.60	2.40	0.63	0.02	60
	Bluff (9)	INCLUDED WITH LOWER A								
	Millenbach (10)	X	X	X	3.92	3.46	4.33	1.64	0.03	44
	Corbet (11)	X	X	X	3.06	3.00	1.96	0.60	0.03	60
	O68 (12)	INCLUDED WITH CORBET								
	Queмонт (11)	X	X		16.35	1.20	1.80	0.54	0.12	40
	Aldermac (18)	X	X	X	2.07	1.48	-	0.20	0.01	-
	Newbec	X	X		0.007	6 to 7				
	Fourcet		X							
	D-62	X								
	Moosehead	X	X							
	Dafault Zinc	X	X		0.50	-	<1.0	-	-	-
	South Rusty Hill		X							
	Bedford		X		0.09	0.89				
	Ribago	RECENT DISCOVERY - TONNAGE/GRADE UNCERTAIN								
	Aldermac	RECENT DISCOVERY - TONNAGE/GRADE UNCERTAIN								
4th Cycle	Deldona (16)	X			0.10	0.30	5.00	0.76	0.12	5
	Delbridge (15)	X	X		0.40	0.55	8.60	2.00	0.07	6
	Gallen (12)	X			3.25	0.07	4.77	0.63	0.02	2
5th Cycle	Mobrun ¹	X	?		3.00	0.62	2.30	0.60	0.50	21
	New Lens	TONNAGE/GRADE UNCERTAIN								
Uncertain	Magusi	X			4.11	1.20	3.60	0.90	0.03	25
	New Insc0	X	X		1.15	2.11	-	0.50	0.03	-
	Horne (mined) (14)	X	X		60.26	2.20	-	0.40	0.17	-
	Horne #5 ²	X	X		144	1.0	0.9			52

(2) refers to former or operating mines and "uneconomic deposits" respectively.

¹ Some Cu-rich ore removed during earlier mining.

² Tonnage and grade of Horne #5 zone from Sangster (1980) and combined with mined tonnage.

Data from Boldy (1979) and unpublished compilations by D. MacNeil (Corp. Falconbridge Copper) and B. Bancroft (Noranda).

Table IV: Grade, tonnage and stratigraphic positions of VHMS deposits of the Noranda Volcanic Complex. From Gibson and Watkinson (1990).

parallel flexure folds with an original NNW orientation. The second phase (D_2) produced open, asymmetric flexural folds with an EW orientation. The first phase folds are commonly re-oriented by the second folding. The folds and associated penetrative schistosity are interpreted to have resulted from D_1 , a NNE-SSW compression and D_2 , a NS-oriented compression.

Alternatively, a series of investigations have interpreted the structural elements of the SVZ as resulting from the subsidence of komatiite-dominated volcanic basins (Goodwin and Smith, 1980; Jensen, 1985). This model involves gravitational instabilities caused by the subsidence of the volcanic basins. Subsidence would have entrained the diapiric ascent of tonalitic plutons between basins, resulting in a dome-and-basin geometry. Subsidence followed by a N-S compression was suggested in a model by Dimroth et al. (1983a).

Investigations by Hubert et al. (1984), Ludden et al. (1986) and Hubert (1990) interpreted diamond-shaped fault patterns in the Southern Volcanic Zone to have resulted from a single episode of oblique convergence. A sinistral wrench-fault tectonic model was proposed to explain this particular geometry. In a similar model based on information gathered in the area influenced by the Larder Lake-Cadillac Fault Zone between Rouyn-Noranda and Val d'Or, Robert (1989) recognized two main compressional orientations, one N-S and the other NW-SE both resulting from a single dextral transpression.

Desrochers et al. (1993) and Desrochers and Hubert (1996) have documented the complex structural history of the Southern Volcanic Zone through a comprehensive study of the Malartic Composite Block in the Val d'Or area (Table I). The authors provide evidence for a pre-2705 Ma D_1 tectonic event. The D_1 event is interpreted to have resulted from early accretion of ultramafic to mafic rocks of the Malartic Composite Block. The Val d'Or Domain (2705 Ma) unconformably overlies rocks affected by D_1 , indicating that D_1 occurred prior to 2705 Ma. D_2 is divided into three increments resulting from the same progressive deformation that occurred between 2687 and 2680 Ma. The three increments are attributed to a rotation in the principle compressional direction from NE-SW to N-S and finally NW-SE. A minor D_3 event producing local conjugate kink folds is attributed to an E-W shortening.

The peak of the Kenoran orogeny is constrained by relationships between the Cléricy syenite and the Kewagama sedimentary group. The Cléricy syenite (2682 ± 3 Ma) intruded the Kewagama sedimentary group, which yielded detrital zircon ages as young as 2687 Ma (Mortensen, 1993). Since intrusion of the Cléricy syenite postdates the main period of Kenoran deformation, the peak in the Kenoran orogeny is constrained to an interval between 2687 and 2679 Ma.

1.1.4 The Blake River Group

The Blake River Group (BRG) (Fig. 1.4) is located between the EW-trending Larder Lake-Cadillac Fault to the south and Porcupine-Destor Fault to the north. The BRG is divided into three subgroups (Péloquin et al., 1994): (1) the Noranda

Bouchard (1980)	Tourigny (1984)	Bahineau (1985)	Hubert et al. (1984); Hubert (1990)	Sansfaçon and Hubert (1990)	Robert (1991)	This study
		D ₁ : NE-SW:NW-SE:V Fo ₁ : NW-SE S ₁ : NW-SE	D ₁ : NE-SW:V:NW-SE Fo ₁ : NW-SE S ₁ : NW-SE F ₁ : NW-SE and NE-SW	D ₁ Fo ₁ : NE-SW, iso	D ₁ Fo ₁ : NE-SW, iso	D ₁ : NE-SW:NW-SE:V Fo ₁ : NW-SE S ₁ : NW-SE F ₁ : NW-SE
D ₁ : N-S:E-W:V Fo ₁ : E-W, iso S ₁ : E-W/V	D ₁ : NE-SW:NW-SE:V Fo ₁ : E-W, dex S ₁ : 285°/V	D ₂ : N-S:E-W:V Fo ₂ : E-W, dex S ₂ : E-W/V	D _{2,1} : N-S:E-W:V Fo _{2,1} : E-W, iso S _{2,1} : E-W/V L _{2,1} : steep	D ₂ : NE-SW:NW-SE:V Fo ₂ : N315° S ₂ : N315°/mod-V	D ₂ : N-S:E-W:V Fo ₂ : ±E-W, iso S ₂ : NW-SE to E-W/V L ₂ : steep	D _{2,1} : N-S:E-W:V Fo _{2,1} : NW-SE S _{2,1} : NW-SE
			D _{2,2} S _{2,2} : N080°/V, pressure-solution cleavage	D ₂ Fo ₂ : N280°, sin S ₂ : N280°/mod-V		D _{2,2} Fo _{2,2} : E-W, dex S _{2,2} : E-W/V L _{2,2} : variable
D ₂ : N350°:N080°:V Fo ₂ : E-W, dex S ₂ : N082°/V	D ₂ : N-S:E-W:V Fo ₂ : E-W:V S ₂ : 278°/V		D _{2,1} Fo _{2,1} : E-W, dex S _{2,1} : E-W/V ECC ₁ and ECC ₂		D ₂ : NW-SE:NE-SW:V Fo ₂ : E-W, dex S ₂ : E-W to ENE-WSW	D _{2,1} Fo _{2,1} : E-W, dex S _{2,1} : E-W
D ₁ Kink, N305°, sin; N045°, dex	D ₁ : E-W:N-S:V Kink, NNW-SSE, sin; NE-SW, dex	D ₁ Kink, NW, sin; NE, dex	D ₁ : E-W:N-S:V Kink, N330°, sin; N030°, dex	D ₁ Kink, NW-SE, sin; NE-SW, dex		D ₁ Kink, N330°, sin; N035°, dex

Notes: Orientation of inferred principal strain axis: Z:Y:X (V, subvertical), Fo, folding; F, fault; iso, isoclinal; sin, asymmetric sinistral folds; dex, asymmetric dextral folds; mod, moderate.

Table I: Comparison of structures and deformation events in the Southern Volcanic Zone measured by several authors (Desrochers and Hubert, 1996).

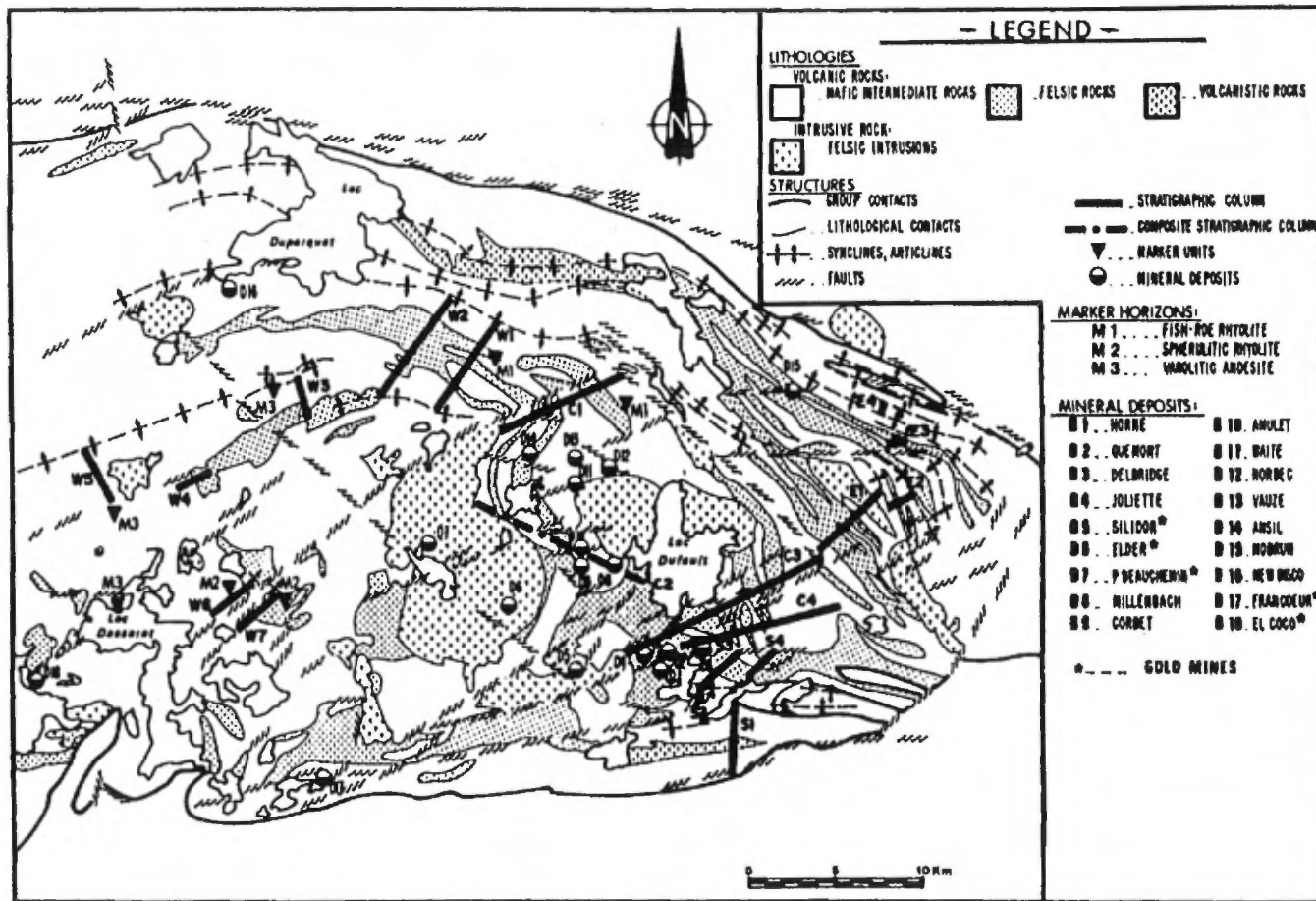


Figure 1.4: Simplified geological map of the eastern Blake River Group in Quebec. From Pêloquin et al. (1990).

subgroup consists of a bimodal andesite-rhyolite sequence that forms the Noranda Volcanic Complex (see Section 1.1.5); (2) the Garrison-Bowman subgroup, located south of the Noranda subgroup, is composed of tholeiitic basalt and andesite; and (3) the Misema subgroup, located west of the Noranda subgroup, is composed of andesite and minor rhyolite. The Misema subgroup is similar to the Noranda subgroup and may represent a lateral equivalent (Péloquin et al., 1990). Based on a stratigraphic reconstruction, the total thickness of the Blake River Group is estimated to be 14 km (Péloquin et al., 1990).

1.1.5 The Noranda Volcanic Complex

The Noranda Volcanic Complex (NVC) (de Rosen-Spence, 1976; Dimroth et al., 1983a; Gélinas et al., 1984; Gibson and Watkinson, 1990; Paradis, 1990; Péloquin et al., 1990) has an approximate diameter of 35 km and is estimated to represent a total thickness of 7.5 to 9 km, erupted between 2703 and 2698 Ma. The NVC is composed of transitional tholeiitic-calcalkaline rhyolite, andesite and basalt flows with minor pyroclastic rocks.

The NVZ was originally divided into five separate "rhyolitic zones" (Spence, 1967) which are now defined as cycles (Gibson and Watkinson, 1990). Each cycle consists of an andesite basal unit and mixed rhyolitic and andesitic upper unit (Table II). Cycles 1 and 2 are interpreted as pre-cauldron sequences, whereas Cycle 3, which hosts the majority of the volcanic-hosted massive sulphide (VHMS) deposits, is interpreted to have been deposited during two phases of subsidence. Cycle 4 is viewed as a late to post-cauldron sequence in which volcanism caused the subsidence

structure to fill with lava that eventually spilled over the edges of the subsiding basin. Cycle 5 has the same age as Cycle 2 and may be a tectonic repetition of Cycle 2 (Mortensen, 1987).

SPENCE (1967) DE ROSEN-SPENCE (1976)	GIBSON AND WATKINSON (1990)	SEQUENCE
Rhyolite Zone 5 Andesite	Cycle 5	
Rhyolite Zone 4 Andesite	Cycle 4	Post-Cauldron
Rhyolite Zone 3 Andesite	Cycle 3 Mine Sequence	Cauldron
Rhyolite Zone 2 Andesite	Cycle 2	Pre-Cauldron
Rhyolite Zone 1	Cycle 1	

Table II: Lithostratigraphic subdivisions of the Noranda Volcanic Complex. From Gibson and Watkinson (1990).

Cycle 3, which hosts the Flavrian pluton, was first recognized as an extrusion within a syn-volcanic subsidence structure by de Rosen-Spence (1976). The structure was originally referred to as a caldera (Lichtblau and Dimroth, 1980; Dimroth et al., 1982; Gibson et al., 1984; Gibson and Lichtblau, 1986), and was re-defined as a cauldron by Gibson and Watkinson (1990) due to the uncertain shape of the original structure. The Noranda cauldron is located between the Hunter Creek and Cranston Faults in the north and the Quernont and Horn Creek Faults in the

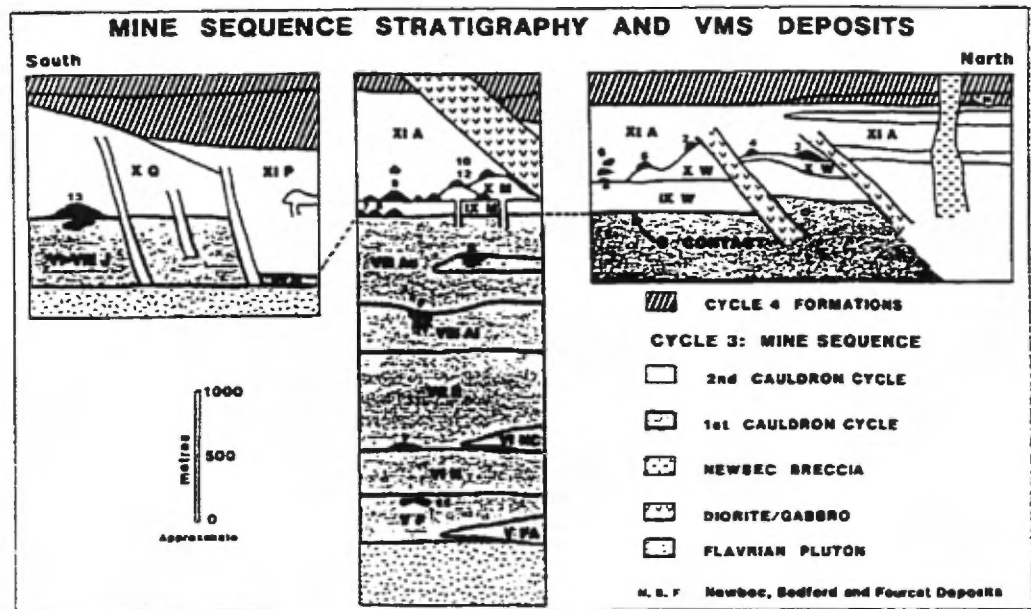


Figure 1.6: Stratigraphic position of VHMS deposits within the Noranda cauldron. Map symbols from Tables III and IV. After Gibson and Watkinson (1990).

cycle therefore marks a well-defined time interval where intra-cauldron VHMS deposits were concentrated.

Intra-cauldron VHMS deposits are spatially associated with volcanic vents localized on syn-volcanic faults and ill-defined paleostructures. The paleostructures are preferentially oriented (1) ENE and (2) WNW to NW (See CHAPTER 2) and allowed cross-stratal permeability for ascending hydrothermal fluids.

Porphyry Cu-Mo-Au

Cu-Mo-Au mineralization occurs in porphyry-type deposits and prospects within the Flavrian and Powell plutons. However, these deposits are presently not economic, due to their low grades. The Don Rouyn deposit was mined as a source of Cu-rich siliceous flux for the Horne smelter (Goldie, 1976). Estimated mined tonnage is 5.5 Mt grading 75% SiO₂ and 0.15% Cu, with reserves of 36 Mt of similar grade. Hosted in trondhjemite and diorite within the Powell pluton, the deposit was cylindrical in shape, trended ENE and plunged steeply to the south. The deposit contained Cu, Mo, Au and W, and was concentrically zoned. A central core of chalcopyrite and bornite gradually gave way to a pyrite-rich outer zone. Both the concentration of chalcopyrite and the chalcopyrite/pyrite ratio decrease outward from the central bornite zone (Goldie, 1976).

The St-Jude breccia is a Mo-Au prospect located at the Flavrian pluton's western contact with andesite. The prospect may represent a high-level explosion breccia related to the intrusion of trondhjemite (Kennedy, 1984).

Gold deposits

The Noranda area has produced significant amounts of gold from several deposits (Fig. 1.4). However, the largest production of gold was from the Horne mine, a VHMS deposit. All other gold deposits in the Noranda area are spatially associated with major geologic structures: the Larder Lake-Cadillac Fault, the Horne Creek Fault and the Smokey Creek Fault.

Deposits associated with the Larder Lake-Cadillac Tectonic Zone (LCTZ) in the Rouyn-Beauchastel area, are located in a 20 km segment that straddles the Blake River and the Timiskaming Groups (Gauthier et al., 1990). The deposits occur as veins or disseminations in highly deformed ultramafic with mafic volcanic rocks and sediments. Deposits spatially associated with the LCTZ include Astoria, McWatters and O'Neil Thompson.

Within the Noranda Volcanic Complex, many gold deposits are spatially associated with the Horne Creek and Smokey Creek (Mouilleuse) Faults. Deposits located along the Horne Creek Fault, that include Francoeur, Wasamac and Donald, occur in a variety of styles including veins and fracture-controlled structures.

Several gold deposits and prospects are spatially associated with the NW-trending Smokey Creek Fault. This fault displaces Proterozoic units, indicating activity over a long period of time. Granitoid-hosted gold deposits in the Noranda area are located within the Flavrian and Powell plutons, in third order structures that are possibly related to the Smokey Creek Fault (see CHAPTER 5). Deposits occur

as veins and/or fracture-related disseminations in trondhjemite (Richard et al., 1991; Carrier, 1994). Locally, deposits are commonly associated with diorite dikes crosscutting the host trondhjemite. Table V lists granitoid-associated deposits within the NVC.

Mine	Intrusion	Tonnage	Grade (g/t)	Au (kg)	Au (oz)
P. Beauchemin	Flavrian	1 956 000	5,1	10 195	327 771
Boulder Hill	Flavrian	272 000	4,6	1 251	40 220
Elder	Flavrian	2 353 833	5,4	12 805	411 684
Silidor	Powell	3 650 000	5,2	18 980	610 211
Powell-Rouyn	Powell	2 807 000	4,4	12 350	397 055
Senator-Rouyn	Powell	2 106 960	4,6	9 692	311 560
New Marlon	Powell	149 140	6,6	984	31 636

Table V: Granitoid-hosted gold deposits within the Noranda Volcanic Complex.

Gold mineralization in the Noranda area occurred during several episodes of hydrothermal activity associated with a variety of geotectonic events spanning as much as 150 Ma. Descriptions by Kerr and Mason (1990) at the Horne mine clearly indicate that gold was introduced to the NVC during volcanism at about 2700 Ma. However, the intimate relationship between gold mineralization and Z-shaped folds within the LCTZ suggests that gold mineralization also occurred during late-stage movements associated with D₂, the NW-SE-oriented compression, at about 2680 Ma (Robert, 1990). Furthermore, post-orogenic hydrothermal activity is commonly viewed as an important source of gold mineralization. Geochronologic data (Wong et al., 1991; Zweng et al., 1993), support an auriferous event mineralization event between 2630 and 2580 Ma.

1.2 The Flavrian Pluton

The Flavrian pluton is composed mainly of trondhjemite (quartz-rich tonalite) and tonalite, as well as minor amounts of quartz-diorite. A plot of modal quartz-alkali feldspar-plagioclase (Fig. 1.7) shows that rocks from the Flavrian pluton occur mainly within the tonalite field. Samples that occur in fields 3, 4 and 9 (granite, granodiorite and quartz-monzodiorite) are probably altered. Paradis et al. (1988) showed that samples from the Flavrian pluton straddle the tholeiitic and calcalkaline domains on an AFM plot (Fig. 1.8). However, Na_2O enrichment in trondhjemites is probably, at least partially, due to Na-metasomatism. In addition, an Al_2O_3 vs Yb plot clearly indicates that the Flavrian pluton occurs within the low- Al_2O_3 or "oceanic" field (Fig. 1.9).

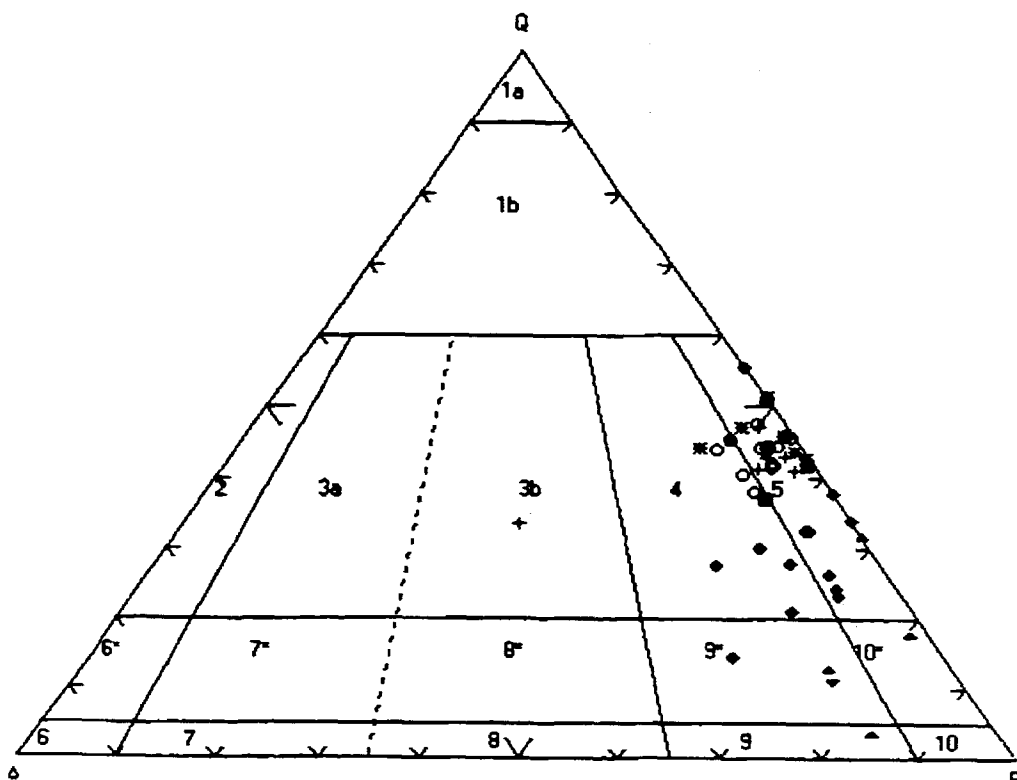


Figure 1.7: Quartz-alkali feldspar-plagioclase diagram based on normative values (LeMaitre, 1989). Data from this study. 1a = quartzolite (silexite); 1b = quartz-rich granitoids; 2 = alkali-feldspar granite; 3 = granite; 4 = granodiorite; 5 = tonalite; 6* = quartz alkali-feldspar syenite; 7* = quartz syenite; 8* = quartz-monzonite; 9* = quartz monzodiorite/quartz monzogabbro; 10* = quartz-diorite/quartz-gabbro/quartz-anorthosite; 6 = alkali-feldspar syenite; 7 = syenite; 8 = monzonite; 9 = monzodiorite/monzogabbro; 10 = diorite/gabbro/anorthosite. Legend for symbols is presented in Figure 3.1.

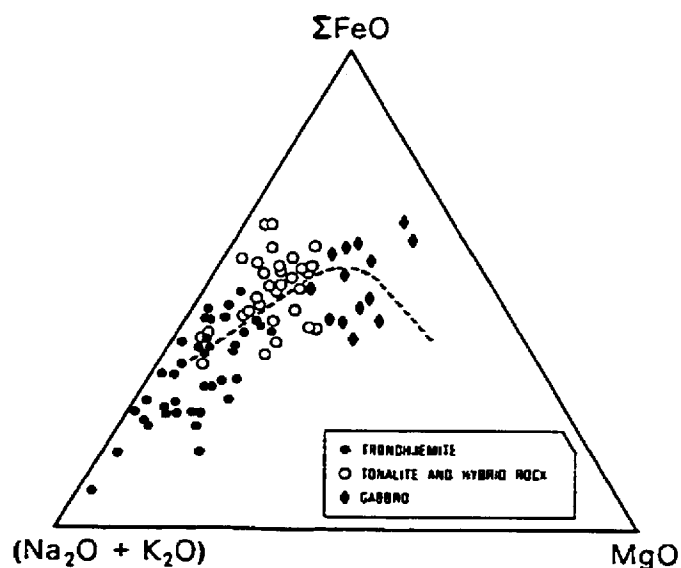


Figure 1.8: AFM diagram for three facies of the Flavrian pluton. The dashed line separates the tholeiitic and the calcalkaline domains according to the division proposed by Irvine and Baragar (1971). From Paradis et al. (1988).

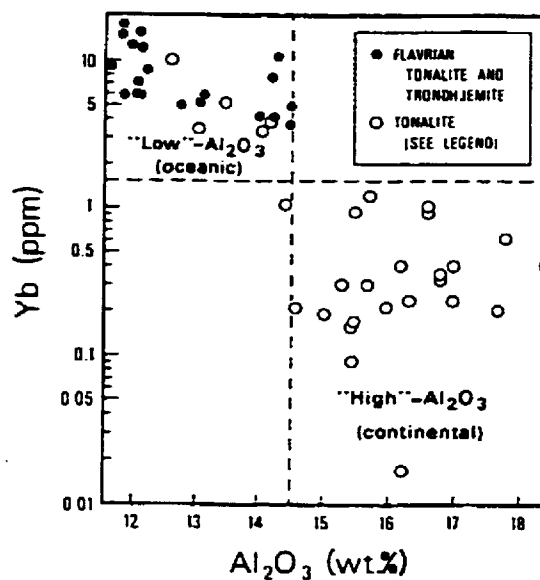


Figure 1.9: Yb vs Al_2O_3 diagram for the trondhjemites and tonalites of the Flavrian pluton (filled circles). Open circles represent tonalites from Arth and Hanson (1972, 1975), Arth et al. (1978), Barker et al. (1976, 1979) and Kay and Senechal (1976). From Paradis et al. (1988).

CHAPTER 2

CHAPTER 2. DESCRIPTION OF INTRUSIVE UNITS, FIELD RELATIONSHIPS AND SEQUENCE OF INTRUSION

2.1 Introduction

The Flavrian pluton is composed of a series of intrusions of various textures and compositions (Fig. 2.1) described in detail by Goldie (1976, 1978, 1979a, 1979b), Kennedy (1984), Paradis (1984) and Paradis et al. (1988). A reexamination of the mineralogical and textural characteristics of intrusive phases is made in this chapter and summarized in Table VI. This revision is complemented by new textural observations, a detailed description of field relationships and the nature and geometry of contacts between intrusive phases and allows a sequence of emplacement of phases to be established in light of new geochronological data. In addition, the shape of the pluton is constrained by describing the contacts between the pluton and host volcanic rocks and combining this information with gravimetric data. The reexamination of the petrographic and geometrical characteristics of the pluton's phases forms the basis for the construction of a mechanical model of emplacement for the Flavrian pluton, the main objective of this chapter.

2.2 Description of Intrusive Units

The intrusive units are described in order of relative emplacement (from oldest to youngest).

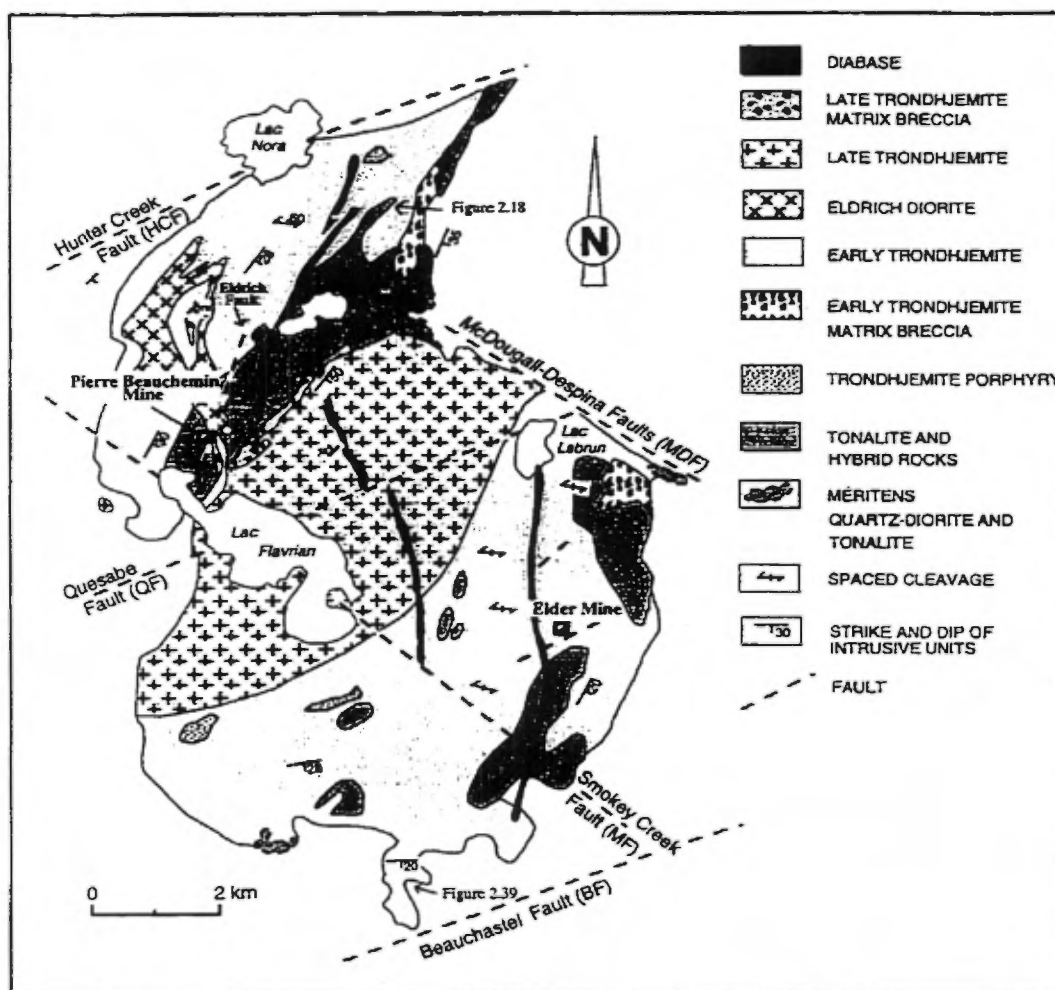


Figure 2.1: Geology of the Flavrian pluton. Compiled from Goldie (1976), Kennedy (1984) and this study.

Rock type	Mineralogy	Textures	Characteristics
Méritens qtz-gabbro	major: plag. ol.-alb. act.-horn. trace: chl., ep., qtz., stilp., ser., ilm.	<ul style="list-style-type: none"> ● dioritic, qtz porphyritic ● microgabbroic ● acicular amphibole 	<ul style="list-style-type: none"> ● closely associated with homogeneous tonalite ● abundant hornblende
Tonalite <i>(1) Homogeneous</i> <i>(2) Heterogeneous and hybrid rocks</i>	major: qtz, alb. trace: act.-horn., chl., ep. stilp., tit., ilm., leuco., ap.	<p>(1) massive with branching and radiating aggregates of act. or horn., stilp. and chl.</p> <p>(2) same as above with irregular zones of trondhjemite and minor granophyre</p> <ul style="list-style-type: none"> ● qtz xenocrysts surrounded by amph. or qtz-alb. intergrowths. ● acicular ap. 	<ul style="list-style-type: none"> ● texturally variable homogeneous and heterogeneous varieties ● hybrid rocks contain lobate inclusions of andesite, qtz-diorite and tonalite in a trondhjemite matrix ● quench textures ● diffuse contacts
Trondhjemite porphyry	major: qtz, alb. trace: act., bio., ep., chl.	<ul style="list-style-type: none"> ● qtz and alb. phenocrysts ● magmatic breccia (minor) 	<ul style="list-style-type: none"> ● characteristically porphyritic ● contains small inclusions of mafic material
Early coarse-grained trondhjemite	major: qtz, alb. trace: ep., chl., act., ap., tit., zr., mt., ilm., rut., hem., all., stilp., leuc.	<ul style="list-style-type: none"> ● medium to coarse granitic ● magmatic breccia ● minor granophyre 	<ul style="list-style-type: none"> ● textural variability (magmatic breccia) ● qtz-ep.-mt. microlitic cavities ● clots of mafic minerals/minerals
Granophyre	major: qtz, alb. trace: act., ep., chl., ap., tit., zr., mt., ilm., rut., hem., all.	<ul style="list-style-type: none"> ● granophyre ● microgranitic ● minor porphyritic 	<ul style="list-style-type: none"> ● fine-grained ● minor pegmatite zones ● variable qtz-alb. intergrowth morphology
Eldrich diorite	major: alb., act.-horn. trace: ep., chl., qtz., leuc., ilm., hem.	<ul style="list-style-type: none"> ● dioritic ● subophitic ● minor plag. phenocrysts 	<ul style="list-style-type: none"> ● grain size correlates with dike size
Late trondhjemite	major: qtz, ol.-alb., act.-horn., trace: chl., ep., ap., tit., zr., mt., ilm., rut., hem., all., leuc.	<ul style="list-style-type: none"> ● coarse granitic 	<ul style="list-style-type: none"> ● contains many mafic inclusions, clots of mafic minerals and obscure zones of early trondhjemite. ● texturally homogeneous

Table VI: Mineralogical and textural features of the various phases of the Flavrian pluton. Observations derived from this study have been compiled with those of previous authors. Abbreviations: quartz (qtz), plagioclase (plag.), oligoclase (ol.), albite (alb.), amphibole (amph.), actinolite (act.), hornblende (horn.), chlorite (chl.), epidote (ep.), biotite (bio.), stilpnomelane (stilp.), sericite (ser.), ilmenite (ilm.), titanite (tit.), leucocoxene (leuco.), apatite (ap.), magnetite (mt.), zircon (zr.), rutile (rut.), hematite (hem.) and allanite (all.).

2.2.1 The Méritens quartz-diorite

The Méritens quartz-diorite unit is the most mafic and least abundant phase of the Flavrian pluton. The quartz-diorite outcrops are generally small, rounded and commonly hosted by tonalite. Weathered surfaces are greyish-green to brown in colour (Fig. 2.2), exposing a well-developed dioritic texture (Fig. 2.3A and 2.3B). The term dioritic is used as a general term describing the intersertal and sub-ophitic to ophitic textures characteristic of quartz-diorite. Identification of quartz-diorite in the field is difficult due to its similarities with phases of tonalite. However, the dioritic texture and the relatively more mafic appearance of the quartz-diorite are generally diagnostic.

The Méritens quartz-diorite occurs at the southern margin of the pluton where it is closely associated with tonalite; it also occurs at the eastern boundary of the pluton where it outcrops and has been reported in drill core along the McDougall and Despina faults beneath the Corbet VHMS deposit (Knuckey and Watkins, 1982). However, the quartz-diorite is best exposed in the northwest part of the pluton, south of Lac Méritens, where an elongated zone of diorite, about 4 km in length, occurs along the contact with the late trondhjemite (Fig. 2.1).

In thin section, no primary minerals are observed, aside from quartz. However, magmatic textures are well-preserved locally. The quartz-diorite is composed mainly of plagioclase and amphibole (mainly hornblende), with minor amounts of quartz, chlorite, epidote, ilmenite and calcite (Fig. 2.4A); apatite and zircon are rare. It



Figure 2.2: Outcrop of Méritens quartz-diorite near the pluton's eastern boundary. Note the mafic inclusions within the quartz-diorite, suggesting at least two phases of emplacement of mafic magma.

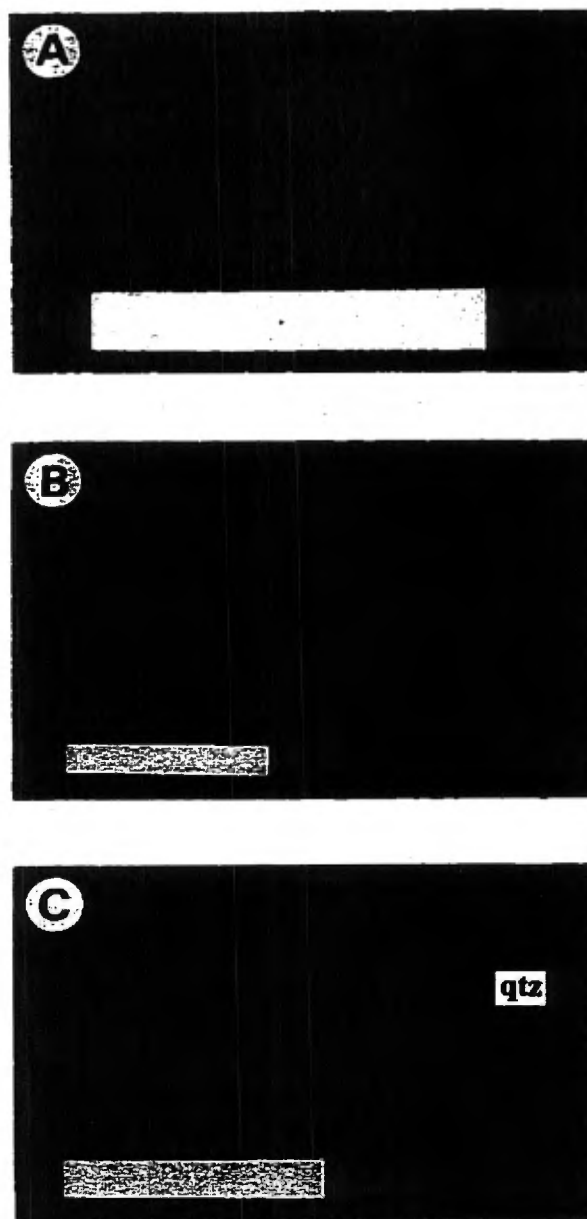


Figure 2.3: Slabbed samples of: A) the Méritens quartz-diorite, showing the typical dioritic texture; B) a fine-grained dioritic phase of the Méritens quartz-diorite; and C) homogeneous tonalite showing characteristic acicular amphibole crystals and an angular-shaped mafic inclusion. Notice the quartz grain in the central right part of photograph (arrow); a rim composed essentially of quartz and albite surrounds the grain. Scale bar for all photographs = 2 cm.

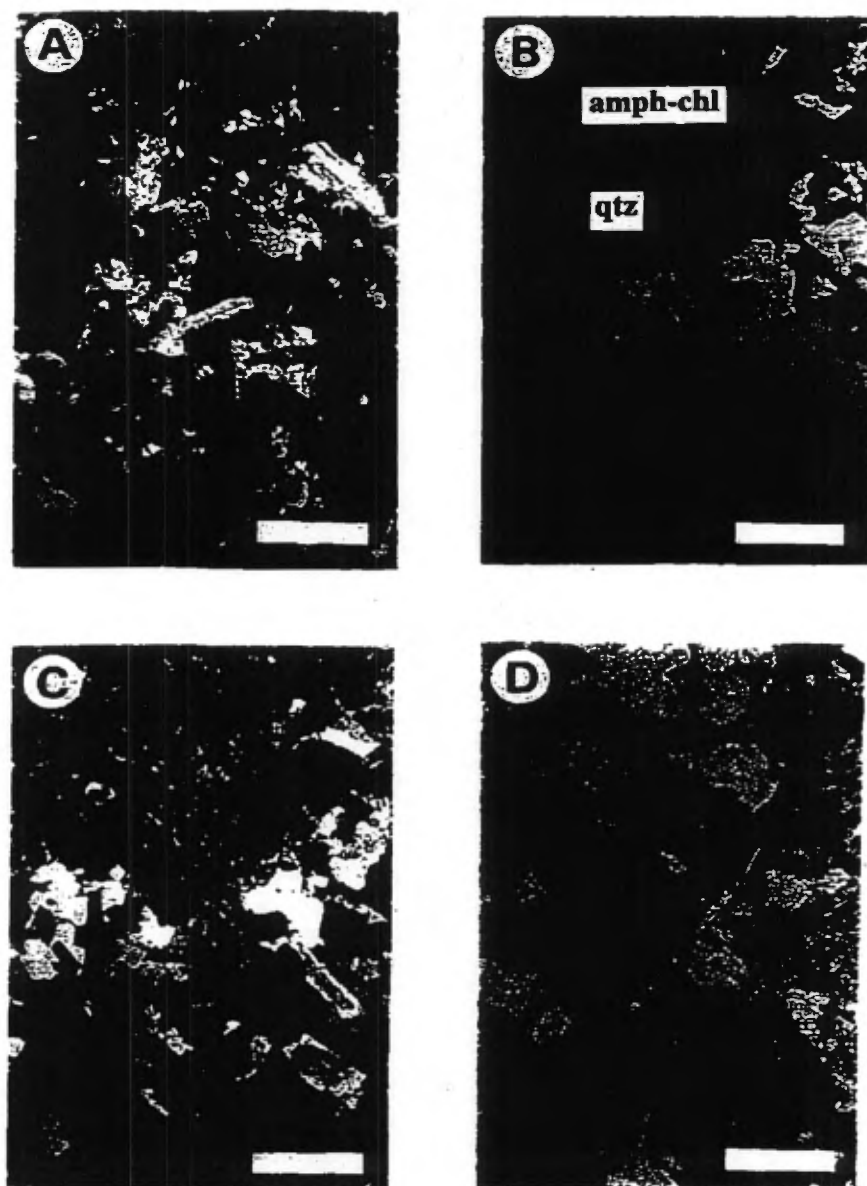


Figure 2.4: Photomicrographs of intrusive phases of the Flavrian pluton: A) Méritens quartz-diorite (crossed-polarized); B) amphibole-chlorite cluster in spotted tonalite (polarized light); C) amphibole-chlorite cluster in spotted tonalite (crossed-polarized light); and D) acicular apatite crystal in tonalite (polarized light). Scale bar = 1 mm.

commonly shows a sub-ophitic texture where euhedral to subhedral plagioclase laths up to 2 mm in length and variably altered to epidote, sericite and chlorite form the framework (60%) for a groundmass of hornblende (35%), anhedral quartz (5%) and minor chlorite. The groundmass is commonly overprinted by a quartz-sericite-carbonate alteration assemblage. Hornblende containing exsolved calcite is also common. Locally, the Méritens quartz-diorite may show textures common to tonalite in which acicular amphibole crystals and equidimensional to elongate aggregates of mafic minerals are characteristic.

2.2.2 Tonalite

Weathered exposures of tonalite occur as brownish-grey to green-coloured rounded outcrops. A pink cast is commonly observed on fresh surfaces. Tonalite is distributed throughout the Flavrian pluton (except in late trondhjemite), as inclusions or small outcrops incorporated within later phases. A large zone of tonalite is associated with Méritens quartz-diorite and hybrid rocks in a NE-trending, sharply bounded zone 1 km wide by 5 km long passing through Lac Méritens (Fig. 2.1). Other concentrations of tonalite are observed near the pluton's southeastern boundary where it occurs as rounded to angular inclusions in early trondhjemite matrix breccia and hybrid rocks (see Sections 2.2.3 and 2.2.5). Tonalite is composed of subhedral to euhedral albite (40% to 60%), anhedral, interstitial quartz (10% to 40%) and actinolite (15% to 30%). Minor constituents are chlorite, epidote, stilpnomelane, sericite, calcite and opaque minerals (ilmenite, magnetite, pyrite and hematite). Trace minerals include titanite, leucoxene, apatite and zircon.

Tonalite shows a variety of textures that have been attributed either to magma mixing (Goldie, 1978) or to the combined effects of intrusion of early trondhjemite into the Méritens quartz-diorite and superimposed hydrothermal alteration (Kennedy, 1984). Based on texture, two major types of tonalite are observed: (1) massive tonalite and (2) heterogeneous tonalite or hybrid rocks. A dominance of one texture commonly grades into areas of the other textures. Within massive tonalite, two dominant textures are observed. Homogeneous tonalite occurs in irregular shaped zones that show distinctive elongate, branching and radiating crystals (up to 4 cm in length) of actinolite and/or hornblende, stilpnomelane and chlorite (Figs. 2.3C, 2.5A and 2.6A). Spotted tonalite is characterized by a blotchy, spotted texture caused by the clustering together of amphiboles, chlorite and/or stilpnomelane to form aggregates of mafic minerals that can attain 1 cm in size (see Figures 2.4B and C, 2.5B and 2.6B). Other mineral clusters in tonalite are composed of plagioclase, amphibole and opaque minerals, together with rare amounts of quartz. Massive zones of homogeneous and spotted tonalite commonly grade into zones of heterogeneous tonalite and hybrid rocks (see Section 2.2.3).

Heterogeneous tonalite was originally described by Goldie (1976). Like spotted tonalite, it is characterized by the clustering of mafic minerals to form relatively large (up to 1 m) irregular-shaped mafic aggregates in a matrix of tonalite or trondhjemite. Heterogeneous tonalite, as described by Goldie (1976), is very similar to hybrid rocks (see Section 2.2.3) and has been mapped here as hybrid rocks. Other diagnostic textures commonly observed in the tonalite include acicular apatite crystals up to 0.5

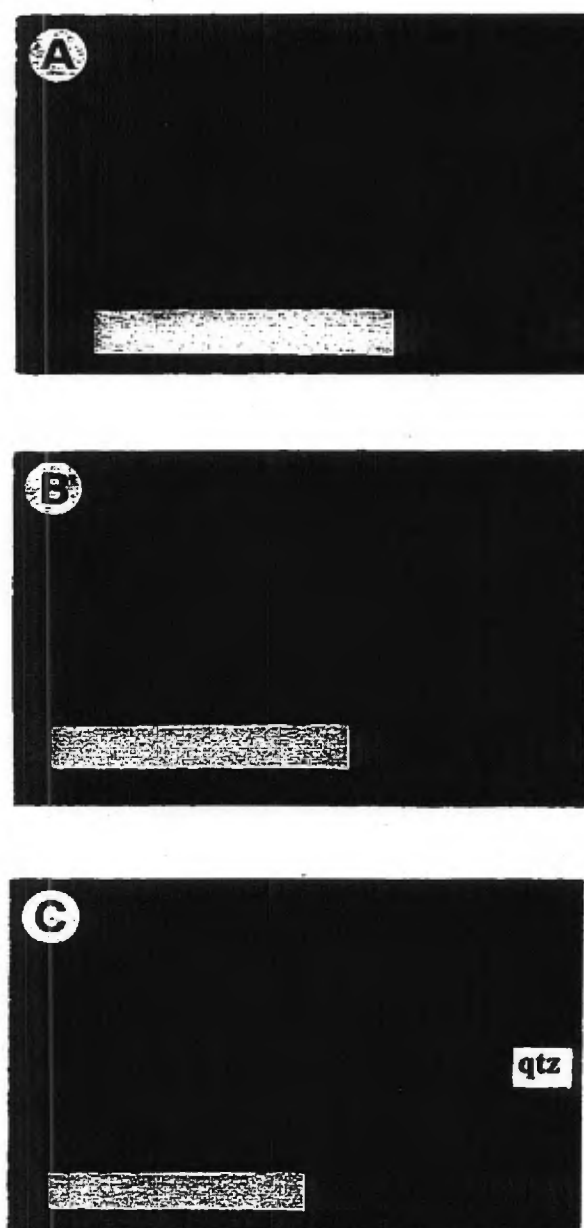


Figure 2.5: Slabbed samples of: A) acicular amphibole within tonalite; B) spotted tonalite; and C) quartz grain surrounded by a rim of quartz-albite intergrowth within tonalite. Scale bar for all photographs = 2 cm.

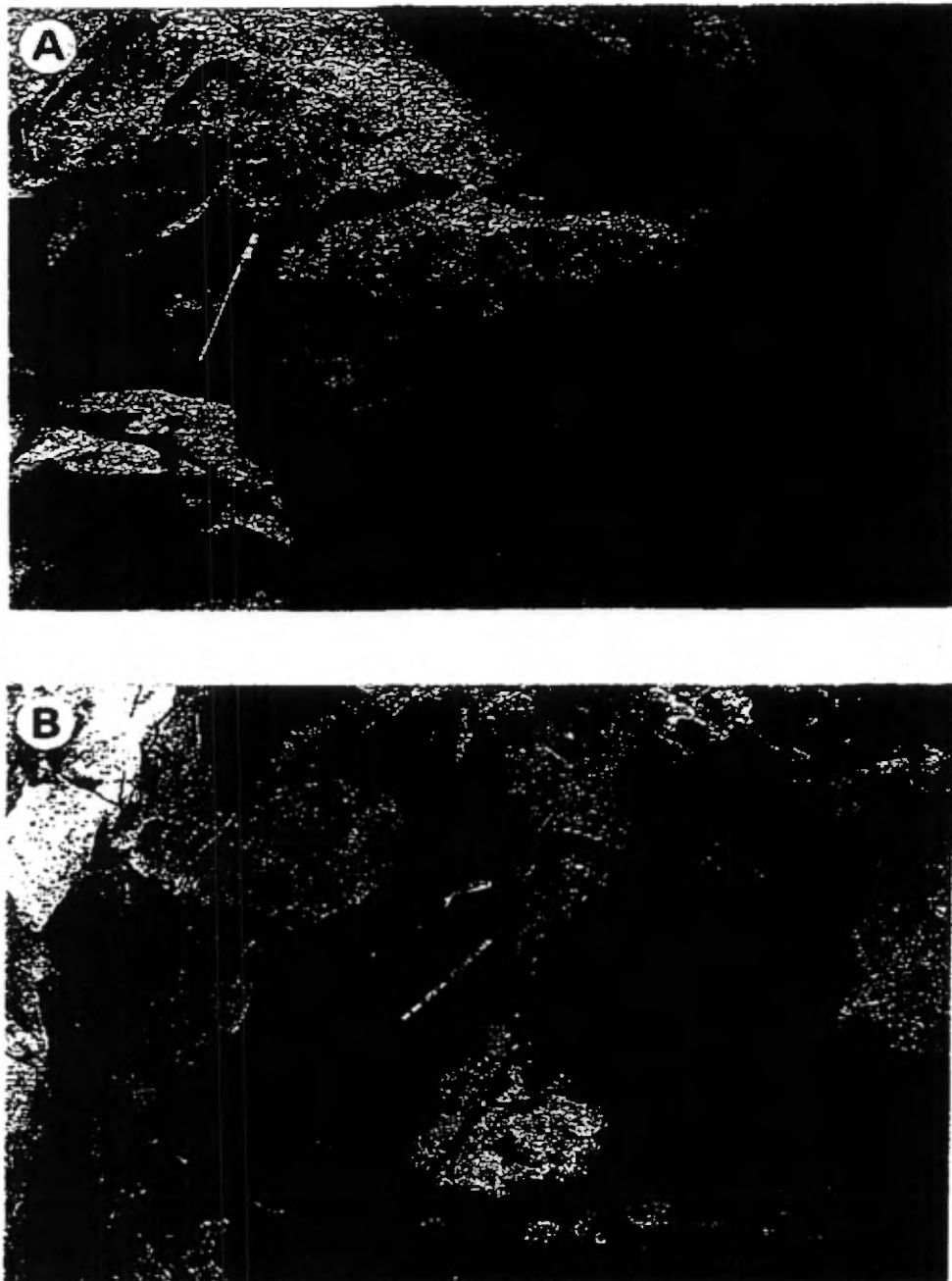


Figure 2.6: Typical field exposures of: A) homogeneous tonalite showing the characteristic acicular amphibole crystals; and B) spotted tonalite, showing the characteristic subrounded spots generally composed of amphibole and chlorite.

mm in length (Fig. 2.4D) and subrounded quartz grains, up to 4 mm across, rimmed by intergrowths of quartz and albite (Figs. 2.3C and 2.5C). Quartz-albite intergrowths commonly occur in the groundmass of tonalite.

Plagioclase crystals in tonalite are albite and are generally weakly to intensely altered and commonly replaced and overprinted to varying degrees by one or a combination of the following minerals: epidote, chlorite, sericite and less commonly calcite and quartz. Zoned plagioclases are scarce and consist mainly of clear albite rims surrounding more calcic cores. Actinolite replacing hornblende, is commonly partially replaced by chlorite and epidote. Stilpnomelane and opaque minerals (magnetite) locally overprint amphibole. Quartz-epidote veinlets 1-2 mm wide commonly transect tonalite and local silicification and albitization of tonalite is indicated by the overprinting of mineral assemblages by anhedral quartz and poikilitic disseminated albite.

2.2.3 Hybrid rocks

Hybrid rocks are a minor transitional phase between tonalite and early trondhjemite. They generally contain rounded to lobate, irregular-shaped inclusions of Méritens quartz-diorite and tonalite hosted within a tonalite or early trondhjemite matrix (Fig. 2.7A and 2.7B). Locally, the matrix is less well-developed and irregular masses and apophyses of microgranitic to fine-grained early trondhjemite occur within a tonalitic host. Hybrid rocks are closely associated with tonalite and early trondhjemite in the northwestern and southeastern parts of the pluton where the early

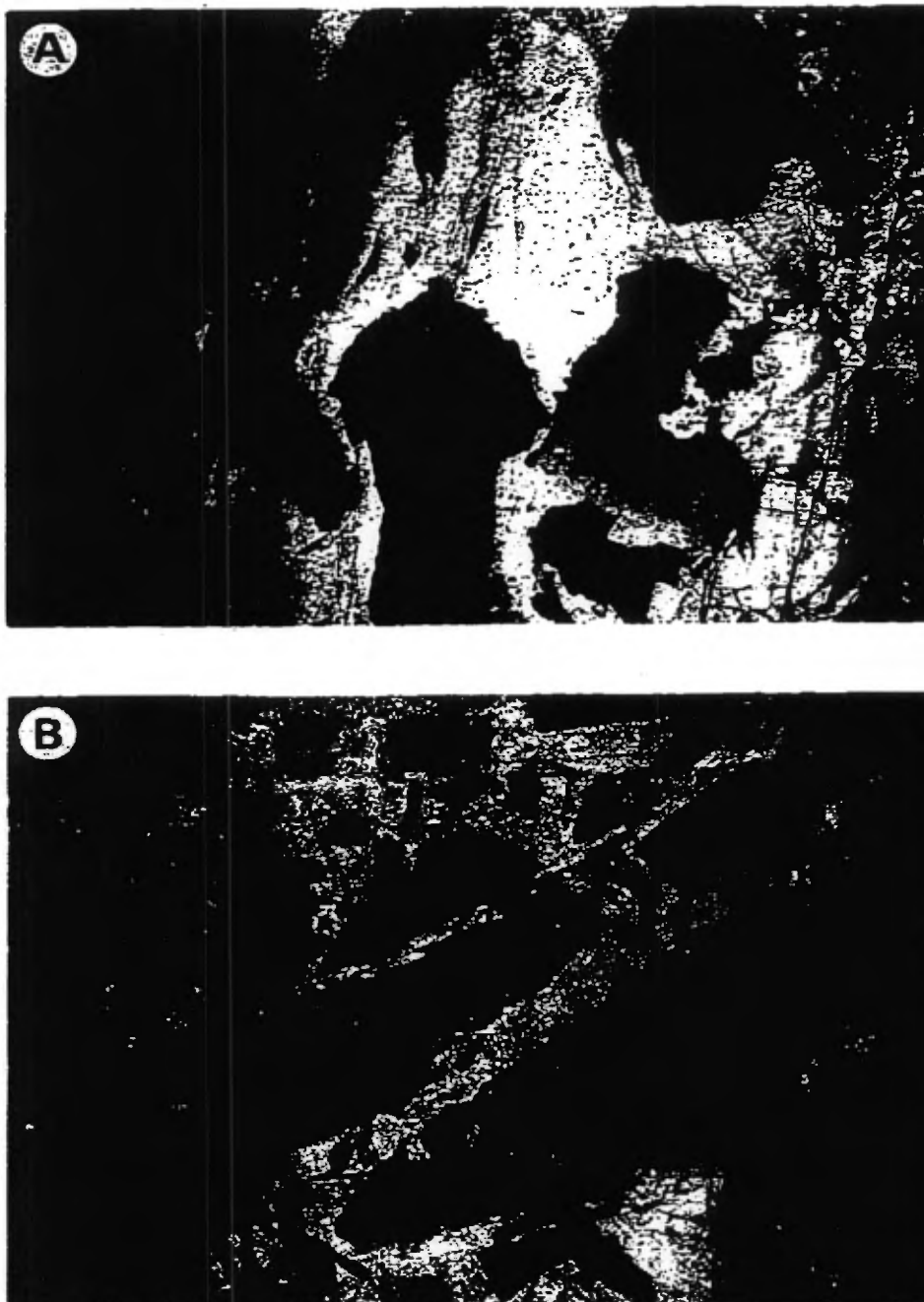


Figure 2.7: Hybrid rocks from levels 6 and 7 at the Pierre Beauchemin gold deposit: A) irregular-shaped inclusions of Méritens quartz-diorite in an early trondhjemite host; and B) angular inclusions of quartz-diorite hosted by early trondhjemite. Pencil magnet in both photographs indicates scale.

trondhjemite is in contact with tonalite and Méritens quartz-diorite. Inclusions in the hybrid rocks are commonly in frequently, ill-defined contact with the host rock. A rim, up to 4 mm wide, essentially composed of quartz and albite, is commonly developed around inclusions that show a relatively sharp contact with the host. Because of the abundant inclusions, hybrid rocks vary in composition and texture over short distances and commonly show most of the textures otherwise seen in tonalite; i.e., hybrid rocks commonly contain quartz grains rimmed by granophyric intergrowths of quartz and albite and acicular apatite.

2.2.4 Early trondhjemite

Two separate masses of early trondhjemite, occupying approximately 50% of the pluton, occur within the Flavrian pluton. The northern intrusion is 8 km long by 1 to 2.5 km wide, trends NE and forms the northernmost part of the pluton. The arc-shaped southern mass, 9 km long by 4 km wide, forms the southern boundary of the Flavrian pluton. The early trondhjemite generally weathers to a distinctive white colour, exposing a rough surface with abundant cavities and patches and/or veins of epidote. Fresh surfaces appear greyish-green. The early trondhjemite occurs in outcrops that can reach several hundred metres across, making it the most abundant exposed phase of the pluton (Fig. 2.1).

Early trondhjemite is composed of quartz and albite with minor amounts of epidote, actinolite and chlorite and accessory amounts of magnetite, sphene, ilmenite, stilpnomelane, apatite and zircon. A wide variety of textures ranging from coarse-

grained equigranular to granophyric are observed within the early trondhjemite. Textural variability is common both at the outcrop and thin section scale; a thin section of a coarse-grained phase may contain minor zones of granophyric quartz-albite intergrowth or porphyritic quartz and albite. Subphases of the early trondhjemite are recognized on the basis of their textures, mineralogy and the nature of their contacts (see Section 2.3). Five subphases of early trondhjemite occur within the pluton: (1) porphyritic trondhjemite; (2) pink trondhjemite; (3) medium- to coarse-grained trondhjemite; (4) microgranitic trondhjemite; and (5) granophyric trondhjemite. The medium to coarse-grained trondhjemite and granophyre phases are the most abundant, both occupying approximately the same area of the pluton.

The trondhjemite porphyry, described initially as a porphyritic rhyolite by Kennedy (1984), weathers to a pinkish grey colour and occurs as xenoliths and rare masses up to 50 m across within the early trondhjemite. The larger masses of trondhjemite porphyry occur in the north part of the pluton, where xenoliths of trondhjemite porphyry up to several metres across are hosted by early trondhjemite. Trondhjemite porphyry also occurs in the southwestern part of the pluton, where a relatively large body of trondhjemite porphyry is hosted by early trondhjemite (Fig. 2.1). Several other small outcrops or xenoliths of trondhjemite porphyry occur along a NE-trending zone in the southern part of the pluton. The trondhjemite porphyry is, in relation to the pluton as a whole, volumetrically insignificant. The trondhjemite porphyry contains up to 10% mafic inclusions 2 to 4 cm across; and its distinguishing feature is its porphyritic quartz and albite phenocrysts (Figs. 2.8A and 2.9A). Clear

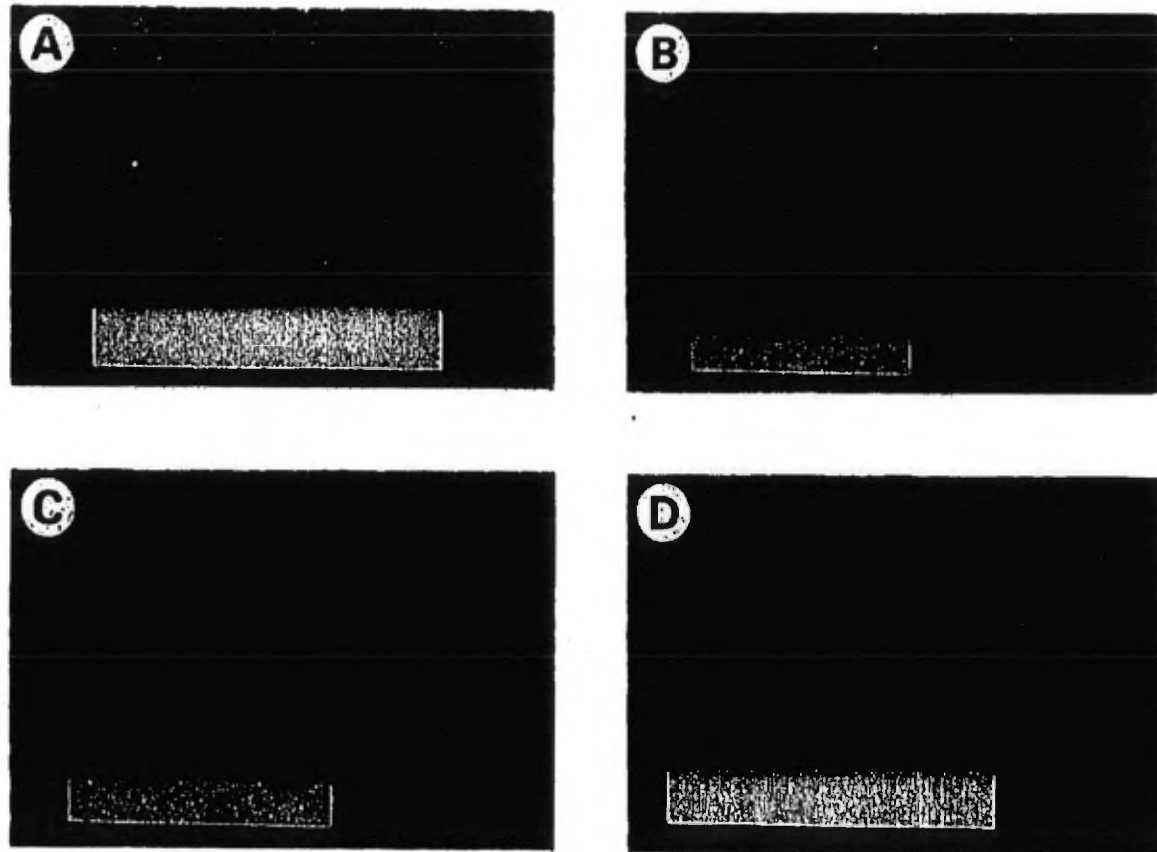


Figure 2.8: Slabbed samples of: A) trondhjemite porphyry; B) coarse-grained trondhjemite; C) pink trondhjemite; and D) granophyre. Scale bar for all photographs = 2 cm.

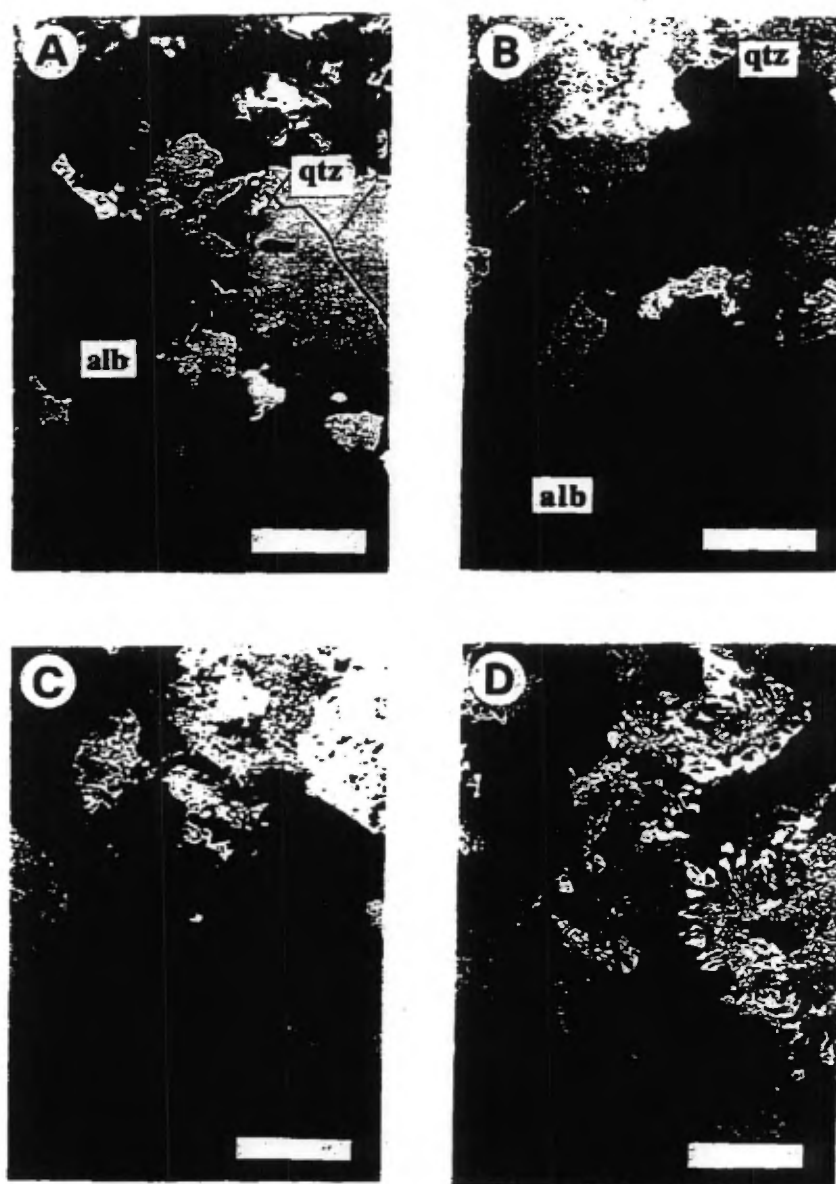


Figure 2.9: Photomicrographs of: A) trondhjemite porphyry; B) coarse-grained trondhjemite; C) chlorite, epidote, magnetite and stilpnomelane in pink trondhjemite (also note the magmatic brecciation texture); and D) granophyric texture in granophyre. Scale bars = 1 mm.

quartz phenocrysts, up to 4 mm across, are irregularly-shaped to subrounded and commonly in optical continuity with quartz in the groundmass. Subhedral to euhedral albite phenocrysts, approximately the same size as quartz, typically show a blurred surface resulting from epidote and lesser sericite alteration. The groundmass is composed of interstitial quartz and euhedral albite that locally show intergrowth textures. Corroded edges of irregular-shaped quartz pools are common. Minor constituents include phenocrysts of amphibole (actinolite or hornblende), biotite, stilpnomelane and accessory chlorite, epidote, potassium feldspar, rutile and opaque minerals.

Medium to coarse-grained early trondhjemite (Fig. 2.8B) is commonly composed of subhedral to euhedral albite (infrequently zoned) and quartz (Fig. 2.9B). Quartz and albite constitute more than 95% of the rock. Grain sizes can reach 8 mm, however, they are commonly 2 to 4 mm across. The mafic minerals, typically less than 5%, are actinolite, chlorite and epidote and commonly occur together either in irregularly-shaped clusters or associated with what seem to be altered amphiboles. Zones of quartz-albite intergrowth may occur within an equigranular matrix. A common texture of the early trondhjemite occurs where mosaic-like clusters, up to 5 mm across, of four or five quartz crystals show sharp, curving edges that appear to be the product of a single quartz grain shattered into several individual pieces (Fig. 2.10). Albite forms the matrix to the shattered quartz fragments. Where quartz crystals appear to have been partially fractured, thin, wedge-shaped zones of albite occur in what appears as partially split quartz grains. The different types of brecciation

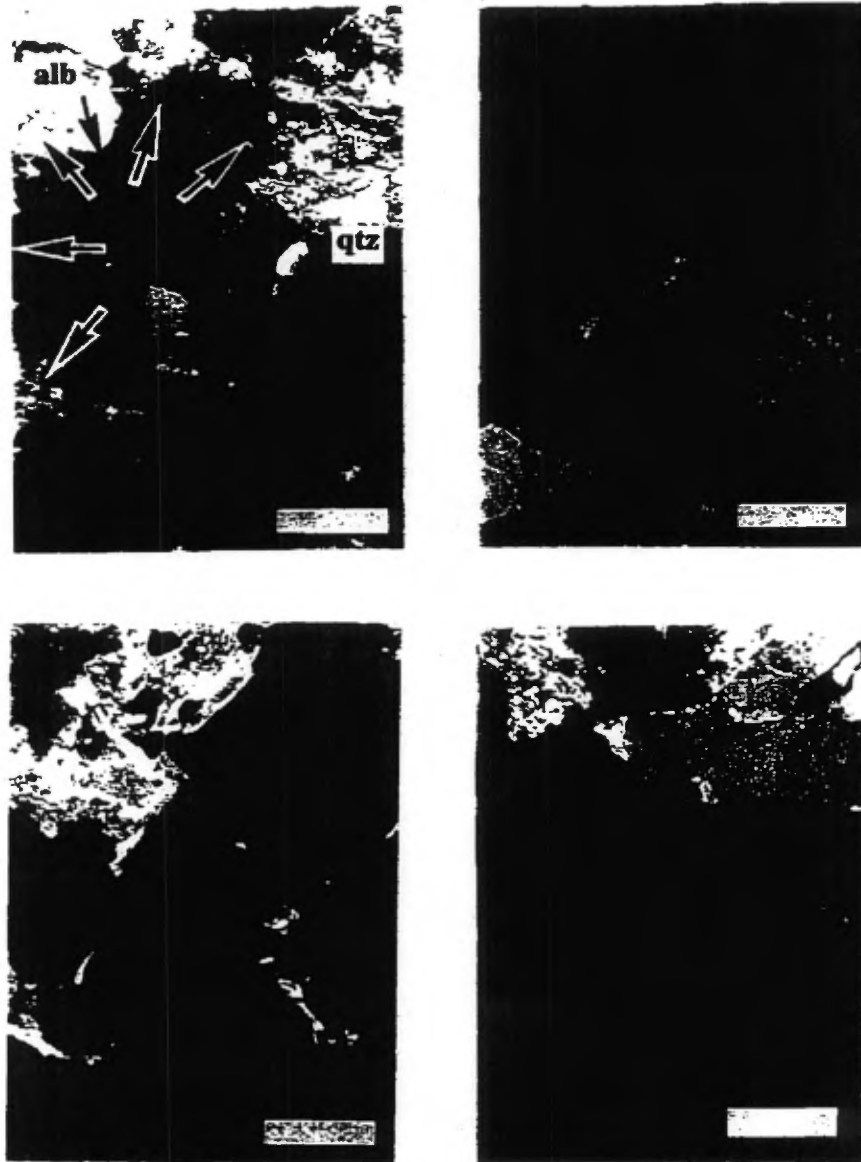


Figure 2.10: Photomicrographs of the magmatic brecciation texture within early trondhjemite; arrows in upper left photograph show breakup directions of several pieces of a single quartz crystal. Scale bars = 1 mm.

textures suggest that intensity of brecciation varied. Another common feature of the coarse-grained trondhjemite's quartz crystals is the interdigitated boundaries that appear to be serrate in section to form a consertal texture (Fig. 2.9B).

Pink early trondhjemite is beige to pink coloured in weathered outcrop. Fresh surfaces may also show the pinkish cast. It is generally medium- to coarse-grained equigranular in texture, with a maximum grain size of 5 mm (Fig. 2.8C), and commonly magnetic due to the presence of magnetite (1-2%). The phase generally occurs with other early trondhjemite phases in both the northern and southern intrusions of early trondhjemite. Pink early trondhjemite is readily distinguished from early coarse-grained trondhjemite by its colour and the presence of magnetite crystals. The pink colour most probably reflects surficial oxidation of magnetite to hematite. Magnetite occurs as irregular-shaped aggregates, up to 1 mm across with hundreds of micro-sized crystals associated with chlorite and lesser epidote \pm stilpnomelane. The lozenge shape of some of the aggregates suggests that the chlorite-magnetite-epidote assemblage replaced amphibole crystals. Magnetite may also occur as single crystals up to 2 mm across within a matrix principally composed of quartz and albite. In this case, a rim of epidote and chlorite up to 0.2 mm wide is commonly developed around the magnetite crystal.

Microgranitic early trondhjemite, like coarse-grained early trondhjemite, appears white in weathered outcrop surfaces. This phase is minor and occurs sporadically throughout the southern intrusion of early trondhjemite. However,

microgranitic early trondhjemite may occur in the northern part of the pluton, since it is difficult to differentiate it from granophyre in outcrop. Euhedral to subhedral albite grains (50%) and anhedral quartz grains (44%), both up to 2 mm across, form the bulk of an equigranular, microgranitic texture. Quartz-albite intergrowths may occur at crystal boundaries, either as true intergrowths or as serrate quartz crystal edges that share boundaries with either quartz or albite. Minor minerals constituting up to 5% of the overall assemblage include actinolite, chlorite and epidote with trace amounts of magnetite. Porphyritic quartz and albite crystals are less commonly observed in microgranitic early trondhjemite.

Outcrops of granophyre are also distinctively white coloured, however, pink weathered surfaces may be observed. Fresh surfaces are grey with a greenish cast. Outcrop surfaces commonly contain cavities up to 1 cm across, giving the phase a "vuggy" appearance. Granophyre is distinguished from other early trondhjemite phases by its extremely fine-grained texture (Fig. 2.8D). The typical granophyric texture may be observed with the naked eye, enabling its distinction from microgranitic early trondhjemite. Granophyre occurs throughout the early trondhjemite, however, concentrations are observed in the northern and southern margins of the pluton. Quartz and albite generally compose more than 95% of the rock with actinolite, chlorite and epidote appearing as minor constituents. Accessory magnetite, ilmenite, hematite, stilpnomelane, carbonate, sericite and zircon may be present. Within the granophyre, zones of granophyric intergrowth appear either throughout the phase and form massive granophyre or as subrounded zones of

intergrowth within a matrix of equigranular textured quartz and albite and form spherical granophyre. In thin section, the radial granophyre's intergrowths appear as circular to ovoid shaped areas, 2 to 5 mm across, suggesting a spherical or ovoid shape in the third dimension. Irregularly-shaped to cuneiform quartz, generally elongate and enlarging outwards, is commonly in optical continuity and centred on a quartz or albite crystal (Fig. 2.9D). Quartz may be intergrown with one or several crystals of albite. Individual spheres of intergrowth quartz-albite may cluster to form zones of intergrowth. Between the spheres, the equigranular, microgranitic matrix is composed of euhedral to subhedral albite and anhedral quartz that is commonly in optical continuity with the quartz in the intergrowths. Quartz and albite in the matrix typically show serrate grain boundaries and minor zones of intergrowth. Chlorite, epidote and lesser amounts of actinolite, magnetite, stilpnomelane and hematite are concentrated in the equigranular matrix. In massive granophyre, intergrowth spheres and clusters are rare to non-existent. Quartz-albite intergrowths occur in no apparent order throughout thin sections. A minor quartz porphyritic phase occurs in the southwestern part of the pluton near the contact between early and late trondhjemite. Quartz crystals (up to 5 mm across) and plagioclase (~1 mm) occur within a groundmass of a quartz-albite intergrowth.

Rare pegmatitic pockets and lenses occur in zones up to a few metres across within granophyre and microgranitic early trondhjemite. These zones (Fig. 2.11A and 2.11B) are composed of euhedral to subhedral quartz up to 5 cm across; euhedral

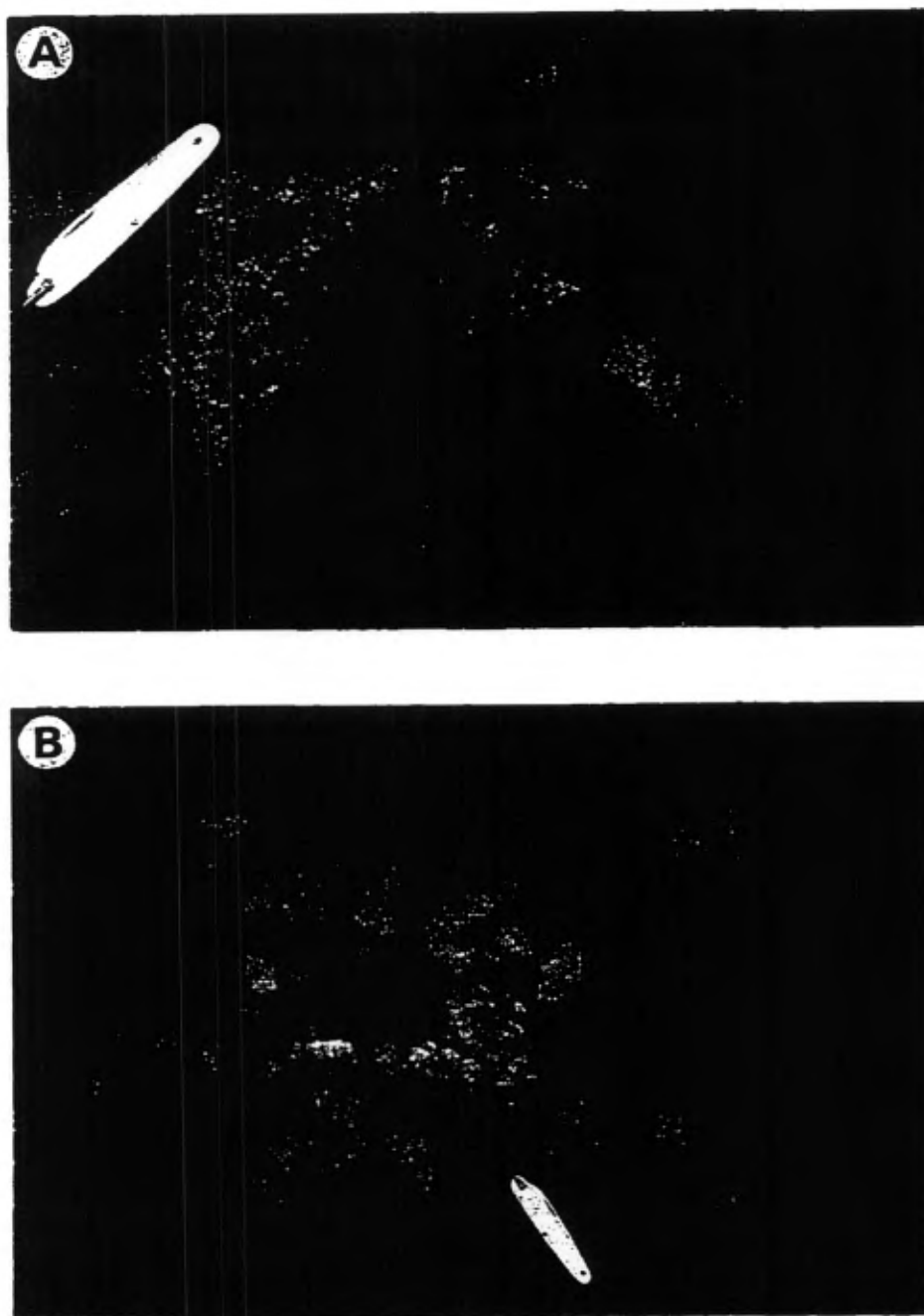


Figure 2.11: Pegmatite lenses within: A) microgranite and B) granophyre, both photographs from the southern part of the pluton.

albite; euhedral acicular actinolite up to 4 cm across; and epidote which occurs either as massive irregular-shaped pockets with minor magnetite or as stains.

The various phases of early trondhjemite are generally altered. Alteration in the form of quartz-epidote \pm magnetite miarolitic cavities, epidote \pm quartz \pm magnetite veinlets and rounded epidote patches and spots are commonly observed in early trondhjemite. Miarolitic cavities range in size from a few millimetres to several centimetres in diameter (Fig. 2.12A and 2.12B). Veinlets range from 1 mm to 10 cm wide, whereas rounded epidote patches and spots up to 10 cm across are common. Generally, plagioclase is weakly to intensely altered and replaced by epidote, sericite and chlorite. Replacement of plagioclase commonly occurs at grain boundaries, where the plagioclase is in contact with quartz, or along cleavage and twinning planes. Granular epidote commonly appears to be sprinkled on the plagioclase's surface, producing a blurred surface. Epidote, chlorite, stilpnomelane and magnetite are alteration products of actinolite. Titanite commonly encompasses ilmenite. Hematite either appears in thin veinlets or forms the grain boundaries of sulphides and magnetite.

2.2.5 Early trondhjemite matrix breccia

The early trondhjemite matrix breccia consists of subrounded to angular clasts of tonalite and/or quartz-diorite, generally 10 cm to 1 m across, hosted within an early trondhjemite matrix (Fig. 2.13). The breccia is a minor phase and occurs sporadically near the early trondhjemite-tonalite contact. It varies from an early trondhjemite

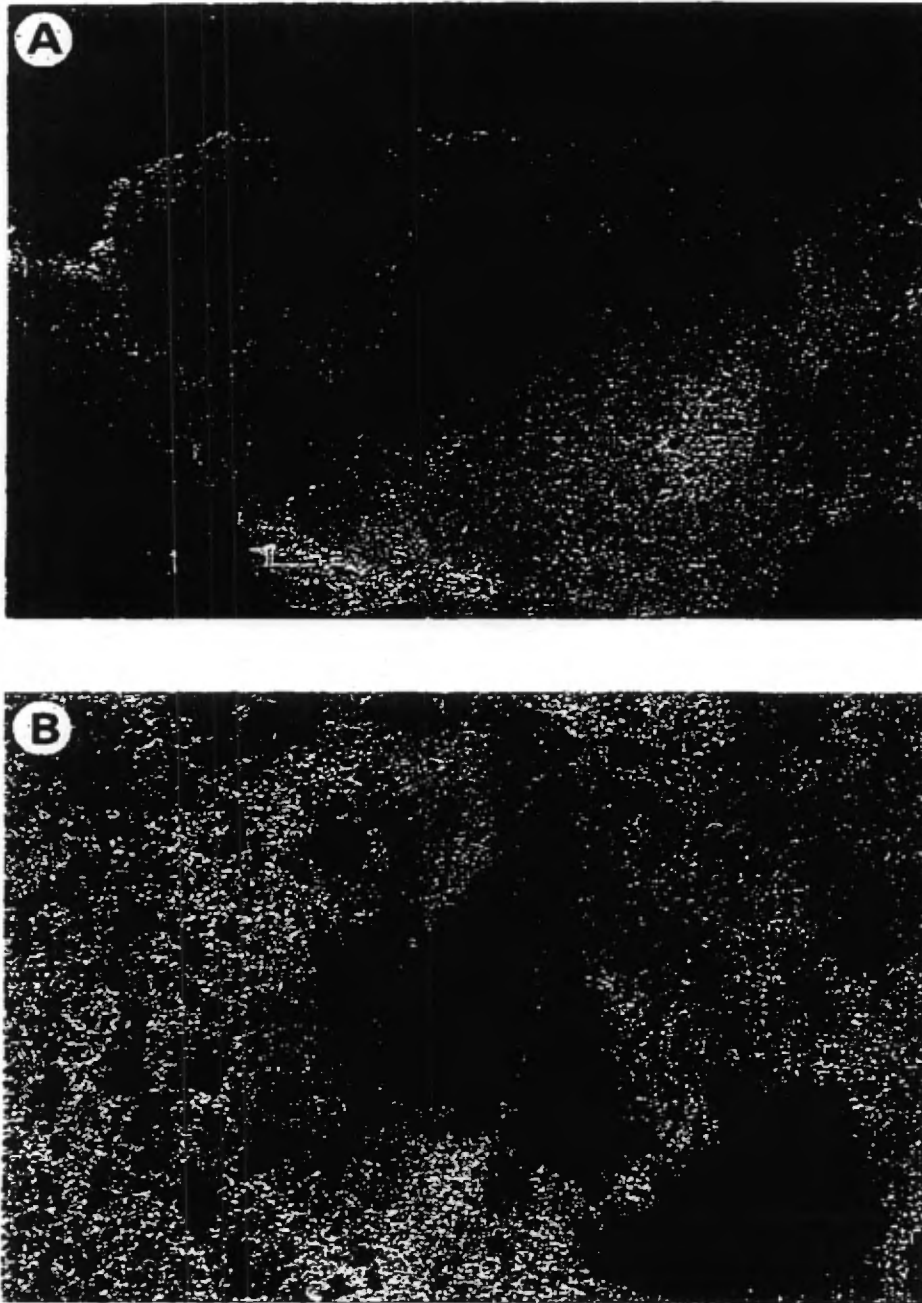


Figure 2.12: Epidote-quartz alteration of: A) microgranite where epidote patches and epidote-quartz miarolitic cavities occur throughout the rock; and B) coarse-grained early trondhjemite where a relatively large epidote-filled cavity is rimmed by quartz. Note the oval pod of granophyre above the miarolitic cavity.



Figure 2.13: Early trondhjemite matrix breccia, northeastern part of Flavrian pluton.

matrix-supported breccia to a phase where the host tonalite dominates and the intruding early trondhjemite is minor. The density of tonalite clasts varies from one area to another. Early trondhjemite dikes or veins commonly transect tonalite and range from sharply bounded, well-defined veins or dikes to irregular-shaped apophyses where the boundaries and terminations are not clear. The early trondhjemite matrix is medium- to coarse-grained and contains epidote spots and patches generally about 0.5 to 3 cm across.

2.2.6 Eldrich diorite

The Eldrich diorite occurs as large dark-green to brown outcrops in the northwestern part of the pluton (Fig. 2.1). The diorite, occupying about 5% of the Flavrian pluton, occurs as several sills and irregular masses and is best observed at surface and underground at the Pierre Beauchemin (former Eldrich) gold deposit. The grain-size of the Eldrich diorite varies according to the size of the intrusive body. It is composed of remnant plagioclase (55%) that is altered to epidote and lesser amounts of chlorite resulting in a blurred surface; euhedral amphibole (actinolite + hornblende, 35%) up to 1 mm in length; and up to 10% anhedral quartz. Accessory phases include magnetite (2%), chlorite, apatite and carbonate. Although alteration has masked many of the textural relationships, dioritic to sub-ophitic textures are preserved (Fig. 2.14A, 2.14B and 2.14C).

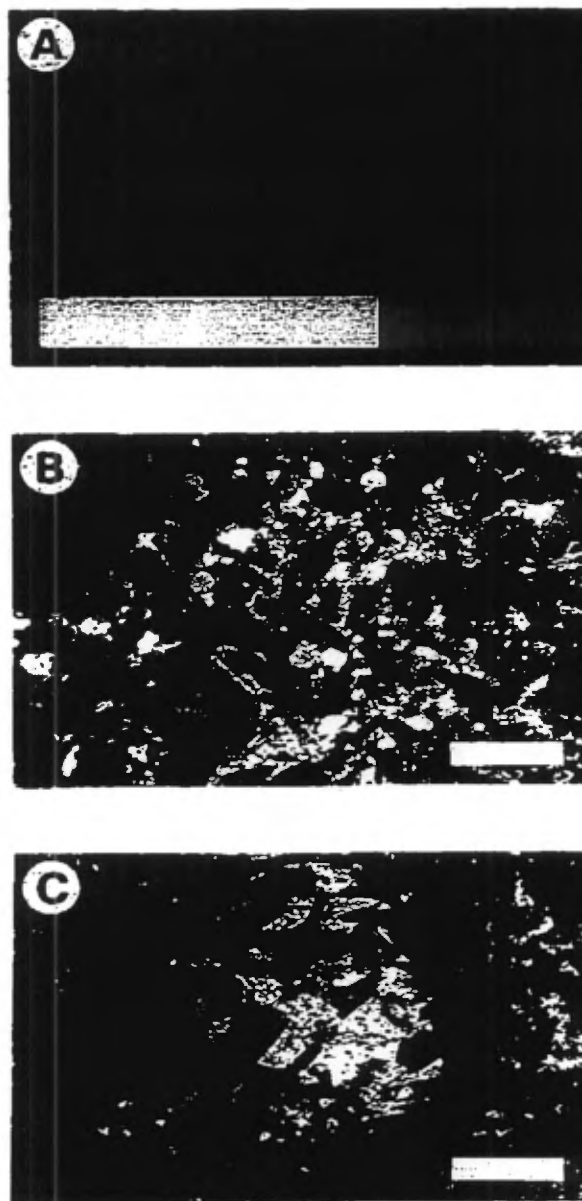


Figure 2.14: A) slabbed sample of Eldrich diorite showing typical dioritic texture; B) photomicrograph of Eldrich diorite showing the dioritic texture; and C) sub-ophitic texture in Eldrich diorite where a large euhedral actinolite crystal hosts smaller euhedral albite laths. Sample 92-90. Scale bar = 2 cm for A and 1 mm for B and C.

2.2.7 Late trondhjemite

The late trondhjemite occurs as large beige-coloured outcrops in the central part of the Flavrian pluton (Fig. 2.1). The phase occupies about 30% of the pluton's surface and is characterized by a homogeneous, well-developed, coarse-grained equigranular texture (Fig. 2.15A). Abundant (up to 20%), irregular-shaped mafic inclusions occur throughout the late trondhjemite (Fig. 2.15C). Euhedral to subhedral stubby grains of plagioclase (45-50%), commonly zoned and up to 4 mm across, generally consist of oligoclase cores and clear albite rims (Fig. 2.15B). Anhedral quartz (45-50%), up to 4 mm across, commonly occurs between the plagioclase laths. Grain boundaries may be serrate where in contact with other quartz grains. Amphibole (up to 10%) is generally actinolite and accessory phases include epidote, chlorite, magnetite, stilpnomelane and zircon. Inclusions are composed of plagioclase and amphibole that have been altered to sericite, epidote and chlorite with accessory opaque minerals and rutile. The replacement of plagioclase by sericite and epidote is widespread. A 2 mm-wide border of hornblende and stilpnomelane commonly rims inclusions within late trondhjemite.

2.2.8 Late trondhjemite matrix breccia

Late trondhjemite matrix breccia occurs in the northwestern part of the Flavrian pluton where late trondhjemite is in contact with the quartz-diorite and tonalite (Fig. 2.1). The breccia is composed of subrounded to angular quartz-diorite and tonalite clasts hosted by late trondhjemite (Fig. 2.16).

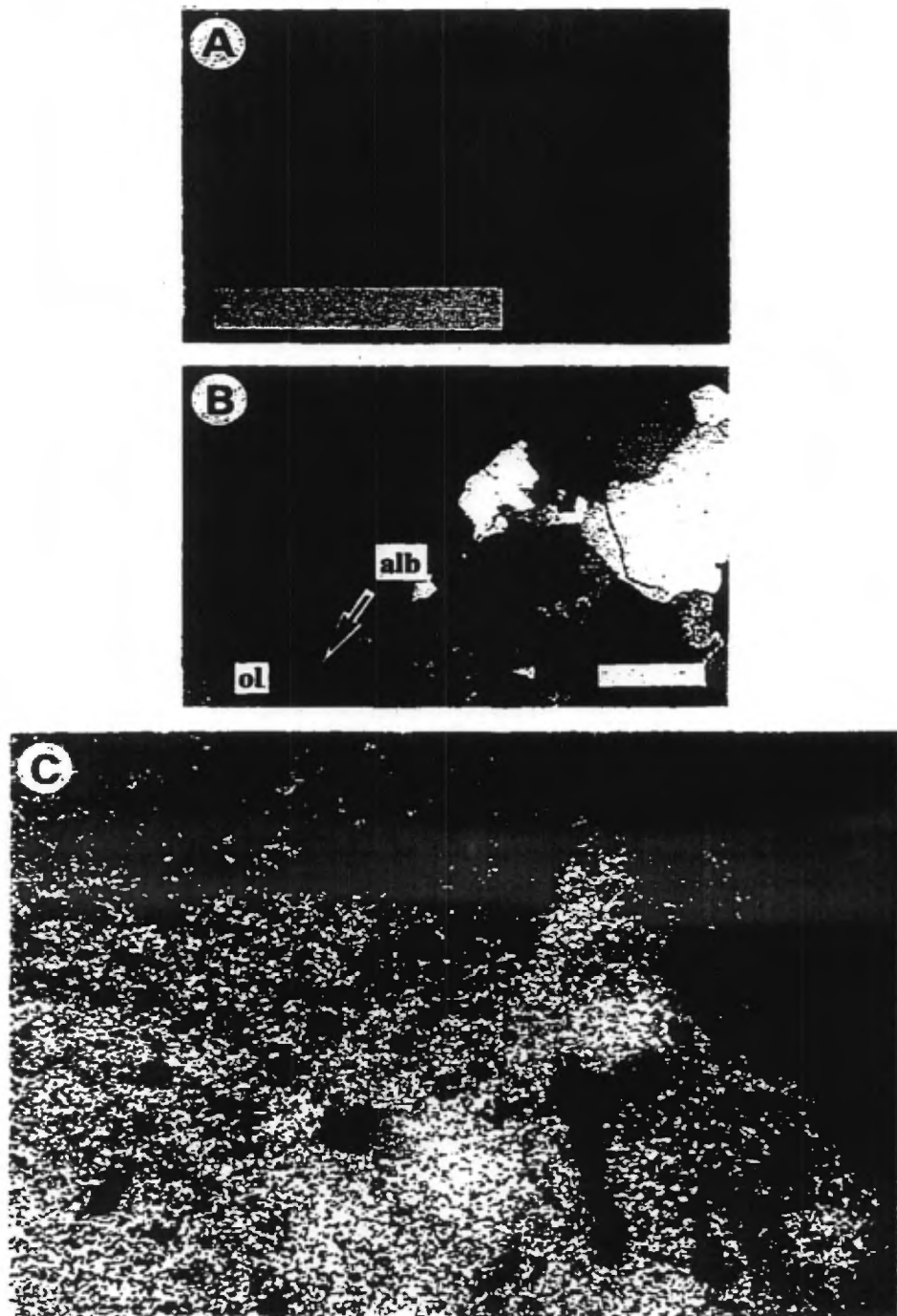


Figure 2.15: A) slabbed sample of late trondhjemite showing coarse-grained equigranular texture; B) photomicrograph of coarse-grained equigranular texture characteristic of late trondhjemite; and C) late trondhjemite showing numerous inclusions. Scale bar = 2 cm for A and 1 mm for B.

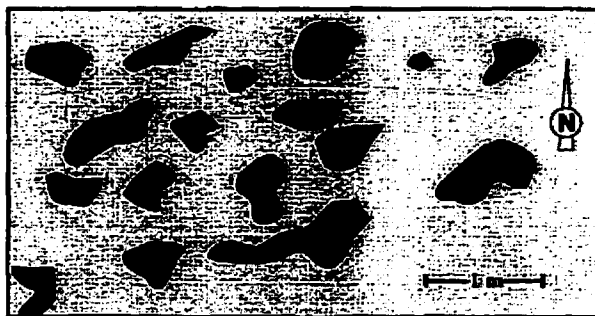


Figure 2.16: Sketch from photograph of late trondhjemite matrix breccia taken 600 m east of the Pierre Beauchemin gold deposit.

2.2.9 Late mafic dikes

Other late mafic intrusions such as diabase, diorite and lamprophyre dikes and sills are also observed in the pluton, however, they are volumetrically insignificant (Fig. 2.1). Although these mafic intrusions have not yet been studied in detail, crosscutting field relations indicate they are clearly younger than all other phases of the Flavrian pluton and they probably correlate with widespread Late Archean to Proterozoic dikes and sills found in many parts of the Canadian Shield.

2.3 Field Relationships and the Sequence of Intrusive Phases

Intrusive relationships between the Méritens quartz-diorite and tonalite are best observed in an elongate zone, about 4 km in length, along the NE-trending contact

between the late trondhjemite and the tonalite in the north-central part of the pluton (Fig. 2.1). Here, the Méritens quartz-diorite occurs as irregularly shaped ill-defined and isolated zones within a tonalitic matrix. The quartz-diorite is distinguished from the homogeneous tonalite by its dioritic texture. Irregular-shaped areas of diorite-textured quartz-diorite grade into zones of typical "tonalitic" textures, as described in Section 2.2. Although isolated zones of Méritens quartz-diorite within tonalite suggest that the quartz-diorite may be older than the tonalite, no clear crosscutting relations are observed. The gradational contact between these units suggests two possible relative ages of formation. Tonalite may be about the same age as the Méritens quartz-diorite and it formed by magma mixing, or the tonalite is younger than the Méritens quartz-diorite and it formed by partial assimilation of the Méritens quartz-diorite by early trondhjemite. The origin of tonalite and its age of formation in relation to other intrusive phases of the Flavrian pluton is a subject of debate (see Goldie, 1978 and Kennedy, 1984).

Like the contact between quartz-diorite and tonalite, contacts between tonalite and hybrid rocks are diffuse and gradational. These hybrid phases were mapped as tonalite in the field. The tonalite phases are therefore considered to be closely associated in time and space with hybrid rocks, occurring where the Méritens quartz-diorite, tonalite and early trondhjemite units have interacted.

The contact between early trondhjemite and tonalite commonly comprises three or four units: early trondhjemite, tonalite, early trondhjemite matrix breccia and/or

hybrid rocks. Two scenario's have been observed in the field: (1) early trondhjemite grades into tonalite via a transitional zone of hybrid rocks and heterogeneous tonalite; and (2) early trondhjemite is in sharp contact with tonalite, commonly generating early trondhjemite matrix breccias.

Scenario 1 occurs in several areas located throughout the pluton, however, it is best observed and well-documented by Kennedy (1984) 2 km north of the Pierre Beauchemin gold mine. As noted previously, tonalite occurs in an elongated zone 4 km long by 1 km wide. A schematic cross-section perpendicular to the tonalite belt illustrates the textural variations (Fig. 2.17).

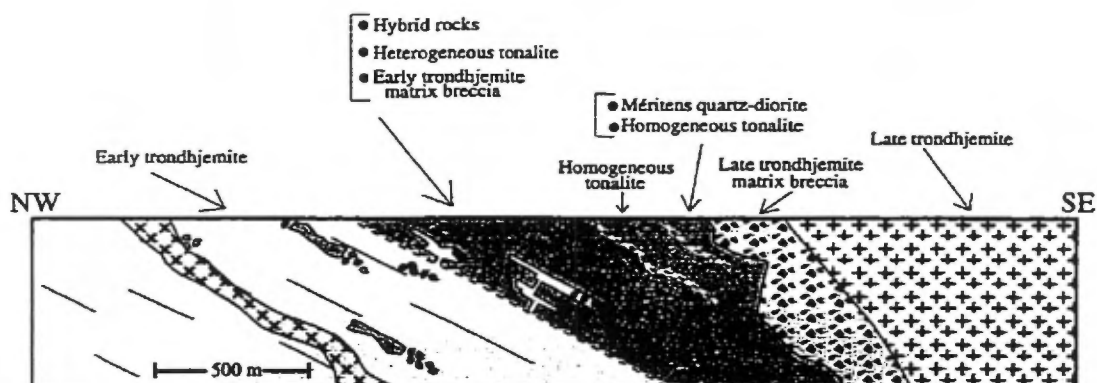


Figure 2.17: Schematic cross-section of the early trondhjemite-tonalite contact in the northwestern part of the Flavrian pluton. Location of cross-section shown on field map in Appendix I. Legend same as in Figure 2.1.

Tonalite is increasingly leucocratic where passing from the southeast to the northwest, towards the early trondhjemite. The variation in colour index corresponds

to a change from massive (homogeneous and spotted) tonalite and quartz-diorite in the southeast to hybrid rocks in the northwest. Although no sharp contacts are seen, hybrid rocks and heterogeneous tonalite are more abundant towards the northwest than the homogeneous variety. A leucocratic variety of tonalite occurs near the contact with early trondhjemite (see Kennedy, 1984 and Goldie, 1976, 1978) where acicular amphibole crystals, several cm in length, are observed.

Field observations of scenario 2 are shown in Figure 2.18, a detailed map of an area in the northeastern part of the pluton. Here, homogeneous tonalite occurs as isolated blocks ranging in size from 10 to 200 m within the early trondhjemite and as smaller blocks (10 cm to 1 m) within the early trondhjemite matrix breccia. Contacts of a large isolated tonalite block, 200 m long by 100 m wide, are sharp and clearly defined at the block's southwestern edge where it is in contact with coarse-grained early trondhjemite. However, contacts are transitional and less well-defined where the tonalite block intrudes and grades into early trondhjemite matrix breccia towards the northeast. Internal textures of the tonalite block shown in Figure 2.18 range from a spotted texture (Fig. 2.5B) at the block's edges near its contact with early trondhjemite, to a homogeneous texture (Fig. 2.3C) in the block's centre. The spotted texture is particularly well-developed at the block's western edge. A transitional zone of early trondhjemite dikes and sills within tonalite occurs where the tonalite block grades into trondhjemite matrix breccia along strike (Fig. 2.18). A close-up of this transitional zone (Fig. 2.19) shows angular to subrounded inclusions of tonalite apparently detached by the intruding early trondhjemite. Within the early

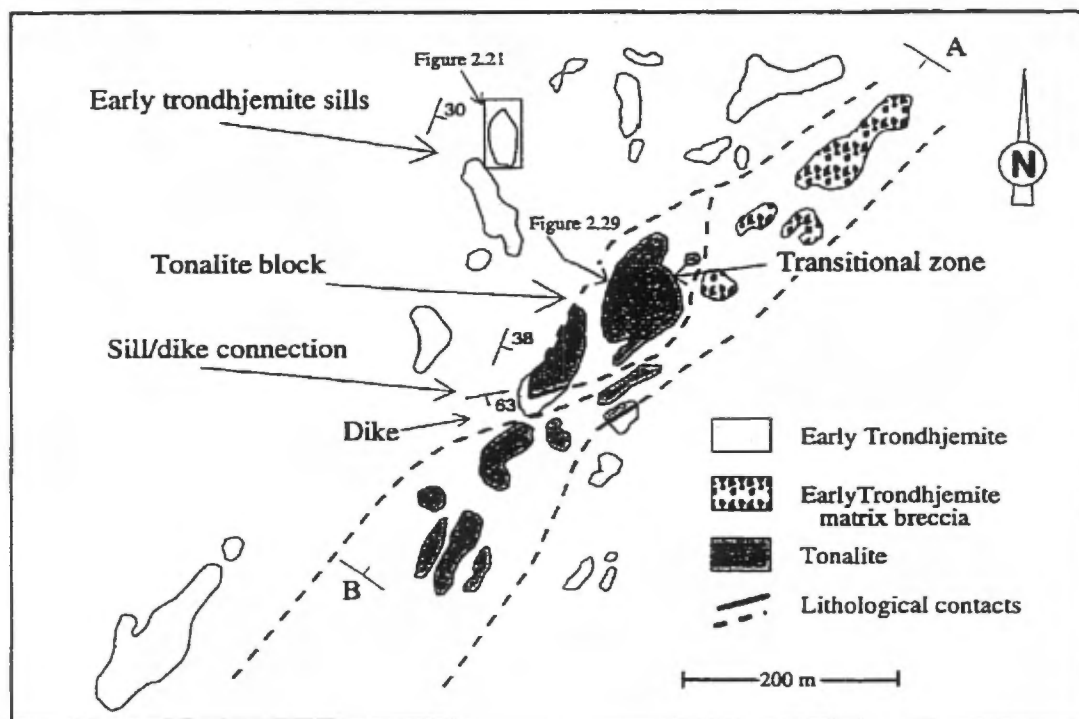


Figure 2.18: Geological map of an area in the northeastern part of the Flavrian pluton, showing structural and contact relationships between the early trondhjemite and tonalite. Location of this figure shown in Figure 2.1.

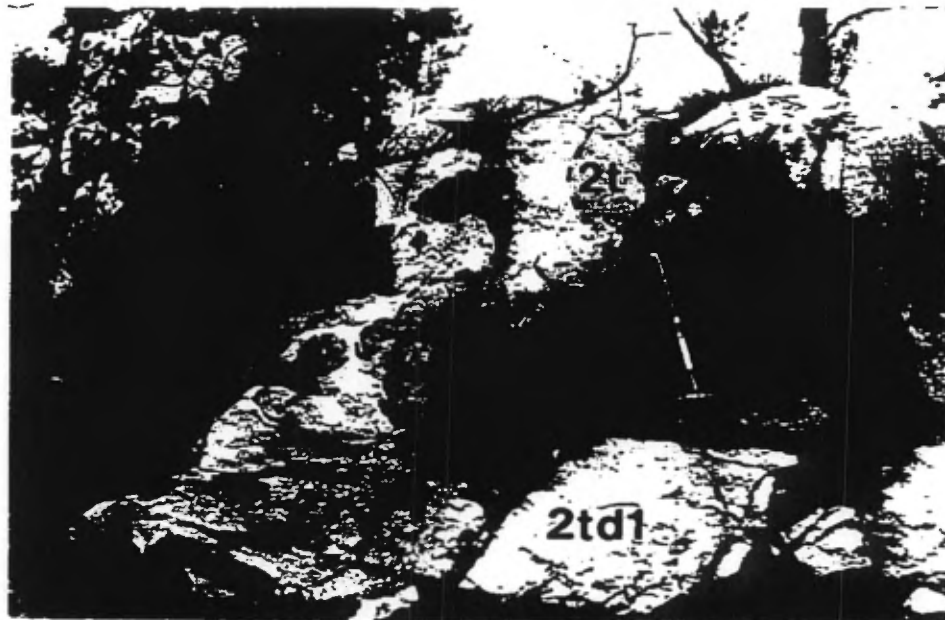


Figure 2.19: Contact area between tonalite and early trondhjemite matrix breccia. Note that early trondhjemite (2td1) appears as dikes detaching tonalite (2t) blocks from the wall rock.

trondhjemite matrix breccia, blocks vary in size and are typically angular and sharply bounded, although some are more rounded and gradational. Textures within the blocks are typically tonalitic and rarely dioritic. Planar to curvilinear, relatively ill-defined veins of fine- to medium-grained early trondhjemite, up to 1 cm across may occur within the blocks. These veins are interpreted to result from the infiltration of early trondhjemite into the tonalite blocks. The observations described above indicate that subrounded, irregular-shaped and angular inclusions and blocks of tonalite were detached from tonalite masses during the intrusion of early trondhjemite. In addition, the sharp contacts suggest that early trondhjemite intruded a solidified host presently represented by tonalite. A schematic section portraying relations noted above is shown in Figure 2.20; the section is oriented parallel to the contact between early trondhjemite and tonalite.

Intrusive relationships between various phases of early trondhjemite are well-exposed two hundred metres northwest of the area shown in Figure 2.18. Mapping at a 1:250 scale (Fig. 2.21) indicates that the early trondhjemite, in this outcrop, is composed of three phases: (1) a coarse-grained inclusion-poor phase showing important textural variations over short distances; (2) a fine-grained phase rich in rounded tonalite inclusions and quartz-epidote vugs and characterized by a well-developed granophyric texture in thin section; and (3) a medium- to coarse-grained, rusty coloured, hematite-rich magnetic phase showing a equigranular texture. Similar relationships were observed in the southern part of the pluton (see Figure 2.22), indicating that the contacts between different phases of early trondhjemite are sharp

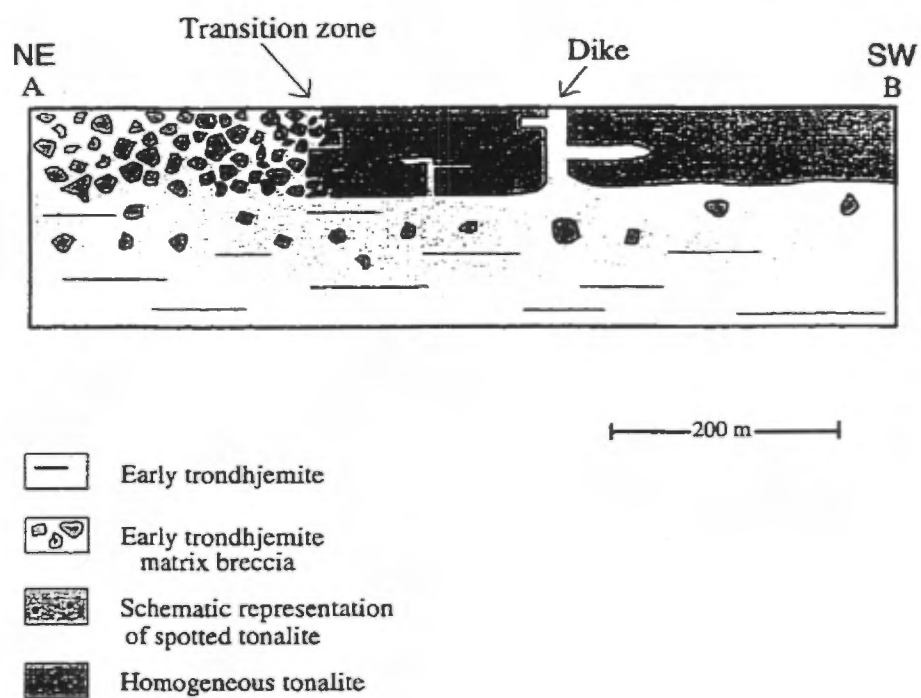


Figure 2.20: Schematic cross-section parallel to strike, showing contacts between early trondhjemite and tonalite. Cross-section location on Figure 2.18.

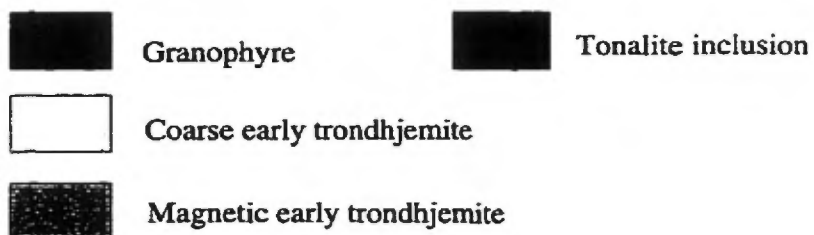
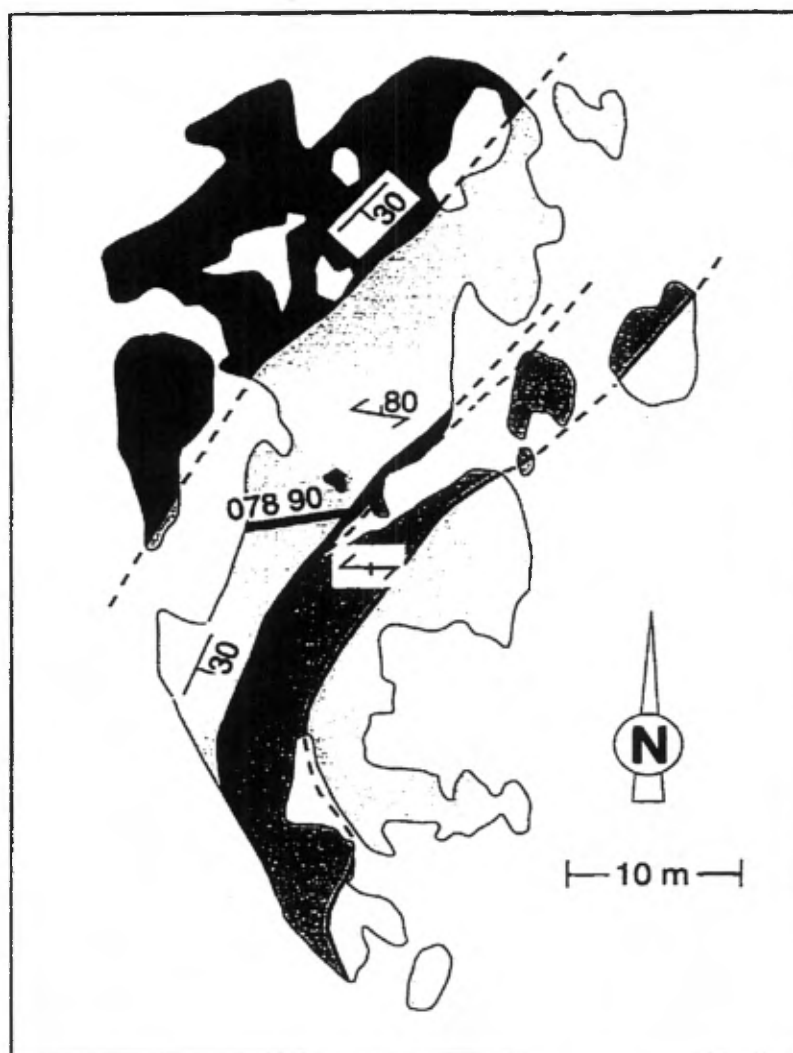


Figure 2.21: Geological map of an outcrop within early trondhjemite, showing internal contact relationships between various phases of early trondhjemite. Location of figure is indicated on Figure 2.18.



Figure 2.22: Contact between pink trondhjemite (above dashed line) and early coarse-grained trondhjemite (below dashed line), southern part of Flavrian pluton. Dashed line marks the contact.

and trend N25°E with a dip of 30° to the southeast. Therefore, early trondhjemite unit is composed of multiple, variably textured, episodically emplaced phases. In addition, the early coarse-grained trondhjemite is transected by an ENE-trending dike of granophyre that connects with a stratigraphically overlying granophyre sill (Fig. 2.21). This crosscutting relationship suggests that the granophyre is younger than the coarse-grained early trondhjemite. Multiple intrusions of early trondhjemite are also commonly observed in the east-central part of the pluton. Intrusive relationships between coarse-grained and microgranitic early trondhjemite are depicted in Figure 2.23 where contacts between both phases are sharp and trend NNE and dip 40° E. A close-up view (Fig. 2.24) reveals the sharp contact and textural differences of the two phases.

Figure 2.25 is a sketch of field observations of early trondhjemite intrusive relationships from an area in the southeastern part of the pluton. Three phases are noted: (1) a greenish-grey coloured quartz-albite porphyritic phase (trondhjemite porphyry); (2) a pink coloured, magnetic, coarse-grained equigranular phase (pink trondhjemite); and (3) a white coloured, medium-grained "vuggy" trondhjemite (coarse-grained trondhjemite). Crosscutting relationships between the three early trondhjemite phases indicate that quartz-albite porphyritic trondhjemite is the oldest phase on the outcrop. It was followed by pink early trondhjemite and then by coarse-grained trondhjemite, the youngest phase.

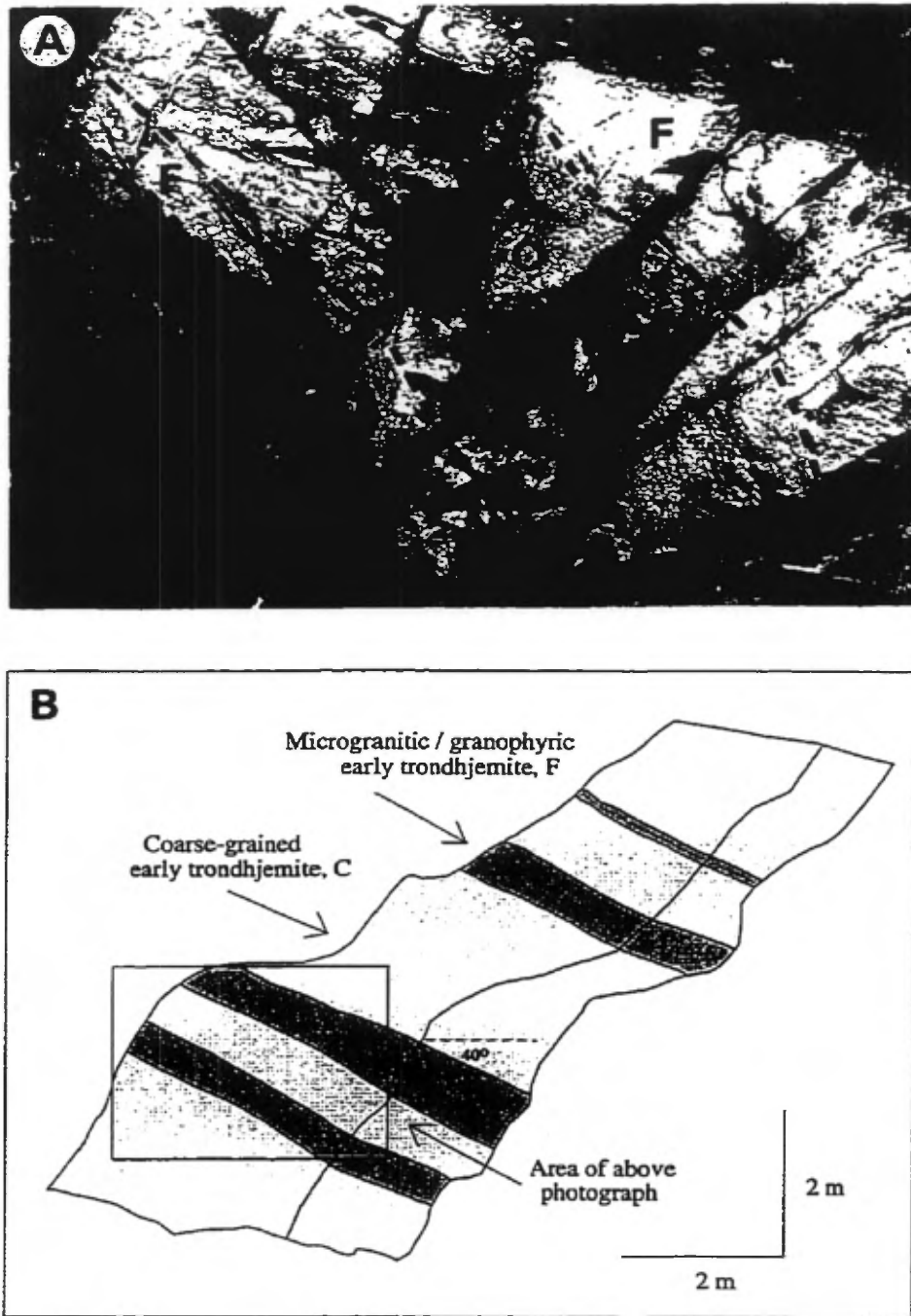
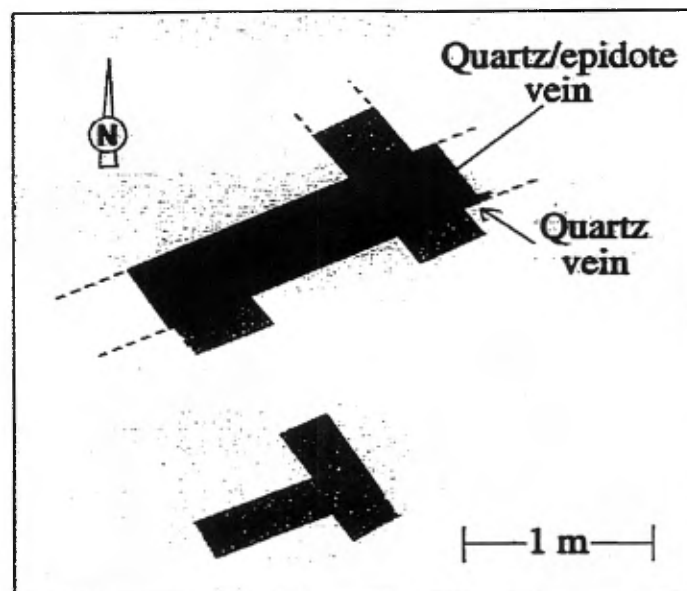


Figure 2.23: A) Contact relationships between coarse-grained (C) and microgranitic (F) early trondhjemite (dashed line marks the contact); and B) sketch of outcrop shown in A.



Figure 2.24: Close-up view of the contact between the coarse-grained and microgranitic early trondhjemite shown in Figure 2.23A.





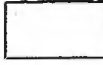
-  White, medium-grained early trondhjemite
-  Pink early trondhjemite
-  Trondhjemite porphyry

Figure 2.25: Sketch from field observations, showing intrusive relationships between various phases of early trondhjemite, eastern portion of the Flavrian pluton.

In the southwestern part of the pluton, greenish-grey coloured quartz-albite porphyritic trondhjemite is hosted by white microgranitic early trondhjemite. The trondhjemite porphyry, commonly containing numerous inclusions interpreted to be andesite and Méritens quartz-diorite, is in sharp contact with and occurs as blocks and inclusions within microgranitic trondhjemite. These relationships suggest that the trondhjemite porphyry is younger than the Méritens quartz-diorite and older than the microgranitic trondhjemite. Relative age relationships between the porphyritic trondhjemite and early trondhjemite are further constrained by the numerous inclusions of trondhjemite porphyry within pink early trondhjemite and early coarse-grained trondhjemite along an ENE-trending zone in the northern part of the southern early trondhjemite intrusion (Fig. 2.1).

The crosscutting relationships shown in Figure 2.25 suggest that the trondhjemite porphyry is older than the pink trondhjemite and medium-grained trondhjemite (coarse-grained trondhjemite). This interpretation, supported by the numerous inclusions of trondhjemite porphyry found within these phases in the southern part of the pluton, suggests that the trondhjemite porphyry is the oldest felsic phase of the pluton. In addition, relationships shown in Figure 2.25 indicate that the emplacement of trondhjemite porphyry was followed by pink trondhjemite and medium-grained early trondhjemite. Evidence of microgranitic trondhjemite and granophyre crosscutting early coarse-grained trondhjemite are given in Figures 2.21 and 2.23. No evidence was found to indicate the relative age relationship between microgranite and granophyre.

The Eldrich diorite is composed of a number of dikes that cut the tonalite and early trondhjemite phases of the pluton, as in Figure 2.1 where the NW-trending Eldrich diorite transects the contact between the tonalite and early trondhjemite. The crosscutting Eldrich diorite is well-documented at the Pierre Beauchemin mine where the dike played an important role in the geometry of ore shoots (see CHAPTER 5).

In the northwestern part of the pluton, the late trondhjemite is in contact with both tonalite and Méritens quartz-diorite. The contact zone consists of a breccia (late trondhjemite matrix breccia) in which late trondhjemite matrix hosts angular inclusions of andesite, tonalite and rarely early trondhjemite. This contact is well-exposed south of Lac Méritens (Fig. 2.1) where, in passing from west to east from tonalite and quartz-diorite to late trondhjemite breccia and finally to late trondhjemite, numerous small dikes of late trondhjemite are observed crosscutting tonalite. In this area, the tonalite is also cut by a series of biotite-filled veins which have been interpreted as part of a metamorphic aureole within the tonalite and Méritens quartz-diorite resulting from the intrusion of late trondhjemite (Kennedy, 1984). The contact between the late trondhjemite matrix breccia and late trondhjemite are best observed on a large outcrop immediately south of Lac Méritens (Fig. 2.26) where an early phase of late trondhjemite is the matrix to the breccia, and a later phase cuts across the breccia. This observation suggests that the late trondhjemite is composed of at least two closely related phases. Away from the contact breccia, the late trondhjemite contains numerous inclusions of tonalite, andesite, Méritens quartz-diorite and early trondhjemite, and is therefore interpreted to postdate these included phases.



Figure 2.26: Contact relationships between late trondhjemite (top of outcrop) and late trondhjemite matrix breccia (bottom of outcrop). The dashed line marks the contact where the long contact segment dips shallowly to the east and the short contact segment dips steeply to southeast. Northern part of Flavrian, near Lac Méritens.

In the centre of the pluton, a distinctively white-coloured xenolith of early trondhjemite, measuring 30 m across, contrasts sharply against the beige colour of the late trondhjemite in which it occurs. The contact between the early and late trondhjemite consists of a dark-green to black coloured rim, 5 to 10 m wide, surrounding the early trondhjemite. The rim is composed essentially of muscovite and chlorite (60%) replacing plagioclase and quartz (40%, and up to 1 mm across). Intergrowth textures are still observed within the early trondhjemite; however the plagioclase is totally replaced by chlorite and muscovite. This rim is interpreted as a metamorphic reaction created around the early trondhjemite block when it was intruded by late trondhjemite.

2.3.1 Geochronology of Flavrian pluton

From U-Pb zircon dating of massive white early trondhjemite, Mortensen (1993) obtained an age of $2700 \pm 2.6 / -1.0$ Ma, which was interpreted to be the best estimate for the crystallization age of this phase of early trondhjemite. This age confirms the 2701 ± 1.5 Ma age published earlier (Mortensen, 1987) for the Flavrian early trondhjemite. A preliminary discordant age of 2679 Ma using the U-Pb zircon method has been obtained for the late trondhjemite (Fig. 2.27). The same sample also yielded ages of 2694 to 2700 Ma and 2712 Ma interpreted to represent ages of inherited zircons. The 2700 Ma age corresponds to the age for the Flavrian early trondhjemite obtained by Mortensen (1993) and is therefore interpreted to have been inherited from this phase. The 2712 Ma date, the oldest age yet recorded for Blake River Group rocks, may correspond to the older zircons found in the Flavrian tonalite

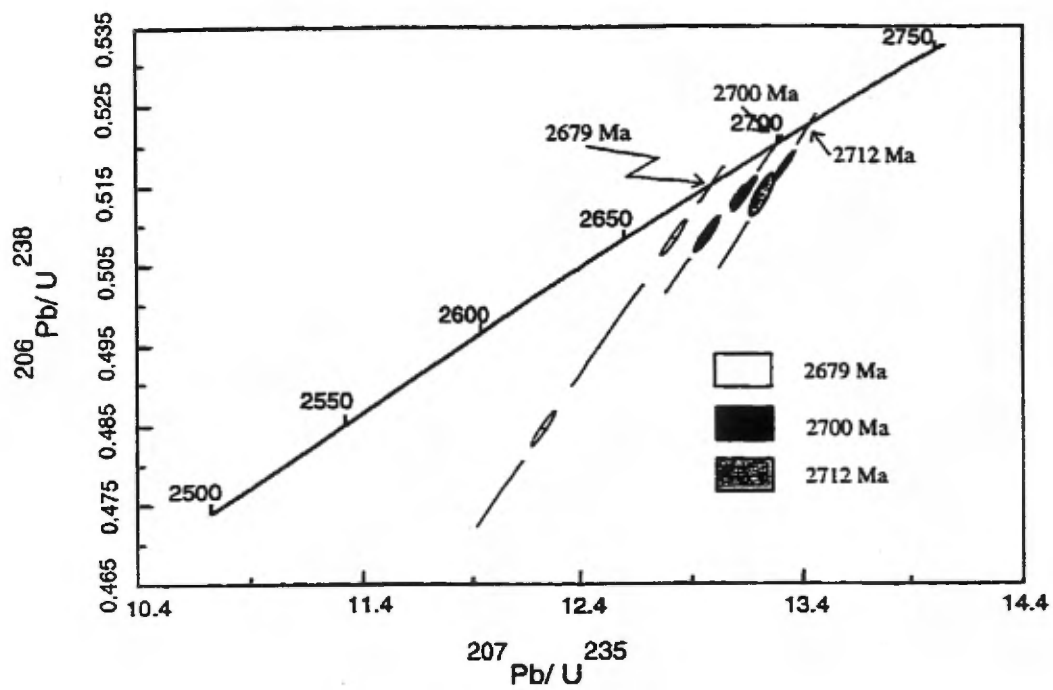


Figure 2.27: Preliminary U-Pb zircon results showing $\text{Pb}^{207/206}$ isochron diagram for the late trondhjemite of the Flavrian pluton.

by Mortensen (1993) and interpreted by him to have been inherited from an older source. Note that these ages are discordant and preliminary (exact errors are not known).

Based on the crosscutting relationships and geochronological data presented above, the following sequence of intrusions is suggested, in general agreement with Kennedy (1984) (from oldest to youngest): (1) Méritens quartz-diorite, homogeneous tonalite, hybrid and heterogeneous tonalite; (2) trondhjemite porphyry; (3) pink trondhjemite; (4) coarse-grained trondhjemite; (5) granophyre and microgranite; (6) Eldrich diorite; (7) late trondhjemite; and (8) late mafic intrusions. All phases except the late mafic intrusions are affiliated with the emplacement of the subvolcanic Flavrian pluton.

2.4 Geometry of the Flavrian Pluton

In the following section, the nature and geometry of contacts between phases, along with the orientations of dikes and sills, are used to establish the internal geometrical features of the pluton. Generally, most contacts between major units of the Flavrian pluton trend $N00^{\circ}$ to $N30^{\circ}E$ and are shallowly dipping (Fig. 2.1). The shallow attitude of contacts and the close parallelism with volcanic units outside the pluton suggest that the contacts represent sill-like intrusions. The sills are cut and fed by a series of dikes whose geometry is discussed below.

2.4.1 Orientations of contacts between internal phases

Contacts between the Méritens quartz-diorite and tonalite are diffuse and therefore orientations were not established. However, at the pluton scale, the zone where Méritens quartz-diorite is most abundant trends N30°E, parallel to the trend of other major units in the northern part of the pluton (Fig. 2.1). Contacts between various phases of early trondhjemite and between tonalite and early trondhjemite also trend NNE and are shallowly dipping at the pluton scale (Fig. 2.1). However, a more detailed examination reveals that in addition to the shallowly dipping, NNE-trending segments, contacts also trend WNW to NW or ENE and are steeply dipping. In plan view, steeply dipping contacts generally occur as relatively short segments compared to shallowly dipping contacts. The steeply dipping contact segments are viewed as dikes (see Figure 2.18) and are described in Section 2.4.2. In the southern part of the pluton, contacts are commonly variable in trend and shallowly dipping. Trends range from northwest in the southwestern part of the pluton to northeast in the southeastern part of the pluton.

The Eldrich diorite is composed of a series of en echelon dikes and sills that transect early trondhjemite and tonalite in the northwestern part of the pluton. The intrusion appears elongate in a NNW orientation; however its northern extremity trends N30°E. Where exposed in the vicinity of the Pierre Beauchemin gold mine, the Eldrich diorite trends N to NNE and dips between 20° and 40°E to ESE. Contacts between the Eldrich diorite and host tonalite and early trondhjemite are well-exposed underground at Pierre Beauchemin (see Section 5.2.3). Where undeformed, contacts

are sharp and a chilled margin, up to 2 cm wide, may occur. However, locally, the contact may be strongly tectonized by post-intrusion faults.

The contact between the late trondhjemite and early trondhjemite was not observed directly. However, as indicated by Figure 2.1, the contact is generally oriented EW to NE. The contact between the late trondhjemite and late trondhjemite matrix breccia was observed in two locations and trends north and dips 30° to 50° E (Figs. 2.1 and 2.26). Figure 2.26 shows the contact between late trondhjemite and late trondhjemite matrix breccia near Lac Méritens where long, sharp north-trending, shallowly dipping contact segments alternate with short, WNW-trending, steeply dipping segments.

2.4.2 Dike orientations

The orientations of 134 early trondhjemite and granophyre dikes crosscutting tonalite were measured in the Flavrian and adjacent Powell plutons. Stereograms (Fig. 2.28) indicate that the dikes are preferentially oriented along three directions: (1) E- to ENE-trending and steeply dipping; (2) WNW- to NW-trending and steeply dipping; and (3) variably trending and shallowly dipping. Except for shallowly dipping dikes, these orientations are also observed in epidote-quartz-magnetite veins that transect the early trondhjemite and granophyre.

Figure 2.29 shows the geometrical relationship between early trondhjemite dikes and sills that cut tonalite in the northern part of the pluton. The vertical,

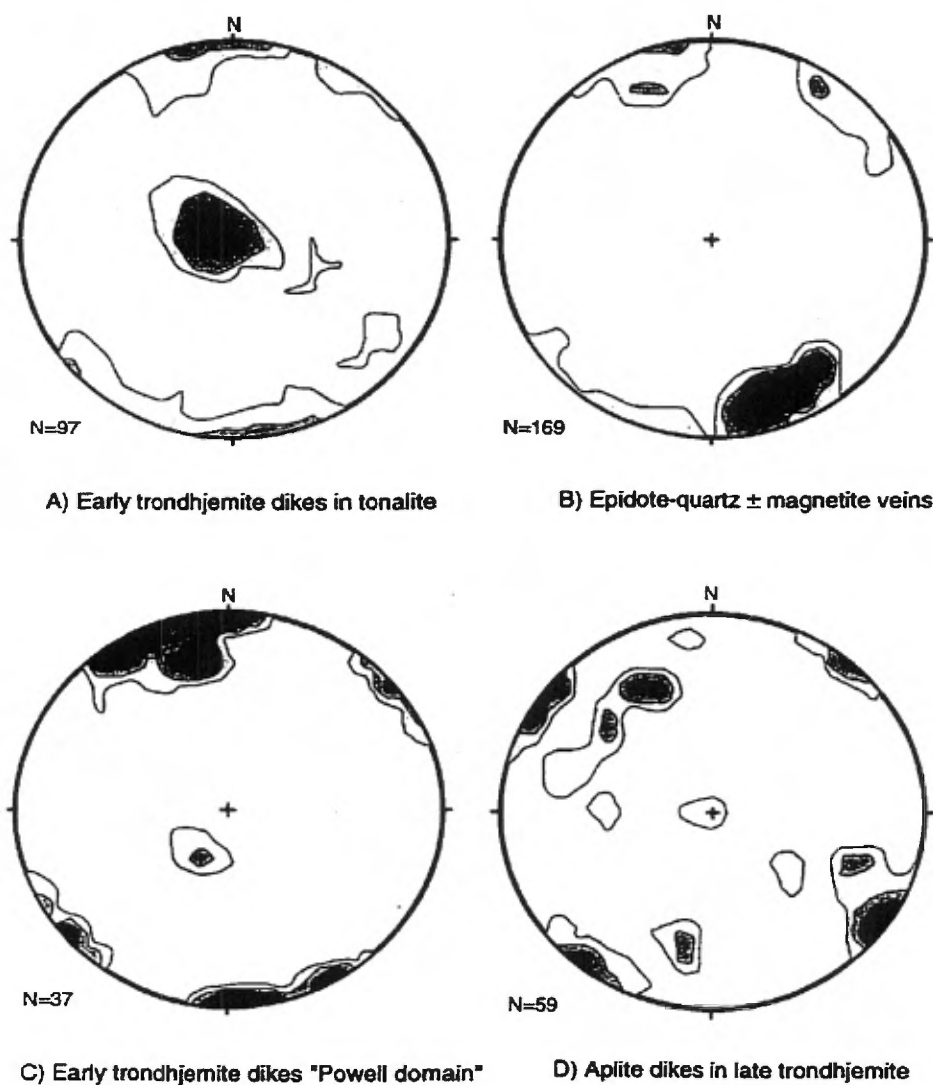


Figure 2.28: Lower-hemisphere equal-area stereographic projections of: A) trondhjemite dikes within the Flavrian pluton; B) epidote-quartz \pm magnetite veins within the early trondhjemite and granophyre; C) trondhjemite dikes within the Powell pluton; and D) aplitic dikes within the late trondhjemite. 2% area contour intervals.

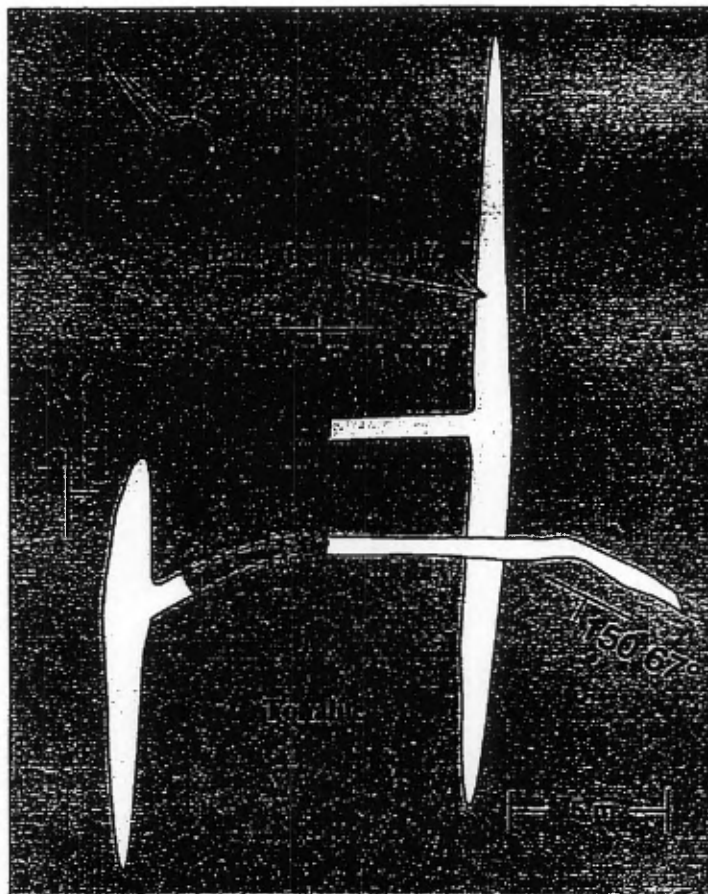


Figure 2.29: Schematic diagram (based on a photograph) illustrating the dike-fed sill geometry of early trondhjemite crosscutting tonalite. Location of these observations is shown by black square in Figure 2.18.

N140°E-trending dike abruptly connects with the N032°E-trending shallowly dipping sill. In turn, the interconnected dike and sill are cut by a second generation of early trondhjemite where a N030°E-trending, shallowly dipping sill-like body connects with a SE-trending, steeply dipping dike. These relationships are also shown in Figure 2.18, where a NNE-trending sill connects with an ENE-trending, steeply dipping dike and Figure 2.21, where an ENE-trending dike connects with a NNE-trending, shallowly dipping sill. Interconnected dikes and sills are commonly observed throughout the pluton. In a large outcrop north of the Elder mine, early coarse-grained trondhjemite is cut by a 30 cm wide dike of a similar composition (Fig. 2.30). These phases are, in turn, transected by a later phase of fine-grained early trondhjemite. The last phase of fine-grained early trondhjemite (possibly granophyre) appears as NE-trending, shallowly dipping sills connected by WNW-trending, steeply dipping dikes. A similar relationship is observed in the northern part of the pluton where steeply dipping dikes of early trondhjemite feed shallowly dipping sills. Note the sharp, shallowly dipping contact between the early trondhjemite and host tonalite beneath the detached tonalite block (Fig. 2.31). WNW-trending, steeply dipping early trondhjemite dikes are also observed underground at the Pierre Beauchemin gold mine. The dikes at this mine are generally 1 m across, consist of early trondhjemite, and show sharp contact relationships with the host tonalite (Fig. 2.32). The sharp, undisrupted nature of a contact between an early trondhjemite dike and tonalite host is shown in Figure 2.33; individual quartz crystals within the early trondhjemite near the contact with tonalite are elongate perpendicular to the dike walls, suggesting that dilation occurred perpendicular to the walls.

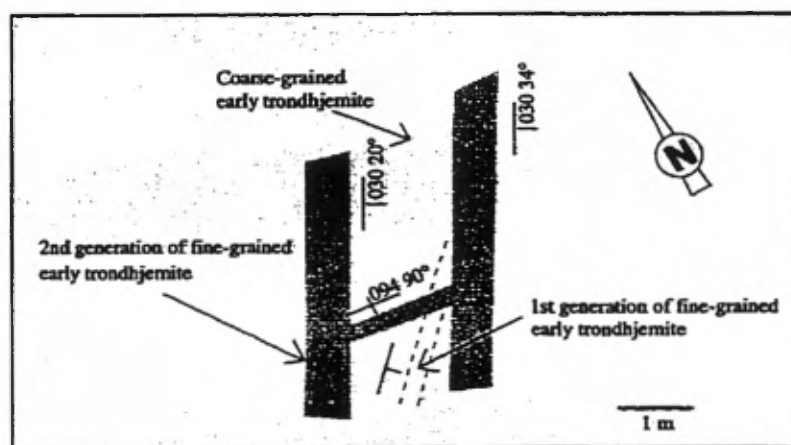


Figure 2.30: Sketch from field observations illustrating geometrical relationships between coarse-grained trondhjemite and two generations of finer-grained sills and dikes. Note the dike-fed sill geometry of the second generation of fine-grained early trondhjemite crosscutting tonalite. Southeastern part of Flavrian pluton.



Figure 2.31: Early trondhjemite crosscutting tonalite along two preferred orientations: 1) N-trending and shallowly dipping; and 2) a steeply dipping orientation. The steeply dipping dikes feed the shallowly dipping sills.



Figure 2.32: Early trondhjemite dike crosscutting tonalite. Level 5, Pierre Beauchemin gold deposit.

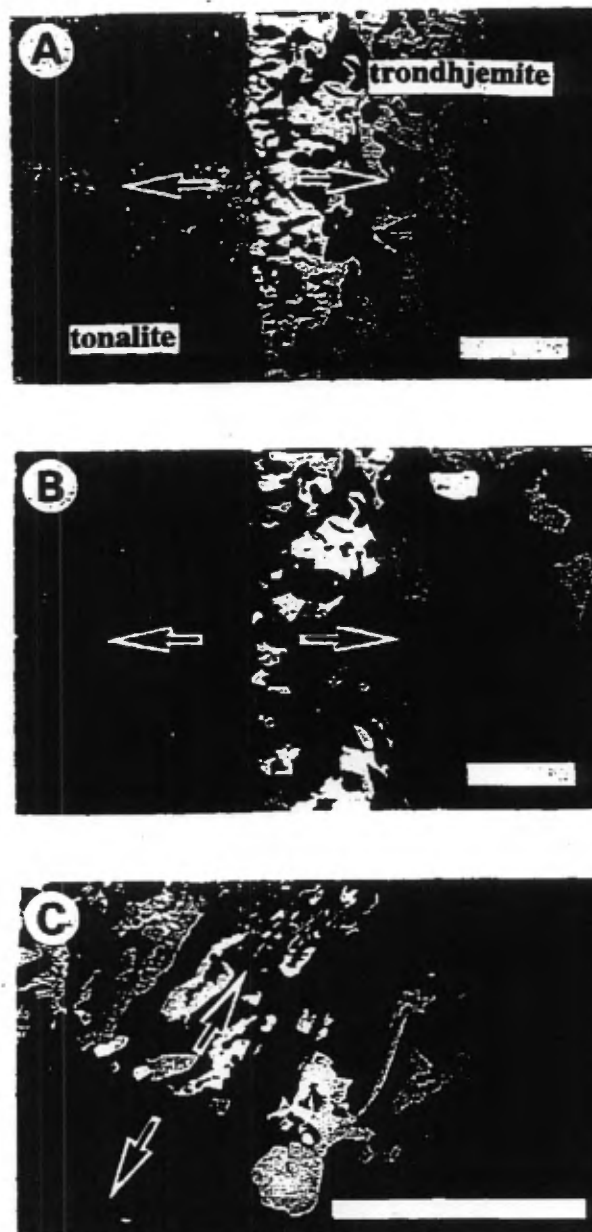


Figure 2.33: Photomicrographs of the contact between early trondhjemite dike and host tonalite. Arrows indicate the direction of extension perpendicular to the dike walls: A) polarized light; B) crossed-polarized light; and C) close-up. Scale = 1 mm for A and B and 0.63 mm for C.

Figure 2.34 shows several generations of sharply bounded dikes of various compositions crosscutting quartz-diorite in the eastern part of the Powell pluton. The dikes have an overall WNW trend; however, they typically zigzag with dike segments trending both WNW to NW and ENE. The geometry and episodic nature of the dikes suggest multiple episodes of extension in both the WNW to NW and ENE subvertical planes. A closer look at a dike connecting two segments of an early trondhjemite dike transecting tonalite within the Flavrian pluton is presented in Figure 2.35A and 2.35B. Where the sharply bounded NE-trending dike segment connects with the NW-trending segment, a fragment of the tonalite host rock appears to have been slightly displaced from its original position. The angular shape of the fragment suggests that it was subjected to little movement or rotation during the emplacement of the early trondhjemite dike. The sharp and angular dike segments are characteristic of "zigzag dikes" as defined by Hoek (1992). Where zigzag dikes show strongly preferred orientations, they are interpreted by Hoek to have been emplaced along preexisting planes of weakness such as fractures, faults or lithological contacts.

2.4.3 Internal deformation

Mapping of the pluton revealed no significant internal deformation, apart from relatively thin and brittle shear zones and faults observed in drill core and brittle-ductile shears observed at the contacts of diorite dikes. Intensity of deformation and alteration is clearly higher in the Powell pluton, as noted by Goldie (1976). The Powell pluton hosts a prominent, inhomogeneous, N60°-oriented steeply dipping fabric. The intense alteration and the abundance of N60E°-oriented dikes in the

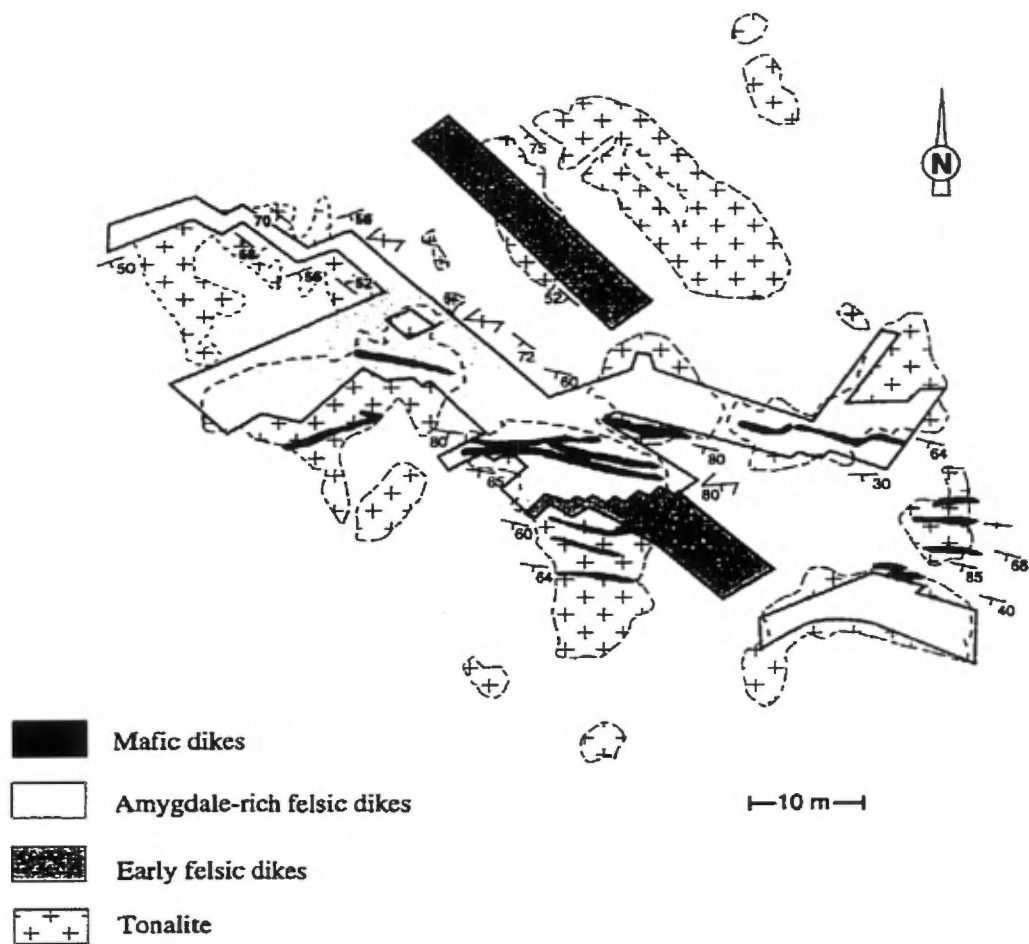


Figure 2.34: Detailed geological map showing multiple generations of dikes crosscutting tonalite within the eastern part of the Powell pluton. Note the sharp, angular dike segments. Dashed lines outline outcrops.

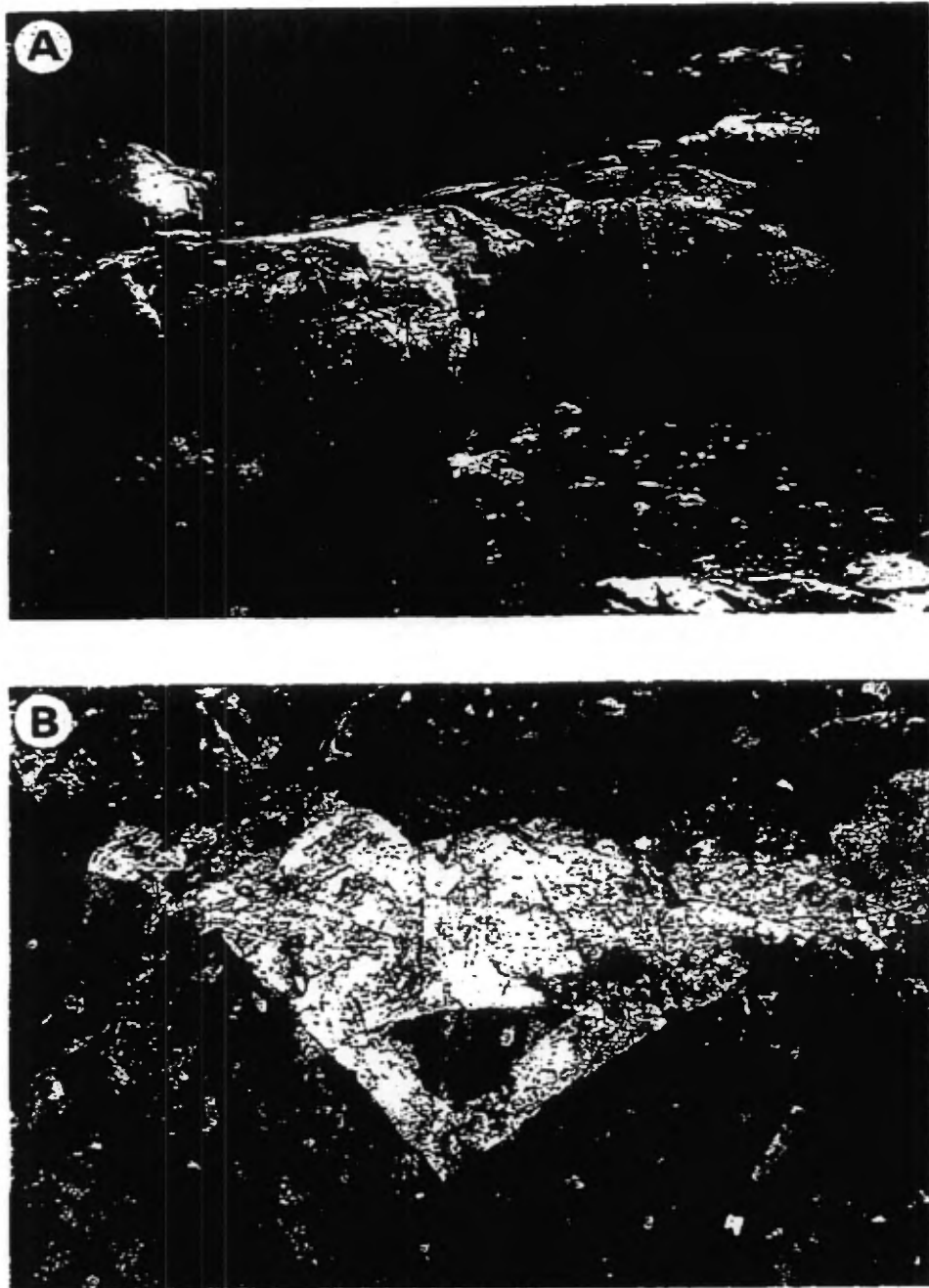


Figure 2.35: A) Early trondhjemite dike crosscutting tonalite and B) a close-up of the dike where an angular tonalite fragment, detached from the wall, occurs where the dike passes from an ENE to a NW orientation.

Powell pluton may have significantly influenced the orientation of the overprinted fabric. In the Flavrian pluton, however, internal deformational features are much less well-developed. An EW- to ESE-trending, steeply dipping fabric (S_1) is observed throughout the pluton (Fig. 2.1). The fabric commonly contains chlorite, sericite, quartz and hematite (Fig. 2.36) and is interpreted as a late secondary spaced cleavage. The spaced cleavage is developed to variable intensities in different areas and suggests that a N-S to NNE-directed compression produced a minor post-emplacement imprint on the pluton. Most of the post-emplacement deformation of the pluton appears to have been focused along relatively thin faults. Shears associated with diorite dikes play an important role in the distribution of gold within the Flavrian pluton and are discussed in detail in CHAPTER 5. The Eldrich fault, located in the northwestern part of the pluton trends NNE and dips between 30° and 50° ESE. The fault influences an area about 4 km long and 75 m wide at the contact between the Eldrich diorite dike and the host granitoid rocks. The fault hosting the Pierre Beauchemin gold deposit (Fig. 2.1) was mapped in detail and is discussed in CHAPTER 5. Where deformation was more intense, thin bands of recrystallized quartz grains encompass zones of less deformed host rock, forming a tectonic breccia texture. These breccias are commonly associated with mineralized zones at the Pierre Beauchemin gold mine (see CHAPTER 5). The Quesabe fault trends $N60^\circ E$ and dips steeply towards the southeast. Within the Flavrian pluton, it is best inferred between Lac Flavrian and Lac Lebrun (Fig. 2.1). The fault, which does not outcrop, manifests itself at the surface by a topographic low. The fault was intercepted in drill core and is described as a narrow zone (50 m) of variable brecciation, silicification.

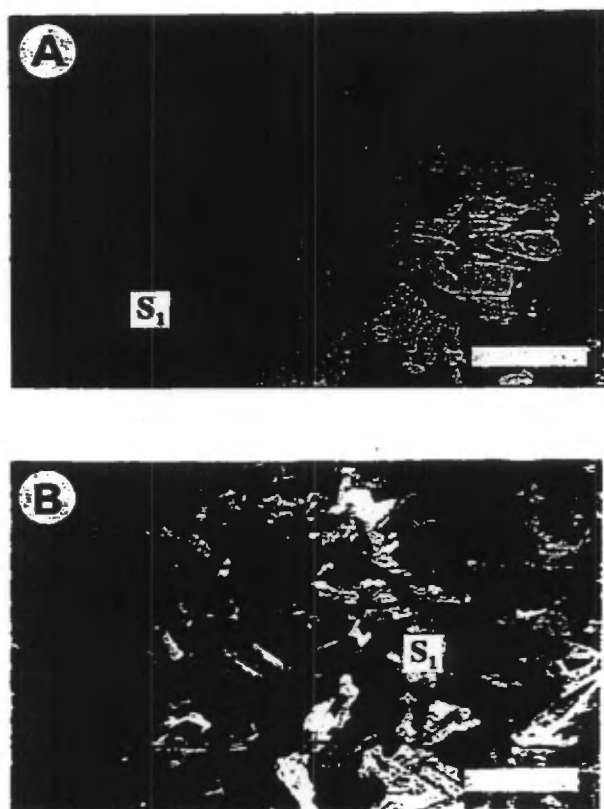


Figure 2.36: Photomicrographs of ZY section view of the (S_1) spaced cleavage transecting early trondhjemite. Both A and B are from the southern part of the Flavrian. Top of photograph indicates north. Scale bars = 1 mm.

chloritization and locally, gold mineralization (R. Potvin personal communication). Large outcrops of massive late trondhjemite show no visible deformation features near the fault in the central part of the Flavrian pluton. Localized areas of alteration expressed as quartz and quartz-epidote vugs or dark chloritic zones are observed near the fault.

The sharp contacts between intrusive phases suggests that emplacement occurred passively. Early trondhjemite matrix breccias and late trondhjemite matrix breccias commonly observed at contacts do not contain folds, foliations or any structural elements indicating forceful emplacement. Primary magmatic flow textures related to magma emplacement were severely altered during regional albitization and may be represented by local zones of textural variability. Subhorizontal textural variations within early trondhjemite paralleling contacts between phases observed underground at the Pierre Beauchemin gold deposit (Fig. 5.3A) may reflect primary magmatic layering.

Post-emplacement deformation of the Flavrian pluton has not significantly modified the internal or external geometry of the pluton. The geometric relationships between phases within the pluton are therefore considered to have been produced by primary emplacement mechanisms; the systematically oriented dikes and sills that form the pluton were intruded along three preferred orientations and were not significantly modified by later structural events.

2.4.4 Shape of the Flavrian pluton and relationship to the host BRG volcanic rocks

The northeastern contact between the Flavrian pluton and the volcanic rocks of the Noranda cauldron (Fig. 2.1) is sharp, trends N20°E and dips between 20° and 50° ESE where it is well-exposed in outcrop and reported in drill core beneath the Ansil Cu-Zn deposit. Attitudes of volcanic rocks external to the pluton parallel those between phases internal to the pluton, i.e., the pluton is concordant with volcanic rocks in this area.

East of the Flavrian pluton, the Norbec, D-zone, East Waite and Old Waite Cu-Zn deposits of the Central Noranda cauldron are aligned along the Old Waite dike swarm, a major N70°E-oriented steeply dipping dike-in-dike structure (Gibson and Watkinson, 1990). This structure is truncated by the late trondhjemite of the Flavrian pluton which is in turn cut by the Quesabe fault (Fig. 2.37). At the surface, the regular geometry and internal textures of the late trondhjemite are not disrupted by the fault. Therefore the Quesabe fault appears to have been activated both as an early syn-volcanic structure related to the Old Waite dike swarm and a late post-volcanic structure crosscutting the late trondhjemite unit of the Flavrian pluton.

The eastern margin of the central part of the pluton is fault bounded and defined by the McDougall and Despina faults (Fig. 2.1). The McDougall and Despina faults strike northwest, are steeply dipping and merge at depth (shown as a single fault on Figure 2.1) (Knuckey and Watkins, 1982). Watkins (1980) and Knuckey and Watkins (1982) demonstrated the syn-volcanic nature of the fault, along with the role it played

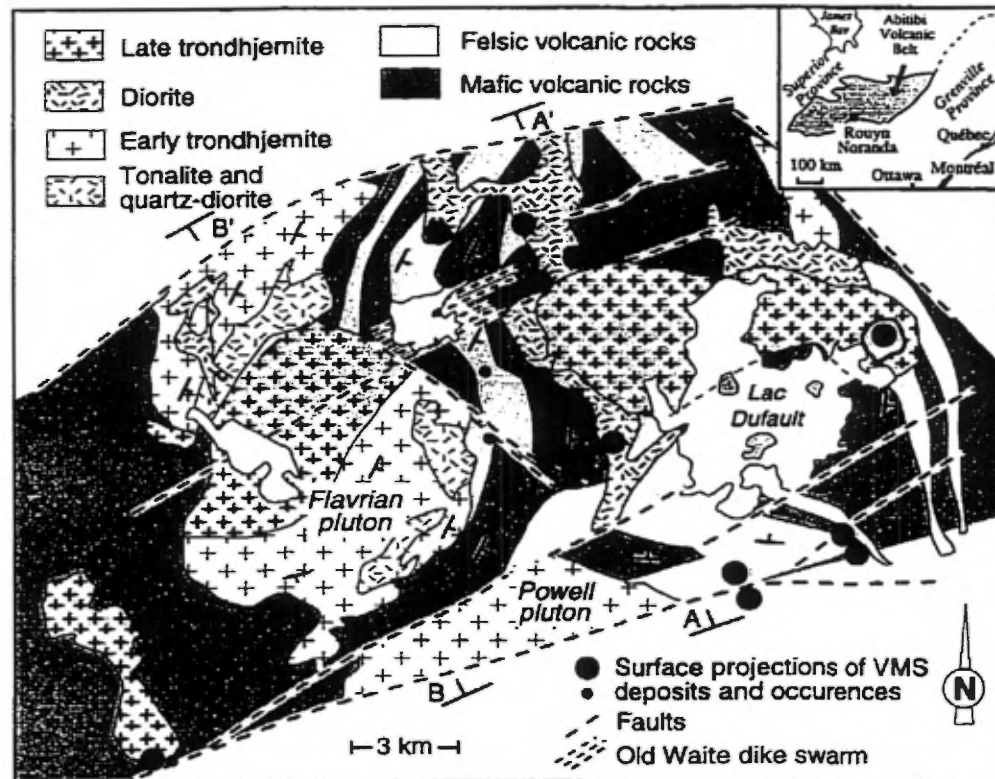


Figure 2.37: Simplified geology map of the Noranda cauldron area. Modified from Gibson and Watkinson (1990).

in the formation of the Corbet massive sulphide deposit. They also demonstrated that rock units on the west side of the fault dropped at least 700 m relative to the east side before intrusion of the Flavrian trondhjemite (see Figure 2.38). Field investigations indicate that the trondhjemite referred to by Watkins (1980) and Knuckey and Watkins (1982) corresponds to the early trondhjemite described in this paper.

The Flavrian pluton is bounded on the north by the Hunter Creek fault (HCF). Using drill core data and stratigraphic relations, Camiré and Watkinson (1990) indicate that the fault trends N240°-250°, dips about 70° northwest and had an apparent north-side-up dextral movement. This interpretation contrasts with that of Péloquin and Verpaelst (1989) who stated that an apparent left-handed movement along the HCF is indicated by the relative displacement of the Fishroe rhyolite, a chemically distinct felsic volcanic unit observed on each side of the fault. The HCF has been considered syn-volcanic by many authors (de Rosen-Spence, 1976; Litchblau and Dimroth, 1980; Dimroth et al., 1982; 1985; Gélinas et al., 1984 and Hubert et al., 1984); however, Camiré and Watkinson (1990) suggest that there is no evidence to support this interpretation. The contact between the Flavrian pluton and volcanic rocks is not exposed to the north. Scattered outcrops of tonalite, diorite dikes (Eldrich diorite) and early trondhjemite near the northern boundary of the pluton in the Lac Nora area (Fig. 2.1) commonly show variably oriented brittle fractures. Near the inferred contact with volcanic rocks, 20 cm-wide shears transect tonalite and diorite with trends parallel to the HCF and dipping between 55° and 80° south. These shears suggest late shearing of the pluton near its contact with the

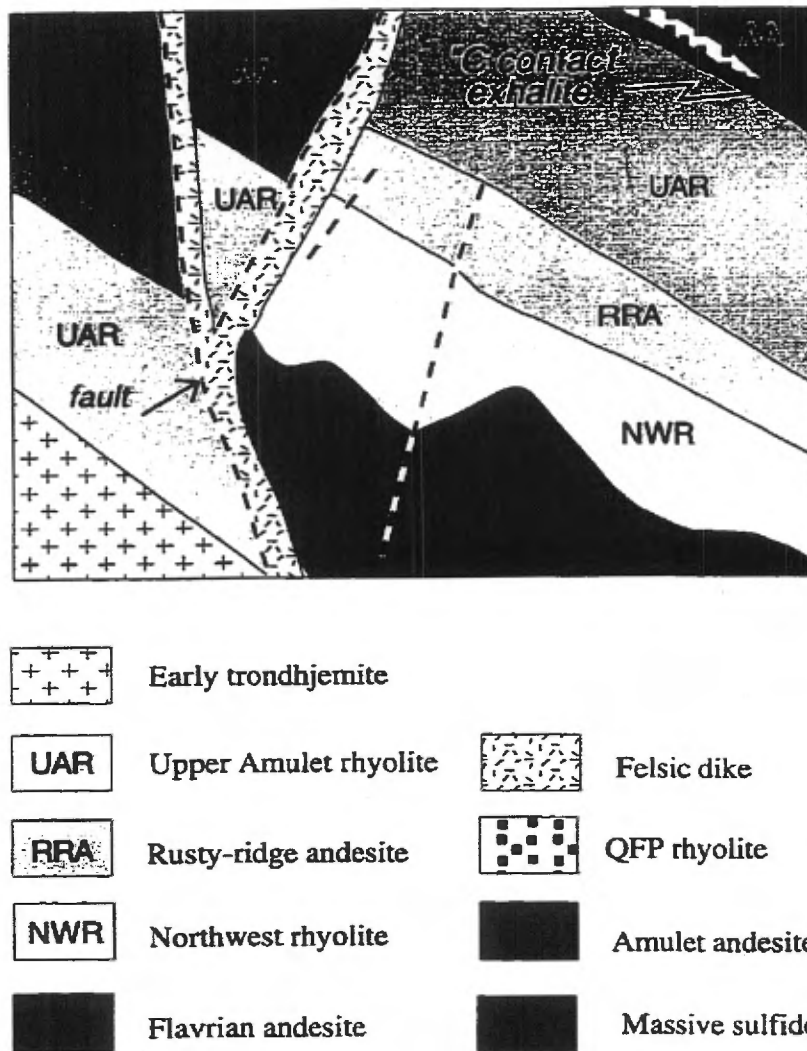


Figure 2.38: East-west cross-section through the Corbet massive sulphide deposit showing down-dropped stratigraphy on the west side of the McDougall and Despina faults. Note that the early trondhjemite must have intruded the volcanic sequence after movement along the fault because it does not appear on the east side of the fault. After Knuckey and Watkins (1982).

volcanic rocks. Based on observed late shears and evidence presented by numerous authors suggesting that the fault was syn-volcanic, the HCF is interpreted as a reactivated syn-volcanic fault.

Where exposed to the south, contacts among internal phases of the Flavrian pluton trend E to ENE and dip 20° to 30° S to SE. These attitudes are reflected at the southern contact between the pluton and andesitic volcanic rocks where a 20 m exposure of the contact is characterized by a 10 cm-wide shear zone that hosts many small shear veins filled with quartz, chlorite and minor amounts of sulphides. Slickenlines on shear planes suggest that movement was dip-slip. A sketch map of the contact is shown in Figure 2.39. At the contact, greenish coloured, altered early trondhjemite is composed of anhedral to intersertal quartz and weakly to moderately altered albite. Quartz and albite commonly show serrate crystal edges and intergrowth textures. Albite is altered to sericite, chlorite and lesser amounts of epidote. No recrystallization or deformation features are observed within the early trondhjemite. Thin (centimetre-wide) quartz veins commonly occur in both the early trondhjemite and the volcanic rocks on both sides of the contact. Evidence of deformation is shown within andesite by a weakly developed foliation parallel to the contact with the pluton. The sheared contact between the Flavrian pluton and the andesite volcanic rocks, along with the penetrative fabric observed in the andesite, are interpreted to be products of a regional N-S compression following emplacement of the pluton. South of the Flavrian pluton, the Beauchastel fault trends $N60^{\circ}E$ and, due

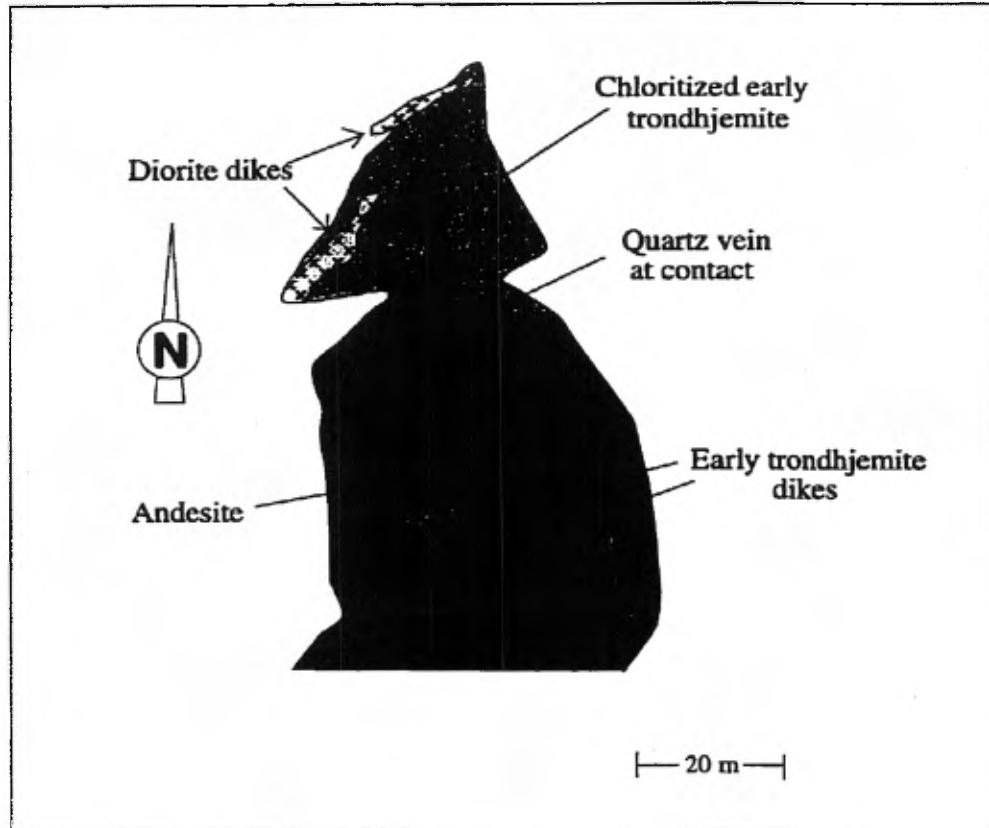


Figure 2.39: Geological map of the southern contact between the Flavrian pluton and the andesitic rocks. Location shown of Figure 2.1.

to lack of outcrop, it is inferred to mark the contact between the Powell pluton and shallowly dipping andesitic volcanic rocks (see Appendix I).

Approximately 100 m east of the Pierre Beauchemin mine, coarse-grained, pink coloured early trondhjemite intrudes andesite volcanic rocks showing preserved pillow structures. The andesites form the NNE-trending Eldrich pendant (see Kennedy, 1984) which is about 1.5 km long by 200 m wide. At the contact, the andesite is metamorphosed, giving it a hornfels appearance (Fig. 2.40). The contact is sharp, trends NNE and dips 30° ESE.

Evidence presented above indicates that the Hunter Creek fault, McDougall and Despina faults and Beauchastel fault mark steeply dipping boundaries of the Flavrian and Powell plutons trending either NW or ENE. The steeply dipping boundaries contrast with shallowly dipping contacts at the Flavrian's northeast and southern contacts with volcanic rocks.

High-resolution seismic reflection data have been obtained from a section through the northern part of the central Noranda area as part of LITHOPROBE's^{*} Abitibi-Grenville project. The subhorizontal to moderate dips of the apparent stratigraphic reflectors are interpreted to be contacts between diorite dikes and

* LITHOPROBE is a national multidisciplinary geoscience project.

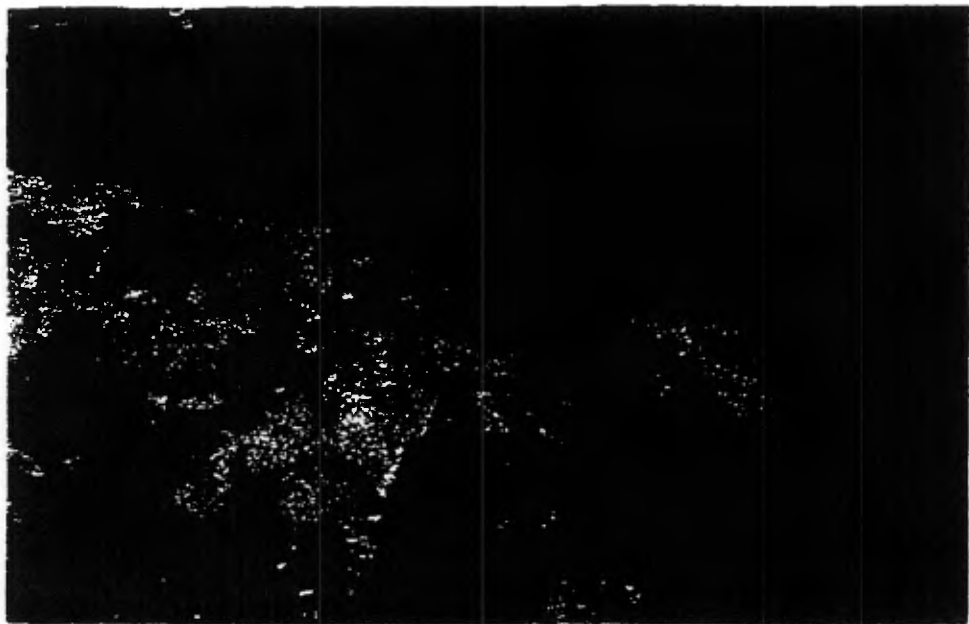


Figure 2.40: Contact between the early coarse-grained trondhjemite and andesite of the Eldrich pendant located 100 m east of the Pierre Beauchemin gold mine.

volcanic rocks. The contacts between volcanic rocks of the Noranda cauldron and the upper contact of the Flavrian pluton are also well-imaged, and although the lower contact of the pluton cannot be determined with confidence, the seismic data do support the concordant sill-like configuration proposed by Goldie (1976), Hubert et al. (1984), Kennedy (1984), Paradis et al. (1988) and Richard et al. (1990).

A detailed gravity survey undertaken in the eastern Blake River Group (Chouteau and Deschamps, 1989) has been reprocessed and reinterpreted by Bellefleur (1992; see Figure 2.41). His 2.5D model of the Bouguer anomaly through the Flavrian pluton uses specific gravity and aeromagnetic data along with geological information to constrain a modelled section. The section clearly portrays the Flavrian pluton as a thin tabular body, the preserved part of which increases significantly in thickness to the south, from a point 3 km south of the Quesabe fault to beyond the southern contact. The southern part of the pluton is estimated to be 1200 m thick. The Powell pluton to the southwest has a similar thickness, whereas in the north, the Flavrian pluton is interpreted to be only 500 m thick. Field relations and geophysical data indicate that the Flavrian pluton is a sill-like body generally concordant with the overlying volcanic rocks of the Noranda cauldron, as originally suggested by Goldie (1976).

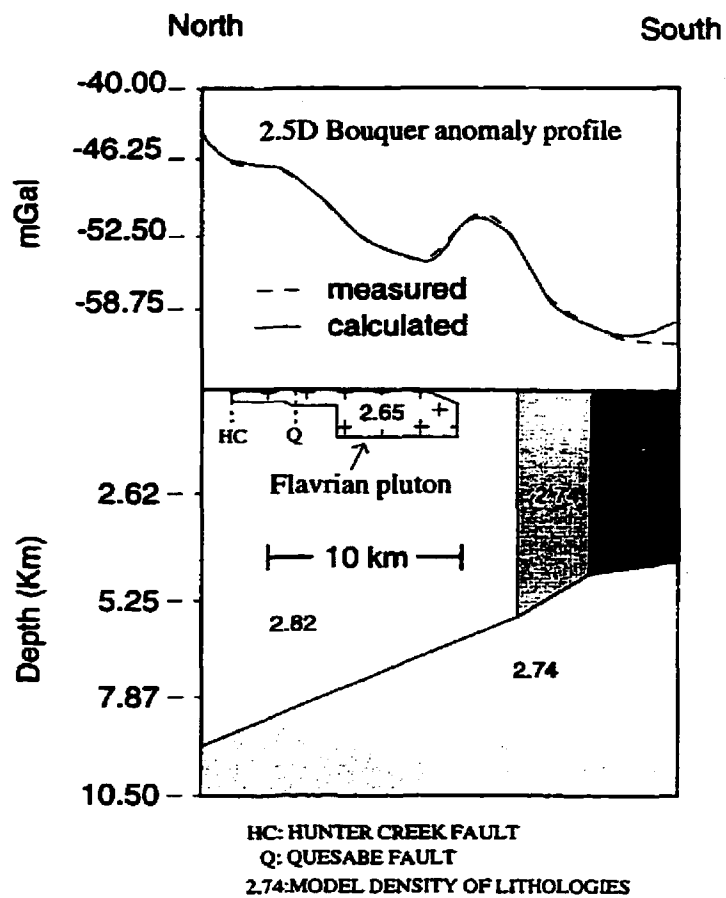


Figure 2.41: Schematic diagram depicting the shape of the Flavrian pluton relative to surrounding rocks, as interpreted from a 2.5D Bouguer anomaly profile. Modified from Bellefleur (1992).

2.5 Summary and Discussion

Textural variability and episodic, high-level emplacement

The Flavrian pluton is composed of a series of intrusions of various compositions and textures. Early trondhjemite composes 50% of the pluton and is the most abundant phase. Early trondhjemite is composed of several intrusive phases and shows a wide variety of textures. Geochronological and field relation data suggest that the late trondhjemite, which forms about 30% of the outcropping pluton, is a distinctly younger phase of the pluton. This interpretation supports Kennedy (1984), who suggested that the centre of the Flavrian pluton was a relatively late phase. The homogeneous coarse-grained equigranular textures found throughout the late intrusive phase contrasts with the textural variability observed for the early trondhjemite (Table VI) and suggests that conditions during emplacement and cooling differed for both phases. Evidence for emplacement of the Flavrian pluton at a high crustal level is found in the abundance of large quantities of granophyre, magmatic brecciation textures, the absence of gneissic structures and the preserved pillows in the Eldrich pendant.

Textural variability is characteristic of the pluton in general and especially evident in phases older than the late trondhjemite. The variations provide evidence of changing pressure and temperature during emplacement of the principal intrusive phases. For example, granophyric textures occurring as minor zones within tonalite and trondhjemite porphyry, as isolated zones within coarse-grained and microgranitic

trondhjemite and as the dominant texture within granophyre (Fig. 2.9D) are generally interpreted as evidence for rapid cooling (Bard, 1980, p. 136; Lowenstern et al., 1997). Rapid cooling may be due to rapid devolatilization resulting from sudden changes in pressure at high levels in the crust. However, granophyric textures are also interpreted to result from crystallization at eutectic temperatures or compositions. Crystallization at eutectic temperatures and compositions is easily envisaged for granophyre, the last phase of early trondhjemite to crystallize. In addition, the commonly observed fragmentation of quartz grains along curved fractures within pink and coarse-grained trondhjemite and trondhjemite porphyry (Fig. 2.10) is usually attributed to abrupt changes in temperature and/or pressure (Bard, 1980, p. 136). The shattered quartz grains are engulfed in a matrix of quartz and albite. The quartz fragments show a "puzzle-like" fit, indicating that they were not significantly displaced or rotated during their breakup and the subsequent crystallization of the matrix. This observation suggests that the shattering of quartz crystals and the crystallization of the matrix were contemporaneous, indicating a link between sudden pressure/temperature variations and crystallization. As further support for this interpretation, the long, radiating and branching acicular amphibole crystals and acicular apatite grains in the tonalite and hybrid rocks (Table VI) are also interpreted as quench products indicating supercooling (Bard, 1980, p. 117). Quenching occurs when a magma becomes metastable as the magma temperature rapidly falls below its liquidus temperature and is commonly attributed to a sudden drop in temperature due to the mixing of magmas or to the interaction of magma and cool host rocks (Castro, 1990).

Textural and compositional variability among units and within individual units of the Flavrian pluton indicate that the pluton was formed by numerous magmatic pulses. These features, along with diagnostic textures indicating that quenching, supercooling and sudden pressure variations occurred during emplacement, suggest episodic emplacement of intrusions in an environment of abrupt changes in pressure and/or temperatures.

Internal dike-and-sill geometry of the pluton

The sill-like shape of the Flavrian pluton and its emplacement at a high crustal level beneath the Noranda cauldron probably results from a combination of factors involving both magma and host rock. The level to which magma ascends and forms chambers in the crust depends on many factors, such as magma temperature, composition, volatile content, viscosity, volume, shape and depth of source. Relevant contributions from the host rock may include volatile content, density and mechanical properties such as strength and degree of anisotropy (Best, 1982, p. 334). The level at which the density/depth profile of the magma intersects the density/depth profile of the lithosphere is the horizon of neutral buoyancy (HNB) (Ryan, 1987). At this horizon, the magma is in gravitational equilibrium (Walker, 1989), above which rocks are less dense than the magma and below which rocks are denser than the magma. Magma rises to the HNB and tends to spread out laterally along that horizon because of the opposing gravitational forces exerted from the top and bottom parts of the magma chamber. The relatively low density inferred for the early trondhjemite

magma as opposed to the host andesite suggest that the early trondhjemite would have easily risen to a near-surface position where the subvolcanic chamber could have developed and spread laterally along the HNB. Buoyancy of the early trondhjemite may have been increased significantly due to a high volatile content.

The detailed mapping of geometrical relationships within and between intrusive phases provides information relating to structural conditions that prevailed in the chamber at the HNB. Contact relationships between phases and between sills and dikes within a particular phase indicate that intrusion occurred as multiple magmatic injections (Figs. 2.21, 2.22 and 2.23). In addition, the distinctive geometry, portrayed by preferentially oriented and interconnected dikes and sills (Figs. 2.18, 2.21, 2.29, 2.30 and 2.31), suggest that magma injection was governed by tectonic forces that produced complex but systematic geometrical relationships.

It is generally accepted that dikes tend to be intruded along planes perpendicular to the least principal stress (Anderson, 1951). Therefore, steeply dipping dikes are intruded perpendicular to a subhorizontal least principal stress vector. The emplacement of horizontal intrusions (sills) implies a vertically oriented least principal stress. The general sill-like shape of the Flavrian pluton indicates that the least principal stress vector was subvertical through much of the pluton's evolution. However, the pluton's characteristic internal geometry of interconnected dikes and sills indicates that stress vectors were locally reoriented. Interconnected dikes and

sills must have been intruded contemporaneously because they are compositionally identical.

Vector reorientation may be explained by a model involving principal stress vector reversals caused by slight pressure fluctuations of the chamber within a general environment of gravitational stability. The sharp contacts between interconnected sills and dikes within the Flavrian subvolcanic pluton suggest that magma was injected into fractures during periods of slight fluctuations of the lithostatic pressure (L_p) and magmatic pressure (M_p). The variations would have caused incremental fluctuations and possible reversals of the relative principal stress vectors (Fig. 2.42).

A model involving pressure fluctuations was proposed by McCarthy and Thompson (1988) in order to explain the intrusion of horizontal sills in an extensional terrain. In a tectonically extensional volcanic environment, dikes would be intruded vertically, perpendicular to the least principal stress direction. Figure 2.42A and B shows how two perpendicular, interconnected dikes form due to a horizontal rotation in the least principal stress direction. The two main dike orientations observed in the Flavrian (WNW-NW and ENE) indicate that a horizontal rotation of about 90° in the least principal stress vector occurred during dike intrusion. Horizontal rotation of the least principle stress vector may have been caused by a number of events including dilation of wall rock during magma ascent (Iida and Kumazawa, 1986), variable loading or variations in the regional stress field. If the lithostatic stress became least (vertical least principal stress), sill intrusion would occur (Fig. 2.42C). In this case,

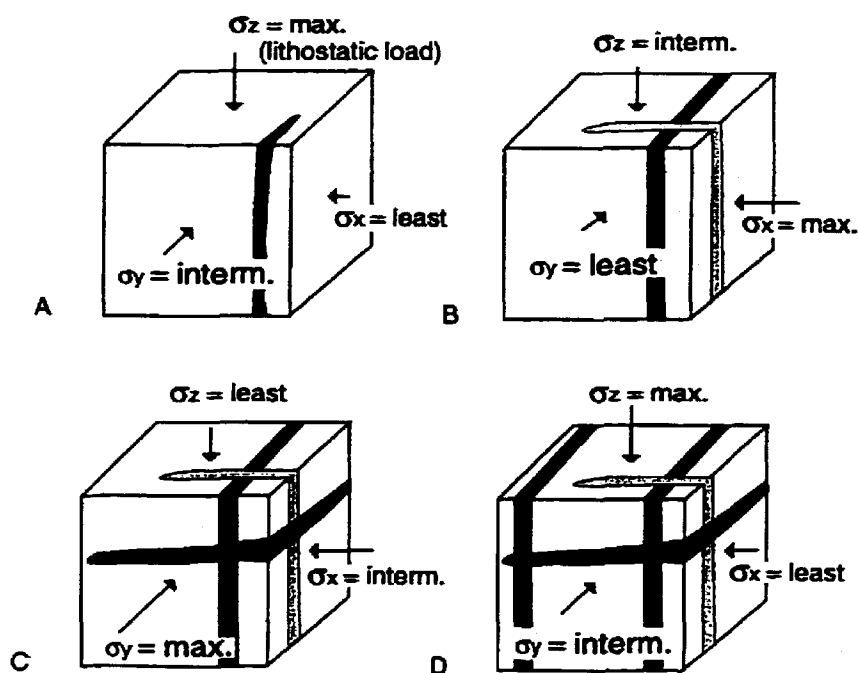


Figure 2.42: Schematic explanation for the intrusion of horizontal sills fed by vertical dikes, after McCarthy and Thompson (1988): A) dike intruding perpendicular to σ_x , the least principal stress; B) horizontal rotation of least principle stress from σ_x to σ_y , a new dike intrudes perpendicular to σ_y ; C) vertical rotation of least principle stress until σ_z becomes least, in which case subhorizontal sills are emplaced; and D) least principle stress reverses back to the situation where σ_x is least, creating another vertical dike perpendicular to σ_x .

magma pressure would be strong enough to float the overlying column of rocks, i.e., $M_p = L_p$ and sills would form. Figure 2.42D presents the results of a renewed rotation of the least principal stress vector following development of sills.

This model suggests that slight pressure fluctuations can determine the geometry of an intrusion. Slight pressure fluctuations at the HNB would cause a change in the relative magnitudes of the principal stress vectors, disrupting equilibrium. Fluctuations could be caused by variations of the lithostatic pressure (L_p) due to loading, dike inflation (as described by McCarthy and Thompson, 1988), rupture of the magmatic reservoir by seismic relief (leading to extrusion), magma replenishment, variations of magma flow rates (extrusion or replenishment), and far-field structural effects such as regional extension. Relative pressure variations may have caused cyclical changes that affect the HNB incrementally. Therefore, the HNB controls the level at which the subvolcanic magma reservoir is developed, however, the exact shape and form (sill, dike) that the magma takes, although regulated by and developed along the HNB, also depends on parameters influencing the balance between lithostatic pressure (loading) and magma pressure. For example, magma intruded along the HNB may occur in the form of dikes (as is the case for dikes intruding the rift zones at Kilauea) or sills where continued magma influx to a chamber leads to fluid pressures above lithostatic and sill inflation (Ryan, 1988). The dike-and-sill relations shown in Figures 2.18, 2.21, 2.29, 2.30, 2.31 and 2.34 are common throughout the pluton and provide evidence for multiple episodes of

extension along WNW to NW, ENE and subhorizontal planes during the emplacement of the entire Flavrian pluton.

The diverse yet consistent orientations of the Flavrian sills and dikes, along with their sharp contacts, suggest a structurally controlled emplacement. Intrusions possibly occurred along preexisting planes of weakness such as fractures or faults, as indicated by the sharp and angular dike segments. Intrusions along the three principal extensional planes, as demonstrated by the model in Figure 2.42, is compatible with emplacement governed by an extensional tectonic environment.

Shape of the pluton and relationship to host volcanic rocks

Several models of pluton emplacement have been suggested which are based on the internal and external contact relationships of plutons. Intrusion is forceful when the surrounding rocks are deformed by the rising pluton, and passive if the host rocks are not affected by the emplacement of the magma body. Furthermore, whether an intrusion is emplaced forcefully or passively depends on the host-rock rheology or more specifically on the viscosity contrast between the magma and the surrounding rock body. The intensity of viscosity contrast may be evaluated in the field from intrusion-related deformation characteristics, and it is assumed to have been low where the enveloping rocks are concordantly wrapped around the pluton, as in the case of diapiric emplacement (Pitcher, 1987). Examples of diapiric ascent are given by Billings (1945), Buddington (1959), Stephansson and Johnson (1976), Coward (1981), Schwerdtner et al. (1983), Bateman (1984, 1985), Castro (1985), Ramsay

(1989) and Paterson and Fowler (1993), although the ascent mechanism is now disputed (Schwerdtner, 1990; Clemens and Mawer, 1992). On the other hand, viscosity contrast was high if the internal structures of the pluton are discordant with the surrounding rocks (Billings, 1945; Buddington, 1959; Pitcher and Berger, 1972; Myers, 1975; Castro, 1987). Generally, ductility contrasts are high in the upper levels of the crust and low at deeper levels, although areas showing evidence of both brittle and ductile mechanisms at a single level in the crust have been reported (Pitcher and Berger, 1972; Pitcher, 1979; Davies, 1982). Where both brittle and ductile behavior occurred, the plutons commonly intruded major faults and shear zones where variable fluid pressures had an important influence on ductility (Sylvester et al., 1978; Castro, 1985; 1986; Guineberteau et al., 1987; Hutton, 1988; Hutton et al., 1990).

The sharp contacts between phases internal to the Flavrian pluton and between the pluton and the host volcanic rocks, along with the presence of numerous dikes, suggest a high level, brittle environment of emplacement where ductility contrasts between the magma and host rocks were high. However, the Flavrian pluton shows a relatively concordant relationship with the overlying volcanic rocks of the Noranda cauldron, suggesting a passive mode of intrusion. The seemingly contradictory characteristics of concordance and high level emplacement are explained by the fact that the Flavrian pluton is syn-volcanic (Goldie, 1976; Paradis et al., 1988), simultaneously intruding at a high level in the crust and producing its own volcanic pile at surface. Considering that the surrounding host rocks were not significantly deformed by intrusion of the Flavrian pluton, the ascending magma apparently filled

voids (fractures) within the volcanic rocks. The filling of fractures is best explained by passive intrusion in an environment dominated by extensional tectonics. Emplacement in an extensional tectonic environment is supported by the geometrical relationship between dikes and sills that indicate three alternating directions of extension for a single intrusive unit.

Another significant relation between the Flavrian pluton and the overlying volcanic rocks is the coincidence in orientation between steeply dipping dikes, as depicted in Figure 2.28, and the steeply dipping syn-volcanic faults or fractures in the area of the Noranda cauldron (Fig. 2.37). The WNW- to NW- and ENE-trending steeply dipping dikes correspond closely in orientation with the faults that control the location of VMS deposits (e.g., the McDougall and Despina faults and the Old Waite structure). These orientations also coincide with the orientations of the steeply dipping contacts of the Flavrian pluton with the host volcanic rocks (e.g., the Hunter Creek and McDougall-Despina faults). The coincidence in orientation of steeply dipping contacts of the Flavrian pluton, of dikes within the pluton and of syn-volcanic faults and fractures within the overlying volcanic rocks suggest that emplacement of both the pluton and volcanic rocks were governed by extensional tectonics. The close agreement in orientation between these structures also suggests that important information concerning the geometry of syn-volcanic faults and fractures may be gained by mapping the underlying subvolcanic pluton, recognizing of course that these relations could be distorted by later deformation.

Model for intrusion of the Flavrian pluton

Plutons emplaced at high crustal levels (i.e., subvolcanic plutons; see Billings, 1945; Buddington, 1959; Pitcher and Berger, 1972) are commonly emplaced by one or more of the following mechanisms: stopping, dike propagation and/or cauldron subsidence. A subvolcanic or high-level emplacement model is supported by the episodic nature of magmatic pulses and the rapid changes in pressure and temperature that governed the intrusion of the Flavrian pluton. The model is consistent with development of a magma chamber at a near-surface HNB due to the inferred low density of the early trondhjemite magma. It is also compatible with the constant relation between the orientation of magma ascent via dikes and the systematically oriented faults and fracture system created during subsidence in a regional extensional tectonic regime.

From measured fault offsets and stratigraphic reconstruction, Gibson and Watkinson (1990) interpreted the Noranda cauldron to have subsided asymmetrically, with a minimum of 0.5 km displacement along its northern margin and 1.2 km along its southern margin during the eruption of the Cycle 3 or Mine Sequence volcanic rocks. The uneven subsidence appears to have been compensated for by the unequal thickness (500 m in the north and 1200 m in the south) of the underlying Flavrian intrusion, as demonstrated by gravity models (Bellefleur, 1992). These observations suggest a link between subsidence and intrusion and indicate that the thickest part of the pluton coincides with the area where cauldron subsidence was greatest. This relationship may suggest that the magma chamber was asymmetric and that chamber

inflation and deflation were greater where the magma chamber and residual magma was thickest. Alternatively, the uneven thickness could be the result of southward regional tilting of a uniformly thick pluton by either volcanic or tectonic forces, and differential erosion of the northern part of the pluton. Field observations and petrographic studies indicate that both the northern and southern parts of the Flavrian pluton contain large portions of granophyre suggesting that the erosion level is similar for the north and south, favoring an asymmetrically shaped magma chamber. An asymmetric magma chamber is in agreement with interpretations of Gibson and Watkinson (1990) who suggest that the south margin of the cauldron was more structurally and volcanically active and characterized by greater subsidence. Evidence linking subsidence and intrusion is also shown in Figure 2.38 from which Watkins (1980) and Knuckey and Watkins (1982) demonstrated that the rock units on the west side of McDougall-Despina faults dropped at least 700 m relative to the east side before intrusion of the Flavrian early trondhjemite.

In summary, the evidence and interpretations presented above suggest that the Flavrian pluton is a composite sill-shaped intrusion emplaced at high crustal levels during asymmetric subsidence of a cauldron (Fig. 2.43). This interpretation is supported by Spence and de Rosen-Spence (1975) and Gibson and Watkinson (1990) who suggest that volcanism in the Noranda cauldron was piecemeal and coeval with progressive subsidence. Emplacement in an extensional tectonic regime is supported by the geometry of the numerous dikes and sills, by the concordant relation between the pluton and the surrounding volcanic rocks, and by an observed link between

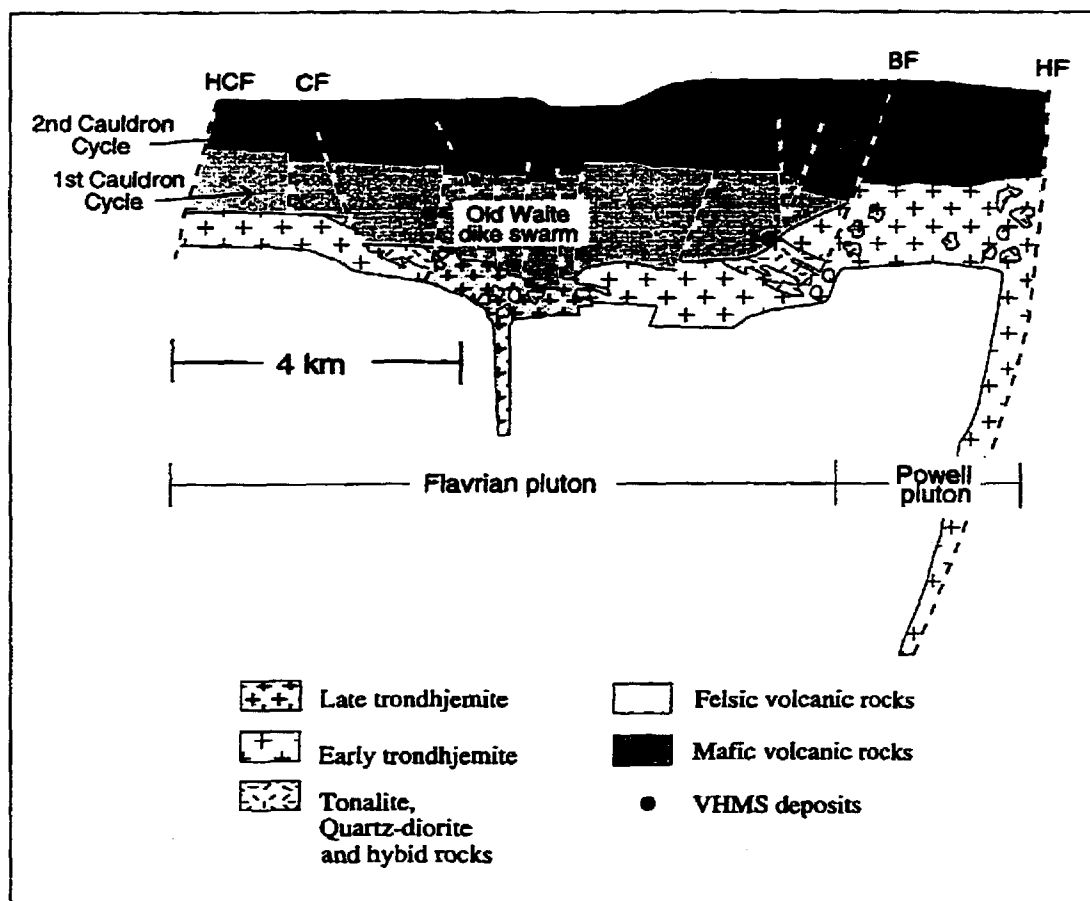


Figure 2.43: Composite cross-section of the Noranda cauldron, after Gibson and Watkinson (1990). Geology of volcanic rocks are interpreted from section A-A' of Figure 2.37; geology of pluton, from section B-B'. Abbreviations: (HCF) Hunter Creek Fault, (CF) Cranston Fault, (MF) McDougall Fault, (DF) Despina Fault, (BF) Beauchastel Fault, (HF) Horne Creek Fault. Vertical scale same as horizontal scale.

subsidence and intrusion. This concept is consistent with the interpretation of subsidence in response to a partial evacuation of an underlying magma chamber, now represented by the Flavrian pluton (Goldie, 1976; Gibson and Watkinson, 1990).

CHAPTER 3

CHAPTER 3. GEOCHEMISTRY OF THE FLAVRIAN PLUTON

3.1 Introduction

The objectives of this chapter are to (1) characterize each of the lithologic phases within the pluton in terms of their major element, trace element and rare earth element (REE) geochemistry, (2) describe groupings, trends and breaks in trends of geochemical data, and (3) discuss and interpret results. The data used in this chapter are presented in Appendix IV. Forty-four samples collected from the various phases of the Flavrian pluton were prepared for analysis by the author. Data from three samples of quartz-diorite are from Paradis et al. (1988). Sample locations are presented in Appendix I. The objectives of this chapter are to (1) characterize each of the lithologic phases within the pluton in terms of their major element, trace element and rare earth element (REE) geochemistry, (2) describe groupings, trends and breaks in trends of geochemical data, and (3) discuss and interpret results. The data used in this chapter are presented in Appendix IV.

3.1.1 Sample preparation, method of analysis and precision

Thirty-six of the forty-seven analyzed samples were collected in the field by the author. Samples SP-8, SP-15, SP-20, SP-43, SP-51-82, SP-67, SP-71a and SP-75 were collected earlier by Suzanne Paradis (1984) for a M.Sc. thesis. These samples were prepared and analyzed by the author. Data from samples SP-28, SP-70 and FL-3 are from Paradis et al. (1988).

Samples measuring about 20 to 25 cm across were collected from outcrops using a sledgehammer. Samples were split into 4 cm fragments using a hydraulic splitter. Care was taken to rid all samples of visible veining or alteration. Two stages of crushing, and pulverizing using an agate shatterbox were conducted to produce the desired powders. The crushers and shatterbox were thoroughly cleaned (first with high-pressure air and then ethanol) and pre-contaminated with the sample to be analyzed for each individual preparation. Silica powder was also used as a pre-contaminant in the shatterbox.

Analysis of major element concentrations (Si, Ti, Al, Fe, Mg, Ca, Na, K and P) as well as Cr, V and Ba, were obtained from glass pellets using X-ray fluorescence (XRF) techniques at McGill University. Pellets were produced from dry sample powders were mixed with a lithium tetraborate flux, then fused and quenched (see Norrish and Hutton (1969) for a detailed description of methods used in sample preparation). Detection limits are 0.01% for major elements, 15 ppm for Cr and 10 ppm for V and Ba.

Trace element analyses (Cr, Ni, Cu, Zn, Rb, Sr, Nb, Y and Zr) were conducted on powder pellets made by combining sample powder with a polyvinyl glue and boric acid powder. The mixture was then compressed into a pellet at about 12 tonnes of pressure. Trace element concentrations were determined by XRF at the Université de Montréal, with a typical analytical precision of about 5%. REE and other trace elements (Th, U, Ba, Hf, Ta, Sc, Cs and W) were analyzed by instrumental neutron activation analysis (INAA) using the SLOWPOKE II nuclear reactor at the l'École

Polytechnique de Montréal. Samples were irradiated for 4 hours and counted for a period of over a month. Precision is about 5% for trace elements and the light rare earth elements (LREE), whereas it is about 10% for Ce, Nd, Ho, Lu and Tb.

Sample preparation and major and trace element analyses of samples 93-02 and 93-02a were conducted at Activation Laboratories (ACTLABS), Ancaster, Ontario. Samples were analyzed by inductively coupled plasma emission spectrometry on fused powders (ICP-fusion). ACTLABS quotes a detection limit of 0.01% for major elements, whereas the detection limits for trace elements are shown in parenthesis as follows: Ba (2 ppm), Sr (2 ppm), Rb (2 ppm), Y (2 ppm), Zr (2 ppm), Nb (2 ppm), Ga (5ppm), Ni (1 ppm), V (5 ppm), Sn (5 ppm), S (50 ppm), and Cu (1 ppm), Pb (5 ppm), Zn (1 ppm), Ag (0.4 ppm), Cd (0.5 ppm), Bi (5 ppm) and Be (2 ppm). Other trace and rare earth elements were analyzed by INAA with similar detection limits as samples analyzed at l'École Polytechnique.

3.2 Description of Geochemical Characteristics of Intrusive Phases

3.2.1 Méritens quartz-diorite

Whole-rock major element analyses indicate that some of the Méritens quartz-diorite samples actually plot as tonalite. The difficulty in obtaining true Méritens quartz-diorite samples in the field supports descriptions presented in CHAPTER 2 indicating the diffuse and ill-defined nature of the contacts between Méritens quartz-diorite and tonalite. As a result, geochemical data from three samples of Méritens

quartz-diorite from Paradis et al. (1988), samples SP-28, FL-3 and SP-70, were added to our database.

Méritens quartz-diorite is characterized by 49.69 to 57.25% SiO_2 and is the most mafic phase of the pluton (see Figure 3.1 for major element variations). TiO_2 concentrations vary between 0.94 and 1.26%, which are low values compared to the Eldrich diorite (1.6% TiO_2) and therefore permit a distinction to be made between the two intrusive phases. However, TiO_2 concentrations fall within the range characteristic of tonalite. Méritens quartz-diorite is further characterized by relatively high Al_2O_3 (15.26 to 20.11%), Fe_2O_3^* (between 7.44 to 13.36%), MgO (3.96 to 6.90%) and CaO (7.59 to 11.11%) compared to other phases that compose the pluton. A single Méritens quartz-diorite sample contained 0.15% MnO , which is low compared to Eldrich diorite. Na_2O concentrations are generally lower in Méritens quartz-diorite compared to tonalite, with concentrations ranging between 2.54 and 4.08%. K_2O concentrations are not diagnostic and range between 0.14 and 0.53%, and P_2O_5 concentrations vary between 0.09 and 0.44%.

Méritens quartz-diorite may be distinguished from tonalite and other more felsic phases in the pluton by its relative enrichment in compatible trace elements such as Cr (14 to 124 ppm), Ni (25 and 90 ppm) and Co (23 to 41 ppm) (see Figure 3.2 for compatible trace element variations). On the other hand, concentrations of

* Fe_2O_3 includes FeO converted to Fe_2O_3

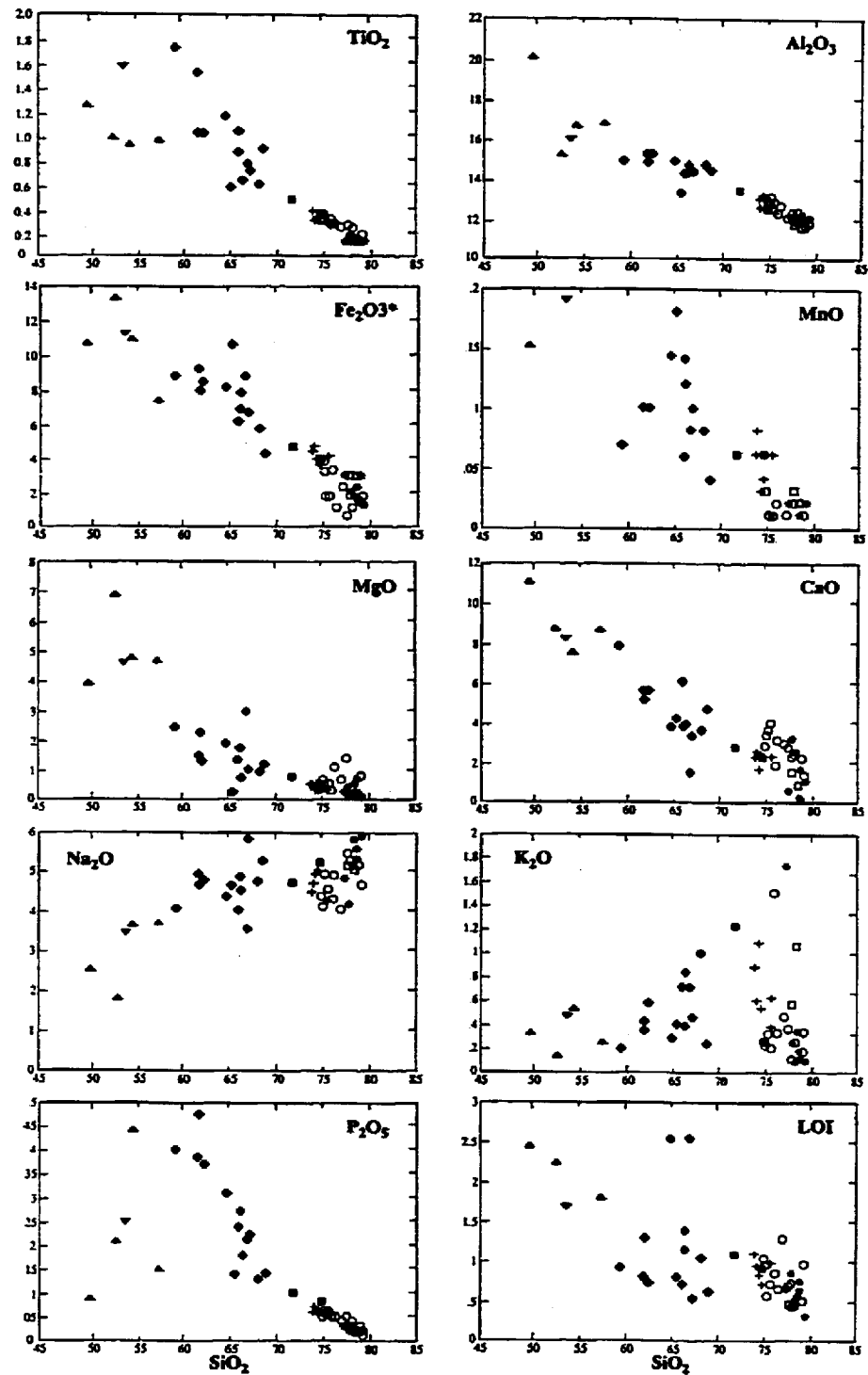


Figure 3.1: Major element variation diagrams of intrusive phases of the Flavrian pluton. Δ = Méritens quartz-diorite; \bullet = tonalite; \blacksquare = trondhjemite porphyry; \square = pink trondhjemite; \circ = coarse-grained trondhjemite; \ast = granophyre; ∇ = Eldrich diorite; \dagger = late trondhjemite. Concentrations in weight %.

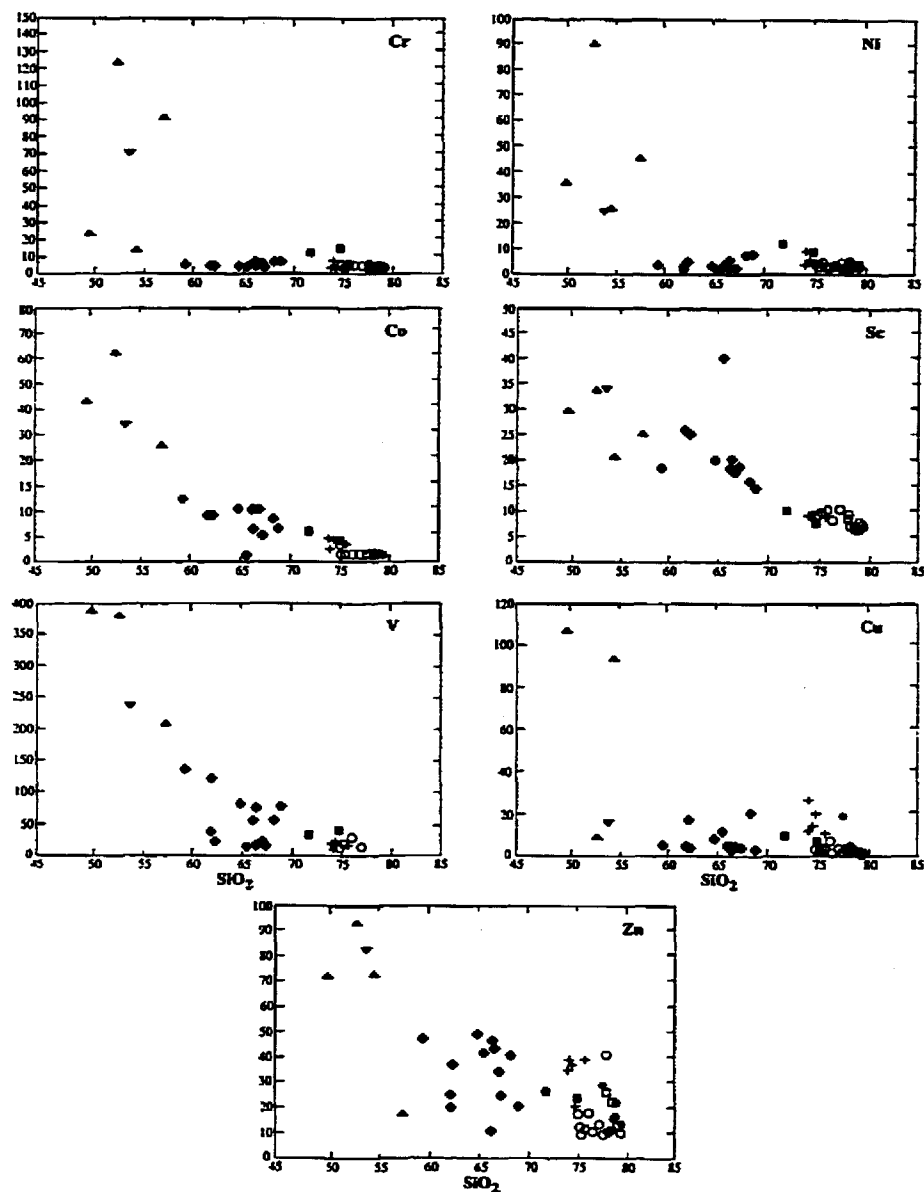


Figure 3.2: Compatible trace element variation diagrams of intrusive phases of the Flavrian pluton. \blacktriangle = Méritens quartz-diorite; \blacklozenge = tonalite; \blacksquare = trondhjemite porphyry; \square = pink trondhjemite; \circ = early coarse trondhjemite; $*$ = granophyre; ∇ = Eldrich diorite, $+$ = late trondhjemite. SiO_2 in weight % and trace elements in ppm.

these elements for the Méritens quartz-diorite fall in the range of those for Eldrich diorite. Equally, relatively higher V concentrations (209 to 389 ppm) within Méritens quartz-diorite distinguish it from tonalite; however, it does not differentiate it from Eldrich diorite. Cu concentrations are generally below 20 ppm in all phases of the Flavrian pluton. However, two samples of Méritens quartz-diorite contain 100 ppm Cu, considerably higher than other more felsic phases. In addition, Méritens quartz-diorite and Eldrich diorite are significantly enriched in Zn (70 to 95 ppm) relative to more felsic phases of the pluton which contain no more than 50 ppm.

Méritens quartz-diorite contains lower concentrations of Nb (4.4 to 8 ppm), Y (12 to 18 ppm), Zr (43 to 115 ppm) and Hf (0.9 to 2.7 ppm) than tonalite (see Figure 3.3). Therefore, a clear chemical distinction can be made between the two intrusive phases. Concentrations of Ta and Th are also generally lower in Méritens quartz-diorite than in tonalite, however, there is significant overlap.

Méritens quartz-diorite and Eldrich diorite cannot be distinguished on the basis of their respective REE concentrations (Fig. 3.4). However, Eu and, to a lesser extent Yb and Lu, are slightly enriched in the Eldrich diorite relative to Méritens quartz-diorite. REE abundances increase systematically between samples 92-76 and SP-28 for Méritens quartz-diorite (Fig. 3.4). REE patterns are slightly fractionated and do not show significant depletion in Eu (Fig. 3.5). Fractionation of the LREE is reflected in La/Yb ratios (Fig. 3.6A and 3.6B) that vary from 3.9 for sample 92-76 to 7.4 for sample SP-28. The increase in the La/Yb ratio correlates with increasing SiO₂

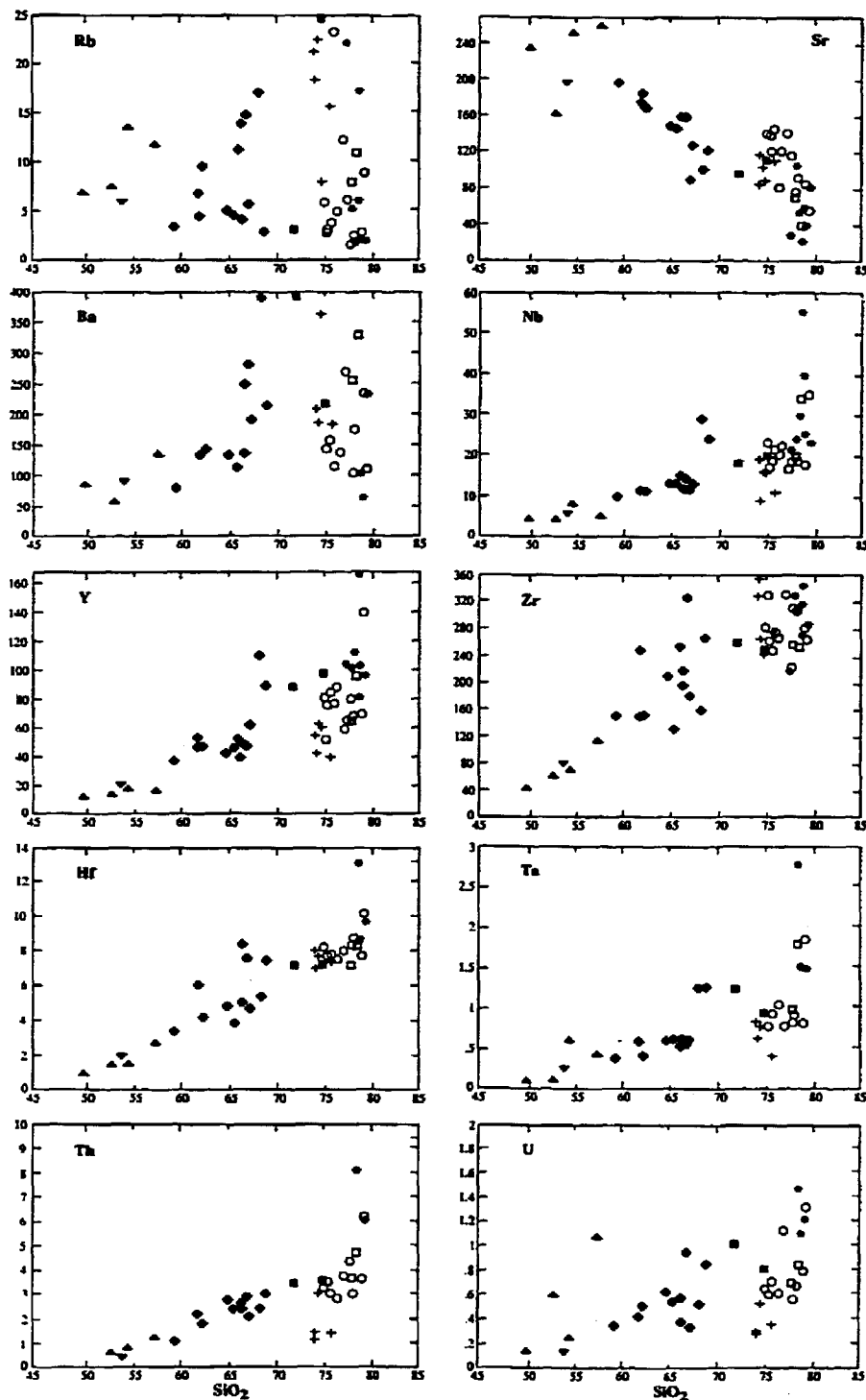


Figure 3.3: LILE and incompatible trace element variation diagrams of intrusive phases of the Flavrian pluton \blacktriangle = Méritens quartz-diorite; \blacklozenge = tonalite; \blacksquare = trondhjemite porphyry; \square = pink trondhjemite; \circ = early coarse trondhjemite; $*$ = granophyre; ∇ = Eldrich diorite; $+$ = late trondhjemite. SiO_2 concentrations in weight % and trace elements in ppm.

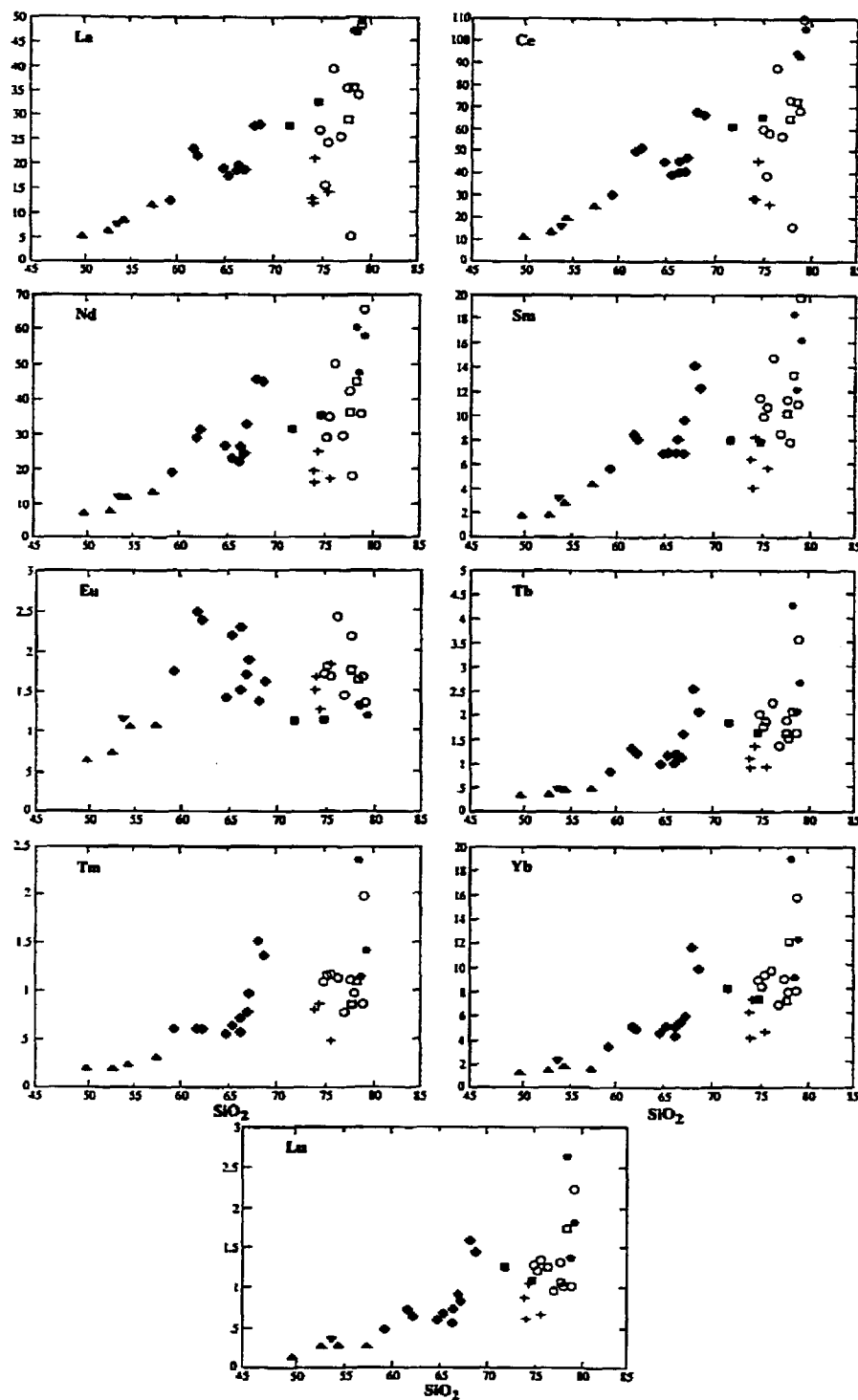


Figure 3.4: Rare earth element variation diagrams of intrusive phases of the Flavrian pluton. \blacktriangle = Méritens quartz-diorite; \blacklozenge = tonalite; \blacksquare = trondhjemite porphyry; \square = pink trondhjemite; \circ = early coarse trondhjemite; \bullet = granophyre; \blacktriangledown = Eldrich diorite; \blackdagger = late trondhjemite. SiO₂ concentrations in weight % and REE in ppm.

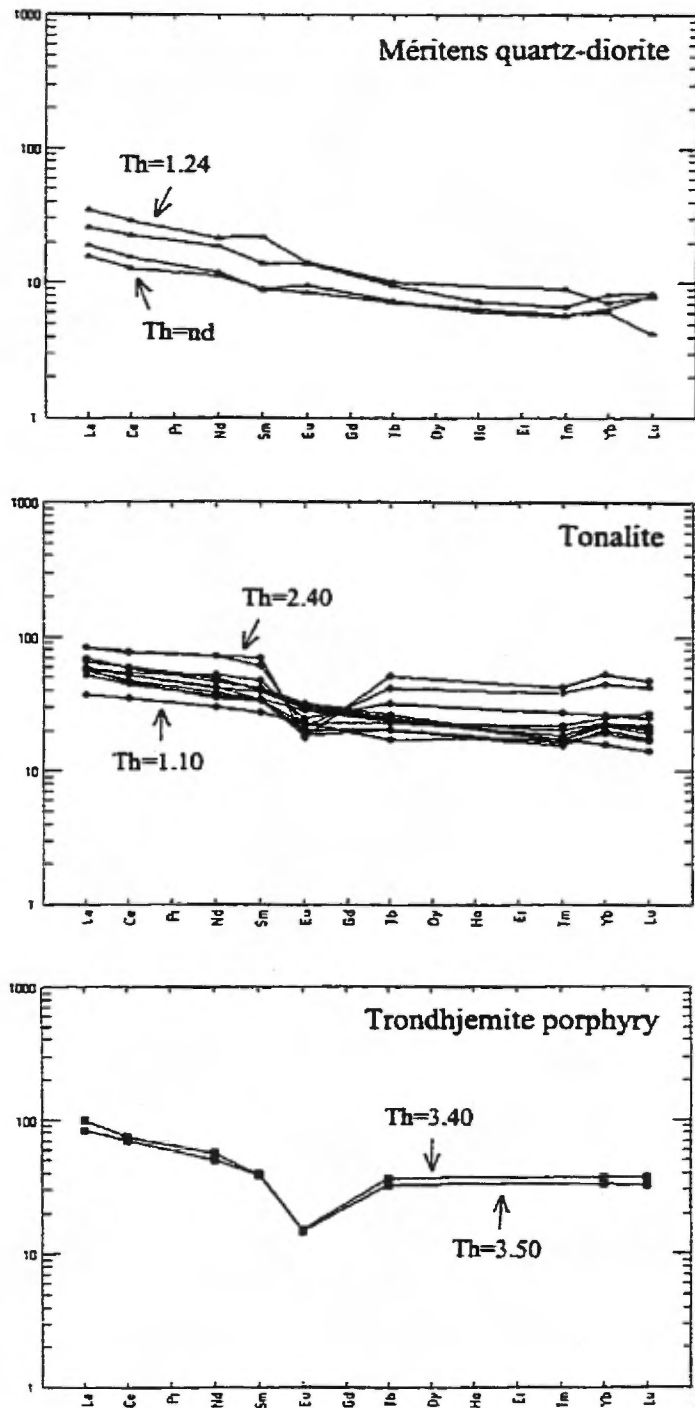


Figure 3.5: Chondrite-normalized REE patterns of Méritens quartz-diorite, tonalite and trondhjemite porphyry. Th concentrations in ppm: nd = not detected. Normalization factors from Sun (1982).

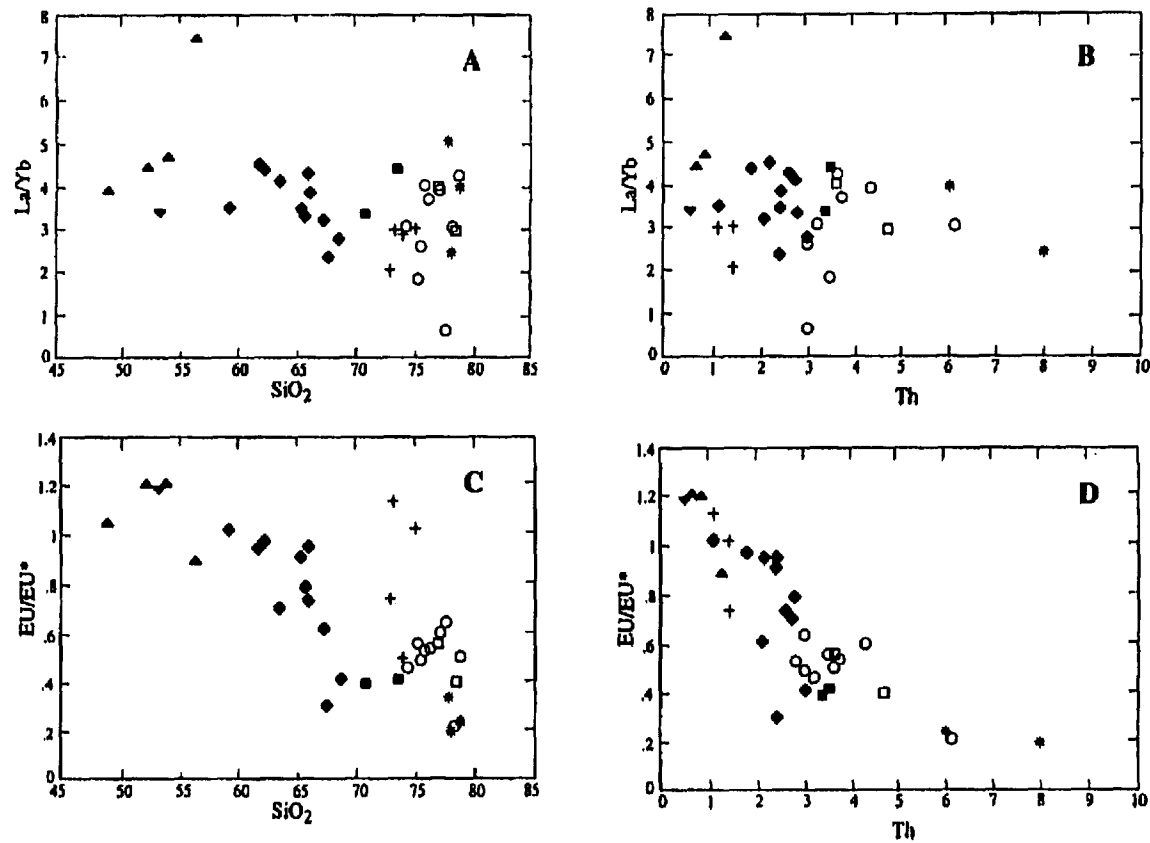


Figure 3.6: La/Yb and Eu/Eu* vs SiO₂ and Th diagrams of intrusive phases of the Flavrian pluton. * = Méritens quartz-diorite; • = tonalite; ◐ = trondhjemite porphyry; ◑ = pink trondhjemite; ◒ = early coarse trondhjemite; ◓ = granophyre; ◔ = Eldrich diorite; + = late trondhjemite. SiO₂ concentrations in % and other trace elements concentrations in ppm. Eu* calculated by linear interpolation between Sm and Tb.

and to a lesser extent Th. The REE patterns Eu/Eu^* range between 0.9 to 1.2 (Fig. 3.6C and 3.6D).

3.2.2 Tonalite and hybrid rocks

Tonalite and hybrid rocks are intermediate in composition between Méritens quartz-diorite and trondhjemite. The textural variety that characterizes tonalite (see Section 2.2.2) is reflected in its chemical signature. Analyses were conducted on tonalite samples showing various textures i.e. homogeneous, spotted, heterogeneous and hybrid in order to obtain data representing the textural variety. In this descriptive section of the chapter, the various tonalites and hybrid rocks will be simply referred to as tonalite. A discussion of the various geochemical signatures of tonalite is presented in Section 3.2.2.

Tonalite ranges between 59.3 and 68.8% SiO_2 and shows relatively well-developed negative correlations for TiO_2 , Al_2O_3 , $Fe_2O_3^*$, CaO, P_2O_5 with SiO_2 (see Figure 3.1), although significant scatter is observed. MnO and MgO show ill-defined negative correlations with SiO_2 , with significant variabilities in abundances. TiO_2 , Al_2O_3 , $Fe_2O_3^*$ and P_2O_5 concentrations in tonalite are distinctively higher than for the various trondhjemites that compose the pluton. Although MnO concentrations are low and near detection limits, two trends are observed on the MnO vs SiO_2 plot for tonalite: (1) a positive correlation with SiO_2 between 0.07% MnO and 0.18% MnO; and (2) a well-defined negative correlation with SiO_2 between 0.18% MnO and 0.04% MnO. Therefore, an inflection point occurs at 0.18% MnO. The inflection point corresponds to a $Fe_2O_3^*$ and MnO high and a TiO_2 and MgO low for tonalite. MnO

concentrations are higher for tonalite than for pink trondhjemite, coarse-grained trondhjemite and granophyre. However, MnO concentrations within tonalite overlap with those of trondhjemite porphyry and late trondhjemite. Significant scatter is observed in tonalite for Na₂O and K₂O concentrations when plotted against SiO₂ (Fig. 3.1). Values range between 2.73 and 5.89% Na₂O and 0.21 and 0.99% K₂O.

Cr and Ni concentrations in tonalite (Fig. 3.2) are relatively low (less than 7 ppm). However, a slight increase in Ni concentration (7.6 ppm) is observed in the felsic end-members of tonalite which correspond to samples 92-83 and 92-88, which are inclusions of tonalite within trondhjemite. Co concentrations (1 ppm to 12 ppm) are generally higher in tonalite than in the trondhjemite phases. However, sample 92-77 is depleted in Co (1 ppm) relative to other tonalite samples. The relative Co depletion is accompanied by relative Sc enrichment in sample 92-77. V concentrations show significant scatter for tonalite (Fig. 3.2). Two separate groups are noted: (1) high-vanadium tonalite, with 57 to 135 ppm V and (2) low-vanadium tonalite, 15 to 37 ppm V. Within the low-vanadium group, sample 92-77 contains the lowest V concentration of all tonalites.

Nb and SiO₂ show a positive correlation for tonalite. However, Nb concentrations are significantly enriched relative to other tonalites in samples 92-83 and 92-88, which contain 24 and 29 ppm Nb respectively (Fig. 3.3). These samples correspond to tonalite inclusions within trondhjemite. The inclusions also are relatively enriched in Y, Ta and U. Tonalite samples in the 64.8 and 68.8% SiO₂ range show significant variations in Zr and to a lesser extent Hf concentrations (Fig.

3.3). However, apart from the tonalite inclusions (samples 92-88 and 92-83), these variations are not observed for Nb and Y, which show relatively good clusters at the 64.8 and 68.8% SiO₂ interval.

Tonalite contains higher REE abundances than Méritens quartz-diorite and Eldrich diorite; however, REE concentrations for tonalite fall in the range of the various trondhjemite phases (Fig. 3.4). The REE patterns are only slightly fractionated, with negative Eu anomalies occurring in the more differentiated tonalite and in tonalite inclusions within early trondhjemite (Fig. 3.5). La/Yb ratios range from 2.37 to 4.56 and decrease with increasing SiO₂, indicating that the REE pattern flattens with increasing SiO₂ (Fig. 3.6A and 3.6B). Eu/Eu* ranges from 1.0 for the low-silica tonalites to 0.3 for tonalite inclusions within trondhjemite (samples 92-83 and 92-88).

3.2.3 Trondhjemite porphyry

Trondhjemite porphyry contains between 71.76 and 74.82% SiO₂ and between 0.36 and 0.48% TiO₂ (Fig. 3.1). Concentrations of SiO₂, TiO₂, Fe₂O₃*, MnO and P₂O₅ within trondhjemite porphyry are generally intermediate between tonalite inclusions and pink trondhjemite, coarse-grained trondhjemite and granophyre. However, trondhjemite porphyry is similar in major element composition to late trondhjemite and a clear distinction between the two phases cannot be made on the basis of major element geochemistry.

Trondhjemite porphyry is readily distinguished from other intermediate to felsic intrusive phases in the pluton by its higher Cr concentrations (Fig. 3.2), which range between 12 and 14 ppm. Ni concentrations (12 and 9.1 ppm) also are enriched relative to other intermediate and felsic phases in the pluton. However, sample 92-44a of late trondhjemite contains similar concentrations of Ni (9.1 ppm) to trondhjemite porphyry. The intrusive phase is further distinguished from both pink and coarse-grained trondhjemite by its relatively higher Co concentration (3.9 to 5.6 ppm) (Fig. 3.2). The trondhjemite porphyry's high Fe_2O_3^* , Cr, Ni and Co concentrations compared to pink trondhjemite, coarse-grained trondhjemite and granophyre may be due to the presence of mafic inclusions (see Section 2.2.4).

In terms of high-field strength elements, trondhjemite porphyry is distinguished by relatively higher Y abundance (90 to 100 ppm) than coarse-grained trondhjemite and late trondhjemite and by slightly lower Hf concentrations (7.2 ppm) than coarse-grained trondhjemite (see Figure 3.3). In addition, trondhjemite porphyry is readily distinguished from late trondhjemite by its relatively higher Ta, Th and U concentrations.

Trondhjemite porphyry samples lie along the positive correlation trend defined by Méritens quartz-diorite and tonalite for the LREE, La (28 and 32 ppm), Ce (61 and 65 ppm) and Nd (31 and 36 ppm) on a REE vs SiO_2 plot (Fig. 3.4). Although these concentrations lie within those of pink trondhjemite and coarse-grained trondhjemite, they enable a clear distinction between trondhjemite porphyry and late trondhjemite. Consequently, late trondhjemite is typically depleted in LREE relative to

trondhjemite porphyry. Sm concentrations for trondhjemite porphyry (8 ppm) are at the low end of those exhibited by coarse-grained trondhjemite (7.8 to 20 ppm) and at the high end of those for late trondhjemite (4 to 8.2 ppm). In addition, Tb (1.6 to 1.8 ppm), Yb (7.2 and 8.1 ppm) and Lu (1.1 and 1.3 ppm) abundances are either higher or at the high end for those of late trondhjemite. Trondhjemite porphyry may be further distinguished from other trondhjemite phases by its low concentration in Eu (1.1 ppm) (see Figure 3.4). Eu concentrations of trondhjemite porphyry are among the lowest of all trondhjemite phases. The REE pattern for trondhjemite porphyry is slightly fractionated and shows a pronounced negative Eu anomaly (Fig. 3.5). La/Yb ratios for trondhjemite porphyry are 3.40 and 3.48, values which are distinctively more LREE-fractionated than the La/Yb ratios of 2.06 to 3.05 of late trondhjemite (Fig. 3.6A and 3.6B). Eu/Eu* values are 0.39 and 0.42, indicating that the relatively well-developed negative Eu anomalies in both trondhjemite porphyry samples are generally not apparent in late trondhjemite (Fig. 3.6C and 3.6D). REE abundances and ratios enable a clear distinction to be made between trondhjemite porphyry and late trondhjemite.

3.2.4 Pink trondhjemite

Pink trondhjemite ranges between 77.80 and 78.44% SiO₂. This range is within the spectrum of SiO₂ concentrations for granophyre and at the high end of SiO₂ concentrations for coarse-grained trondhjemite. The high SiO₂ content clearly distinguishes pink trondhjemite from porphyritic and late trondhjemites (see Figure 3.1). Pink trondhjemite is readily distinguished from other phases in the pluton by its relatively low Al₂O₃ concentrations (between 11.60 and 11.75%), which are the

lowest of any phase of the pluton. Similarly, the pink trondhjemite's low MgO concentrations (0.1%) are among the lowest observed in the pluton. Pink trondhjemite and granophyre are similar in terms of their low concentrations of TiO_2 (0.14 to 0.16%), CaO (0.81 to 1.52%) and P_2O_5 (0.02 to 0.03%) relative to porphyritic trondhjemite, coarse-grained trondhjemite and late trondhjemite. In addition, relatively high Fe_2O_3^* concentrations in the pink trondhjemite (2.92%) compare with the high end of Fe_2O_3^* concentrations for granophyre; but are distinctively lower than Fe_2O_3^* concentrations in trondhjemite porphyry and late trondhjemite. The relatively high Fe_2O_3^* content of pink trondhjemite reflects its magnetic character (see Section 2.2.4). Lower MnO (0.03%) also distinguishes pink trondhjemite from trondhjemite porphyry and late trondhjemite.

On REE vs SiO_2 diagrams (see Figure 3.4), La (29 to 35 ppm), Ce (65 to 72 ppm) and Nd (36.4 to 72 ppm) abundances within pink trondhjemite are intermediate between those of granophyre, which are higher, and late trondhjemite which are lower. Sm concentrations within pink trondhjemite (10.2 and 13.3 ppm) are distinctively higher than within late trondhjemite (4 to 8.2 ppm). Pink trondhjemite is further distinguished from late trondhjemite by the relative abundance of heavy rare earth elements (HREE), which are generally higher (with some overlap) for pink trondhjemite. Eu (1.7 to 1.8 ppm), Tb (1.6 to 2 ppm) and Tm (0.9 and 1.1 ppm) concentrations within pink trondhjemite are at the low end of concentrations for granophyre and therefore provide further distinction between the two phases (Fig. 3.4). The REE pattern is slightly fractionated and shows a pronounced negative Eu anomaly (Fig. 3.7). Its abundance in HREE is reflected in an upward shift in the

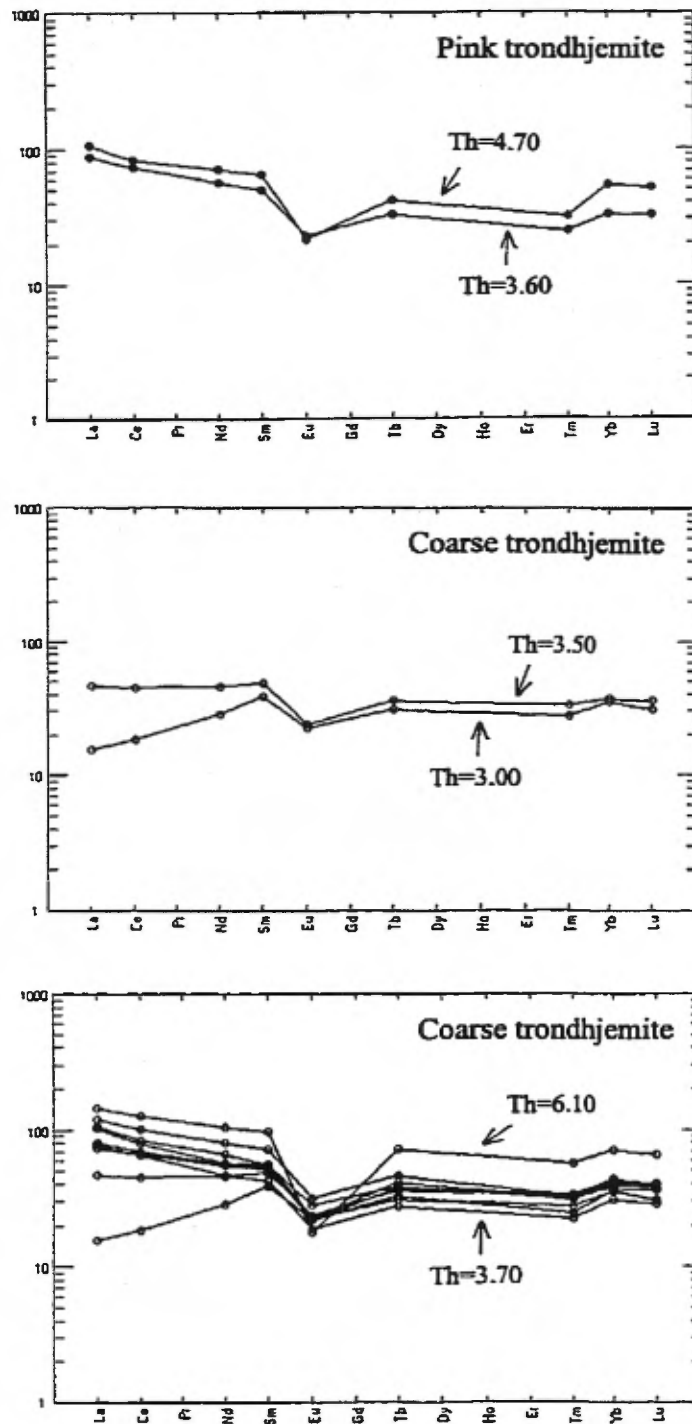


Figure 3.7: Chondrite-normalized REE patterns of pink and coarse-grained trondhjemite. Th concentrations in ppm. Normalization factors from Sun (1982).

pattern for Yb and Lu. The La/Yb ratios for pink trondhjemite (2.97 and 4.07) are not distinctive and are within the range of ratios for other intrusive phases (Fig. 3.6A and 3.6B). The negative Eu anomalies are reflected in the Eu/Eu* ratios of 0.4 to 0.56.

3.2.5 Coarse-grained trondhjemite

The suite of coarse-grained trondhjemite samples ranges between 75.00 and 79.16% SiO₂ and between 0.13 and 0.35% TiO₂ (Fig. 3.1), which is generally lower than trondhjemite porphyry but higher than pink trondhjemite and granophyre. Concentrations of Fe₂O₃* (between 0.62 and 3.82%) and MnO (0.01 to 0.03%) within Coarse-grained trondhjemite are generally lower than for trondhjemite porphyry and late trondhjemite. In addition, lower P₂O₅ concentrations (0.01 to 0.06%) also distinguish coarse-grained trondhjemite from trondhjemite porphyry.

Coarse-grained trondhjemite is characterized by relatively large variations in LREE abundance. La (5.1 to 48 ppm), Ce (16 to 109 ppm) and Nd (18 to 66 ppm) (Fig. 3.4) vary significantly. The Sm abundance within coarse-grained trondhjemite is clearly higher than within late trondhjemite, enabling a clear distinction to be made between the two phases. The distinction is further supported by slightly higher abundances of HREE in the coarse-grained trondhjemite compared to late trondhjemite. Apart from sample 92-95, HREE show much less variation compared to the LRRE in coarse-grained trondhjemite. HREE values (Tm = 1 ppm, Yb = 8 ppm and Lu = 1.2 ppm) tend to cluster and are not as scattered.

Coarse-grained trondhjemite La/Yb ratios vary between 0.66 and 4.32, showing significant variation over a restricted SiO₂ range and to a lesser extent Th intervals (Fig. 3.6A and 3.6B). The large variation in La/Yb ratios is caused by variations in La (see Figure 3.4). LREE mobility has been documented within the alteration zone associated to the Ansil deposit (Barrett et al., 1991) and is interpreted to have resulted from high temperature alteration of the host rocks beneath Ansil. The LREE depletions are typical of rocks that were subjected to high temperature alteration; whereas LREE additions reflect precipitation of the LREE at lower fluid temperatures (MacLean, 1988). The breccia texture, characteristic of coarse-grained trondhjemite, is interpreted to have resulted from separation of an aqueous fluid phase (see Section 3.5). This fluid probably interacted with the crystallized and molten parts of the early coarse-grained trondhjemite, effectively remobilizing the LREE.

Samples 92-100 and 92-87 showing significantly lower La concentrations than other coarse-grained trondhjemites. A slightly positive (92-87) to obviously positive (92-100) slope shown by the chondrite normalized LREE in these two samples differs from other coarse-grained trondhjemite which show negative slopes for the LREE (Fig. 3.7). These variations are reflected in their odd-shaped REE patterns. Both samples are essentially composed of quartz and albite set in a magmatic breccia texture (see CHAPTER 2), with minor amounts of actinolite, epidote, sericite, apatite and zircon. Shattered and resorbed quartz crystals lie in an albite matrix. Albite is moderately altered to epidote and sericite; however, twinning planes are visible. Similar LREE depleted patterns are reported from samples of oceanic plagiogranite in the Troodos ophiolite (Coleman and Peterman, 1975; Kay and Senechal, 1976). Two

hypotheses may explain the LREE-depleted samples: (1) they represent a separate intrusion of trondhjemite, or (2) they are coarse-grained trondhjemite subjected to a secondary or late magmatic process that depleted the LREE. The presence of abundant quartz-epidote veins and orbicules within the coarse-grained trondhjemite suggests that high temperature fluids (supercritical?) altered the intrusive phase. These late magmatic fluids may have mobilized the LREE, causing the wide range of La/Yb ratios. The REE patterns show negative Eu anomalies that increase with increasing REE abundance (Fig. 3.7). Eu/Eu* range between 0.21 and 0.64 and do not show any definitive correlations with SiO₂ or Th (Fig. 3.6C and 3.6D). These fluids may have enhanced the europium anomaly in coarse-grained trondhjemite through the breakdown of plagioclase.

Sample 92-95 contains the highest abundance of REE and the most significant Eu anomaly of all coarse-grained trondhjemites, and the REE pattern of this sample 92-95 resembles that of granophyre (Fig. 3.7). Consequently, although it is coarse-grained, sample 92-95 shows all the geochemical characteristics of granophyre. Therefore, the granophyre intrusion may have some coarse-grained geochemical equivalents that are indistinguishable in the field from early coarse-grained trondhjemite.

3.2.6 Granophyre

SiO₂ contents within granophyre range between 77.90 and 79.23%. This range falls at the high end of coarse-grained trondhjemite concentrations and distinctively higher than trondhjemite porphyry and late trondhjemite (Fig. 3.1). Al₂O₃ (from 1.89

to 12.24%), Fe_2O_3^* (1.27 to 2.97%) and MnO concentrations (0.01 to 0.02%) are lower than those of trondhjemite porphyry and late trondhjemite, enabling further distinctions to be made. Although some overlap occurs, lower P_2O_5 (0.02 to 0.03%), TiO_2 (0.13%), and higher Na_2O concentrations (4.14 to 5.97%) distinguish granophyre from other trondhjemite except pink trondhjemite.

Granophyre contains higher immobile trace element concentrations than any other phase in the pluton. Nb, Hf and Y abundances within granophyre are at the high end of those for coarse-grained trondhjemite and are clearly enriched relative to late trondhjemite (Fig. 3.3). In addition, Ta, Th and U concentrations, although exhibiting some overlap with samples 92-73 and 92-95, are enriched in granophyre relative to other phases in the pluton.

Granophyre shows much less LREE variation than coarse-grained trondhjemite (Fig. 3.4). LREE concentrations of granophyre (La 47 ppm, Ce 93 to 106 ppm, Nd 48 to 60 ppm, and Sm 12 to 18 ppm) are the highest in the pluton, except for two coarse-grained trondhjemite samples. Granophyre contains low Eu concentrations (1.2 to 1.3 ppm) relative to pink trondhjemite and trondhjemite porphyry. In addition, granophyre is clearly distinguished from late trondhjemite by its higher HREE abundances (Fig. 3.4). In contrast to LREE, HREE show relatively wide variations in granophyre. La/Yb ratios vary between 2.5 and 5.1 over a narrow SiO_2 range and, to a lesser extent, over Th intervals. The low abundance of Eu is reflected in the negative Eu anomaly (Eu/Eu* ratios vary between 0.2 and 0.34), which is the largest of any phase in the pluton (Figs. 3.6C and 3.6D and 3.8).

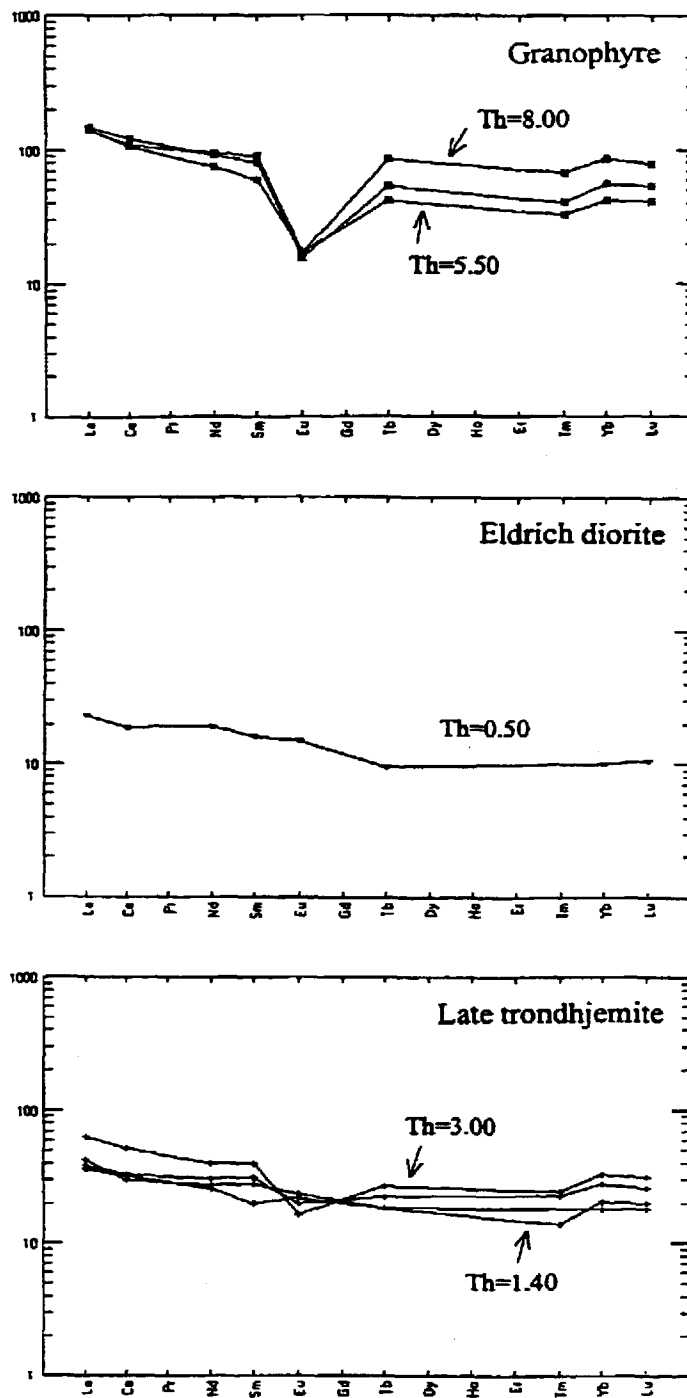


Figure 3.8: Chondrite-normalized REE patterns of granophyre, Eldrich diorite and late trondhjemite. Th concentrations in ppm. Normalization factors from Sun (1982).

3.2.7 Eldrich diorite

Our single analyzed sample of Eldrich diorite contains 53.64% SiO_2 . Its concentration in TiO_2 (1.59%) clearly distinguishes it from Méritens quartz-diorite which contains about 1% TiO_2 (Fig. 3.1). Another characteristic feature is the Eldrich diorite's relatively high MnO concentration, the highest in the pluton. All other major elements show similar concentrations in both Eldrich diorite and Méritens quartz-diorite. Equally, Eldrich diorite is generally not distinguished from Méritens quartz-diorite by compatible trace element concentrations. However, Ni concentrations within Eldrich diorite (25 ppm) are at the low end of concentrations for Méritens quartz-diorite (Fig. 3.2). Eldrich diorite contains lower concentrations of Nb (4.4 to 8 ppm), Y (12 to 18 ppm), Zr (43 to 115 ppm) and Hf (0.9 to 2.7 ppm) than tonalite (see Figure 3.3). Generally, Eldrich diorite is not distinguished from Méritens quartz-diorite in terms of REE abundance. However, slight variations are noted. Eu concentrations are slightly higher in the Eldrich diorite relative to the Méritens quartz-diorite (Fig. 3.4) and Tm values are below detection in Eldrich diorite, whereas they are detected in Méritens quartz-diorite. The chondrite normalized REE pattern for Eldrich diorite (Fig. 3.8) is relatively flat and less fractionated than the pattern for Méritens quartz-diorite. This difference is indicated by a La/Yb ratio of 3.41, which contrasts with values of 3.92 and 7.43 for Méritens quartz-diorite.

3.2.8 Late trondhjemite

Late trondhjemite is characterized by its lack of significant internal chemical variation for major elements relative to the coarse-grained trondhjemite. The phase

can be distinguished from coarse-grained trondhjemite, pink trondhjemite and granophyre by its higher concentrations of Fe_2O_3^* , MnO and P_2O_5 and its lower SiO_2 content (Fig. 3.1). It is compositionally similar to trondhjemite porphyry, but the late trondhjemite's slightly lower concentration of P_2O_5 and MgO may distinguish it from trondhjemite porphyry. Late trondhjemite and trondhjemite porphyry contain similar Co concentrations (4 ppm), slightly higher than the other trondhjemites (Fig. 3.2). Cu and Zn concentrations in late trondhjemite are enriched relative to those of coarse-grained trondhjemite.

Late trondhjemite generally contains lower concentrations of Nb (between 9.1 and 19 ppm) and Y (50 ppm) than the trondhjemite porphyry, pink trondhjemite and granophyre (Fig. 3.3). In addition, late trondhjemite shows unusually wide variations in Zr concentrations (242 to 354 ppm). However, generally lower abundances of Th within late trondhjemite distinguish it from early coarse-grained and pink trondhjemite.

Late trondhjemite is depleted in REE (Fig. 3.4) and is clearly distinguished from other trondhjemite phases by its REE content. La (11.95 to 20.94 ppm), Ce (26.23 to 4.21 ppm), Nd (16.2 to 25.2 ppm), Sm (4 to 8.2 ppm), Tb (0.91 to 1.34 ppm), Tm (0.48 to 0.87), Yb (3.97 to 7.23 ppm) and Lu (0.62 to 1.06 ppm) are depleted in late trondhjemite. Late trondhjemite REE concentrations lie at the low end of a steeply dipping, somewhat scattered, trend that characterizes the REE concentrations of other felsic intrusive phases. Eu abundances fall within the range of other trondhjemites except trondhjemite porphyry. The late trondhjemite's REE

pattern is flat to slightly fractionated, with a small Eu anomaly occurring in sample 92-35, a REE-abundant sample (Fig. 3.8). Eu/Eu^* varies between 0.5 and 1.1.

Sample 92-35 consistently plots in fields defined by coarse-grained trondhjemite. Given the distinct geochemical signature of the late trondhjemite, sample 92-35 is likely a coarse-grained trondhjemite. It is not clear however, whether sample 92-35 was misidentified in the field, or the sample number is erroneous. Sample 92-35 may represent a weakly altered inclusion of early coarse-grained trondhjemite within late trondhjemite.

3.3 Description of Trends, Breaks and Inflections in the Geochemical Data

3.3.1 General statement

A broad negative correlation is observed for Al_2O_3 , Fe_2O_3^* , MgO , CaO and volatiles (L.O.I.) with SiO_2 (Fig. 3.1). However, the clear interpretation of trends is inhibited by scattered data, a common feature for major elements. Concentrations of relatively compatible elements, such as Cr, Ni and Co, are generally low in the Flavrian pluton because it is dominated by intermediate to felsic intrusive phases. However, broad negative correlations are observed between Co, Sc and V with SiO_2 (Fig. 3.2). In addition, Zn shows a crude, widely scattered, negative correlation with SiO_2 .

Rb, Sr and Ba are generally considered to be mobile during alteration or metamorphism. Rb and Ba show large scatters on Harker variation diagrams.

possibly due to secondary processes (Fig. 3.3). Sr appears less scattered and a negative correlation trend is inferred between Sr and SiO₂ for tonalite. Rb concentrations show extreme scatter for both individual intrusive phases and throughout the pluton as a whole. However, the highest absolute concentrations of Rb for each of the phases increase with increasing SiO₂, such that a crude positive correlation is inferred. Equally, an ill-defined positive correlation is inferred between Ba and SiO₂ for the Méritens quartz-diorite.

Generally, Nb, Y, Zr, Hf, Ta, Th and U show positive correlations with SiO₂ (Fig. 3.3). Scattered U concentrations may be due to low concentrations (near the detection limits) or may indicate that U was mobile during metasomatic processes. Th, Ta and Nb show a relatively well-defined positive correlation with SiO₂ for the Méritens quartz-diorite, tonalite, trondhjemite porphyry and coarse-grained trondhjemite. These elements seem to have been relatively immobile during the evolution of the pluton. However, their concentrations vary significantly in granophyre. Important variations in the concentrations of immobile trace elements suggest non-characteristic behavior depending on SiO₂ contents. These variations are described in the following sections.

From a general perspective, REE abundances (apart from Eu) increase with increasing SiO₂ content. However, this increase is not systematic, and several variations in REE concentrations prevent a smooth trend. La/Yb ratios remain constant with increasing SiO₂ and Th (Fig. 3.6A and 3.6B), whereas Eu/Eu* shows a broad negative correlation with SiO₂ for all phases except late trondhjemite. A well-

defined negative correlation is observed between Eu/Eu^* and Th. In the following section, specific SiO_2 intervals are described, showing important variations in concentration.

3.3.2 The Méritens quartz-diorite / tonalite transition

TiO_2 concentrations in Méritens quartz-diorite (Fig. 3.1) are clearly lower than within the least differentiated tonalite. Méritens quartz-diorite samples are isolated from the relatively well-defined negative correlation trend shown by tonalite and trondhjemite for TiO_2 vs SiO_2 . Similarly, P_2O_5 is relatively enriched in tonalite and a negative correlation between P_2O_5 and SiO_2 clearly distinguishes tonalite from the scattered values observed in Méritens quartz-diorite. The geochemical transition from Méritens quartz-diorite to tonalite is also marked by variations in the behavior of Cr and Ni. Significant scatter of the relatively enriched Cr and Ni concentrations for Méritens quartz-diorite (Fig. 3.2) is followed by a sudden decrease in Cr and Ni concentrations with the appearance of tonalite (sample 92-68) and the successively more felsic phases of the pluton. However, the oldest felsic phase of the pluton, the trondhjemite porphyry, contains distinctively higher concentrations of Cr than other trondhjemite and tonalite. As previously noted, the Cr enrichment in trondhjemite porphyry is probably due to the presence of abundant mafic inclusions.

The positive slopes observed for Nb, Y, Zr, Hf, Ta and Th vs SiO_2 in Méritens quartz-diorite are relatively well-defined and are, for the most part, extrapolated to tonalite. Therefore, a smooth chemical transition is observed between Méritens quartz-diorite and homogeneous tonalite in terms of their systematic enrichment in

the immobile high-field strength elements. However, slight disturbances are observed. Tonalitic composition corresponds to an abrupt Y enrichment in sample (92-68) relative to the trend developed by systematic Y enrichment in Méritens quartz-diorite (Fig. 3.3).

The geochemical transition from Méritens quartz-diorite to tonalite also seems to have affected the behavior of certain REE. The LREE (La, Ce, Nd and Sm) are not affected by the transition, but a clear break in the trend occurs at sample 92-68 for SiO_2 vs Eu and SiO_2 vs Tm which are enriched compared to the differentiation trend (Fig. 3.4). Subtle increases in abundances are observed in sample 92-68 for Tb, Tm, Yb and Lu relative to the differentiation trend.

At 62% SiO_2 , Zr and Hf in homogeneous tonalite sample 92-90 are enriched relative to other samples with similar SiO_2 contents (Fig. 3.3). In addition, the homogeneous tonalite samples 92-90 and 92-71 are relatively enriched in LREE compared to the differentiation trend formed by Méritens quartz-diorite and the homogeneous tonalite sample 92-68 (Fig. 3.4). This feature is also observed for Sm and Eu.

In summary, the transition between Méritens quartz-diorite and tonalite is marked by a break in TiO_2 , an inflection for P_2O_5 , depletions in Cr and Ni, and slight disturbances in high field strength element (HFSE) and REE concentrations. The relatively smooth transition for incompatible elements suggests that tonalite may have, at least in part, formed by differentiation of Méritens quartz-diorite. However,

the chemical disturbances at or near the transition are interpreted to have been caused by the interaction between Méritens quartz-diorite and early trondhjemite. This interaction may have been in the form of magma mixing or assimilation (see discussion on the origin of tonalite in this chapter).

3.3.3 Geochemical variations within tonalite

All major elements show significant scatter in tonalite samples between 64.8 and 68.8% SiO₂. However, two trends may be defined by the MnO vs SiO₂ plot (Fig. 3.1): (1) a positive correlation with SiO₂ between 0.07% and 0.18% MnO for the low-silica tonalite and (2) a well-defined, steep negative correlation between 0.18% and 0.04% MnO for high-silica tonalite. Sample 92-77 lies at the inflection point for MnO and is also characterized by the lowest MgO and highest Fe₂O₃* concentrations for tonalite. The inflection point also corresponds to a Co low and a Sc high. It is important to note, however, that MnO concentrations are near the detection level.

Significant variations in immobile element abundances occur at the 64.8 to 68.8% SiO₂ interval. Zr concentrations are most variable, with concentrations ranging between 133 ppm (sample 92-77) and 325 ppm (sample SP-51) (Fig. 3.3). Nb, Y and Ta show significant enrichments for samples 92-83 and 92-88 (tonalite inclusions within trondhjemite). No significant variations in Th concentration are observed for tonalite.

The REE define two groups between 64.8 and 68.8% SiO₂. Between 64.8 and 67% SiO₂, La, Ce, Nd, Tm, Yb and Lu form a well-defined cluster. However, sample

92-82 lies outside the cluster for Nd (33 ppm) and Tb (1.6 ppm) vs SiO₂. The second group is defined by two silica-rich samples (tonalite inclusions), which are enriched in all REE except Eu relative to other tonalite (see Figure 3.4). Between 64.8 and 68.8% SiO₂, tonalite samples (92-78, 92-77, SP-51 and 92-81) have similar Sm concentrations (7 ppm) and evolve with increasing SiO₂ into a positive trend showing relatively wide variations in Sm concentrations (8 ppm to 14 ppm). Samples showing the higher Sm concentrations include 92-70, 92-82, 92-83 and 92-88, which are the "high-silica" end members of the tonalite group. The second break occurs at 68.4% SiO₂ and is also marked by a significant enrichment of LREE and HREE and by depletions in Eu for samples 92-83 and 92-88, which are tonalite inclusions in a trondhjemite matrix. Both La/Yb and Eu/Eu* show broad negative correlations with SiO₂. The large variation of Eu/Eu*/Th in tonalite reflects the variety of textures that characterize this intrusive phase. Textural variability in tonalites is interpreted to have resulted from the phases various origins (see Section 3.5 on the origin of tonalite).

3.3.4 Geochemical variations within trondhjemite

Large variations in Zr, Y and Nb abundances occur between 73.8 and 79.2% SiO₂. Much of the variation below 77% SiO₂ is seen in late trondhjemite, which contains lower concentrations of Nb and Y relative to other trondhjemites. Large variations in the immobile elements, especially in LREE, occur between 77 and 79.2% SiO₂, the most felsic rocks in the pluton. Variations within the 77 to 79.2% SiO₂ interval are accompanied by an order of magnitude variation in La and Ce and to a lesser extent in Ta and Th (see Figures 3.3 and 3.4). Th shows a relatively well-

defined positive correlation with SiO_2 for Méritens quartz-diorite, tonalite, trondhjemite porphyry and coarse-grained trondhjemite. However, concentrations increase significantly and show relatively important variations for samples having the highest SiO_2 concentrations (77 to 79.2%).

The LREE define a positive correlation with silica for quartz-diorite, tonalite and trondhjemite porphyry, which may be attributed to differentiation (Fig. 3.4). This trend contrasts markedly with large variations in LREE abundances between 73.8 and 79.2% SiO_2 . Therefore, the inferred differentiation trend from Méritens quartz-diorite to coarse-grained trondhjemite abruptly terminates with significant LREE enrichments in granophyre, distinctive LREE depletions in late trondhjemite and LREE variations in coarse-grained trondhjemite. Granophyre enriched in LREE and HREE and relatively depleted in Eu compared to other trondhjemite phases occurs at the enriched end of the differentiation trend.

3.4 Trace Element and REE Variation Diagrams

Two-element variation diagrams for elements having contrasting bulk partition coefficients (i.e., for compatible vs incompatible elements) enable a clear distinction to be made between groups of rocks within the Flavrian pluton based on their chemical affinities. Samples are grouped according to their relative order of appearance in the pluton (groups 1 through 7), with trondhjemite porphyry and pink trondhjemite shown together, because both are older than coarse-grained trondhjemite. Group 1 = Méritens quartz-diorite, group 2 = tonalite, group 3 =

trondhjemite porphyry and pink trondhjemite, group 4 = coarse-grained trondhjemite, group 5 = granophyre, group 6 = Eldrich diorite and, group 7 = late trondhjemite.

On a plot of compatible TiO_2 vs incompatible Th (Fig. 3.9A), tonalite sample 92-68 contains a higher concentration of TiO_2 than any sample of the more mafic Méritens quartz-diorite. Also, a series of Méritens quartz-diorite and tonalite samples contain relatively constant TiO_2 concentrations of about 1%. Group 3, formed by trondhjemite porphyry and pink trondhjemite, is closely related to coarse-grained trondhjemite (group 4). Granophyre (group 5) forms a distinct low Ti, high Th group distinguishable from pink trondhjemite and trondhjemite porphyry. However, granophyre appears as a high-Th end member to coarse-grained trondhjemite. Late trondhjemite (group 7) is clearly distinguished from trondhjemite porphyry and pink trondhjemite (group 3) and coarse-grained trondhjemite (group 4).

A similar sort of behavior is observed on an Al_2O_3 vs Th plot (Fig. 3.9B). Al_2O_3 decreases with increasing Th from Méritens quartz-diorite to early trondhjemite, which include trondhjemite porphyry, pink trondhjemite and coarse-grained trondhjemite. Groups 3 and 4 are formed by early trondhjemite groups and clearly overlap. Granophyre is distinguished by its relatively high Th concentrations. Equally, late trondhjemite clearly forms a separate low-Th group, not related to coarse-grained trondhjemite.

Figure 3.9C, 3.9D and 3.9E shows plots of compatible trace element Sc against incompatible elements Th and Ta and La. A negative correlation between Sc and

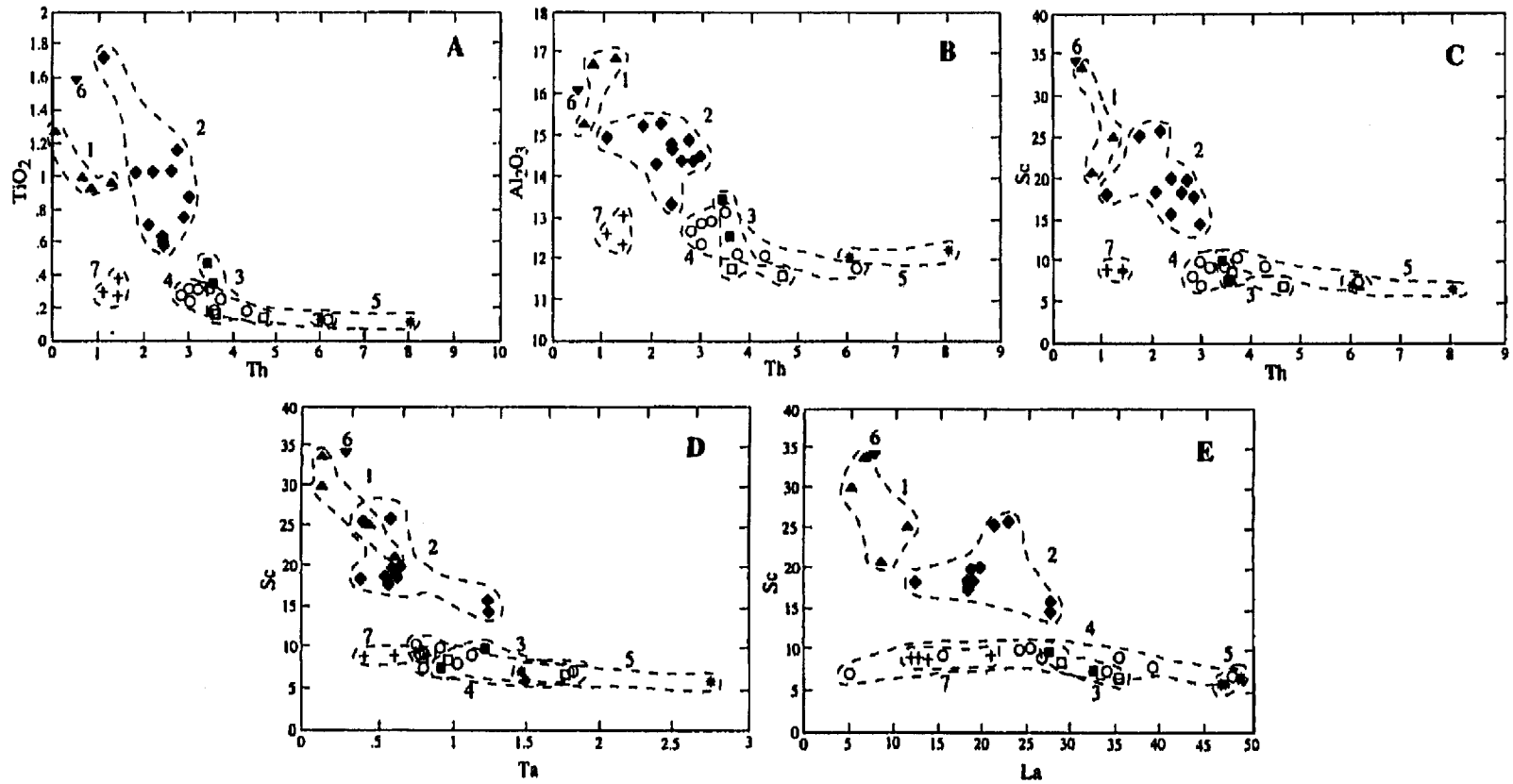


Figure 3.9: Compatible vs incompatible trace element diagrams of intrusive phases of the Flavrian pluton. \blacktriangle = Méritens quartz-diorite; \bullet = tonalite; \blacksquare = trondhjemite porphyry; \square = pink trondhjemite; \circ = early coarse trondhjemite; \ast = granophyre; ∇ = Eldrich diorite; \dagger = late trondhjemite. Concentrations in ppm.

incompatible elements is well-defined for Méritens quartz-diorite to early trondhjemite, with some scatter observed in tonalite samples. Again, groups 3 and 4 (early trondhjemite) show significant overlap. In addition, late trondhjemite (group 7) and granophyre (group 5) are clearly separate phases. Late trondhjemite is depleted in incompatible trace elements and granophyre is enriched in incompatible trace elements relative to early trondhjemite.

Variation diagrams of incompatible elements suggest an evolution of the pluton from a different perspective. A crude positive correlation is observed between Hf and Zr for Méritens quartz-diorite and tonalite samples (Fig. 3.10A), and significant overlap, occurs for early and late trondhjemite. This overlap is likely caused by significant variations in Zr concentrations. Granophyre sample 92-72 contains significantly higher Hf concentrations than group 3, 4 and 7 trondhjemites. Granophyre samples may lie on a positive correlation trend that is clearly distinguished from the relatively flat trend defined by pink trondhjemite and trondhjemite porphyry (group 3), coarse-grained trondhjemite (group 4) and late trondhjemite (group 7).

Similar observations can be made for Hf vs Th (Fig. 3.10B). A crude positive correlation exists for Méritens quartz-diorite and tonalite. This correlation ends abruptly with four tonalite samples (92-90, 92-78, 92-81, 92-83) showing a possible negative correlation between Hf and Th. Tonalite samples 92-70, 92-83, SP-51 and 92-88 contain higher Hf concentrations than other tonalite and plot within the field defined by coarse-grained trondhjemite. Early trondhjemite clusters at about 8 ppm

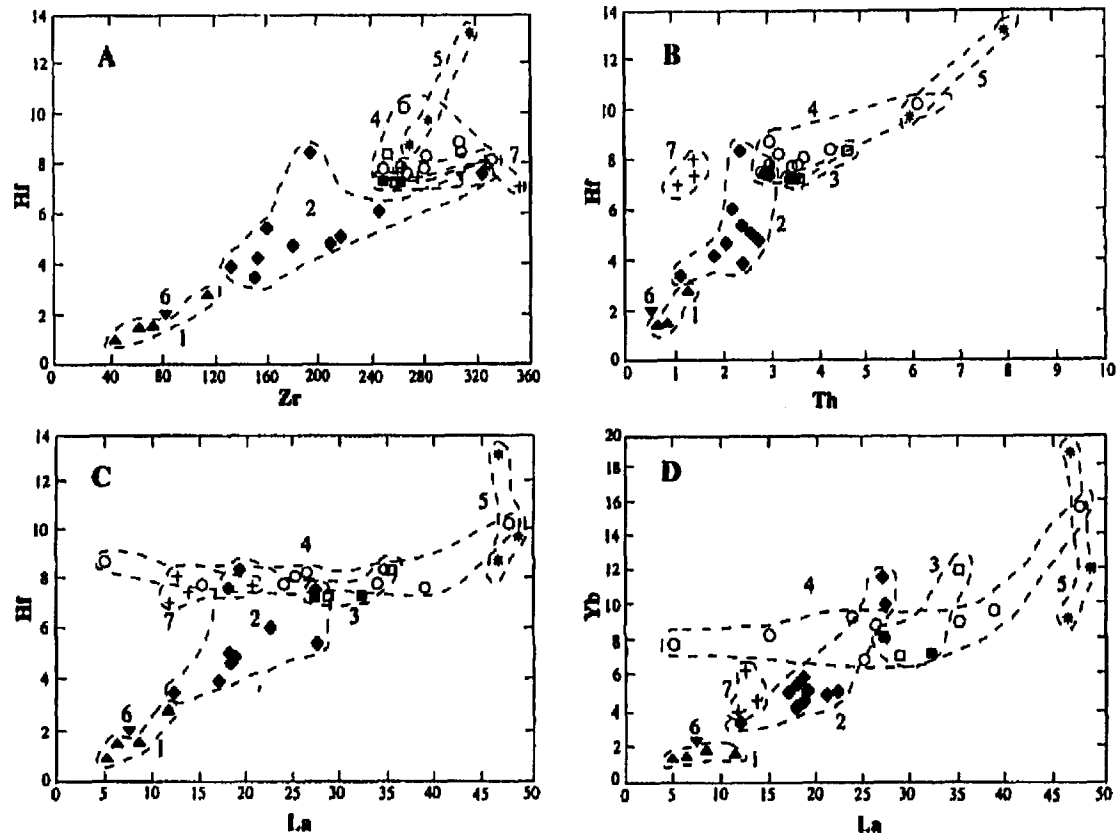


Figure 3.10: Incompatible vs incompatible trace element diagrams of intrusive phases of the Flavrian pluton. \blacktriangle : Méritens quartz-diorite, \bullet : tonalite, \blacksquare : trondhjemite porphyry, \circ : pink trondhjemite, \square : early coarse trondhjemite, $*$: granophyre, \blacklozenge : Eldrich diorite, $+$: late trondhjemite. Concentrations in ppm.

Hf, whereas the trondhjemite porphyry and pink trondhjemite group is distinguished from coarse-grained trondhjemite by a relative enrichment in Th. Granophyre is distinctively enriched in both Th and Hf, whereas late trondhjemite has clearly lower Th concentrations.

For Hf vs La (Fig. 3.10C), a clear positive correlation occurs for Méritens quartz-diorite, tonalite, porphyritic trondhjemite and pink trondhjemite. However, coarse-grained trondhjemite shows relatively constant Hf and variable La concentrations. This pattern contrasts with the positive trend defined by the combinations of groups 1, 2 and 3. Tonalite samples SP-51, 92-70 and 92-88 plot within the coarse-grained trondhjemite field at relatively higher Hf concentrations than other tonalite. Late trondhjemite occurs at the low La end of the trend, along with two early trondhjemite samples (92-87 and 92-100) of the coarse-grained trondhjemite trend. Furthermore, samples 92-67, 92-72, 92-95 and 92-93 are clearly distinguished from other trondhjemites by their higher La and Hf concentrations and distinctive vertical trend, varying significantly in Hf at a constant La content.

Similarly for Yb vs La (Fig. 3.10D), a clear change in La behavior is noted for coarse-grained trondhjemite compared to Méritens quartz-diorite and tonalite. Again, the granophyre shows variations in Yb concentrations at constant La concentrations (group 5). A clear distinction is made between group 4 (coarse-grained trondhjemite) and group 5 (granophyre), based on the behavior of La. Yb concentrations are constant with increasing La in coarse-grained trondhjemite, whereas Yb concentrations vary extensively at constant La values in granophyre. The behavior of

La exemplifies the behavior of LREE: incompatible element plots of Zr vs La and Y vs La (not shown) further support the observations made on the other diagrams discussed here.

3.5 Discussion

Geochemical characterization

The distinct geochemical signatures of phases composing the Flavrian pluton support field investigations and indicate the occurrence of eight separate intrusive phases. Field observations (Section 2.2.4) and subtle geochemical differences indicate that early trondhjemite can be subdivided into three separate phases: (1) trondhjemite porphyry, (2) pink trondhjemite, and (3) coarse-grained trondhjemite. Granophyre is also related to early trondhjemite but its chemistry is more distinct. Although pink trondhjemite and trondhjemite porphyry are volumetrically minor, they provide evidence of early (pre-coarse-grained trondhjemite) felsic magmatism.

However, coarse-grained trondhjemite is volumetrically significant, occupying about 50% of the total early trondhjemite. Coarse-grained trondhjemite is composed mainly of quartz and albite with lesser amounts of epidote and chlorite. It is silica-rich, with concentrations ranging between 75 and 79.2%. CaO and Sr enrichment relative to other trondhjemite phases is likely due to the presence of epidote either in the form of disseminated alteration of plagioclase or as fillings of miarolitic cavities which are abundant throughout coarse-grained trondhjemite (see Section 2.2.4). Na₂O concentrations of 4 to 5.5% are reflected in abundant euhedral albite in coarse-

grained trondhjemite. Albite commonly forms the matrix of magmatic breccia textures described in Section 2.2.4. Well-developed albite crystals in the matrix suggest that they crystallized relatively slowly. The breccia texture is unusual because the quartz fragments do not appear to have been rotated (Section 2.2.4). Therefore, although the shattered and resorbed quartz crystals indicate the sudden infiltration of albite, the size of the albite crystals suggests relatively slow cooling.

These microbreccias (see Section 2.2.4 and Figure 2.10), which are generally interpreted to reflect abrupt pressure and/or temperature changes (Bard, 1980, p.139), are similar to hydrobreccias related to high fluid pressures and/or high fluctuations in fluid pressure. Magmatic brecciation occurs throughout the coarse-grained trondhjemite, indicating the scale and importance of the mechanism causing the brecciation. The coarse-grained trondhjemite's enrichment in HFSE and REE suggests that this phase represents a late-stage, SiO_2 - and Na_2O -rich magma that crystallized under relatively stable conditions following sudden pressure fluctuations. Subsolidus metasomatic processes most likely enhanced Na_2O enrichment. The breccia texture may have been caused by expansion of a fluid phase as it passed from a dissolved component in magma to a separate aqueous fluid during cooling and/or in situ decompression. The formation of a free aqueous fluid phase represents oversaturation of fluid in the silicate melt and is commonly termed resurgent boiling (Clarke, 1992, p. 160). A sudden drop in pressure could have been induced by expansion of the fluid-rich magma as it rose to a level in the chamber where lower lithostatic pressure would have caused the aqueous fluid to separate from the magma. Equally, the sudden drop in pressure may have been triggered by breaching of the

saturated magma reservoir through seismic activity. Widespread miarolitic cavities filled with epidote, quartz and less commonly magnetite suggest degassing or boiling during emplacement and/or cooling of coarse-grained trondhjemite (Fig. 2.12). The occurrence of pegmatites, although uncommon, further supports the formation of a separate volatile-rich fluid phase (see Figure 2.11). The large variations in La/Yb at a given level of Th are caused by variations in La and interpreted to result from late magmatic alteration of the coarse-grained trondhjemite by a free aqueous fluid that separated from the trondhjemite magma. LREE mobility is interpreted to have resulted from high temperature alteration of the trondhjemite. The incompatible element-rich aqueous fluid would have interacted with both solid and molten coarse-grained trondhjemite. The resorbed quartz fragments in the breccia are interpreted as evidence of the alteration capacity of the aqueous fluid. The aqueous fluid probably altered plagioclase, enhancing Eu depletion. Variations in the intensity of brecciation within the early coarse-grained trondhjemite directly reflect the large variations in its geochemistry.

Granophyre is enriched in SiO_2 , Na_2O , HFSE, Th, U and REE relative to coarse-grained trondhjemite. It also shows a pronounced negative Eu anomaly. Eu/Eu* ratios of 0.2 to 0.34 are the lowest in the pluton. Paradis et al. (1988) suggested that the large increase in the negative Eu anomaly in "enriched trondhjemite" (granophyre) relative to coarse-grained trondhjemite was attributed to volatile transfer during magma degassing (Flynn and Burnham, 1978) or interaction with seawater (Humphris, 1984). Paradis et al. indicated that igneous fractionation could not have been the controlling mechanism responsible for Eu depletion because

the large increase in Eu depletion occurred over a small SiO_2 interval with no significant variation in Nb, Y and Ta. However, our studies indicate that granophyre is enriched in HFSE, including Nb, Y and Ta, compared to coarse-grained trondhjemite. Therefore, igneous fractionation (crystallization of feldspar) may have caused Eu depletion in granophyre.

Crosscutting relationships clearly indicate that granophyre is a separate, later phase than coarse-grained trondhjemite. Granophyre's enrichment in SiO_2 , Na_2O , HFSE, Th, U and REE and depletion in Eu compared to coarse-grained trondhjemite suggests that granophyre represents an increased level of differentiation relative to coarse-grained trondhjemite. The most probable means to produce a more differentiated magma enriched in incompatible elements is by crystallization of feldspar. Feldspar fractionation would have enriched the residual melt in incompatible elements and depleted the residual melt in Eu.

Granophyre's characteristic texture (Figs. 2.8D and 2.9D) indicates either quenching or crystallization at eutectic conditions. The numerous miarolitic cavities in granophyre suggest that devolatilization occurred; supporting sudden cooling due to degassing. However, degassing may have occurred at eutectic conditions. Consequently, field relationships presented in Section 2.3, along with the SiO_2 content, texture and geochemical signature are diagnostic of granophyre and clearly identify granophyre as a late-stage, SiO_2 , Na_2O and incompatible element-enriched differentiate of trondhjemite that cooled rapidly.

The role of seawater interaction

Interaction with seawater probably played an important part of the evolution of the Flavrian pluton. The high Na₂O content of various intrusive phases suggests seawater interaction. Although Na₂O concentrations increase from Méritens quartz-diorite to coarse-grained trondhjemite, they are generally similar for tonalite and trondhjemite, suggesting that albitization may have occurred after or during crystallization of coarse-grained trondhjemite. The high Na₂O content of intrusive phases within the pluton is reflected in the composition of plagioclase. From microprobe analysis of plagioclase for various phases of the Flavrian pluton Kennedy (1984) clearly shows that the plagioclases is albite-rich (Table VII). However, the late trondhjemite contains cores of K-spar or oligoclase rimmed by albite, suggesting that albitization did not affect the late trondhjemite as much as it did other phases.

Kennedy (1984) recognized the importance of seawater interaction in the evolution of the Flavrian pluton, suggesting that the relatively light $\delta^{18}\text{O}$ values obtained for intrusive phases were due to interaction of the pluton with evolved seawater containing a substantial component of magmatic or metamorphic fluids (see Table VII). The Méritens quartz-diorite yielded a whole-rock $\delta^{18}\text{O}$ value of 1.48, the lightest in the pluton. This value approaches that of SMOW and suggests that the Méritens quartz-diorite was intensely altered by seawater. The pluton's interaction with evolved seawater is supported by the presence of epidote and iron-rich actinolite. Kennedy's evidence for a subsolidus interaction between seawater and coarse-grained trondhjemite is based on the observation of a large isotopic fractionation between quartz and albite (δ_{qt}), probably indicating an important disequilibrium. The isotopic

Phase	Plagioclase Composition (mean)	$\delta^{18}\text{O}$ Whole Rock	$\delta^{18}\text{O}$ Quartz	$\delta^{18}\text{O}$ Feldspar	$\delta^{18}\text{O}$ δ_{QF}	T (°C)
Late trondhjemite	Ab _{2.69} An _{0.29} Or _{97.02}	+5.62 (mean)	+7.14 (mean)	+5.74 (mean)	+0.97	770
	to Ab _{96.24} An _{2.35} Or _{1.21} (albite rims)	+5.09 +6.31 +5.45	+7.15 +7.13	+6.18 +5.30		
Eldrich diorite		+3.55				
Granophyre	Ab _{98.3} An _{0.9} Or _{0.2}	+6.79 (mean)	+8.08 (mean)	+6.04 (mean)	+3.16	243
		+7.50 +7.16 +6.30 +6.19	+9.55 +7.82 +7.50 +7.46	+6.39 +5.73 +6.01	+1.77 +1.45	505 650
Coarse trondhjemite	Ab _{93.6} An _{5.6} Or _{0.9}	+4.97 (mean)	+7.19 (mean)	+4.05 (mean)	+2.07	416
		+4.41 +6.00 +4.50	+6.08 +8.86 +6.63	+4.01 +4.49 +3.64	+4.37 +2.99	160 263
Tonalite	Ab ₈₉ An _{10.5} Or _{0.2}	+3.38 (mean)	+5.40 (mean)	+3.01 (mean)	+1.86	493
		+2.56 +5.57 +3.66 +2.09 +3.04	+4.81 +6.60 +4.81 +5.39	+2.95 +3.07	+1.74	515
Trondhjemite porphyry	Ab _{93.6} An _{4.4} Or ₂					
Méritens diorite	Ab ₉₀ An _{9.2} Or _{0.8} and Ab _{77.9} An _{26.9} Or _{0.2}	+1.48				

Table VII: Summary of plagioclase compositions and oxygen isotope values for several phases of the Flavrian pluton. Data from Kennedy (1984).

fractionation observed by Kennedy is consistent with petrographic observations of breccia textures and resorbed quartz crystals (described above and in Section 2.2.4), clearly indicating disequilibrium between the early quartz and later albite-rich matrix. However, Kennedy obtained normal $\delta^{18}\text{O}$ values and an insignificant δ_{qf} for granophyre, not consistent with subsolidus alteration of granophyre by seawater. Kennedy interpreted the granophyre's isotopic signature as resulting from either a change in the fluid composition or a decrease in alteration temperature, but not from crystallization at magmatic temperatures because his calculated isotopic temperatures range from 243 to 650°C. He also suggested that the granophyric texture is caused by subsolidus alteration.

This study indicates that granophyre is younger than coarse-grained trondhjemite, commonly forming thin sills and interconnected dikes within the coarse-grained trondhjemite (Fig. 2.21). The dike-and-sill geometry of granophyre clearly indicates that granophyre is a separate intrusion. Subsidius alteration cannot account for the granophyric texture because the texture does not dominate in coarse-grained trondhjemite. In addition, granophyre is enriched in SiO_2 , Na_2O , HFSE, Th, U and REE and it is depleted in Sr relative to coarse-grained trondhjemite indicating that granophyre is chemically differentiated compared to early trondhjemite. Furthermore, a volatile-rich magma may occur at temperatures of 650°C, suggesting that Kennedy's calculation of 650°C for crystallization of granophyre is correct and that the granophyre could be interpreted to have resulted from a crystallization of volatile-rich magma. The simplest explanation of the increase in incompatible elements is that granophyre crystallized under magmatic conditions. Consequently,

either Kennedy's temperatures for the crystallization of granophyre are erroneous or there are two types of granophyre.

The origin of alkali-rich fluids containing significant amounts of incompatible elements is the subject of a long-standing debate (Kinnaird and Bowden, 1987). The evidence for seawater interaction during the intrusion of the Flavrian pluton is seemingly unquestionable, however the timing of the interaction remains unclear and the possible role of seawater remains open to questions. Was the source rock of the Flavrian magma altered by seawater? Could seawater have mixed with certain portions of the magma chamber early in the differentiation process? Or did seawater have a simple post-emplacement effect on the pluton? The field, textural and geochemical evidence described above, along with the isotopic data provided by Kennedy (1984), suggest that late-stage magmatic-hydrothermal fluids played an important part in the emplacement and post-emplacement history of coarse-grained trondhjemite and granophyre.

Late trondhjemite

The distinctive geochemistry of late trondhjemite supports field observations and geochronological data indicating that the late trondhjemite was a separate phase of the pluton. Late trondhjemite is characterized by a lack of significant internal chemical variations for major elements relative to coarse-grained trondhjemite. The homogeneous and coarse-grained nature the late trondhjemite is consistent with a uniform internal chemistry. The following chemical characteristics indicate that the late trondhjemite is a distinct, less differentiated intrusion, not directly related to early

trondhjemite. Late trondhjemite is enriched in Fe_2O_3^* , MnO and P_2O_5 and it is depleted in SiO_2 relative to pink trondhjemite, coarse-grained trondhjemite and granophyre. It is compositionally similar to trondhjemite porphyry, but the late trondhjemite's slightly lower concentrations of P_2O_5 and MgO may distinguish it from trondhjemite porphyry. A lower level of differentiation is supported by the late trondhjemite's enrichment in Co, Cu and Zn and its depletion in Nb, Y, Th and REE (except Eu) compared to early trondhjemite. The late trondhjemite's lower Th and La concentrations enable it to be clearly distinguished from early trondhjemite on plots of compatible vs incompatible (e.g., Al_2O_3 vs Th, Fig. 3.9) and incompatible vs incompatible elements (e.g., Hf vs Th, Fig. 3.10). Figure 3.9 shows a negative correlation between Al_2O_3 and Th for Méritens quartz-diorite, tonalite and early trondhjemite (including trondhjemite porphyry, pink trondhjemite and coarse-grained trondhjemite) and granophyre. The negative correlation between Al_2O_3 and Th indicates that the pluton evolved through different magmatic pulses, with each pulse further depleted in Al_2O_3 and enriched in Th compared to the previous pulse (see sequence of intrusion in CHAPTER 2). The negative correlation suggests that differentiation occurred by crystallization of feldspar and that the Méritens quartz-diorite, tonalite, early trondhjemite and granophyre are related to the same parental magma. On the other hand, late trondhjemite plots as a separate group on the Al_2O_3 vs Th plot, suggesting that it was derived from a separate magma source.

Kennedy (1984) suggested that the late trondhjemite phase of the pluton (his "plagiogranite") was similar to the Lac Dufault granodiorite located about 2 km east of the Flavrian pluton. Kennedy's interpretation was based on the geochemical

similarities between the granodiorite and late trondhjemite. However, unpublished REE data provided by Dr. John Ludden (1994) from three samples of the Lac Dufault granodiorite contradict Kennedy's interpretation (Fig. 3.11). The REE patterns for the Flavrian late trondhjemite are clearly different from those of the Lac Dufault pluton, which are significantly more fractionated. La/Yb ratios range between 8.67 and 10.83 for the Lac Dufault granodiorite, considerably higher than the 2.06 to 3.05 range of late trondhjemite (Section 3.2.8). Consequently, the late trondhjemite phase of the Flavrian pluton cannot be correlated with the Lac Dufault granodiorite.

The origin of tonalite

The origin of tonalite within the Flavrian pluton is a matter of debate. Whether tonalite was formed by magma mixing (Goldie, 1976), by the combined effects of trondhjemite intrusion into Méritens quartz-diorite (metamorphic assimilation) and superimposed hydrothermal alteration (Kennedy, 1984), or possibly by partial melting of basalt remains a question. However, several observations described in this chapter help to clarify the problem.

The tonalite's chemical variability reflects its ill-defined contacts and textural heterogeneity described in Sections 2.2.2 and 2.2.3. Field relationships indicate that the contact between Méritens quartz-diorite and tonalite is transitional, with Méritens quartz-diorite generally grading into homogeneous tonalite (see Section 2.3). Geochemically, the transition from Méritens quartz-diorite to tonalite is characterized by a SiO₂, Na₂O, TiO₂, HFSE and REE enrichment and an Al₂O₃, MnO, MgO and V depletion. In addition, abrupt depletions in Cr and Ni are observed at the

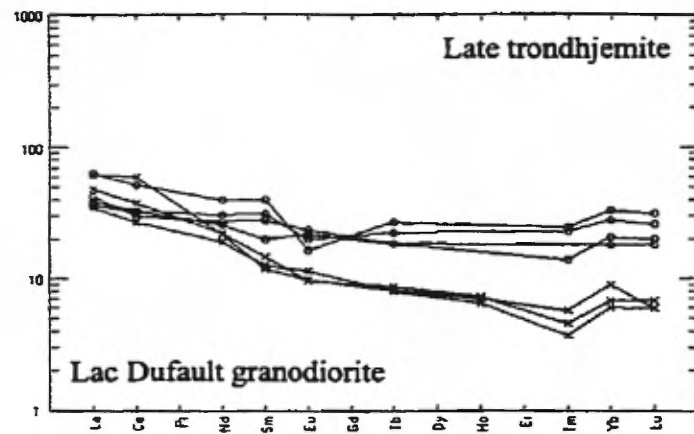


Figure 3.11: Chondrite-normalized REE patterns of late trondhjemite and Lac Dufault granodiorite. Th concentrations in ppm. Normalization factors from Sun (1982).

transition. The transition is also characterized by an inflection for P_2O_5 , probably reflecting the onset of apatite crystallization because acicular apatite crystals (Fig. 2.4D) are commonly observed in tonalite (Section 2.2.2).

The systematic increase in HFSE and REE with increasing SiO_2 for Méritens quartz-diorite and homogeneous tonalite suggests that differentiation by crystal fractionation may have taken place. However, the presence of acicular apatite and amphibole in tonalite are evidence for quenching (see CHAPTER 2) which in turn suggests that tonalite may have been the product of some sort of interaction between what is now represented by Méritens quartz-diorite and early trondhjemite.

The transition from homogeneous tonalite to spotted tonalite, heterogeneous tonalite and hybrid rocks approaching trondhjemite generally corresponds to an increase in SiO_2 and decreases in TiO_2 , Al_2O_3 and P_2O_5 . The two distinct trends for MnO vs SiO_2 in tonalite correspond to a change from homogeneous tonalite to spotted and heterogeneous tonalite and hybrid rocks (Fig. 3.1). The low-silica trend is composed of homogeneous tonalite, which shows a steep positive correlation between MnO and SiO_2 . The inflection point corresponds to MnO, $Fe_2O_3^*$ and Sc highs and TiO_2 , Al_2O_3 , MgO and Co lows for tonalite. Sample 92-77 lies on the inflection point which occurs at about 65% SiO_2 and is described as tonalite characterized by long acicular and curved amphibole needles (up to 1 cm), zoned plagioclase, locally intergrown quartz and plagioclase, acicular apatite, zircon, stilpnomelane replacing amphibole and opaque minerals replacing amphibole.

With increasing SiO_2 , spotted tonalite, heterogeneous tonalite and hybrid rocks dominate, and MnO decreases with increasing SiO_2 . Significant variations in immobile element abundances occur in the high-silica tonalite. Samples show an enrichment in Sm, Tb, Tm and Lu and depletion in Eu with increasing SiO_2 , and LREE generally cluster and do not show systematic increases until samples 92-83 and 92-88. Samples 92-83 and 92-88 are inclusions of tonalite hosted by a trondhjemite matrix. These samples correspond to the felsic end-member of tonalite or (heterogeneous tonalite and hybrid rocks) and contain the highest concentrations of immobile elements such as Nb, Y, Ta and REE (except Eu) of all tonalites. However, Th concentrations in the inclusions were not affected by the interaction with trondhjemite. The high REE abundances in tonalite inclusions suggest that the host trondhjemite is not coarse-grained trondhjemite because of its relatively low concentration in Nb, Y and Ta compared to the inclusions. Instead, the intruding trondhjemite must have been one of the later phases.

Significant variations in immobile trace element concentrations such as Nb, Y, Zr and REE over relatively small SiO_2 intervals emphasize the complex history of the tonalite. However, field and petrographic observations discussed in Sections 2.3 and 2.5, indicate two scenarios: (1) early trondhjemite grades into tonalite (regionally, outcrop scale and in thin section), producing homogeneous tonalite and hybrid rocks and (2) early trondhjemite is in sharp contact with tonalite, generating early trondhjemite matrix breccias. The geochemical data indicates tonalite to be intermediate to Méritens quartz-diorite and early trondhjemite, and variability in incompatible trace element concentration suggests that interaction did occur.

However, differentiation of Méritens quartz-diorite may have produced homogeneous tonalite. Field evidence presented in Sections 2.3 and 2.5 indicate that both gradational and sharp contacts occur between tonalite and trondhjemite; suggesting that tonalite (heterogeneous) is a product of interaction between trondhjemite and quartz-diorite. Interaction likely occurred in two states: (1) trondhjemite magma and quartz-diorite magma and (2) trondhjemite magma and solid quartz-diorite and tonalite. This is likely since several generations of trondhjemite intrude the pluton.

Summary

The geochemical evolution of the Flavrian pluton from Méritens quartz-diorite to granophyre is characterized by a general enrichment in SiO_2 , Na_2O , Y, Nb, Zr, Hf, Ta, Th, U and REE and relative depletion in Al_2O_3 , Fe_2O_3^* , MnO, MgO, CaO, Co, Sc, V and Sr. La/Yb ratios remained relatively constant and Eu was depleted as the more differentiated phases were introduced into the pluton with some variations occurring in the silica-rich phases.

Scatter in the trends of mobile elements, e.g., K_2O and Ba is likely due to alteration. However, scatter in the 64.8 to 68.8% SiO_2 range is largely caused by the interaction between what is now represented by Méritens quartz-diorite and early trondhjemite. The interaction is reflected in the trends of most elements except Th and to a lesser extent Ta and Nb. This interaction likely occurred by magma mixing and partial assimilation of Méritens quartz-diorite by trondhjemite. Both mechanisms are consistent with the numerous phases of trondhjemite. Significant variations in incompatible element concentrations and La/Yb ratios occur between 75 and 79.2%

SiO₂ for coarse-grained trondhjemite and granophyre. The variations in coarse-grained trondhjemite were likely caused by the separation of an aqueous fluid phase from the trondhjemite magma. The formation of a supercritical fluid was likely caused by a boiling event triggered by sudden drops in pressure. Boiling produced late magmatic breccias similar to hydrobreccias. The aqueous fluid-rich breccias probably interacted with seawater, effectively lowering their $\delta^{18}\text{O}$ values and altering their chemical compositions. Scatter observed for elements that are generally immobile such as Zr and La may also be due to crystallization of refractory phases enriched in these elements (Gromet and Silver, 1983), i.e. zircon and allanite. Allanite, which can contain 40% LREE has been reported in the trondhjemite phases of the Flavrian pluton by Kennedy (1984) and Paradis et al. (1988).

Between 77 and 79.2% SiO₂, the increase in incompatible elements is due to the intrusion of granophyre, which was a late-stage high SiO₂, Na₂O and incompatible-element enriched phase that quenched due to rapid cooling.

The distinct geochemistry of late trondhjemite supports field investigations and geochronological data indicating late trondhjemite to be a separate later phase of the pluton that was produced from a separate magma. However, chondrite-normalized REE patterns suggest that late trondhjemite is not equivalent to the Lac Dufault granodiorite, as was previously suggested by Kennedy (1984).

A broad negative correlation occurs between compatible and incompatible elements for Méritens quartz-diorite to early trondhjemite. Samples of trondhjemite

porphyry, pink trondhjemite and coarse-grained trondhjemite show significant overlap at the bottom end of the trend. Granophyre is clearly distinguished by its relative enrichment in incompatible elements, and possibly represents a late-stage differentiate of trondhjemite. Therefore, Méritens quartz-diorite, tonalite, early trondhjemite and granophyre are genetically linked. Late trondhjemite shows a distinct depletion in incompatible elements suggesting it was related to a different magmatic source. Variation diagrams of incompatible elements generally show a crude positive correlation for Méritens quartz-diorite to early trondhjemite and large variations in granophyre. However less overlap occurs between the group consisting of trondhjemite porphyry and pink trondhjemite and coarse-grained trondhjemite. Again, late trondhjemite is clearly distinguished from the other phases. The general negative correlation between Eu/Eu^* and Th suggests that feldspar crystallization played an important role in the differentiation process.

CHAPTER 4

CHAPTER 4: RELATIONSHIP BETWEEN THE FLAVRIAN SUBVOLCANIC PLUTON AND VOLCANIC ROCKS OF THE NORANDA CAULDRON

4.1 Introduction

The Flavrian pluton has been regarded by many authors as the remains of a magma chamber from which were extruded the volcanic rocks of the Noranda cauldron (Goldie, 1976; Gibson and Watkinson, 1990; Kerr and Gibson, 1993). The chamber would have driven the hydrothermal systems responsible for the formation of the Cu-Zn deposits located within the volcanic stratigraphy (Franklin, 1992; Galley, 1996). This hypothesis is largely based on geochronological and geochemical evidence which indicate that the pluton and overlying volcanic rocks were contemporaneous and cogenetic (Goldie, 1976; Paradis, 1984; Mortensen, 1993). The pluton-driven model is supported by isotopic data that suggest that a large zone of isotopic alteration is centred on the pluton (Cathles, 1993).

However, the emplacement history of the pluton was complex and consisted of numerous intrusions of various chemical compositions (see CHAPTERS 2 and 3). Therefore, the exact role played by the pluton in the formation of volcanic-hosted massive sulphide (VHMS) deposits is not yet well-understood. In this chapter, correlations between the phases of the Flavrian pluton and the volcanic rocks of the Noranda cauldron are made based on crosscutting relationships and geochemical comparisons between particular phases of the pluton and volcanic formations. The

principal aim of this chapter is to determine which parts of the pluton were emplaced during the formation of the Noranda cauldron and associated Cu-Zn deposits.

4.2 Field Relationships Between the Flavrian Pluton, the Volcanic Rocks and VHMS Deposits of the Noranda Cauldron

The periodic nature of the bimodal volcanism in the Noranda area has led to a stratigraphic subdivision comprised of five main volcanic cycles (Spence and de Rosen-Spence, 1975; Gibson and Watkinson, 1990) (see review of the geology of the Noranda Volcanic Complex in the Introduction). Volcanic cycles 1 and 2 are located west of the Flavrian pluton and appear to lack significant massive sulphide mineralization. The third cycle, which overlies and is partly intruded by the Flavrian pluton, is interpreted to be a cauldron fill sequence (Gibson and Watkinson, 1990). This cycle, described as the Noranda cauldron, hosts most of the massive sulphide deposits. The stratigraphy of volcanic units and the positions of massive sulphide deposits within the Noranda cauldron are shown in Tables II and III. Cycle 4 is viewed as a late to post-cauldron sequence where volcanism spilled over the edges of the subsidence structure. Cycle 4 strata, which also host VHMS deposits, are interpreted to have formed during a third period of subsidence and volcanism after the main phase of cauldron subsidence of Cycle 3 (Gibson and Watkinson, 1990). Cycle 5 occurs near the top of the Blake River Group (Péloquin et al., 1990). However, its stratigraphic position is not certain and repetition may have occurred by faulting. Cycle 5 hosts the Mobern VHMS deposit.

The geological compilation map in Appendix I shows the Flavrian pluton intruding volcanic rocks of the Noranda cauldron. At the southern contact, early trondhjemite intrudes the Amulet Andesite (Gibson and Watkinson, 1990). This andesite, which belongs to the 2nd cauldron cycle, is the youngest volcanic formation cut by the Flavrian pluton. These relationships indicate that at least part of the early trondhjemite intruded the Noranda cauldron after the deposition of the Amulet Andesite and after the deposition of second cauldron cycle and the VHMS deposits located at the C contact stratigraphic horizon.

4.2.1 Timing of intrusion relative to the formation of the Ansil Cu-Zn deposit

In this Section, we will look at key relationships between the Flavrian pluton and the Ansil and Corbet VHMS deposits of the 1st volcanic cycle. Drill core data from Minnova Inc. (now Inmet Mining Corp.) (Labrie, 1993, written communication) was used to examine the nature of the Flavrian pluton beneath the Ansil Cu-Zn deposit. The Ansil deposit (Galley, 1994; Barrett et al., 1991; Riverin et al., 1990) occurs within the 1st cauldron cycle at the contact between the Northwest Rhyolite and the Rusty Ridge Andesite. The holes were drilled through and into the footwall of the Ansil deposit and its alteration pipe where they intersect the Flavrian pluton (Fig. 4.1A). The black dots represent drill hole locations as they intersect the Flavrian pluton. The thin dashed lines represent the interpreted topographic contours of the pluton's surface, beneath the deposit. The thick dashed lines are faults (interpreted from drill core data) projected on the surface of the intrusion whereas the shaded area represents Ansil's alteration pipe at the pluton's surface. The Ansil deposit, which is located about 350 m above the pluton is also projected on the plane.

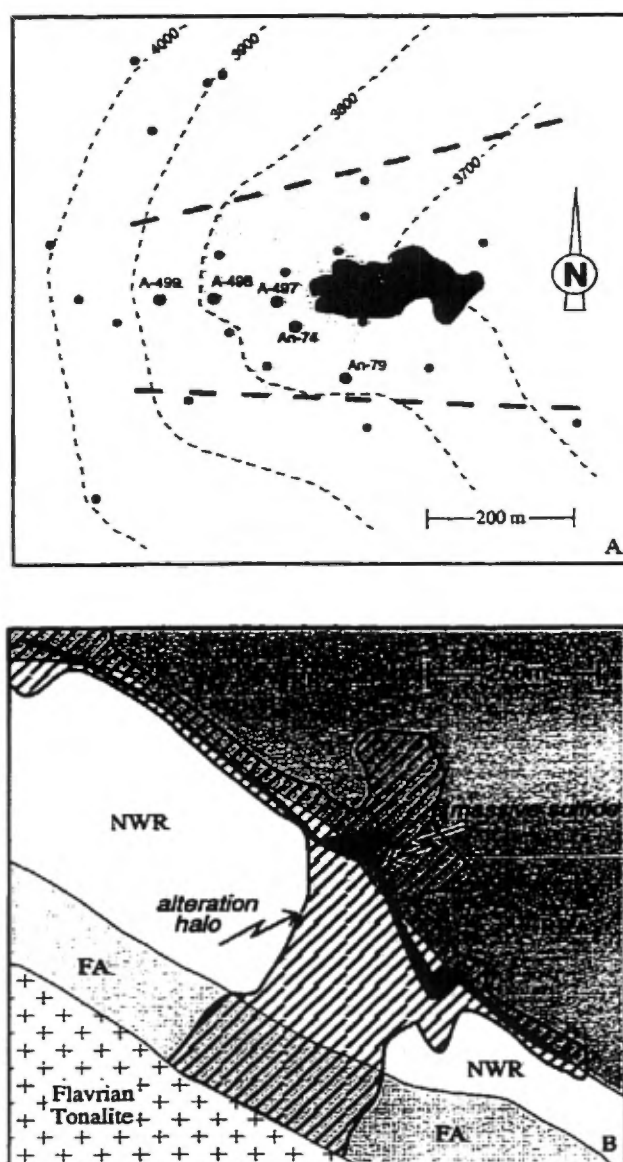


Figure 4.1: A) Composite plan of the Ansil VHMS deposit and the intruding Flavrian pluton beneath Ansil. The black dots represent drill hole locations as they intersect the pluton. Thin dashed lines represent interpreted topographic contours of the pluton's surface beneath the deposit. Thick dashed lines are faults (interpreted from drill core data) projected onto the surface of the intrusion, whereas the shaded area represents alteration pipe of the Ansil deposit on the pluton's surface. From Labrie (1993, personal communication). B) Geological cross-section 46590 N of the Ansil deposit. Modified from Riverin et al. (1990).

Drill holes A-497, A-498, A-499, An-74 and AN-79 were sampled for thin section analysis, and are shown as target symbols.

The contact between the Flavrian pluton and the overlying Flavrian Andesite beneath Ansil is sharp. In hole An-79, early trondhjemite occurs at the contact with the overlying andesite at 1545 metres depth (from collar). The early trondhjemite is medium- to coarse-grained and contains scattered epidote patches and rare chlorite and quartz-carbonate veinlets. A thin section of the early trondhjemite reveals significant granophyric intergrowths. Deeper within the pluton (1595 to 1645 m), a fine- to medium-grained diorite textured intrusion occurs in sharp contact with early trondhjemite.

Fine- to medium-grained, grey-coloured, quartz-porphyrific, variably textured tonalite is observed between 1645 and 1676 metres. Epidote patches and chlorite veinlets are scattered within the tonalite. Petrographic studies of a sample from 1652 metres depth show that quartz occurs with epidote, chlorite, actinolite and sericite in a remnant intergrowth texture where epidote, sericite and chlorite replace albite. Actinolite and chlorite also form irregular zones or clots within the quartz-albite (i.e. altered) matrix.

In drill hole AN-74, the sharp contact between the Flavrian andesite and the pluton occurs at 1588 metres. Fine- to medium-grained grey-coloured quartz-diorite shows a dioritic texture near the contact and grades into a coarser-grained phase deeper within the pluton. A thin section analysis of a sample from 1602 metres

shows abundant quartz and albite altered to epidote, sericite and lesser amounts of chlorite. Quartz and altered albite commonly form a relic intergrowth texture. Actinolite, chlorite and opaque minerals (3%) occur together in irregular-shaped clusters. The contact between the Flavrian Andesite and the Flavrian pluton occurs at a depth of 354 metres in hole A-497. The contact is sharp and the intrusive phase shows a typical quartz-porphyritic diorite texture. Analysis of a sample at 367.5 metres shows local quartz-albite intergrowths and irregular-shaped zones of hornblende, actinolite, and magnetite with minor amounts of sericite and stilpnomelane. In drill hole A-498, where the contact is observed at 337 metres depth, the intrusive border phase is fine- to medium-grained and quartz-porphyritic. Petrographic analysis shows a medium-grained texture composed of euhedral albite and intersertal quartz. Albite is weakly altered to sericite and epidote. Actinolite and chlorite occur in irregular zones associated with trace amounts of opaque minerals. Carbonate, epidote and chlorite are observed in a veinlet. In hole A-499, the contact between the andesite and the Flavrian pluton occurs at 307 m. The intrusive border phase is grey-coloured, fine- to coarse-grained and quartz-porphyritic. A diorite texture is observed in hand specimen. A weakly altered coarse-grained early trondhjemite occurs at 341 metres (deep within the pluton).

Consequently, the Flavrian pluton beneath Ansil is composed of several phases. Megascopically, quartz-porphyritic diorite-textured phases dominate near the pluton's contact with the Flavrian andesite. However, early trondhjemite also is observed at the contact. In thin section, intergrowth textures are abundant with albite commonly altered to sericite and epidote. Textures characteristic of tonalite (amphibole clots

and irregular-shaped zones within a matrix of quartz and plagioclase) are also common. In addition, some ill-defined trondhjemitic zones have been documented in drill logs and observed in thin section, suggesting the presence of heterogeneous tonalite and hybrid rocks.

Table VIII shows selected major element concentrations of the intrusive phases beneath Ansil, from Inmet's drill logs. The ranges in selected major element concentrations of tonalite from our samples of the pluton's outcrops are shown for comparison. The data indicate that concentrations of selected major elements for intrusive phases beneath Ansil are similar to those of outcropping tonalite. Geochemical data from Barrett et al. (1991) confirm the presence of tonalite beneath the Ansil deposit. However, sample AN-79 (1575 m) is enriched in SiO_2 and depleted in TiO_2 relative to other samples, suggesting that early trondhjemite also occurs at the contact with andesite. An early trondhjemite geochemical signature supports thin section analyses indicating coarse early trondhjemite at the contact. Also, sample A-499 (339 m) is interpreted to be hybrid phase because of its high SiO_2 and high TiO_2 contents.

Chemical discrepancies between surface tonalite and tonalite beneath Ansil are observed in An-74. Na_2O concentrations are lower in samples from beneath Ansil (3.4 to 3.8%) compared to surface tonalite (4.0 to 5.9%). Also, three samples from drill hole An-79 are enriched in SiO_2 (64.3 to 69.7%) relative to the surface tonalites (59.3 to 68.8%). The SiO_2 enrichment in AN-79 is probably due to a hybrid phase

	Surface Tonalite	AN-74 1588 m	AN-74 1590 m	AN-74 1609 m	A-498 353 m	A-499 339 m	AN-79 1575 m	AN-79 1603 m	AN-79 1620 m	AN-79 1651 m	AN-79 1672 m
SiO₂	59.3-68.8	66.7	69.0	67.5	65.9	72.8	73.7	68.9	59.9	69.7	64.3
TiO₂	0.58-1.7	0.9	0.9	0.9	0.9	0.9	0.5	0.8	0.9	0.9	0.8
FeO*	4.3-10.6	8.4	5.5	4.5	5.1	4.31	3.7	4.6	5.4	4.4	4.2
MgO	0.3-3.0	1.0	0.6	0.5	1.9	1.1	0.3	0.6	1.1	0.6	1.2
CaO	1.5-7.9	3.7	2.9	4.4	3.5	4.3	2.6	3.1	6.4	4.5	3.3
Na₂O	4.0-5.9	3.5	3.4	3.8	5.6	5.4	4.6	4.7	2.7	3.9	4.8
K₂O	0.2-1.0	0.5	0.8	0.3	0.3	0.3	0.4	0.2	1.1	0.4	0.5

Table VIII: Selected major element geochemistry of drill core samples from the intrusive border phase of the Flavrian pluton, beneath the Ansil deposit.

because the SiO_2 enrichment is accompanied by TiO_2 concentrations of 0.8 and 0.9% typical of tonalite.

The Ansil deposit lies within an envelope of Na-depleted strata that extends as a tabular east-west corridor up to 300 m wide and over 2000 m long (Galley, 1994). The discordant alteration zone extends from the contact of the Flavrian intrusion up through the Flavrian andesite, the Northwest Rhyolite and Rusty Ridge Andesite (Fig. 4.1B). It is characterized by the destruction and replacement of albite formed during spilitization to chlorite and/or sericite. The discordant zone of Na depletion is defined by a boundary of less than 3% Na (Galley, 1994). The Na-depleted zone beneath the Ansil deposit is characterized by a chlorite-sulphide mineral assemblage.

Although samples of tonalite beneath Ansil commonly show alteration of albite crystals, their concentrations in mobile major elements are similar to tonalite samples collected at the pluton's surface. One exception is AN-74, which is depleted in Na_2O relative to other tonalite samples. However, AN-74 still contains over 3% Na_2O . Consequently, either the tonalite samples beneath Ansil were only weakly affected by alteration related to the development of Ansil or the alteration of tonalite was caused by an unrelated thermal event (e.g., metamorphism).

The relatively high Na content of tonalite samples beneath the Na depletion zone related to the Ansil deposit, along with the lack of distinctive chlorite-sulphide alteration commonly associated with VHMS alteration, suggest that the tonalite beneath Ansil was not subjected to footwall alteration as were the overlying volcanic

formations. Based on observations discussed above, the tonalite beneath Ansil is interpreted to postdate the Na-depleted alteration pipe of the Ansil Cu-Zn deposit and therefore, the intrusion of tonalite postdated the formation of the Ansil deposit and its host Northwest rhyolite.

4.2.2 Timing of intrusion relative to the Corbet Cu-Zn deposit

The Corbet Cu-Zn deposit (Watkins, 1980; Knuckey and Watkins, 1982; Gibson et al., 1993; Barrett et al., 1991) is located in the upper part of the Flavrian andesite. The deposit occurs along the McDougall-Despina fault zone, interpreted to be a syn-volcanic structure (Watkins, 1980; Knuckey and Watkins, 1982). Offset markers on each side of the fault shows a southwest-side-down movement of at least 700 metres (Knuckey and Watkins, 1982). These relationships are presented in Figure 2.38, a cross-sectional view of the volcanic sequence containing the Corbet deposit. The crosscutting relation of the Flavrian early trondhjemite with the Upper Amulet Rhyolite is also observed in this figure. Because the trondhjemite is not observed at the same stratigraphic level on the other side of the McDougall-Despina Fault, it is inferred that the trondhjemite intruded the Upper Amulet Rhyolite following the main-stage movement along the McDougall-Despina Fault.

Based on surface and underground drilling, Gibson et al. (1993) observed that the Méritens intrusions were emplaced along the McDougall-Despina Fault. The contact between the quartz-diorite and the Flavrian andesite is generally sharp, and the quartz-diorite is typically fine-grained and chilled. These observations suggest that the Méritens phase was emplaced after the Flavrian Andesite. However, Gibson

et al. also noted that the Méritens quartz-diorite intrusion is cut by the Na-depleted chloritic alteration pipe of the Corbet deposit, which is located at the top of the Flavrian andesite. Alteration of the Méritens quartz-diorite is characterized by feldspars altered to fine-grained quartz, chlorite and/or sericite and mineralized with disseminated and stringer sulphides. From this evidence, Gibson et al. interpret the Méritens quartz-diorite intrusion at Corbet to have been emplaced along the McDougall-Despina Fault during extrusion of the Flavrian andesite and before formation of the Corbet Cu-Zn deposit.

The crosscutting relationships between the alteration zones of Corbet and Ansil with the Méritens quartz-diorite and tonalite phases of the Flavrian pluton indicate that at least part of the Méritens quartz-diorite was emplaced before the formation of the Corbet deposit and that tonalite was emplaced after the formation of the Ansil deposit. In addition, crosscutting relationships indicate that early trondhjemite transects the Upper Amulet Rhyolite and Amulet Andesite and therefore the early trondhjemite postdates the formation of Corbet, Ansil and other massive sulphide deposits spatially associated with the C contact exhalite.

In terms of relative timing, the formation of Cu-Zn deposits in the Noranda cauldron can be constrained to the interval of intrusion between the Méritens quartz-diorite and early trondhjemite: intrusion of the pluton is therefore associated with the development of the first and second cauldron cycles and their associated Cu-Zn deposits. A direct link based on field evidence can therefore be made between

intrusion of the Flavrian pluton and the formation of the Cu-Zn deposits of the Noranda cauldron.

4.3 Geochemical Comparison with Volcanic Rock of the Noranda Cauldron

4.3.1 Description of selected trace element diagrams

Geochemical data from 51 samples of the volcanic rocks of the Blake River Group (BRG) Flavrian Block of the Noranda cauldron were obtained from Shirley Péroquin (Ph.D. thesis in final preparation). The database includes analyses of samples from each of the volcanic formations of the Noranda cauldron (Table III). This section presents selected trace element plots of geochemical data from the Flavrian pluton and the volcanic rocks of the Noranda cauldron.

In Figure 4.2, the data from the BRG volcanic rocks have been contoured and are shown as shaded areas. The lighter shading represents values from the rhyolite formations whereas the darker shading corresponds to values from the andesite formations. Data from the various phases of the Flavrian pluton are represented by the symbols used in CHAPTER 3. The Fishroe rhyolite has been contoured separately because it is quite distinct and may represent a regional stratigraphic marker (Péroquin et al., 1996). The Norque rhyolite has also been contoured separately because it is Al_2O_3 - and Th-enriched compared to other rhyolites and early trondhjemite.

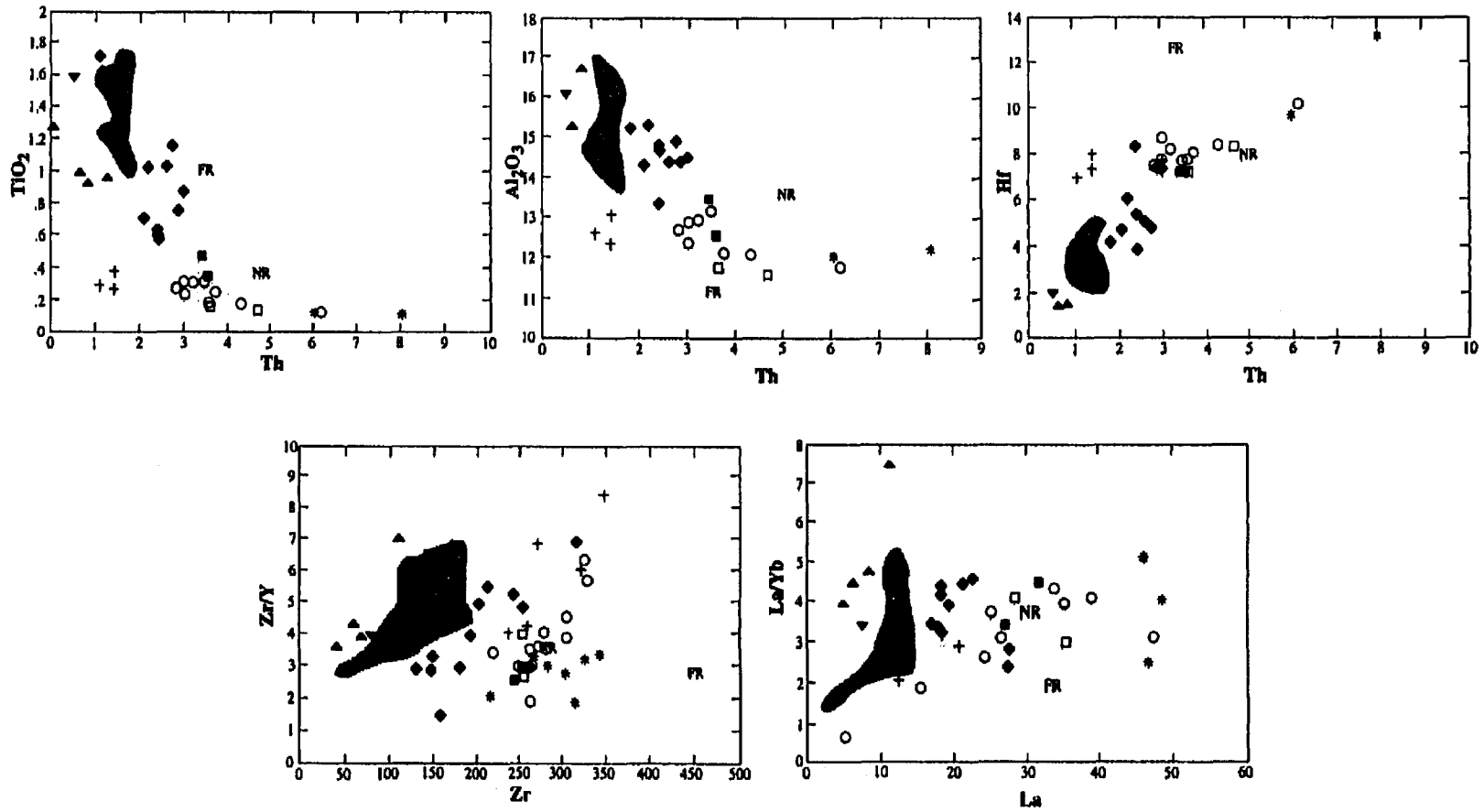


Figure 4.2: Selected geochemical variation diagrams comparing samples from the Flavrian pluton and volcanic rocks from the Noranda cauldron. Symbols legend: ▲: Méritens quartz-diorite, ◆: tonalite, ■: trondjemite porphyry, †: pink trondjemite, ○: early coarse-grained trondjemite, *: granophyre, ▼: Eldrich diorite, †: late trondjemite. Light coloured shading for rhyolite and dark shading for andesite whereas FR is area defined by Fishroe rhyolite and NR, Norque rhyolite. Geochemical data of volcanic rocks from Shirley Péloquin.

The TiO_2 vs Th plot (Fig. 4.2A) shows a broad negative correlation between TiO_2 and Th. At low TiO_2 values, the felsic rocks show large variations in Th. The Méritens quartz-diorite contains lower TiO_2 and slightly lower Th concentrations than the andesites. Tonalite data is significantly scattered and contains higher Th and lower TiO_2 concentrations than andesite. However, tonalite samples contain higher TiO_2 and Th concentrations compared to rhyolite and they plot between andesite and rhyolite. Significant overlap occurs between early trondhjemite and rhyolite with only a few samples of early trondhjemite plotting outside the area defined by rhyolite. Granophyre from the Flavrian pluton is clearly Th-rich compared to rhyolite of the Noranda cauldron, whereas late trondhjemite is Th-poor compared to rhyolite and the Eldrich diorite is clearly Th-poor relative to the andesites. The Fishroe rhyolite is enriched in TiO_2 relative to the early trondhjemite and enriched in Th relative to tonalite.

Similar relationships are observed on the Al_2O_3 vs Th plot (Fig. 4.2B) which shows a broad negative correlation. Méritens quartz-diorite is slightly depleted in Th compared to the andesites, with some overlap occurring between the Al_2O_3 -rich phases. Tonalite is enriched in Th compared to andesite and clearly plots as a separate group. Again, significant overlap occurs between early trondhjemite and rhyolite. However, granophyre clearly plots as a separate Th-rich group, whereas late trondhjemite plots as a Th-poor group. A Th depletion for Eldrich diorite relative to andesite is also observed on this diagram. The Norque rhyolite clearly plots as a separate Al_2O_3 -rich sample.

On a Hf vs Th plot (Fig. 4.2C), a positive correlation is observed for most of the intrusive and extrusive phases, with the late trondhjemite and Fishroe rhyolite plotting in separate fields. The Méritens quartz-diorite is depleted in Hf and Th relative to andesite although some overlap does occur. The tonalite's distinct chemical character is clearly observed, and it forms a well-defined group between rhyolite and andesite. As in the previous diagrams, early trondhjemite, including trondhjemite porphyry, pink trondhjemite and coarse-grained trondhjemite, forms a group that shows significant overlap with rhyolite. Granophyre is distinct in Th, and to a lesser extent, Hf enrichment compared to rhyolite. The Eldrich diorite is distinguished from the andesites by low Hf and Th contents and late trondhjemite is clearly distinguished from the rhyolites by a Th depletion. The Fishroe rhyolite forms a high-Hf, high-Th group that is clearly distinct compared to all intrusive phases.

The Zr/Y vs Zr plot (Fig. 4.2D) shows that intrusive and extrusive phases of the Noranda cauldron have Zr/Y ratios that range between 1.4 for a tonalite sample and 8.3 for a sample of late trondhjemite. The Méritens quartz-diorite forms a group that is slightly depleted in Zr compared to the andesites. Both groups show positive correlation trends that are slightly offset. The tonalites contain Zr concentrations that are intermediate relative to those of andesite and rhyolite. Most of the early trondhjemite samples plot below the area defined by the rhyolites, due to their low Zr/Y ratio. Granophyre forms a distinct group, with a lower Zr/Y ratio than rhyolite. Eldrich diorite is depleted in Zr relative to the andesites and late trondhjemite shows a wide range of Zr/Y ratios, possibly due to the coarse texture of the late trondhjemite

and concentration of these elements in trace minerals. The Fishroe rhyolite is clearly distinguished from the plutonic phases of the Flavrian by its exceptionally high Zr and Y concentrations.

On a plot of La/Yb vs La (Fig. 4.2E), La/Yb ratios vary between 0.66 for an early trondhjemite sample and 7.4 for a sample from Méritens quartz-diorite, with most of the samples ranging between 3 and 4. The volcanic rocks show a positive correlation, whereas the intrusive rocks show a broad flat trend. The Méritens quartz-diorite forms a steeply dipping group that parallels, but does not overlap with the andesites. Therefore, the quartz-diorite is slightly depleted in La relative to the andesites of the Noranda cauldron. However, tonalite contains higher concentrations of La compared to andesite and forms a well-defined group between andesite and rhyolite. Although early trondhjemite shows significant scatter compared to rhyolite, both phases clearly overlap. Granophyre forms a group at the high-La end of the diagram. The characteristic large variations in the La/Yb ratio at constant La concentrations for granophyre clearly distinguish it from the rhyolites. The Eldrich diorite is depleted in La relative to the andesites, and the late trondhjemite shows significant overlap with the andesites.

4.3.2 Interpretation of geochemical data

The Méritens quartz-diorite samples commonly plot on the low-incompatible element side of the andesite. This observation indicates that quartz-diorite is slightly depleted (with some overlap) in Th, Hf, Zr and La relative to the andesites of the Noranda cauldron. Although the depletion is small (~1 ppm in Th and Hf), it is

systematic. The depletion in Zr and La is reflected on the Zr/Y vs Zr and La/Yb vs La plots, where the Méritens quartz-diorite forms a group with a positive correlation that parallels the andesites but is slightly shifted to low Zr and La values. The quartz-diorite's systematic depletion in Th, Hf, Zr and La is interpreted to reflect either (1) differences in primary composition, or (2) preferential leaching of these elements in the quartz-diorite. The parallel trend exhibited by quartz-diorite on the La/Yb vs La plot suggests that both the quartz-diorite and andesites evolved in a similar manner and were closely related.

Tonalite contains higher concentrations of Zr, Th, Hf and La relative to andesites of the Noranda cauldron. The tonalites invariably plot between andesite and rhyolite, with little or no overlap. Therefore, tonalite does not appear to have major extrusive equivalents within the Noranda cauldron. This observation supports similar conclusions by Goldie (1976) and Paradis et al. (1988) indicating that tonalite does not have important extrusive equivalents.

Each of the diagrams shows significant overlap between the pluton's early trondhjemite and rhyolites of the Noranda cauldron. The overlap indicates that both phases were compositionally similar and intimately related. However, the Zr/Y vs Zr plot, shows that early trondhjemite has lower Zr/Y ratios than rhyolite. The lower Zr/Y ratios are due to an enrichment of Y in trondhjemites relative to the rhyolites. The evolutionary paths of early trondhjemite and rhyolite must have been practically identical, with slight variations in Y probably resulting from the crystallization of Y-bearing phases within the pluton.

Granophyre is enriched in Y, Hf, Th and La relative to the rhyolites of the Noranda cauldron. In addition, the enrichment in Y in granophyre is reflected in a lower Zr/Y ratio compared to the rhyolites. The granophyre's distinctive geochemistry indicates that there are no major extrusive equivalents to granophyre within the Noranda cauldron.

Although only one sample was analyzed, the Eldrich diorite is depleted in Th, Hf, Zr and La relative to the andesites. Therefore, the Eldrich diorite did not have any extrusive equivalents within the cauldron.

The late trondhjemite is depleted in Th and La and shows a slightly lower La/Yb ratio compared to the rhyolites. It does, however, show some overlap with the andesites on the La/Yb vs La plot, as well as a partial overlap with rhyolites on the Zr/Y vs Zr plot. As discussed in CHAPTER 3, late trondhjemite shows a distinct geochemical signature relative to early trondhjemite. The overlap in the La/Yb and Zr/Y ratios suggests that, although the late trondhjemite's evolutionary path was different, it was probably derived from a similar source. The depletions in Th and La, along with crosscutting relationships described in CHAPTER 2, identify the late trondhjemite as a separate, late intrusion.

The Fishroe rhyolite is clearly distinct from other rocks in the Noranda area. Although overlap does occur on several plots between the Norque rhyolite and early trondhjemite, the distinctive Al_2O_3 and Th enrichment of the rhyolites suggests that the rhyolites are not directly related to early trondhjemite.

4.4 Discussion

The crosscutting relationships described by Gibson et al. (1993) for the Méritens quartz-diorite at Corbet indicate that a clear association can be made between initial cauldron subsidence, including deposition of the Flavrian Andesite, and intrusion of the Méritens quartz-diorite. In addition, the chemical similarities between the Méritens quartz-diorite and the andesite of the Noranda cauldron suggest that these two lithologies were closely related, with slight differences caused either by primary differences in the compositions of the intrusive and extrusive rocks or by preferential alteration of the quartz-diorite.

Crosscutting relationships between the Flavrian early trondhjemite and the volcanic rocks of the Noranda cauldron indicate that the youngest volcanic formation cut by the early trondhjemite is the Amulet andesite. Therefore, at least part of the early trondhjemite intruded the Noranda cauldron after the deposition of the Amulet andesite, the last volcanic formation of the 2nd cauldron cycle (see Table III). However, the trondhjemites and rhyolites show almost identical geochemical signatures, suggesting that they were cogenetic and related both in time and space. The multi-phase character of early trondhjemite (see CHAPTER 2) implies that early phases of early trondhjemite may have been extruded from the chamber, whereas later phases may have replenished the chamber. The trondhjemite's enrichment in Y relative to the rhyolites may indicate crystallization of Y-bearing minerals within the magma chamber after an extrusion that is now represented by rhyolite.

The chemical compositions indicate that the granophyre, Eldrich diorite and late trondhjemite did not have extrusive equivalents within the Noranda cauldron. Crosscutting relationships described in CHAPTER 2 show these phases to have been the latest of the pluton; i.e., the compositional link between the Flavrian pluton and the volcanic rocks within the Noranda cauldron apparently terminated during intrusion of the early trondhjemite.

From a plutonic perspective, development of the Noranda cauldron is constrained to an interval of time that began with intrusion of the Méritens quartz-diorite and ended before emplacement of the three early trondhjemite phases (trondhjemite porphyry, pink trondhjemite and coarse-grained trondhjemite). The minor amounts of dacite within the Noranda cauldron indicate that tonalite had little or no extrusive equivalent. Thus, only the earliest phases of early trondhjemite could have had direct extrusive equivalents within the Noranda cauldron, because a significant part of the early trondhjemite cuts the tonalite (see CHAPTER 2). Consequently, the trondhjemite porphyry may represent intrusive remnants of Noranda cauldron rhyolite. Trondhjemite porphyry inclusions occur throughout early trondhjemite, especially in an ENE-trending zone within the southern part of the pluton.

The distinct geochemistry of the Fishroe rhyolite and, to a lesser extent, the Norque rhyolite, suggests that these lithologies do not have intrusive equivalents within the pluton. The Fishroe and Norque rhyolites occur within Cycle 4, suggesting that the compositional link between the Flavrian early trondhjemite and

the felsic volcanic rocks of the Noranda cauldron terminated during or before the onset of Cycle 4.

Figure 4.3 depicts an interpretation of the evolution of the Flavrian pluton relative to the development of the volcanic cycles of the Noranda cauldron. Quartz-diorite probably intruded the pre-cauldron volcanic rocks of Cycles 1 before the cauldron development. Magma within the sill-dike complex would have eventually extruded to the surface to form the Flavrian andesite formation during the onset of cauldron development. Early trondhjemite (perhaps trondhjemite porphyry) also would have been channelled via dikes to the surface to form rhyolites of the 1st cauldron cycle. Therefore, magmatic equivalents of Méritens quartz-diorite and early trondhjemite were probably extruded to surface during a period of active volcanism, with little residence time for the melt in the subvolcanic chamber. The subvolcanic and volcanic systems were probably open.

The C contact tuff marks a break in volcanism between cauldron Cycles 1 and 2 (Gibson and Watkinson, 1990). This unit is an extensive, although discontinuous, volcanic exhalative metalliferous sediment stratigraphically associated with VHMS deposits (Kalogeropoulos and Scott, 1989). During the deposition of this sediment, the supply of magma from the Flavrian magma chamber to the volcanic environment must have effectively ceased or considerably diminished. Because the chamber probably contributed significant amounts of magma during extrusion of Cycle 1 volcanic rocks, the chamber would have diminished in size, with volume loss causing subsidence of the overlying volcanic pile. Replenishment of the subvolcanic magma

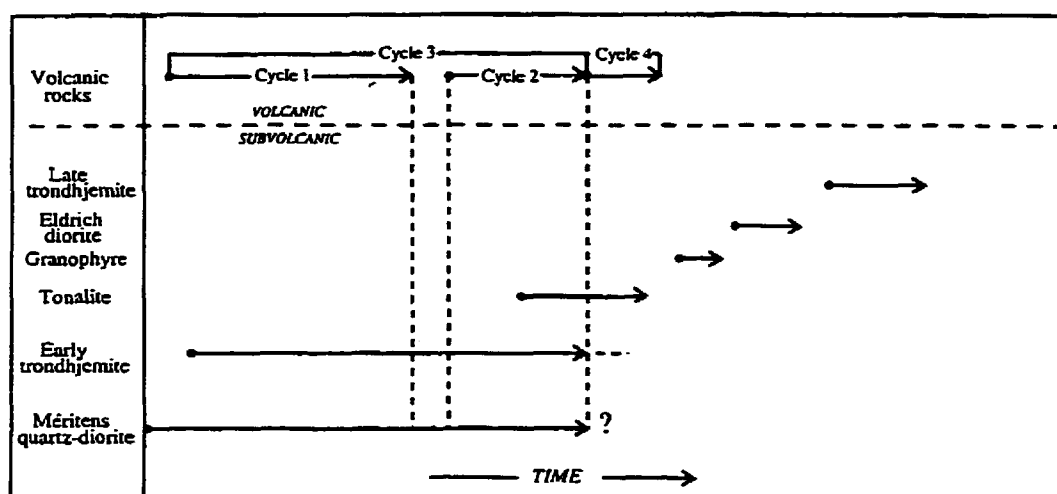


Figure 4.3: Interpretation of the evolution of the Flavrian subvolcanic pluton in relation to volcanic rocks of the Noranda cauldron.

chamber may have occurred with little or no extrusion between the two cauldron cycles. Replenishment of subvolcanic chambers commonly follows major extrusive events (Stix and Gorton, 1993), and replenishment of the underlying chamber, without extrusion, would have caused doming of the volcanic sequence through the reactivation of syn-volcanic faults and fracture zones. Doming of overlying volcanic sequences due to replenishment of an underlying chamber commonly occurs in active volcanic systems (Dzurisin and Yamashita, 1987).

The onset of Cycle 2 volcanism (i.e., extrusion of the Waite and Millenbach rhyolites) was associated with the formation of several VHMS deposits. The magma chamber may have been fully replenished at this point. Renewed extrusion of rhyolite would have, once again, caused volume reduction within the chamber and subsidence of the overlying volcanic rocks. The compositional differences between early trondhjemite and Cycle 4 rhyolite suggests that the link between the chamber and the overlying volcanic rocks terminated before or during the onset of Cycle 4. The system probably closed during intrusion of early trondhjemite. Cycle 5 is probably too far (>12 km) from the Flavrian magma chamber to have been associated with its emplacement. However, another similar pluton (the Cléricy sill) may represent the remnants of a magma chamber related to Cycle 5 volcanic rocks.

The lack of extrusive equivalents to tonalite suggests that the system was closed during formation of this phase of formation of the Flavrian pluton. Tonalite was probably formed by a combination of differentiation of a more mafic magma and interaction with early trondhjemite. Granophyre is probably a late-stage product of

increased differentiation of early trondhjemite. Granophyre has no extrusive equivalents and apparently unrelated to volcanic activity. The crosscutting relationships and compositions of Eldrich diorite and late trondhjemite suggest that they are also unrelated to volcanic activity.

CHAPTER 5

CHAPTER 5. DISTRIBUTION OF GOLD MINERALIZATION AT THE PIERRE BEAUCHEMIN MINE: CONSTRAINTS ON THE TIMING OF GOLD MINERALIZATION WITHIN THE FLAVRIAN PLUTON

5.1 Introduction

The Flavrian subvolcanic pluton hosts a number of gold deposits and prospects that have been mined or explored since 1948. An estimated 66 000 kg (2.1 M ounces) of gold have been extracted from seven deposits located in the Flavrian and Powell plutons (Richard et al., 1991; Carrier, 1994). Most of the production (63%) has come from the Pierre Beauchemin, Elder and Silidor mines. The three deposits are located in third-order structures near their intersection with the Smokey Creek (Mouilleuse) Fault, a northwest-trending second-order structure (Fig. 5.1). Locally, all three deposits are spatially associated with diorite dikes that cut trondhjemitic and tonalitic host rocks, with most of the mineralization occurring at or near the dike-granitoid contact.

The fact that significant gold occurs within the pluton raises questions related to the timing of mineralization. Was gold mineralization within the pluton related to pluton emplacement and/or the formation of VHMS deposits or was it a late-stage event related to regional compression? The aim of this chapter is to describe the geology of the Pierre Beauchemin gold deposit with a focus on the role of metamorphosed mafic dikes in the formation and distribution of auriferous ore lenses

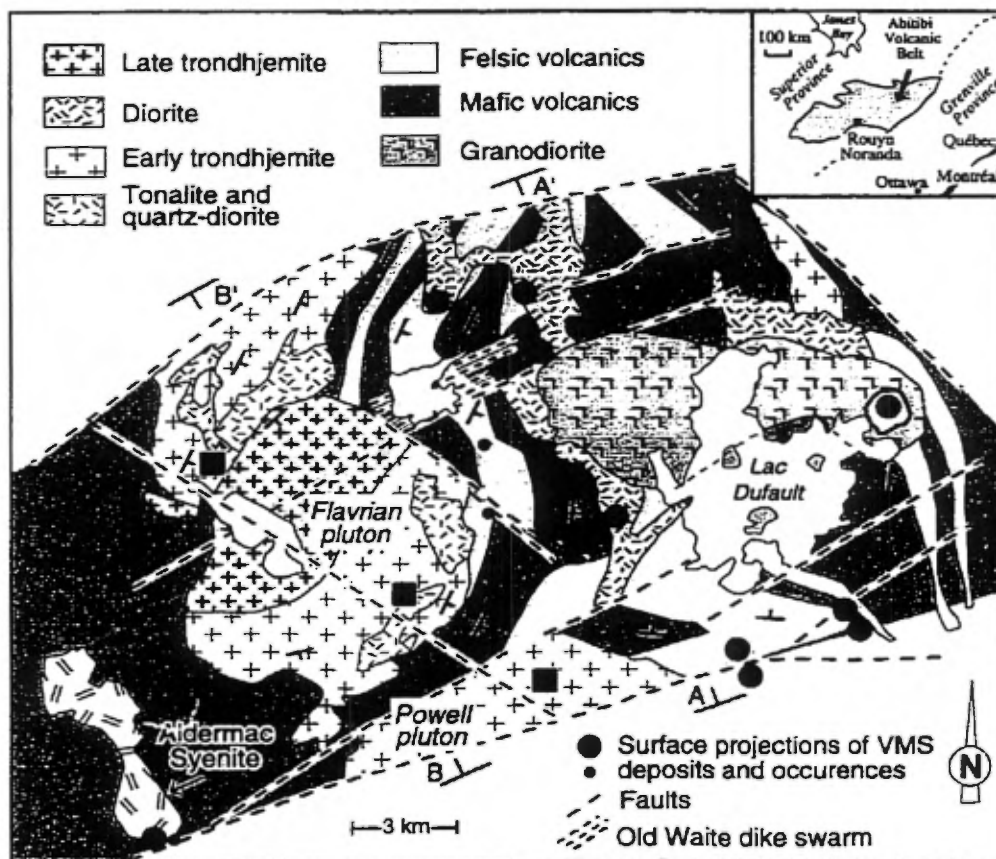


Figure 5.1: Simplified geological map of the Noranda Cauldron showing locations of gold deposits within the Flavrian and Powell Plutons. (1) Pierre Beauchemin Mine, (2) Elder Mine and (3) Silidor Mine. Modified from Gibson and Watkinson (1990).

and ore shoots. A kinematic analysis is conducted using shear and associated slip vector orientations to establish the structural framework that governed the distribution of gold. In addition, vein mineralogy and textures are described and interpretations related to the nature of mineralizing fluids are discussed. Finally, constraints on the timing of mineralization are established in answer to the question presented above.

5.2 Description of Host Rocks at the Pierre Beauchemin Mine

5.2.1 General

The Pierre Beauchemin gold mine (formerly Eldrich mine) produced about 2 Mt of ore grading 5 g/t. It is located at the intersection between the Eldrich Fault and the Eldrich diorite in the northwestern part of the Flavrian pluton (Fig. 5.2). Three major rock types form the host granitoid rocks in the mine area: early trondhjemite, tonalite and hybrid rocks. Contacts between these intrusive phases are gradual to sharp, and trend northeast with dips of approximately 30° to 50° to the southeast. Figure 5.3A shows primary layering within trondhjemite. Petrographic analysis indicates that the layering reflects textural variations.

The granitoid rocks are cut by a series of mafic diorite dikes that generally trend northward and dip 30° east in the mine area. The dikes are characterized by a series of discontinuous masses of metamorphosed and altered diorite that pinch and swell and vary significantly in orientation at the local scale (Figs. 5.3B, 5.4A and 5.4B). The dikes that form the Eldrich diorite unit are described in CHAPTER 2.

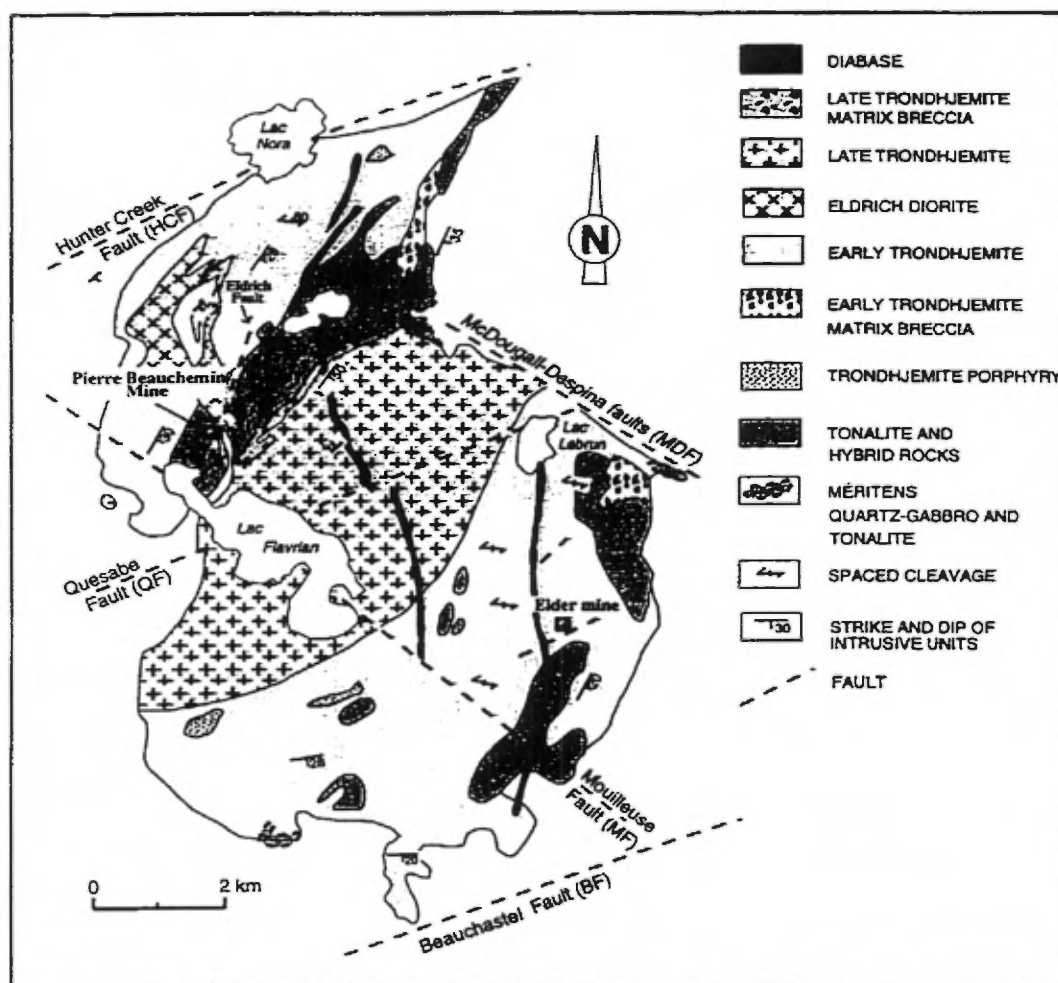


Figure 5.2: Simplified geological map of the Flavrian pluton showing location of the Pierre Beauchemin gold deposit. From Goldie (1976), Kennedy (1984) and this study.

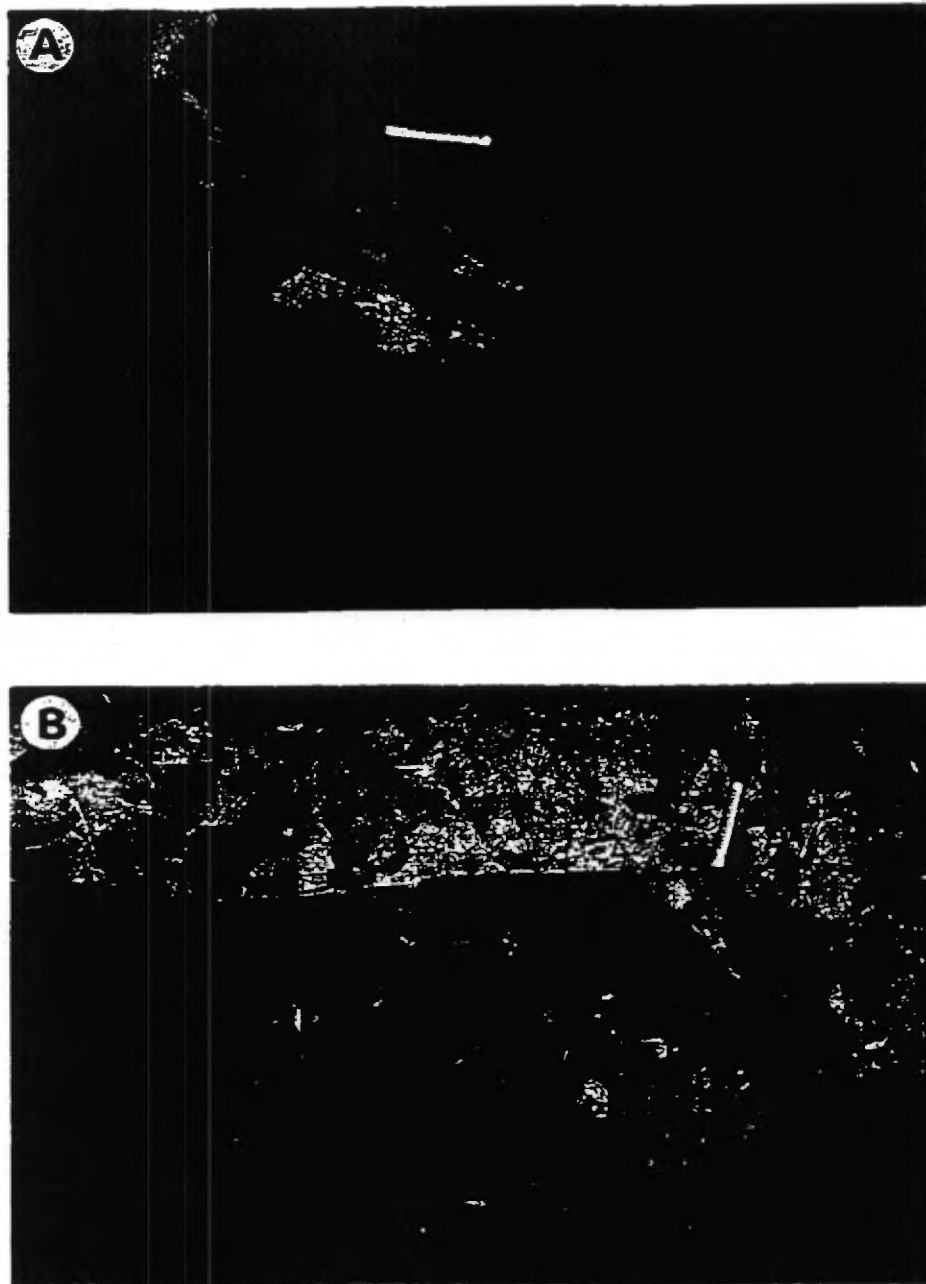


Figure 5.3: A) primary layering within trondhjemite, level 4 south (8+80 N); and B) an undeformed contact between tonalite and diorite, level 4 (13+80 N).

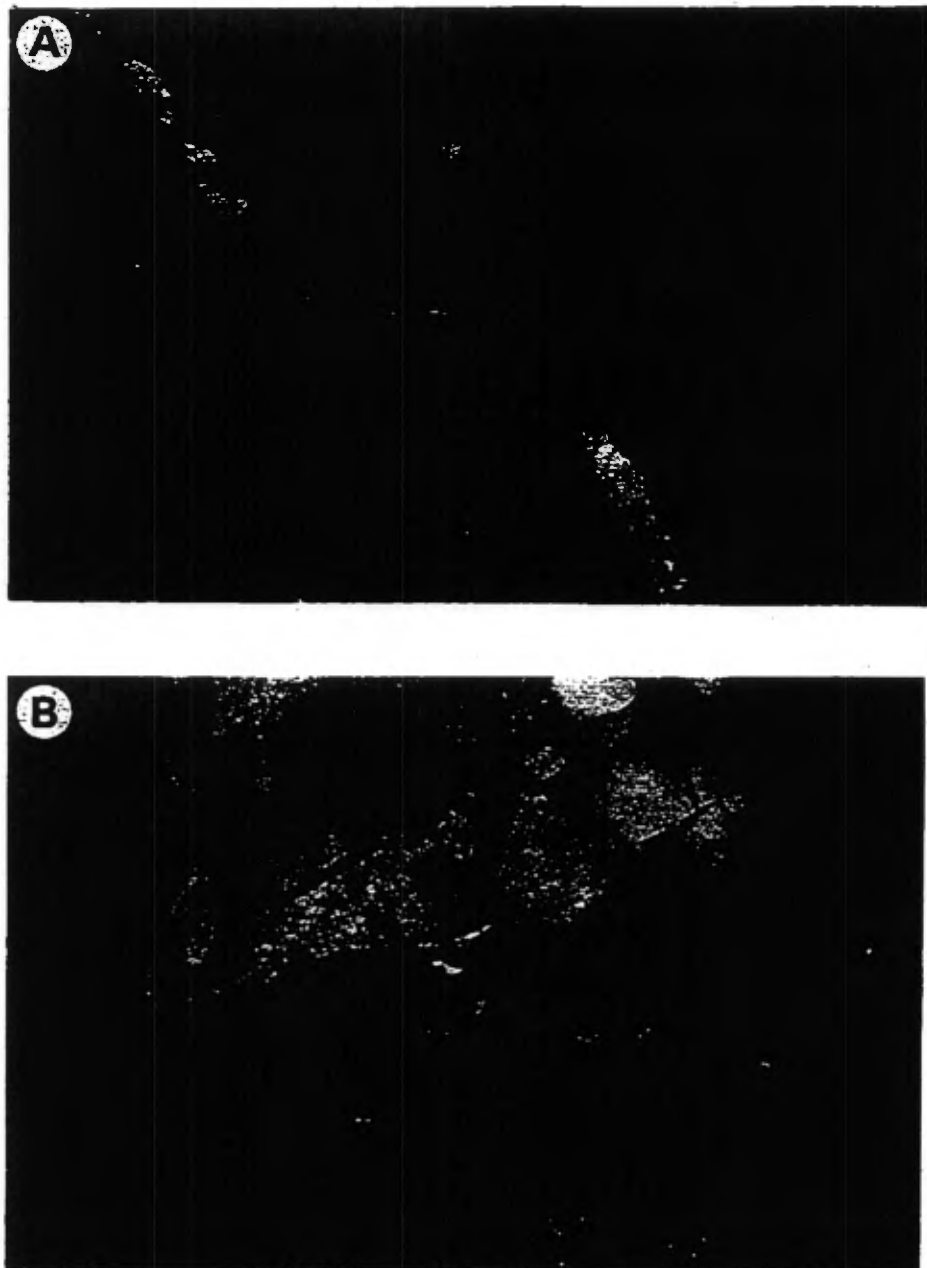


Figure 5.4: A) small diorite dike crosscutting aplite dike within trondhjemite, level 6 (11+80 N) and B) en echelon diorite dikes within tonalite. Note the variation in orientation of the primary contact between diorite and tonalite (shape of the dike), level 6 (11+80 N).

Figure 5.5 presents stereographic polar projections of the unstrained granitoid-diorite contact of the main dike throughout seven levels of mine development. These projections demonstrate that the dike is non-planar and that the strike and dip of the dike's intrusive contacts are distributed along a great circle. The significance of this distribution is discussed later. Other minor rock types in the mine area include aplitic dikes, mafic volcanics and lamprophyre dikes.

5.2.2 The granitoid rocks

The granitoid rocks of the Pierre Beauchemin mine are typical of those described in CHAPTER 2. Early trondhjemite is mainly composed of quartz and plagioclase (An₂ to An₂₅) accompanied by mafic mineral constituents, generally amphibole (actinolite and hornblende), chlorite and epidote. Primary textures in the trondhjemite vary from granitic (Fig. 5.6A) to granophyric to intersertal, and include important grain-size variations (cryptocrystalline to 7 mm). Radiating aggregates of mafic mineral constituents are common in the tonalites where the grain size is more uniform and averages 5 mm. In the mine area, the granitoid rocks are characterized by mineralogical and textural variations defining a series of intrusive sills trending NNE and dip 30°.

Highly strained granitoid rocks exhibit local grain-size reduction, recrystallization and Na-metasomatism of the quartz + plagioclase assemblage to quartz + albite. Fractures containing hydrothermal quartz, chlorite and carbonate transect the rock, giving it a brecciated texture with fragments of highly variable sizes (Fig. 5.6B).

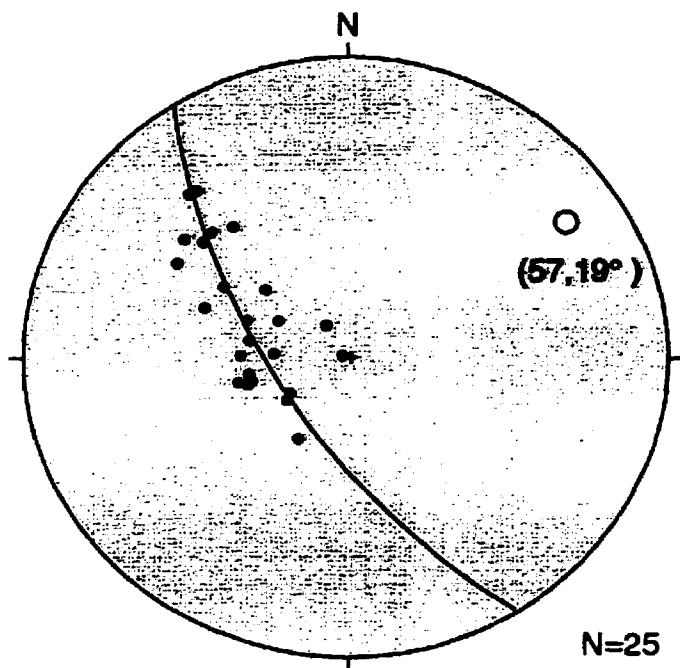


Figure 5.5: Stereographic polar projections of unstrained granitoid-diorite contacts. Measurements were taken from the main dike within domain III throughout 7 levels of the mine. The circle represents the pole of the "best fit" great circle that corresponds to the axis of curvature of the dike. This axis represents the variation of primary emplacement contact orientations of the diorite dike. Lower hemisphere equal-area projection.

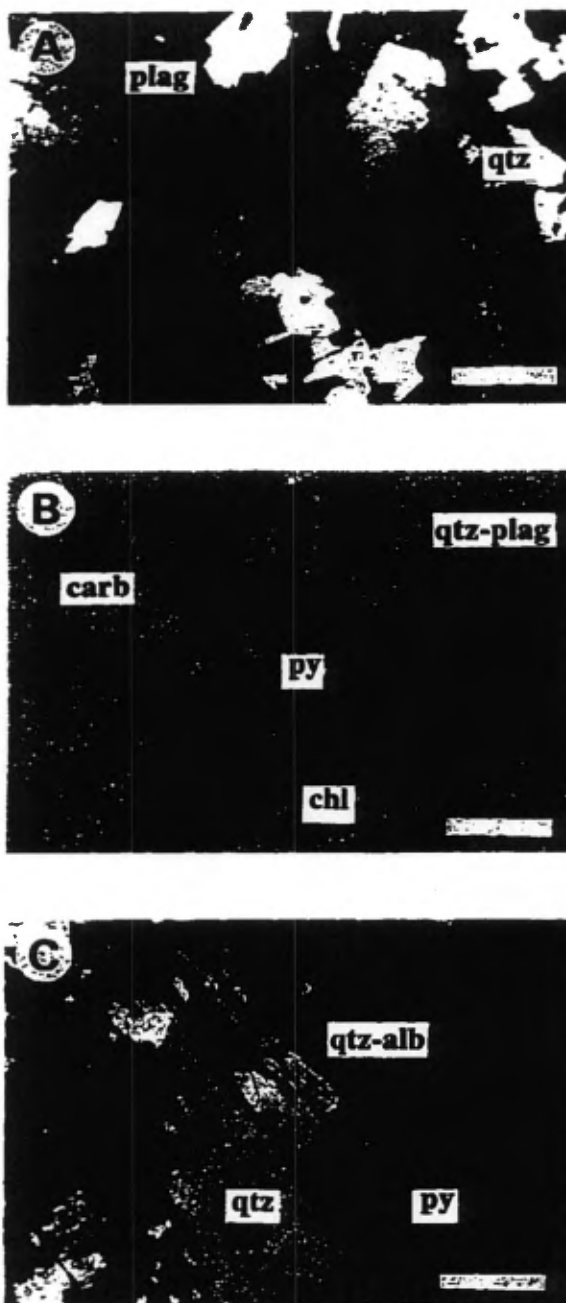


Figure 5.6: Photomicrographs of: A) unstrained trondhjemite showing a typical granitic texture; B) an intersection-type vein in granitoid showing a typical breccia texture; and C) shear vein in granitoid showing breccia texture and recrystallized albite-quartz matrix. Abbreviations: plag: plagioclase; qtz: quartz; act: actinolite; carb: carbonate; ser: sericite; py: pyrite; chl: chlorite; alb: albite. Scale bars = 1 mm.

5.2.3 The Eldrich diorite

Mafic dikes of diorite composition vary from a few centimetres to 40 m in thickness (with an average of 20 m), and account for less than 5% of the total rock mass in the mine area. Where undeformed, the diorite is composed mainly of plagioclase phenocrysts (altered to clay minerals, sericite, epidote and carbonate) set in a chlorite + actinolite + epidote-rich matrix. An intersertal or sub-ophitic to ophitic texture is commonly visible (Fig. 5.7A). These mafic dikes show relatively homogeneous textures compared to the granitoids, and two varieties of diorite are recognized: a coarse-grained type associated with large dikes (for example, 10 m in width), and a fine-grained type associated with small dikes (for example, 20 cm in width).

High strain zones within the diorite are characterized by a well-developed planar fabric where C/S fabric relationships are observed (Fig. 5.7B). Chlorite, sericite and carbonate are present in the strained examples, with phyllosilicates showing a preferred orientation in the direction of slip. The slip planes isolate carbonate-rich areas characterized by low strain.

At the highly strained contacts between dikes and granitoids, the diorite is transformed to a chlorite + sericite + carbonate schist, whereas the granitoid host rock remains relatively undeformed (Fig. 5.8). These features illustrate the difference in deformation styles for both the diorite dikes and the host granitoid rocks.

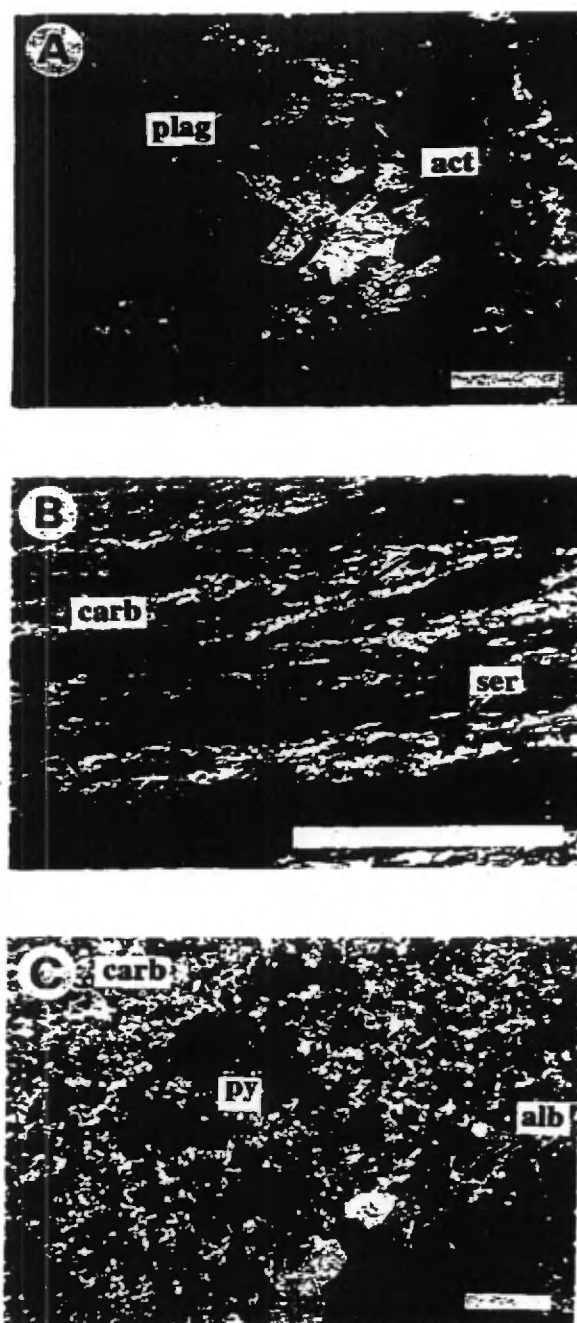


Figure 5.7: Photomicrographs of: A) unstrained diorite showing an inherited ophitic texture; B) highly strained unmineralized diorite, with C/S fabric relationships; and C) a contact vein showing an unstrained intensely altered texture. Abbreviations: plag: plagioclase; qtz: quartz; act: actinolite; carb: carbonate; ser: sericite; py: pyrite; chl: chlorite; alb: albite. Scale bars = 1 mm.

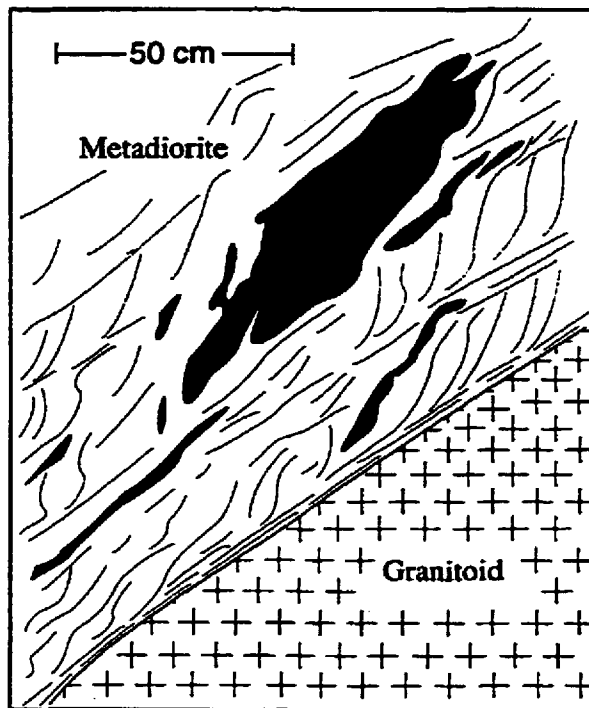


Figure 5.8: Shear zone at a granitoid-dike contact, showing that deformation was concentrated in the less competent diorite dike which has been transformed to a chlorite-sericite-carbonate schist. Black shading is for quartz-carbonate veins. Level 6 N (15+10 N). Sketched from photograph.

The megascopic and microscopic observations described above demonstrate that, where deformed, the diorite dikes show ductile deformation characteristics, whereas the deformed host granitoids show more brittle deformation characteristics. The contrast in deformation style is attributed mainly to the respective mineralogies of the rock type; the diorites being composed dominantly of chlorite, epidote, plagioclase, sericite and carbonate, are less competent than the host granitoid rocks composed chiefly of plagioclase and quartz. The bulk of the deformation was therefore concentrated within the dikes and their contact zones. The difference in competence suggests that deformation may have been initiated in the diorite dikes or at granitoid-dike interfaces (Belkabir et al., 1994).

5.3 The Eldrich Fault Zone

Drill-hole information suggests that the Eldrich Fault zone can be followed along strike for over 3 km. Generally, it trends and dips N25°E/40°SE, and shows a maximum true width of 75 m in the mine area. Detailed mapping of over 7 km of underground workings within the Eldrich Fault at the Pierre Beauchemin gold mine shows that the fault zone is composed of a complex series of anastomosing shear planes and fractures. Highly strained shears separate zones of low strain.

Crosscutting features observed both at the pluton and mine scales clearly indicate that the diorite dikes transect the host tonalite and trondhjemite and that the Eldrich Fault zone, which host the gold mineralization, clearly transects the Eldrich diorite, early trondhjemite and tonalite (Fig. 5.2). This observation indicates that

deformation responsible for the present distribution of gold at Pierre Beauchemin followed emplacement of the Eldrich diorite.

5.3.1 Shear orientations

The Eldrich Fault can be divided into five alternating domains (I, II, III, IV and V) according to their shear-zone orientations and host lithologies. These domains are observed at all mine levels; level 4 is presented in Figure 5.9. Within domains I, III and V, shears trend north, dip 25 to 40° east, and generally lie parallel to and commonly within the diorite dikes (Fig. 5.9A and 5.9B). Within the intervening domains II and IV, shears generally trend N30° with dips of 40° NE as well as N60° with dips of 50 to 60° SE, respectively, and are generally restricted to the granitoid rocks.

Figure 5.9A shows that if all shears (minor and major) are taken into account, small variations in shear orientation are observed in passing from one domain to another. These modest variations are attributed to the relatively high number of measured minor shears that show significant changes in orientation over short distances, causing scatter in the data for individual domains. However, major shears consistently show significant changes in orientation (>30° in strike and up to 35° in dip) as they pass from one domain to another (Fig. 5.9B). Because the major shears commonly contain ore veins, variations in shear orientation significantly affect exploration and exploitation procedures.

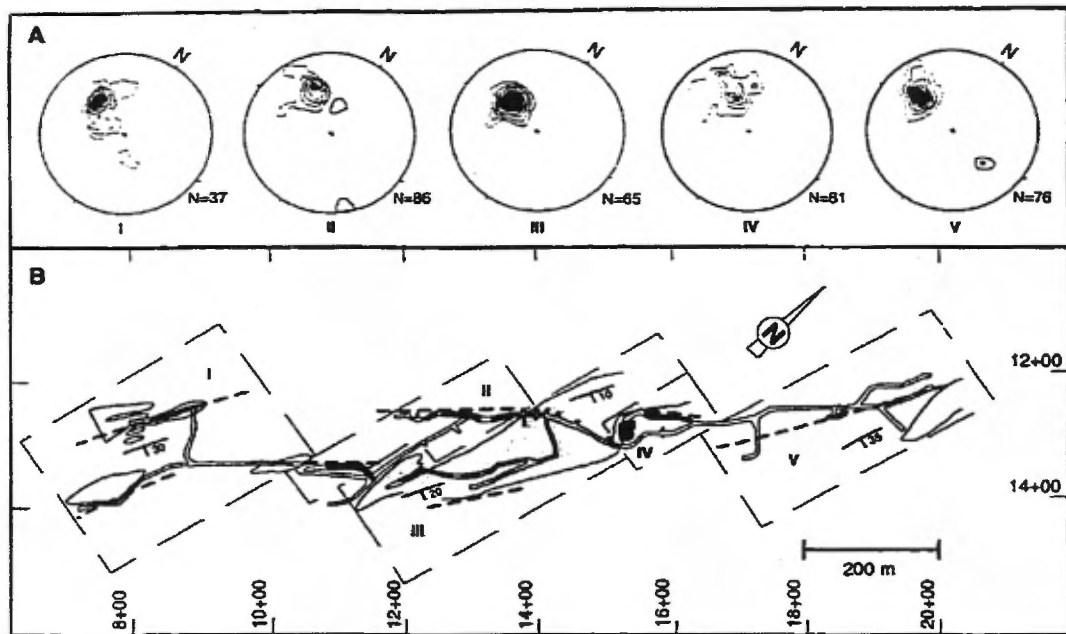


Figure 5.9: A) stereographic polar projections of shear zone orientations measured throughout the mine, showing domains (I through V), lower hemisphere equal-area projection, 2% contour intervals; and B) domains, geology and mineralized zones at level 4. Diorite dikes are lightly shaded whereas mineralized zones are black and major shears are represented by dashed lines. Dip symbols are for diorite-granitoid contacts.

5.3.2 Slip vectors and fault kinematics

Major shears commonly display well-exposed slip surfaces. Slickenline and slickenside measurements demonstrate that north-trending shears within domains I, III and V, had reverse sinistral movements (Fig. 5.10). As in the case of the north-trending shears, the N30°-trending shear planes, show reverse movements with minor sinistral components, whereas the N60°-trending shears show reverse movements with minor dextral strike-slip components.

5.4 Mineralization

5.4.1 Vein types and their orientations

Ore zones can be found in both major rock types (diorite and granitoid) and consist of an echelon rhombohedral-shaped lenses. The lenses are limited to the 75 m width of the Eldrich Fault and are found throughout the 1.2 km of mine development along the strike of the fault. The mineralized bodies vary from a host rock-dominated assemblage containing introduced vein minerals to intensely altered and mineralized zones where original mineral assemblages and textures are totally replaced. Several types of veins are distinguished on the basis of host-rock associations, orientations and textures. The vein types and their respective textures vary where the veins cross different rock types (except for the intersection-type veins which occur at the intersection of both rock types). The principal characteristics of these lenses are presented in Table IX.

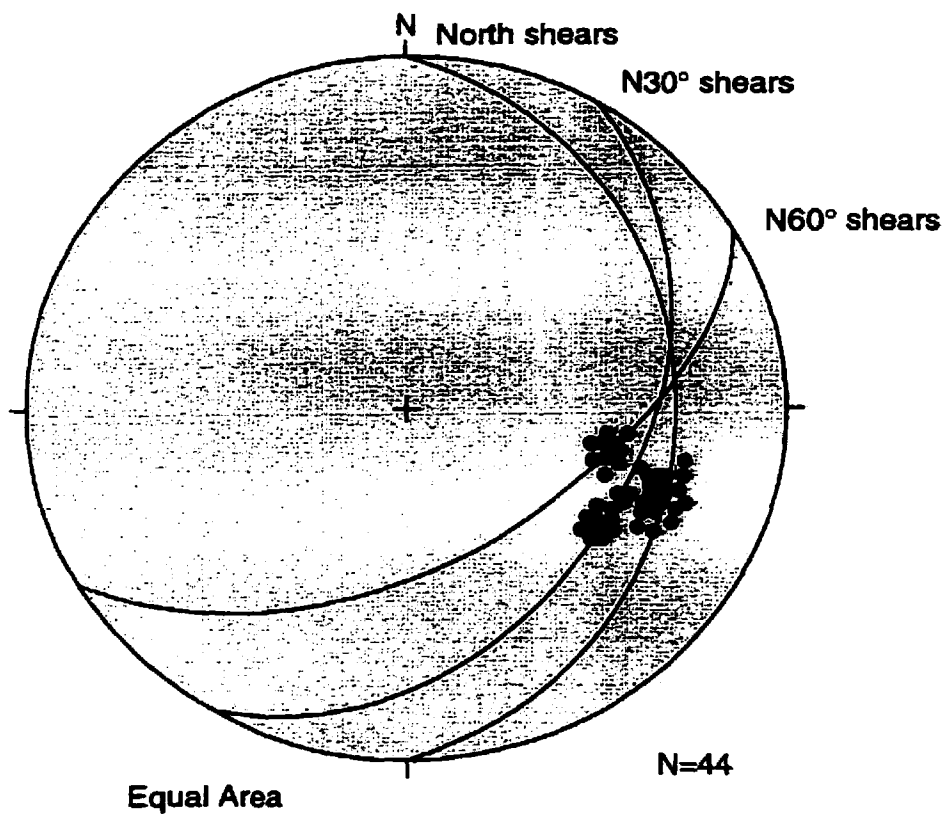


Figure 5.10: Stereographic representation of slip vector orientations measured from slickenlines on major shear surfaces. The orientations of major shears are plotted as great circles on the stereogram. Lower hemisphere equal-area projection.

Ore shoot	Vein type	Texture
Type 1 dike-associated	a) shear-vein within diorite zone.	sheared, brecciated, disseminated
	b) shear-vein and breccia at granitoid-dike intersection. "intersection-type" vein.	sheared and brecciated
	c) intensely altered zone at the tonalite-diorite interface. "contact-type" vein.	disseminated, minor shearing
Type 2 granitoid-associated	a) shear-vein within granitic rocks	brecciated, sheared
	b) extensional veins (minor)	elongated quartz, open space filling
	c) shear-vein and breccia at granitoid-dike intersection. "intersection-type" vein.	sheared and brecciated

Table IX: Ore shoots and their associated veins.

Veins located in domains I, III and V may occur (1) as shear veins occupying north-trending shear planes (Figs. 5.11 and 5.12); (2) as intensely altered segmented zones (contact veins) at granitoid-dike contacts that may be indirectly related to shear zones; or (3) as intersection veins where breccia zones are located at granitoid-dike intersections. Within domains II and IV, granitoid rocks host mineralization. Granitoid-hosted ore lenses occur as shear veins (Figs. 5.11 and 5.12) that typically display a brecciated texture (see Section 5.4.3).

Diorite-associated veins in domains I, III and V dip 10 to 40° east, and lie parallel to the north-south trend of the diorite dikes (Fig. 5.13). The shape of the dikes controls variations in the strike and dip of diorite-associated veins. However, granitoid-associated veins (domains II and IV) are oriented either N30°E/40° SE or N60°E/50 to 60° SSE (Fig. 5.13).

5.4.2 Vein mineralogy

Economic veins hosted either by diorite or granitoid rocks contain carbonate, pyrite, chlorite, quartz, albite ± sericite ± magnetite ± specularite ± rutile ± chalcopyrite and gold. Carbonate occurs as calcite and ferro-dolomite (Trudel et al., 1991), either as fine-grained disseminations of variable abundance or as euhedral to subhedral grains in veins; it is commonly associated with chlorite and pyrite and is abundant in mineralization associated with diorite (Fig. 5.7C). Dark-green chlorite occurs in veinlets and fractures and forms the matrix of chlorite breccia. Chlorite is commonly associated with pyrite in mineralized zones (Fig. 5.6B). Euhedral to subhedral clear albite is associated with quartz in breccia fragments or occurs as

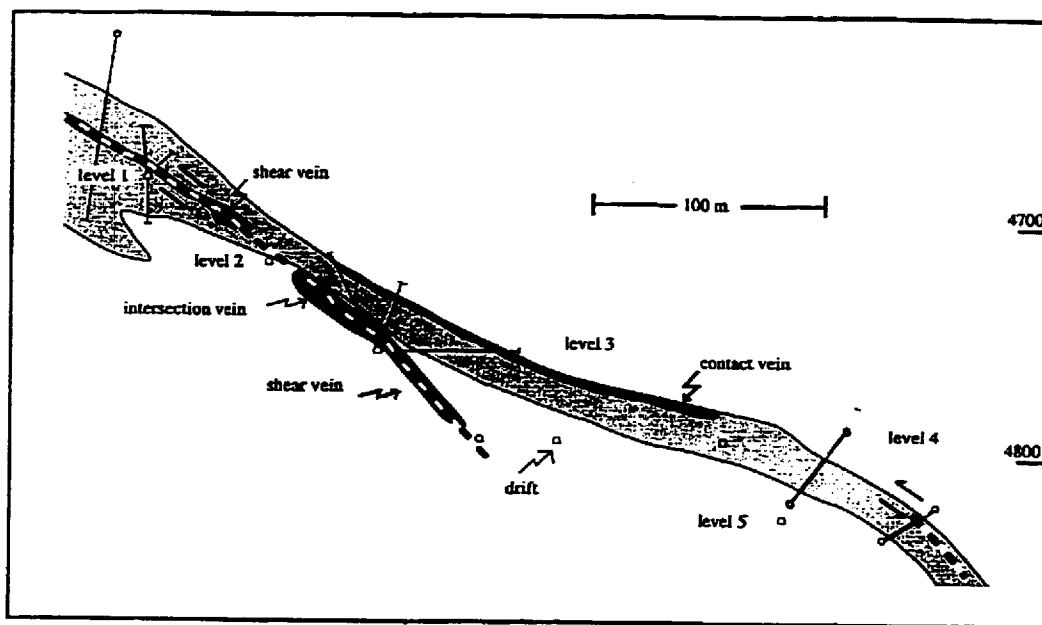


Figure 5.11: Cross-section at azimuth $N90^\circ$, perpendicular to the main diorite dike of structural domain III, showing the non-planar geometry of the dike and various vein types.

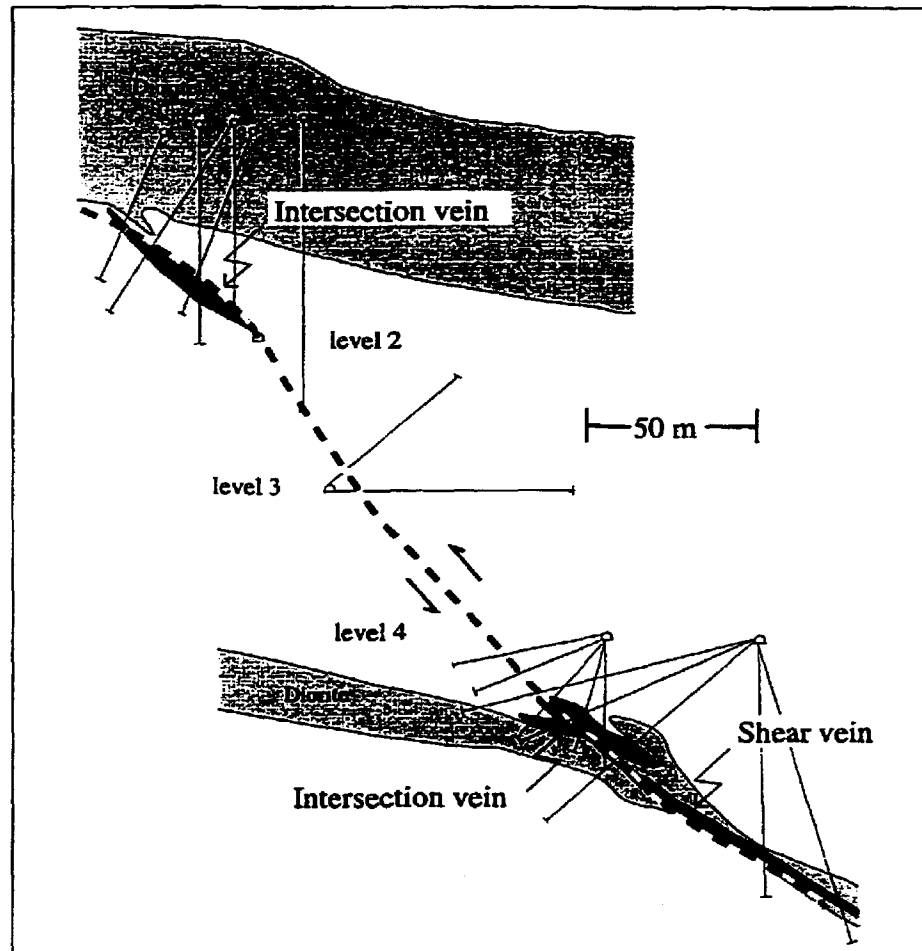


Figure 5.12: Cross-section at 17+40 N, showing sectional shear refraction and various vein types.

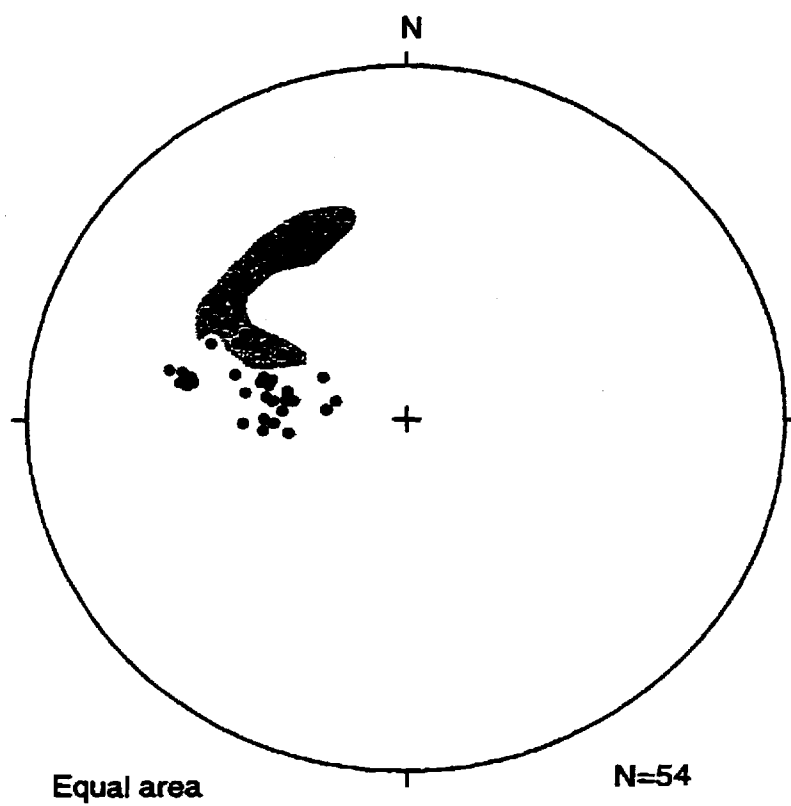


Figure 5.13: Stereographic polar projections of economically mineralized veins; dark shaded area for veins associated with domains II and IV, light-grey shading for veins associated with domains I, III and V. Lower hemisphere equal-area projection.

recrystallized fine-grained matrix in breccia. Albite also occurs, less commonly, as euhedral crystals in intensely carbonatized samples (Fig. 5.7C). Quartz occurs mainly as early fragments within breccia derived from the wall-rocks (Fig. 5.6B). However, it also occurs as vein quartz and as recrystallized grains associated with albite in the matrix of strained granitoid.

Opaque minerals observed in mineralized veins at Pierre Beauchemin include pyrite, magnetite, specularite, chalcopyrite and gold. Pyrite is by far the most common opaque mineral and generally constitutes between 1 and 7% of mineralized rock. Other opaque minerals listed above are normally found in trace amounts. Two distinctive types of pyrite are observed: (1) subhedral to euhedral disseminated crystals (0.5-1.7 mm in size) associated with carbonate \pm quartz \pm chlorite and \pm albite; and (2) fractured crystals commonly with corroded edges in contact with chlorite. Type 2 pyrite hosts numerous inclusions of gangue minerals and other opaque minerals such as magnetite, chalcopyrite, rutile and gold (Fig. 5.14). Magnetite generally occurs as clusters of small grains (<0.1 mm) composing <1% of the mineralized rock. Méthot (1987) reported two types of magnetite: a greyish coloured variety and a brownish-grey variety. Microprobe analysis indicated that the brownish-grey variety contains titanium whereas the grey magnetite did not. Magnetite commonly is closely associated with specular hematite and occurs as inclusions within pyrite (Fig. 5.14B). Specularite composes <1% of mineralized rock and occurs as small laths (~0.2 mm in size) which may be clustered to form irregular aggregates. Specularite is observed within thin crosscutting quartz veinlets and as irregular clusters associated with pyrite and magnetite (Fig. 5.14B). Chalcopyrite is

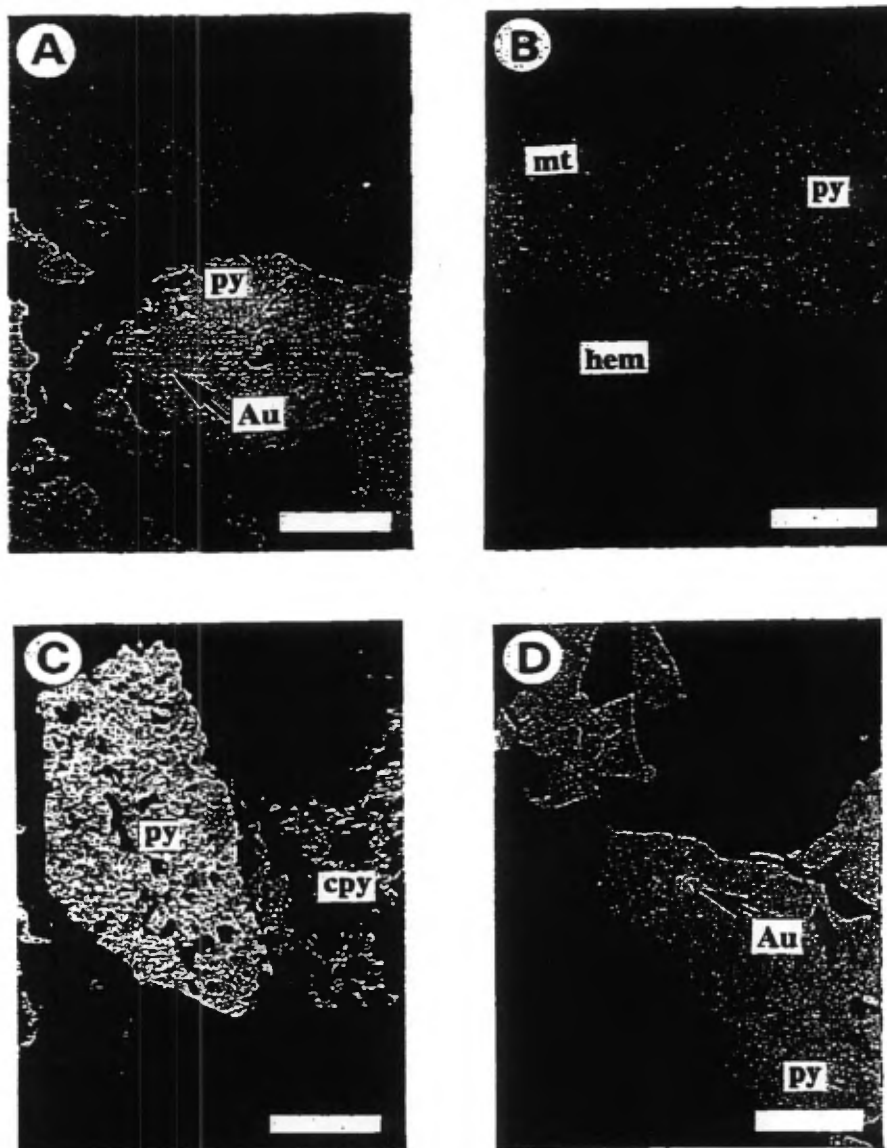


Figure 5.14: Photomicrographs of polished sections showing: A) pyrite crystals hosting inclusions of gangue; note gold included in pyrite; B) inclusions of magnetite within pyrite along side specularite also containing magnetite (from Méthot, 1987); C) pyrite crystal in contact with chalcopyrite; and D) gold associated with microfracture in pyrite. Scale bars = 0.12 mm for A and C, 0.15 mm for B, and 0.06 mm for D.

rarely observed; it occurs in trace amounts associated with pyrite, either as small inclusions or as a separate crystals bordering pyrite (Fig. 5.14C). Rutile occurs in trace amounts, either as small inclusions within pyrite or as separate patches within the host rocks.

Gold is found as free gold within gangue and closely associated with pyrite. It also occurs within pyrite, as rounded inclusions or as thin filaments within microfractures (Fig. 5.14D). Gold grains are generally <0.5 mm across.

5.4.3 Vein textures

Figure 5.6B shows a brecciated texture commonly found in intersection type veins. A matrix composed of chlorite hosts angular fragments composed of quartz, plagioclase (albite), carbonate, and subhedral to euhedral disseminated pyrite, forming a clast-supported breccia. Figure 5.7C shows a typical contact vein exhibiting the complete replacement of original minerals in the diorite by a secondary assemblage composed of carbonate, albite and disseminated pyrite. The breccia texture in a trondhjemite-hosted shear vein (Fig. 5.6C) is characterized by angular broken quartz crystal fragments within a matrix of fine quartz and albite. Pyrite is disseminated within the matrix. A few small sub-economic subhorizontal veins are located in the granitoid rock adjacent to shears.

Other types of breccias observed within the mine are chlorite breccias and hematite breccias. A dark-green to black chlorite breccia on level 2 (13+70 N) and a mineralized chlorite breccia occurs on level 4 (18+40 N). Subangular to irregular-

shaped fragments of quartz, albite and carbonate (1 to 5 cm in size) compose 90% of the rock and are hosted by a dark-green massive chlorite, carbonate, pyrite (~5%) matrix. The second type of breccia is located near line 11+00 S at the southern end of the drift on level 5. This hematite breccia is characterized by numerous veinlets of metallic grey specularite (2-3 mm in size) that transecting a pinkish coloured tonalite. Chlorite, carbonate, pyrite and quartz also occur with specular hematite.

Ore-grade fractures and shear zones of domains II and IV have been found to continue without interruption into domain III, as shown in Figure 5.15, suggesting that various mineralized zones were formed during a single event.

5.4.4 Vein geochemistry

A geochemical study of the mineralized zone at Pierre Beauchemin (Méthot, 1987; Trudel et al., 1989) suggests that diorite, tonalite and trondhjemite were mainly enriched in S, CO₂ and Na₂O and depleted in SiO₂ and K₂O relative to the unmineralized host rocks (see Fig. 5.16). Modest enrichments in MgO and FeO may be due to chloritization and/or the formation of ferro-dolomite during carbonatization. SiO₂, TiO₂ and K₂O are clearly depleted in the mineralized zone. Although quartz is observed in mineralized zones, its depletion in whole rock geochemical analyses indicates that it clearly was not introduced by the hydrothermal fluid. These compositional changes are therefore attributed to pyritization, carbonatization and albitization of the host rocks and are in agreement with observations described above in the present manuscript.

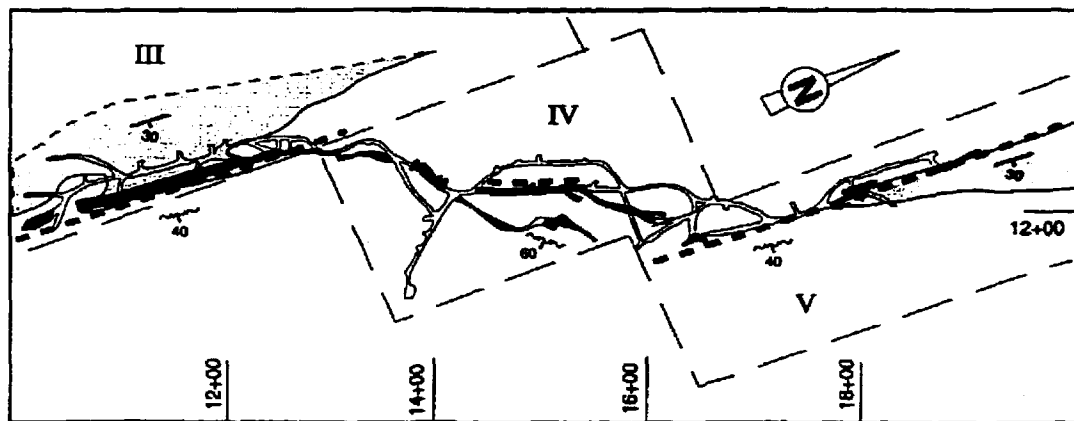


Figure 5.15: Geology of level 1 showing the antidualational jog (domain IV) between diorite dikes (lightly shaded). Mineralized shear planes are black and shears are represented by the heavy dashed lines.

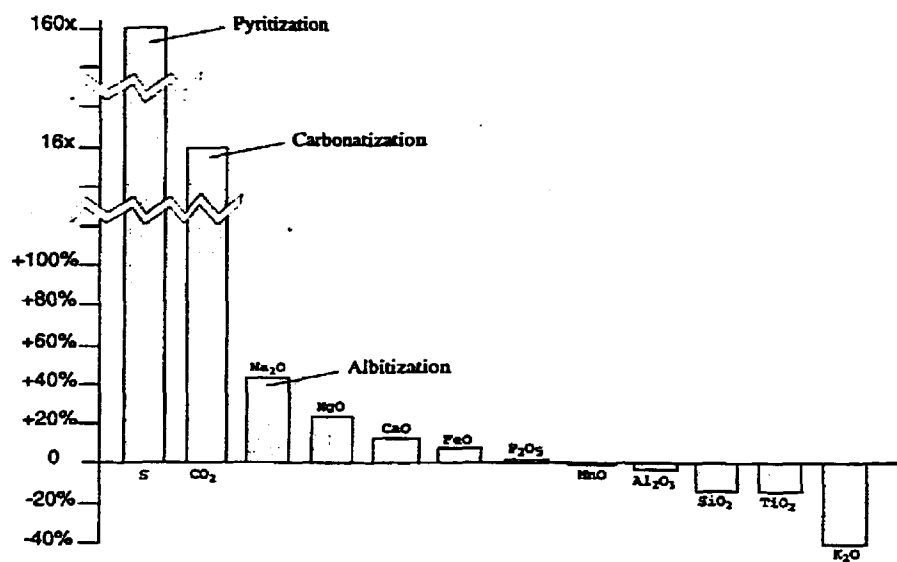


Figure 5.16: Average gains and losses in major elements from samples collected within economically mineralized zones at the Pierre Beauchemin gold deposit. From Trudel et al. (1989) (FeO: total iron expressed as FeO).

5.4.5 Constraints on the sequence of alteration events

Epidote, which commonly occurs in most of the intrusive phases of the pluton (see CHAPTER 2), generally occurs distal to mineralized zones in relatively fresh rocks at the Pierre Beauchemin mine. Epidote occurs as patches or in mm-size fractures where primary textures are preserved in granitoid or diorite. Upon approaching mineralization, the number of fracture-filled veins of chlorite, carbonate, pyrite, hematite and quartz increases and epidote decreases, indicating that alteration assemblages associated with gold mineralization overprint widespread epidotization.

Figure 5.17, a sketch of observations at 15+00 N provides a cross-section of the mineralized zone. Five metres above the mineralized zone, a quartz-carbonate vein occurs at the contact between a diorite dike and tonalite. Primary textures are preserved in the tonalite as far as 1.5 metres from the mineralized zone where the tonalite's primary magmatic textures are obliterated and a marked change in colour is observed. A distinct pink to orange colour, caused by hematitic alteration, surrounds the mineralized zone. The hematitic halo, generally not more than a few metres wide, is in sharp contact with grey- to beige-coloured, pyrite-rich granitoid containing carbonate, chlorite, quartz and economic gold. The sequence shown in Figure 5.17 suggests that hematitic alteration preceded the ore assemblage of pyrite, carbonate, chlorite, quartz and gold. A relatively early episode of hematitization is also supported by observations presented in Figure 5.18 showing a carbonate vein hosting a tonalite fragment. The fragment is cut by a veinlet of specularite that does not transect the carbonate. However, the specularite vein is in turn cut by chlorite veinlets. A chlorite vein transects the carbonate. These relationships suggest that

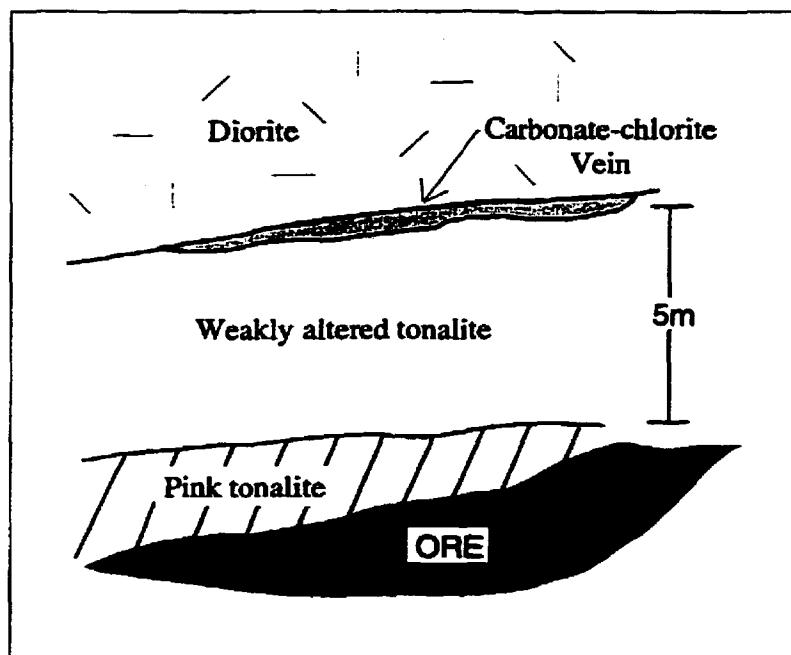


Figure 5.17: Textural and colour variations of tonalite upon approaching a mineralized vein. Primary textures are obliterated by intense hematitic alteration forming a halo, 1-2 metres in width from the pyrite-rich vein. Sketch from notes taken in manway between levels 4 and 5 (15+00 N).

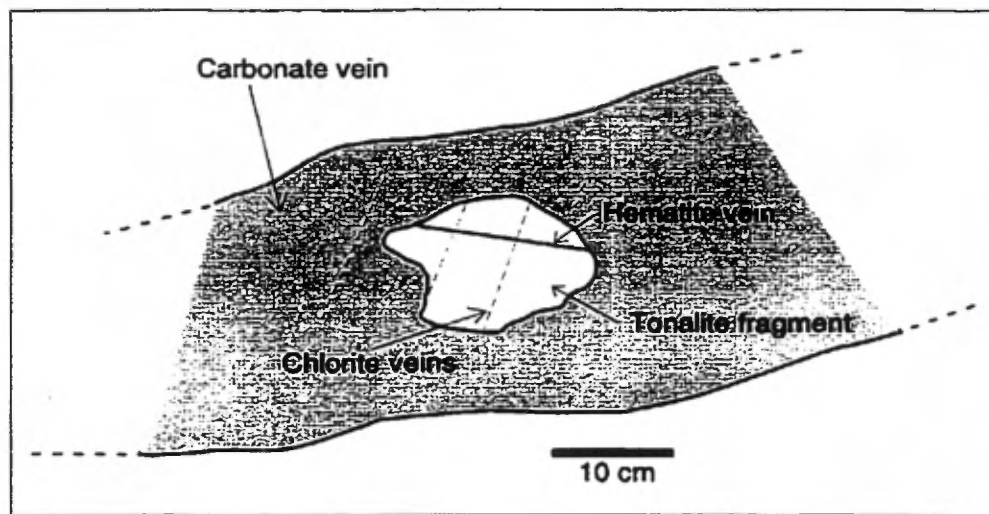


Figure 5.18: Carbonate vein containing a fragment of wall-rock tonalite. The fragment is cut by a specularite veinlet that is cut in turn by chlorite veinlets. Sketch from notes, level 1 survey station 1-48.

hematitic alteration preceded the formation of the carbonate vein and that chlorite veining was the latest event. Pyrite concentrated on the edges of the fragment, suggests that carbonate and pyrite (Au) were synchronous. However, evidence for relatively late hematite includes disseminated specularite overprinting carbonate alteration in a sample from drill core (85-85-1). In addition, Méthot (1987, p.93) presents a photomicrograph of a sample from level 3 (12+60 N) that clearly shows specularite after pyrite.

Figure 5.19 shows a matrix of recrystallized quartz and albite cut by a veinlet containing chlorite, sericite, carbonate and pyrite. This common observation suggests that albitization preceded carbonatization and pyritization. However, Figure 5.7C shows a rare albite crystal overprinting disseminated carbonate.

The diorite dikes invariably show stockwork veinlets of carbonate where approaching a mineralized zone. Intensity of the stockwork increases near the mineralization (Fig. 5.20A). In the mineralized zone, diorite is brownish-beige to grey coloured and rich in disseminated carbonate and pyrite.

Late-stage carbonate veinlets commonly occur throughout the deposit (Fig. 5.20B). These veins, varying between 1 mm and 10 cm across, cut silicified and brecciated host rock. It is not clear that these veins are related to carbonate alteration associated with gold mineralization.

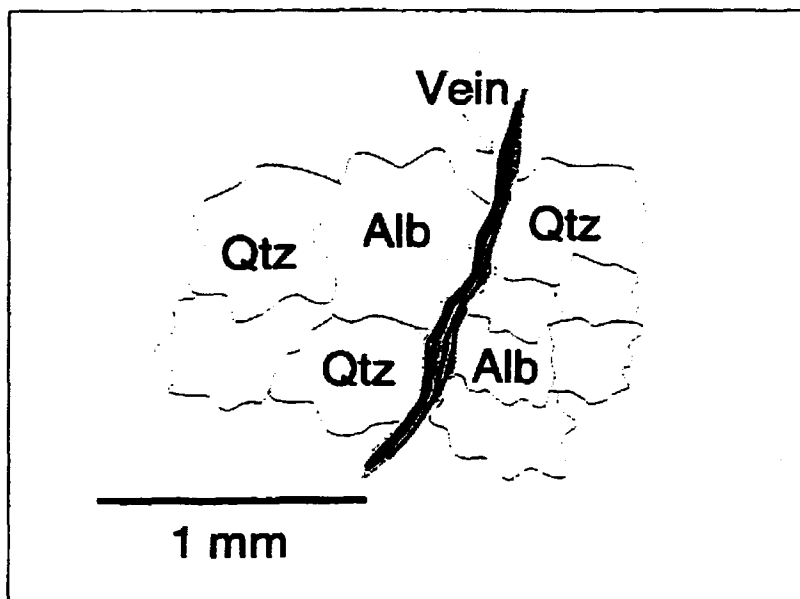


Figure 5.19: Sketch from microscopic observations showing recrystallized quartz-albite matrix transected by a carbonate-chlorite-pyrite veinlet.



Figure 5.20: A) stockwork carbonate veining within diorite; and B) photomicrograph of carbonate veinlet cutting diorite, level 4 (14+20 N). Scale bar = 1 mm.

Figure 5.21 shows a milky quartz vein containing cubic pyrite at the contact between a lamprophyre sill and an aplite dike cutting trondhjemite. These relationships suggest that hydrothermal activity occurred after emplacement of the lamprophyre and probably late in the overall sequence of events. The quartz vein does not contain gold.

5.4.6 Ore shoots

Ore shoots at the Pierre Beauchemin mine are defined as elongate ore bodies composed of several grouped ore veins. Two types are recognized (Table IX): (1) dike-associated shoots, with plunges varying from approximately 10 to 25° NE within the dikes and 40° at the contacts with the granitoid; and (2) granitoid-associated shoots located between diorite dikes, with the ore concentrated in a network of shear veins plunging approximately 50° NE. The plunges of the five principal ore-shoots found within the Pierre Beauchemin deposit (Fig. 5.22) were measured from a three dimensional reconstruction of the mine. Figure 5.23 presents a composite longitudinal view of mineralized zones and diorite dikes projected onto a N30°-oriented vertical plane. In this figure, the differences in the plunges of both ore shoot types is indicated by the difference in the orientations of the two-headed arrows. However, the two types of shoots form a continuum; granitoid-associated shoots become dike-associated where they pass from one rock type to the other. The continuum between these two ore-shoot types is shown in Figure 5.24; a composite planar projection of veins in their respective shoots through levels 1 to 10 of the mine.



Figure 5.21: Milky quartz vein containing fragments of wall rock at a contact between trondjemite and subhorizontal lamprophyre.

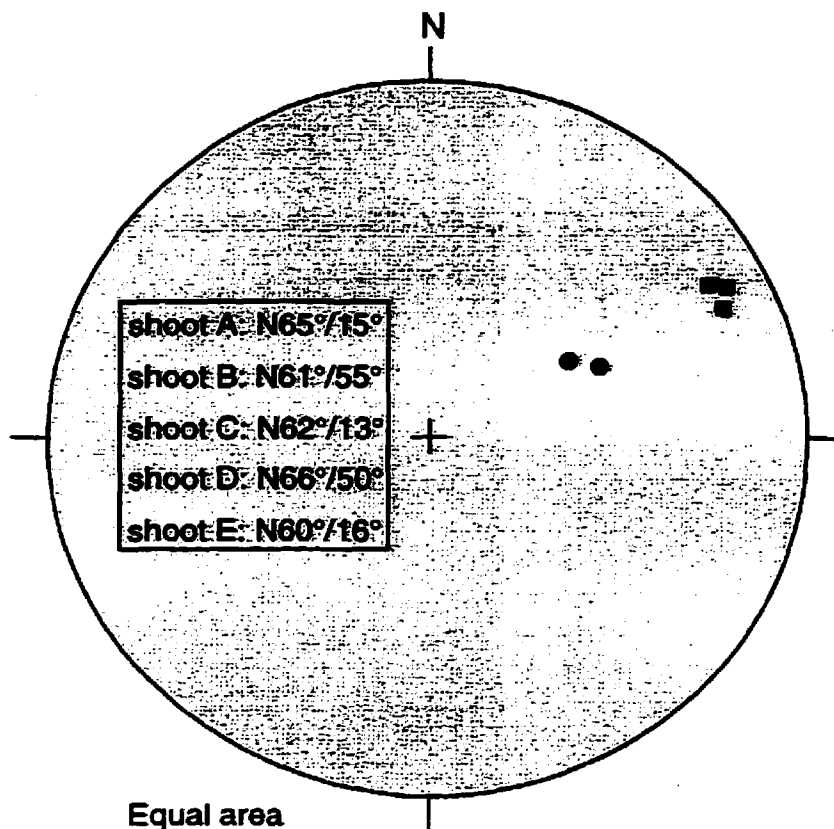


Figure 5.22: Stereographic representation of the orientations of the 5 main ore shoots measured from a three-dimensional reconstruction of the deposit. Squares correspond to type 1 (dike-associated) shoots, whereas circles correspond to type 2 (granitoid-associated) shoots. It is important to note, however, that the shoot plunge varies within a single shoot and that these measurements are end-member orientations. Lower hemisphere equal-area projection.

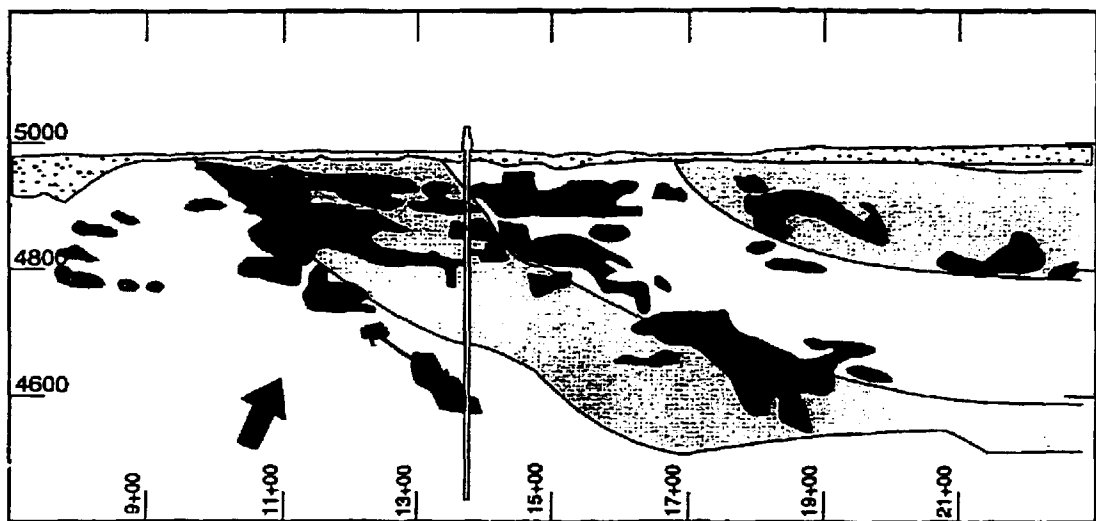


Figure 5.23: Longitudinal projection of diorite dikes and mineralized zones on a vertical plane oriented N30°; light-grey shading for diorite dikes, intermediate shading for dike-associated shoots, and black shading for granitoid-associated shoots.

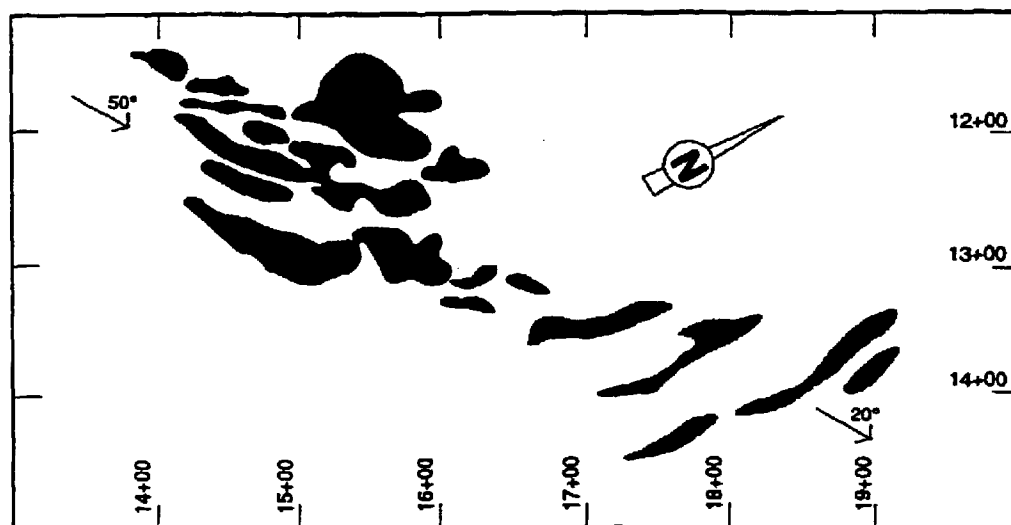


Figure 5.24: Planar composite projection of refracting ore shoots across levels 1 to 10; light-grey shading for dike-associated shoots and black shading for granitoid-associated shoots. Arrows indicate plunges of shoots.

5.5 Discussion

5.5.1 Host-rock competency

Ramsay (1982) relates competence with ductility, which is essentially a measure of strain intensity. The competence of rocks has been defined and used in many different manners, and it may, according to circumstances, involve relative ductility, viscosity or strength (Treagus, 1988). In our case, we define the rigid unit as competent and the ductile unit as incompetent.

Poulsen and Robert (1989) show that, where a rock layer is much weaker than its host, simple shear can be expected to occur mainly in the weaker layer. The contrasting deformation styles, evident in different textures in granitoid and diorite dikes at the Pierre Beauchemin mine, are interpreted here to have resulted from competence contrasts between the two rock types, the diorite dikes being therefore much more ductile and weaker than the host granitoid.

5.5.2 Shear zones

Various structures, including cleavage (Foster and Huddleston, 1986; Treagus, 1988), fractures (Hancock, 1985), and shear zones (Eisenstadt and DePaor, 1987), have been observed to change orientations where they pass between units of different rheologies. Therefore, the rheology of a rock unit is an important factor in the determination of the nature and orientation of structures. Our observations at the Pierre Beauchemin mine indicate that shear zones are refracted, both in strike and dip (Figs. 5.9, 5.11, 5.12, 5.13 and 5.15), in passing from the dikes to the granitoid rock.

This shear refraction is accompanied by a slight change in slip vector orientation, most likely due to the difference in orientation between shear zones and the maximum compression direction. In the mine area, shear zone orientations and their associated slip vectors are best represented by a subhorizontal principal axis of shortening directed in a WNW-ESE orientation; the principal extension axis is subvertical and the intermediate principal axis is perpendicular to the two other axes (Fig. 5.25). As discussed above, shears that trend northward are formed within the diorite and, at their contacts with the granitoid, N30°-trending shears become refracted into north-trending shears where they pass through the granitoid.

However, the origin of the N60°-trending shears remains unclear. These shears and their associated reverse dextral slip may result from the presence of preexisting planes of weakness in the granitoid. Assuming a WNW-ESE-directed compression, the difference in orientation between this compression and the N60° planes of weakness would produce a reverse dextral movement. This interpretation is supported by the observation that steeply-dipping N60°-trending orientations occur as primary anisotropies related to the emplacement of the felsic intrusions (see CHAPTER 2). Another possible interpretation is that, because of competency contrasts, shears were initiated along preferred planes of weakness due to heterogeneities in rock strength (Bott, 1959), such that the planes of weakness correspond to the orientations of dikes and their interfaces with the host granitoid. The dextral offset of the dikes caused the formation of N30°-trending shears where the dike-associated north-trending shear planes refracted to a N30° direction in passing through the granitoid between the offset dikes. The N60°-trending shears and

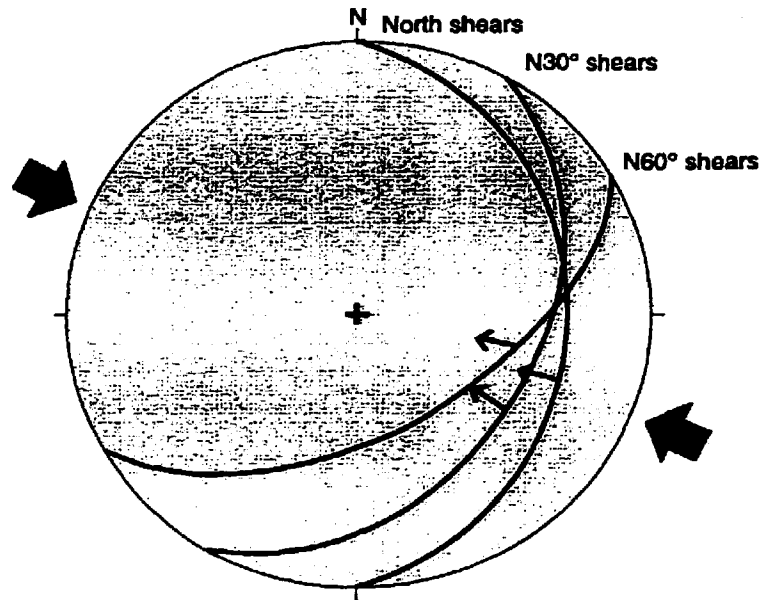


Figure 5.25: Lower hemisphere equal-area stereographic projection of main shear plane orientations and their associated slip vectors. Arrows indicate maximum compression orientation.

fracture planes may have been formed by accumulating stress in the more competent rock volumes between offset shear zones, thereby creating an antidilational jog structure (Sibson, 1987; 1989).

Bott (1959) demonstrated that initial slip along preferred planes of fracture could occur in any direction within the slip plane. The precise direction of slip would depend on the relative values of the three principal pressures, provided that the slip plane is not parallel to any of the principal pressures. This interpretation contrasts with the "Andersonian" fault model (Anderson, 1951) where the relative value of the intermediate principal pressure has no bearing on the direction or incidence of fracture. Our observations suggest that, although shearing was focussed and may have been initiated in the diorite dikes, the general slip orientations of shears within the granitoid show no significant variation compared to the dike-associated shears. Therefore, we propose that the bulk of the granitoid-hosted shears formed in response to shear refraction and that the accumulated stress in the granitoid resulted from the dextral offset of incompetent dikes.

5.5.3 Mineralization

Observations presented above (Sections 5.3 and 5.4) indicate that gold mineralization occurred after the emplacement of the Eldrich diorite. Economic mineralization is clearly associated with shears and fractures developed in and near the Eldrich diorite within the Eldrich Fault zone. Therefore, the present distribution of gold is clearly controlled by structures related to the fault; this does not rule out the

possibility that gold had been pre-concentrated in the area and was remobilized during deformation.

The kinematic analysis presented in Section 5.3.2 suggests that shears developed in response to WNW-ESE compression. This orientation contrasts markedly with the NS-oriented compression responsible for the weak penetrative fabric observed in the central part of the pluton (discussed in CHAPTER 2). In addition, shear and vein development cannot be associated with intrusion of any of the phases of the Flavrian pluton because their emplacement was related to a regional-scale extensional event (see CHAPTER 2) and not compression. Based on these observations, it is suggested that mineralization at the Pierre Beauchemin deposit occurred after the emplacement of the Eldrich diorite during a WNW-ESE-oriented compression.

Contact-type veins, intersection-type veins, diorite-hosted shear veins and granitoid-hosted shear veins are observed at the mine (Table IX). Vein textures vary where the veins transect rock types with differing rheological properties, as discussed by Hodgson (1989b). Vein orientations are also fundamentally controlled by the host-rock rheology. Variations in orientation are associated with the domain in which the veins occur (domains I, III and V are associated with diorite, and domains II and IV with granitoid) (Fig. 5.13).

Contact-type and intersection-type veins are located where the change in dip of the dikes influenced shear-zone dips and was therefore responsible for the formation

of dilation zones when dip-slip movement took place along shears (Figs. 5.11 and 5.12). Diorite-hosted shear veins are commonly linked to intersection-type veins near variations in orientation the shear zones (Figs. 5.11 and 5.12). Granitoid-hosted shear veins commonly occur as a continuum of intersection-type veins and are also related to shear refraction (Fig. 5.11). The recognition of the various vein types and their characteristics is especially essential within this type of deposit because different vein types have repercussions on hanging wall stability (possible dilution) as well as on the grade and tonnage of ore as it is mined.

Veins are generally located in or associated with areas that have undergone some degree of dilation, most of which has been created by changes in orientation of shear zones due to competency contrasts between the dikes and the host granitoid. A schematic diagram showing this model is presented in Figure 5.26. Similar situations are observed in many mineral deposits and have been discussed by Hodgson (1989b) as movement on non-planar shear surfaces, one of six principal deformational mechanisms responsible for generating dilatancy.

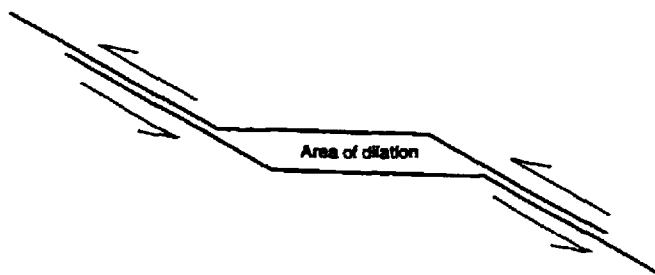


Figure 5.26: Schematic model for the creation of zones of dilation (dilational jog of Sibson, 1987) by the shearing of non-planar surfaces.

Two types of ore shoots are observed at the Pierre Beauchemin mine: (1) diorite dike-associated shoots, and (2) granitoid-associated shoots. In Figure 5.5, the poles for contacts between the diorite dikes and host granitoid rocks within domain III are distributed along a great circle coincident with the axis of dike curvature, demonstrating that the dikes are non-planar bodies. The unstrained nature of several measured contacts between the dikes and the host granitoid indicate that dike curvature is a primary emplacement-related feature which is not in any way related to later flexure. Note that the plunge of the curvature axis corresponds approximately to the general $N65^{\circ}/20^{\circ}$ plunge of the type 1 ore shoots as shown in Figure 5.22. Figure 5.23 demonstrates that the plunges of diorite-associated ore shoots vary between 10° and 40° when projected onto a vertical longitudinal plane oriented $N30^{\circ}$ (i.e., parallel to the Eldrich Fault zone). The long axes of the diorite-associated shoots are apparently perpendicular to slip directions. In fact, there is no simple relationship between slip-vector and shoot orientation because shoots trend $N65^{\circ}E$. This apparent relation is due to the projection of variously oriented and refracting ore zones, and is predicted to be common in anisotropic rock media. Granitoid-associated ore shoots plunge 50° in an ENE direction (Figs. 5.22 and 5.24). In this case, the shoot plunge is controlled by the plunge of the fault bend between the diorite dikes, which is itself related to the plunge of the axis of curvature of the non-planar dikes.

Figure 5.24 is a composite plan of levels 1 through 10 which demonstrates the relationship between type 1 and type 2 ore shoots. Both types of shoots trend in approximately the same direction, although the plunges of shoots vary significantly

along this trend. The variation in plunge corresponds to the passage from one domain to another. The ore shoots are therefore interpreted to have been refracted, with the refraction having been controlled by the axes of curvature of the dikes, as illustrated in Figure 5.27 where shallow-plunging dike-associated ore shoots correspond in orientation to the axis of curvature of the incompetent dike. The plunge of the dike-associated shoots increases as it evolves into a granitoid-associated shoot and vice-versa. A three-dimensional reconstruction of the deposit is presented in Figure 5.28. The reconstruction is based on simplified geological maps of the first 7 levels of the deposit (Appendix V). Note the shape and distribution of the main diorite dike and the fault passing from level to level. Also note that ore zones associated with diorite occurs at the intersection between the dike and the fault. However, granitoid-hosted shoots, are tube-shaped, plunge steeply and occur between the diorite dikes where fault bends occur. A schematic illustration of the deposit is presented in Figure 5.29 where the relationship between dike shape and distribution, shear refraction and shoot orientations are presented. Hodgson (1989a), who indicated that bends or changes in shear orientation commonly control ore shoots, supports these observations. Furthermore, Newhouse (1942) discussed the case where ore shoots developed at a curve or deflection of a shear zone that resulted from its intersection with different rock types. He predicted that the plunge of the ore shoot would not necessarily be perpendicular to slip direction; however, it may be controlled by the plunge of the deflection.

Poulsen and Robert (1989) classified ore shoots according to the nature of their structural control. They distinguished two major types: (1) geometric ore shoots,

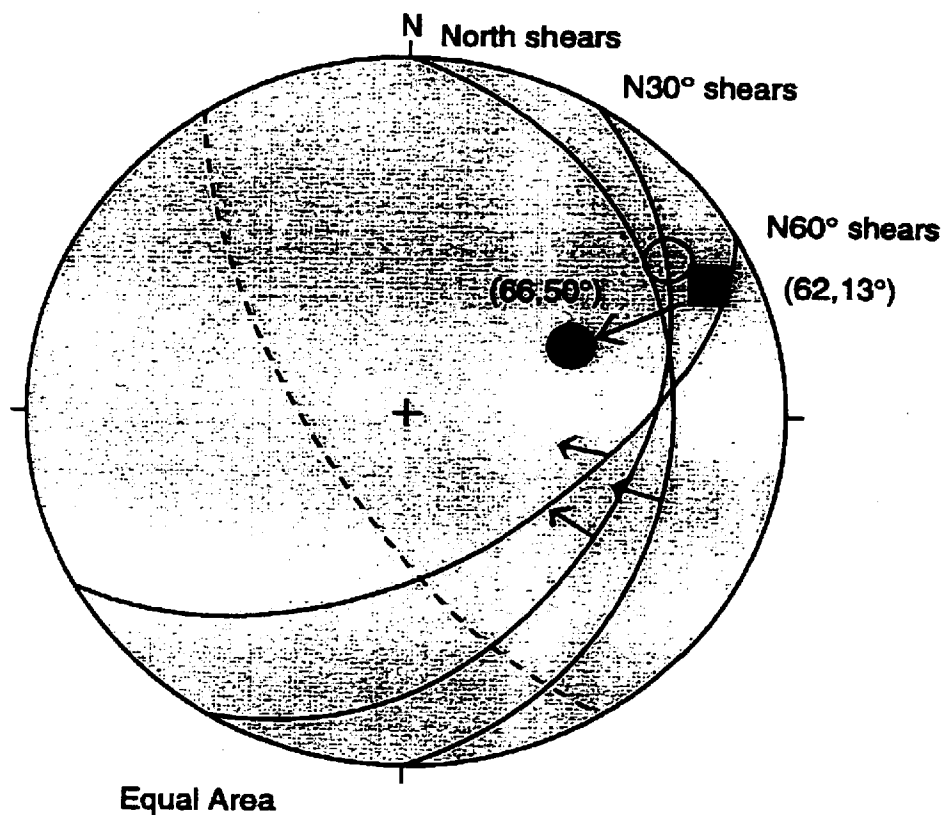


Figure 5.27: Lower hemisphere equal-area stereographic projection of main shear-vein orientations, slip vectors and ore-shoot plunges. The square represents the shallow plunging dike-associated shoots, the black circle represents granitoid-associated shoots, and the arrow shows the trend along which the plunge of the shoots vary. The dashed great circle is the best-fit circle of Figure 5.5; its pole is represented by the open circle.

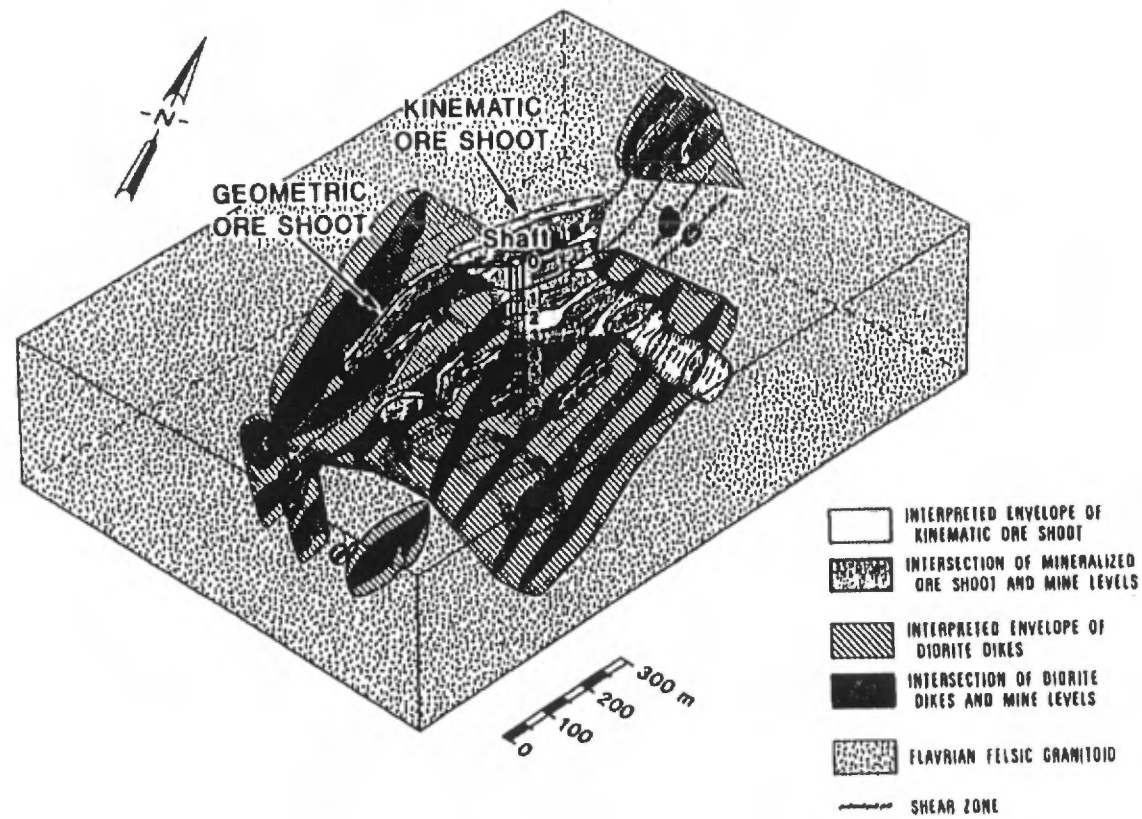


Figure 5.28: Three-dimensional representation of the Pierre Beauchemin gold deposit. Note the contrasting plunges of granitoid and dike-associated ore shoots.

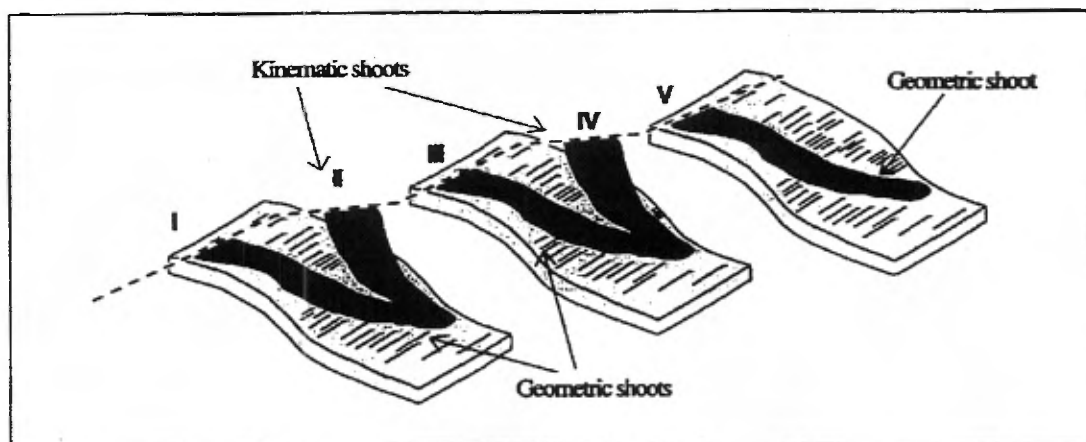


Figure 5.29: Conceptual model of the Pierre Beauchemin gold deposit. Diorite dikes are shown in light-grey and ore shoots (I, II, III, IV and V) are shown in black. The trace of the Eldrich Fault is represented by the dashed pattern and the host granitoid is represented by the white background. Note that the fault changes orientation as it passes from a dike-dominated to a granitoid-dominated domain. Note also that the dike-associated ore shoots (I, III, and V) occur within domains (I, III and V) and that granitoid-associated ore shoots (II and IV) occur in domains (II and IV). Both types of ore shoots have contrasting plunges and may connect at depth.

which form where mineralization along a given shear zone is restricted to the zone of intersection with a favorable preexisting element; the plunge of shoots parallels the intersection of the shear zone with the favorable geological element, and bears no relationship to the direction of slip along the host shear zone; and (2) kinematic ore shoots, which are related to the development of veins and shear zones; these shoots commonly occur at the intersections between different sets of veins and shear zones or as lenticular ore bodies within shear zones. Kinematic shoots are not obviously related to shear zones, and they have generally been interpreted as resulting from openings generated by slip at bends or curvatures in the overall shear-zone trend.

The detailed structural analysis of the Pierre Beauchemin gold deposit indicates that both types of shoots are present and that their locations are controlled by the relative competencies of the deformed rocks (Figs. 5.28 and 5.29). As discussed by Poulsen and Robert (1989), we also observe both types of shoots to be intimately related, as the shoots refract and anastomose into each other along axes defined by the curvature of the weaker dikes.

At the pluton scale, many sub-economic mineralized zones occur in structures within the anisotropic granitoid. However, economic vein-gold deposits have only been mined in areas of the pluton where less competent dikes transect the more competent host granitoid. The difference in competency and volume contrasts may have been the dominant criteria in terms of localizing structures and economic gold concentrations.

Detailed mapping and petrographic analyses indicate that minerals associated with gold-rich veins are carbonate, pyrite, quartz, albite, chlorite \pm sericite \pm magnetite \pm specularite \pm rutile \pm chalcopyrite. Crosscutting relationships suggest that albitization and possibly a phase of hematitization preceded or were coeval with gold precipitation associated with pyritization and carbonatization. The intimate association between specularite, magnetite and pyrite-rich ore has also been observed at the Elder (Trudel et al., 1991) and Silidor deposits (Gaulin, 1992; Carrier, 1994). Both of these deposits occur within the Flavrian-Powell intrusion and both are remarkably similar to Pierre Beauchemin. Based on the presence of hematite and barite in the ore, $\delta^{18}\text{O}$ values of -2‰ and low $\delta^{34}\text{S}$ values, Trudel et al. (1991) suggest that oxidizing fluids played an important role in the emplacement of mineralization at the Elder mine. A mix of two fluids, one oxidizing and the other reduced, is invoked by Trudel et al. (1991) for gold precipitation. Barite and specularite is equally common at Silidor (Gaulin, 1992), again supporting the call for oxidizing conditions during gold mineralization. Kennedy and Kerrich (1982) were the first authors to identify the probable role of oxidizing conditions associated with gold in the Flavrian pluton. Low $\delta^{18}\text{O}$ values (+2‰) measured in quartz veins within the Pierre Beauchemin (then Eldrich) deposit were interpreted as resulting from the influx of meteoric water within the Flavrian pluton during post-volcanic emergence of the Blake River Group. The presence of pyrite, magnetite and specularite together with gold in the ore at Pierre Beauchemin suggests that a combination of oxidizing and reduced fluids may have been involved in the mineralizing event.

In summary, the Pierre Beauchemin gold deposit is a structurally controlled vein deposit in which the distribution of ore veins and shoots was ultimately controlled by the different rheological properties of the host rocks where competent granitoid and less competent diorite behaved differently to a WNW-ENE-oriented compression, creating favorable space for mineralization. Gold mineralization was associated with pyritization, carbonatization, albitization and chloritization of the host rocks. The presence of pyrite, magnetite, specularite and gold in the ore at Pierre Beauchemin suggests that a combination of oxidizing and reduced fluids were involved in the mineralizing event.

**GENERAL DISCUSSION
AND
CONCLUSIONS**

GENERAL DISCUSSION AND CONCLUSIONS

Episodic high-level emplacement in an extensional environment

The Flavrian subvolcanic pluton is composed of the following intrusions: (1) Méritens quartz-diorite, homogeneous tonalite, hybrid and heterogeneous tonalite; (2) trondhjemite porphyry; (3) pink trondhjemite; (4) coarse-grained trondhjemite; (5) granophyre and microgranite; (6) Eldrich diorite; and (7) late trondhjemite. Pink trondhjemite, trondhjemite porphyry, coarse-grained trondhjemite and granophyre are sub-phases of the early trondhjemite. Detailed analysis of the internal and external contacts of the Flavrian pluton indicate that the pluton is a composite sill-like intrusion that was emplaced at high crustal levels during asymmetric subsidence of a cauldron. The sharp nature of internal contacts indicates that ascending magma was emplaced in fractures and along faults, resulting in a dike-fed sill geometry. Evidence of several magmatic pulses during emplacement of individual phases illustrates the episodic nature of emplacement. Episodic magmatic pulses would have caused cyclical internal pressure variations within the pluton. Evidence of pressure variation during emplacement is recorded in many of the textures. The distinct geometry of the numerous dikes and sills, the concordant relation between the pluton and the surrounding volcanic rocks and the observed link between subsidence and intrusion indicate that emplacement occurred in an extensional tectonic regime. The link between intrusion and extension supports the work of several authors who have proposed an extensional environment for the formation of the Noranda Volcanic

Complex (de Rosen-Spence, 1976; Gibson and Watkinson, 1990; Pélouin et al., 1990).

Evolution of the Flavrian subvolcanic pluton and its association with the VHMS deposits of the Noranda cauldron.

The Méritens quartz-diorite is the oldest phase recognized in the Flavrian pluton. It is a minor phase that is closely associated with tonalite and characterized by a dioritic texture with quartz phenocrysts. Quartz-diorite is mainly composed of plagioclase and amphibole (mainly hornblende), with minor amounts of quartz, chlorite, epidote, ilmenite and calcite. Chemically, quartz-diorite is depleted in SiO_2 , Na_2O , Nb, Y, Zr and Hf and enriched in Al_2O_3 , Cr, Ni, Co and V compared to other phases within the pluton. REE patterns of quartz-diorite are slightly fractionated and do not show significant depletion in Eu.

Quartz-diorite occurs in syn-volcanic structures such as the McDougall and Despina Fault zones (Gibson et al., 1993) and also in a NE-trending elongated zone near Lac Méritens. In this area, quartz-diorite consistently occurs stratigraphically above tonalite and grades into tonalite down-section. These relationships are also observed beneath the Ansil deposit and suggest that the Méritens quartz-diorite also occurred as sill-like bodies. Consequently, during the earliest stages of development, the Flavrian pluton was likely composed of a series of dike-fed sills of quartz-diorite (Fig. D.1). The contact between Méritens quartz-diorite and tonalite is transitional, with Méritens quartz-diorite generally grading into homogeneous tonalite.

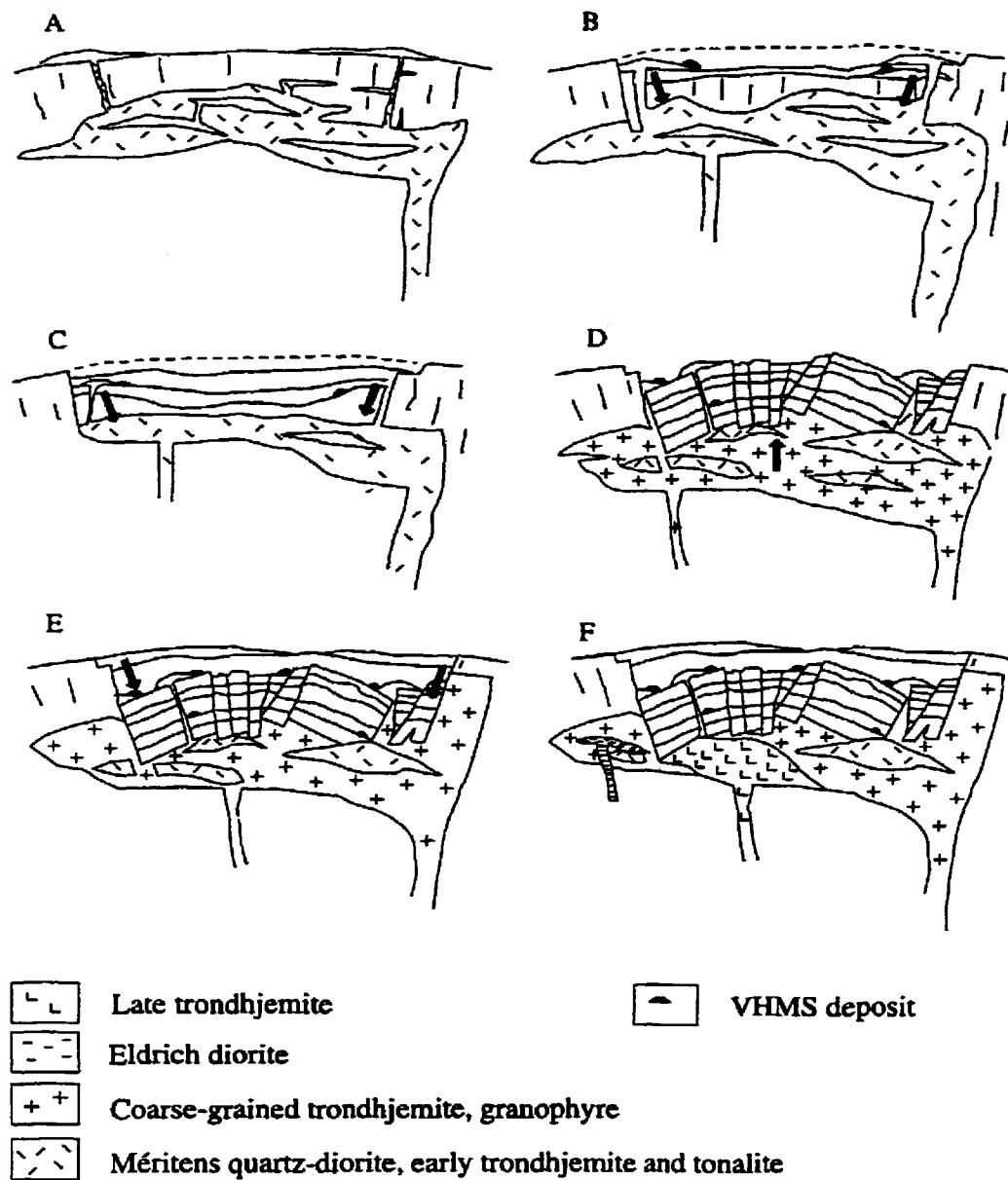


Figure D.1: Cartoon depicting the evolution of the Flavrian pluton in relation to the Noranda cauldron. Black arrows indicate either subsidence or resurgence.

Enrichments in SiO_2 , Na_2O , TiO_2 , HFSE and REE and depletions in Al_2O_3 , MnO , MgO and V characterize the transition from quartz-diorite (stratigraphically above) to tonalite (stratigraphically below). The nature of the contact and the chemical variations suggest that Méritens quartz-diorite may have undergone chemical fractionation to form homogeneous tonalite. However, TiO_2 enrichment in tonalite suggests a more complex mechanism of differentiation. Méritens quartz-diorite is probably the remnant of a large amount of mafic magma that passed through the "Flavrian" magmatic reservoir and was eventually extruded within the Noranda cauldron. This is supported by the link between the onset of subsidence, volcanism of the Flavrian andesite and intrusion of quartz-diorite.

The oldest felsic intrusive phases within the Flavrian pluton are trondhjemite porphyry and pink trondhjemite. Pink trondhjemite is a minor phase characterized by the presence of magnetite. The role of pink trondhjemite in the evolution of the pluton is not clear. However, it does mark a separate early pulse of trondhjemite magma. Magnetite-chlorite-epidote pseudomorphs after amphibole in pink trondhjemite may have resulted from early alteration or contact metamorphism. Trondhjemite porphyry occurs as inclusions within coarse-grained early trondhjemite throughout an ENE-trending zone in the southern part of the pluton and as large masses in the northern part of the pluton. The southern zone may mark the location of an early ENE-trending feeder structure. Trondhjemite porphyry contains abundant mafic inclusions, suggesting that it is younger than the quartz-diorite. However, the distinguishing feature of trondhjemite porphyry is its quartz and albite phenocrysts.

Trondhjemite porphyry is depleted in SiO_2 and enriched in TiO_2 , Fe_2O_3^* , MnO , P_2O_5 , Cr , Ni , Co and Y relative to other trondhjemites. It is readily distinguished from late trondhjemite by higher Ta , Th , U and REE concentrations, along with its LREE-fractionated REE pattern and Eu anomaly.

Trondhjemite porphyry and Méritens quartz-diorite are interpreted as remnants of the earliest magma to have been injected into the pluton. Crosscutting relationships constrain intrusion of these phases to the onset of cauldron development. In addition, geochemical similarities to the overlying volcanic rocks suggests that these phases represent magmas that fed the overlying volcanic pile during the 1st cauldron volcanic cycle. Figure D.1B shows the shallow-level Flavrian magma chamber feeding volcanic rocks of the 1st cauldron cycle. No mixing textures, apart from the mafic inclusions, were observed within the trondhjemite porphyry, suggesting that both the mafic and felsic magmas occurred in separate areas or at different levels in the subvolcanic environment.

The 1st cauldron cycle is interpreted to have been deposited during subsidence (Gibson and Watkinson, 1990) with magma being injected from the subvolcanic chamber to the volcanic environment. Extrusion of magma from the Flavrian chamber during subsidence associated with the 1st cauldron cycle is shown in Figure D.1B and C. The Corbet and Ansil VHMS deposits were formed during volcanism and associated subsidence of the 1st cauldron cycle. The deposits were likely short-lived hydrothermal systems occurring in an environment of high-energy, rapid

volcanism (Hoy, 1993). Extrusion of the 1st cauldron cycle volcanic rocks would have considerably diminished the chamber's size, with volume loss entraining subsidence of the overlying volcanic pile. Subsidence may have also been caused by a difference in magma flow rate (Johnson, 1992). The flow of magma into the chamber from below may not have compensated for the magma flowing out of the chamber en route to surface. Also, cauldron subsidence may have been due to regional extension (Dzurisin et al., 1994). The study of modern active volcanoes indicates that eruption of magma normally results in a decrease in the internal pressure of the magma reservoir as it extrudes (Johnson, 1992). This is consistent with subsidence caused by the collapse of the underlying chamber.

The high-energy environment of active volcanism and subsidence that occurred during the formation of Cycle 1 volcanic rocks was followed by a sudden interruption in volcanism, that coincided with the development of the C Contact tuff (Gibson and Watkinson, 1990). During this period, the supply of magma from the underlying chamber to the volcanic environment must have stopped or considerably diminished. Closure of the combined subvolcanic-volcanic system may have been caused by a lack of magma within the low-pressure environment of the subvolcanic chamber following the major episode of Cycle 1 volcanism.

Following eruption of the first cauldron cycle and during the subsequent period of quiescence, pressures within the underlying chamber probably increased gradually. Chamber pressurization may be attributed to a several factors. At Kilauea, the

decrease in pressure within the summit magma chamber following eruption is interpreted to have been compensated (1) by elastic expansion of the remaining magma and gas, (2) by additional exsolution of gas dissolved in the magma, and (3) by contraction of the volcanic edifice (Johnson, 1992). In addition, pressurization can result from transfer of magma to the subvolcanic chamber from a deeper source zone. Evidence presented by Stix and Gorton (1993) suggest that input of silicic magma into the magma chamber followed volcanism and collapse of the Toledo caldera in New Mexico. Pressurization of the Yellowstone caldera has been attributed to a combination of magmatic devolatilization and magma intrusion into the magma chamber (Dzurisin et al., 1994). Gradual pressurization of the chamber may also be caused by fractional crystallization (Tait et al., 1989). Fractional crystallization would slowly increase volatile content and therefore internal pressure, possibly leading to eruption.

Reservoir degassing is favored when internal pressure is low, such as after major eruption and deflation (Johnson, 1992). From this perspective, the period of quiescence marked by the C Contact tuff was probably accompanied by degassing of the chamber. Hot gases emanating from the chamber would have transferred heat (and possibly metals) to the seafloor. Sustained hydrothermal activity may have been due to injection of new magma to the chamber or differentiation by crystal fractionation. Both mechanisms increase pressurization and heat flow from the chamber. Pressurization of the underlying chamber would have increased to a point where magma pressure would equal lithostatic pressure. Under these conditions, the

formation of sills is favored in the high-level chamber. The episodic intrusion of coarse-grained trondhjemite sills probably caused incremental pressurization of the magma chamber. Further increases in pressure (magma overpressure) would have caused doming of the volcanic sequence through the reactivation of syn-volcanic faults and fracture zones. Figure D.1D shows that intrusion of coarse-grained trondhjemite into the underlying Flavrian magma chamber up-lifted the 1st cauldron cycle volcanic rocks. The trondhjemite magma probably originated from a deeper source zone, ascended, and replenished the Flavrian chamber. Most of the differentiation by crystal fractionation probably occurred within this deeper zone because no cumulate textures are observed within the Flavrian pluton. Doming of overlying volcanic sequences due to replenishment of an underlying chamber commonly occurs in active volcanic systems (Dzurisin and Yamashita, 1987). Regional tumescence due to doming is inferred to occur before mineralization in several VHMS districts (Hodgson and Lydon, 1977; Gibson and Watkinson, 1990).

Pressure within the Flavrian chamber must have reached the point where rupture of the reservoir would have caused new magma to be extruded to surface. Numerous rhyolitic domes mark the onset of the 2nd cauldron cycle within the Noranda cauldron. These domes are commonly associated with VHMS deposits (Gibson and Watkinson, 1990), and they are compositionally identical to early trondhjemite.

Our studies suggest that the emplacement of medium to coarse-grained early trondhjemite may have played an important role in the formation of the VHMS deposits related to the onset of the 2nd cauldron cycle. Coarse-grained trondhjemite is commonly composed of subhedral to euhedral, uncommonly zoned, albite and quartz that constitute more than 95% of the rock. The mafic minerals, typically less than 5%, are composed of actinolite, chlorite and epidote and commonly occur together, either in irregular-shaped clusters or associated with what seem to be altered amphibole. Coarse-grained trondhjemite shows a characteristic emplacement geometry of interconnected dikes and sills, indicating that stress vectors were locally reoriented. Stress vector reorientation may be explained by slight pressure fluctuations within the chamber due to loading, dike inflation, rupture of the magmatic reservoir by seismic relief leading to extrusion, magma replenishment, variations of magma flow rates (extrusion or replenishment) and/or far-field structural effects such as regional extension. The coarse-grained trondhjemite's enrichment in SiO₂ and Na₂O reflects the dominance of quartz and albite as the main rock-forming minerals. CaO and Sr enrichment relative to other trondhjemite phases is probably due to the presence of epidote, either in the form of alteration of albite or within miarolitic cavities. Coarse-grained trondhjemite is characterized by relatively large variations in LREE abundance and significant variations of La/Yb ratios over a restricted SiO₂ (and to a lesser extent Th) interval. The REE patterns show negative Eu anomalies that increase with increasing REE abundance but do not show any definitive correlations with SiO₂ or Th.

The characteristic breccia texture formed by shattered quartz fragments within an albite matrix occurs throughout the early coarse-grained trondhjemite. The breccia is interpreted to have resulted from major pressure variations that induced boiling within the magma. The widespread nature of this texture suggests that boiling of the volatile-rich trondhjemite magma must have occurred either over a long period of time (throughout the emplacement history of the coarse-grained early trondhjemite) or during one explosive event that would have affected the early coarse-grained trondhjemite following its emplacement. Boiling would have caused expansion of a fluid phase as it passed from a dissolved component in magma to a separate aqueous fluid phase. Mirolitic cavities filled with epidote, quartz and less commonly magnetite occur throughout the coarse-grained trondhjemite and suggest degassing or boiling during emplacement and/or cooling of the phase.

Crosscutting relationships presented in CHAPTERS 2 and 4 indicate that development of the Noranda cauldron and its associated VHMS deposits was constrained to an interval of time that began with intrusion of the Méritens quartz-diorite and ended before complete emplacement of the group of phases that compose the early trondhjemite. Boiling of the early coarse-grained trondhjemite may have been caused by a large drop in pressure within the chamber associated with extrusion and the onset of the 2nd cauldron cycle. Renewed subsidence and extrusion of the 2nd cauldron cycle volcanic rocks is depicted of Figure D.1E. Boiling would have caused expansion of a free aqueous fluid phase. These high temperature aqueous fluids probably altered the residual early trondhjemite, causing the large variations in

incompatible elements. Degassing of early trondhjemite would have enhanced heat transfer from the subvolcanic chamber to the surrounding rocks. The liberated volatile-rich aqueous fluids would have mixed with large amounts of seawater as they rose, stripping metals from the surrounding rocks. These fluids may have eventually deposited metals near or at the surface, forming the VHMS deposits associated with the onset of the 2nd cauldron cycle. Textures indicating boiling of the early coarse-grained trondhjemite are considered to be strong indirect evidence of magmatic-hydrothermal activity associated with the formation of VHMS deposits at Noranda. The breccia texture within the coarse-grained trondhjemite is distinctive and it may represent a major episode of degassing in the evolution of the Flavrian pluton. In addition, boiling of the coarse-grained trondhjemite may explain the fact that the majority of the VHMS deposits within the Noranda cauldron occur at one specific stratigraphic level.

The compositional differences between early trondhjemite and Cycle 4 rhyolite suggests that the link between the chamber and the overlying volcanic rocks terminated before or during the onset of Cycle 4. Closure of the subvolcanic-volcanic system may have occurred with the end of Cycle 3.

Tonalite is composed of albite, anhedral quartz and actinolite, with minor amounts of chlorite, epidote, stilpnomelane, sericite, calcite and opaque minerals (ilmenite, magnetite, pyrite and hematite). Tonalite shows a variety of textures, suggesting a complex history of emplacement and evolution. Homogeneous tonalite

is closely associated with Méritens quartz-diorite, whereas spotted tonalite occurs along or near contacts with early trondhjemite. Massive zones of homogeneous and spotted tonalite commonly grade into zones of heterogeneous tonalite and hybrid rocks. Heterogeneous tonalite and hybrid rocks generally contain rounded to lobate, irregular-shaped inclusions of Méritens quartz-diorite and tonalite hosted within a tonalite or early trondhjemite matrix. The matrix may be less well-developed where irregular masses and apophyses of microgranitic to fine-grained early trondhjemite occur within a tonalitic host.

Tonalite is intermediate in composition between Méritens quartz-diorite and trondhjemite. The chemical variability observed for tonalite reflects its ill-defined contacts and textural heterogeneity. Significant variations in concentrations of immobile trace element such as Nb, Y, Zr and REE over relatively small SiO_2 ranges further emphasize the complex history of emplacement of tonalite. However, field and petrographic observations indicate two scenarios: (1) early trondhjemite grades into tonalite, producing homogeneous tonalite and hybrid rocks, and (2) early trondhjemite is in sharp contact with tonalite, generating early trondhjemite matrix breccias. Geochemical data indicates tonalite to be intermediate in composition between Méritens quartz-diorite and early trondhjemite, and the variability in incompatible trace element concentration suggests that interaction between trondhjemite and quartz-diorite occurred in two physical states: (1) mixtures of trondhjemite magma and quartz-diorite magma, and (2) mixtures of trondhjemite magma and solidified quartz-diorite and tonalite. The production of tonalite by

various mechanisms is suggested by the occurrence of several generations of trondhjemite intruded the pluton.

The lack of extrusive equivalents to tonalite suggests that the subvolcanic and volcanic systems were closed during the formation of subvolcanic tonalite. Tonalite was likely formed by a combination of differentiation of a more mafic magma and interaction with early trondhjemite. Because no mafic intrusive phases cut tonalite (apart from the much later Eldrich diorite), tonalite must have formed during the late stages of mafic magma extrusion.

Granophyre is distinguished from other early trondhjemite phases by its extremely fine-grained texture. Granophyre occurs throughout the early trondhjemite, but its principal concentrations are observed near the north and south margins of the pluton. Quartz and albite generally compose more than 95% of the rock, with actinolite, chlorite and epidote appearing as minor constituents. Granophyre is enriched in SiO_2 , Na_2O , HFSE, Th, U and REE relative to coarse-grained trondhjemite. It also shows a pronounced negative Eu anomaly (the largest among all phases in the pluton). Crosscutting relationships clearly indicate that granophyre is a separate phase, emplaced later than coarse-grained trondhjemite. The granophyre's distinct geochemistry and late emplacement suggests that granophyre represents a level of increased differentiation relative to coarse-grained trondhjemite. The increase in Eu/Eu^* with increasing Th and SiO_2 , from early coarse-grained trondhjemite to granophyre, suggests that feldspar fractionation played an important

role in the production of granophyre. The granophyre's characteristic texture suggests quenching or sudden cooling and/or crystallization at eutectic conditions. The numerous miarolitic cavities, suggest that devolatilization may have occurred in granophyre. Consequently, field relationships presented in Section 2.3, along with this phase's SiO_2 content, texture and geochemical signature, clearly identify granophyre as a late-stage, SiO_2 -, Na_2O - and incompatible element-enriched differentiate of trondhjemite. However, the abundance of granophyric textures in tonalite from the margins of the pluton (e.g., beneath the Ansil deposit) suggests that granophyric intergrowth textures may have resulted from quenching of magma as it intruded cool, seawater-rich host rocks. Granophyre is enriched in Y, Hf, Th and La relative to the rhyolites of the Noranda cauldron, and an enrichment in Y is reflected in its lower Zr/Y ratio compared to the rhyolites. This distinctive geochemistry indicates that there are no major extrusive equivalents to granophyre within the Noranda cauldron.

The Eldrich diorite occupies about 5% of the Flavrian pluton and occurs as dikes and sills and irregular masses. Diorite is composed of remnant plagioclase that is altered to epidote and lesser amounts of chlorite resulting in a blurred surface; euhedral amphibole (actinolite + hornblende) and anhedral quartz. Accessory phases include magnetite, chlorite, apatite and carbonate. Although alteration has masked many of the textural relationships, dioritic to sub-ophitic textures are preserved. The Eldrich diorite clearly cuts early trondhjemite, and therefore it is the latest mafic intrusive phase of the pluton. In the single sample analysed, the Eldrich diorite shows

major element concentrations similar to Méritens quartz-diorite. However, higher TiO_2 concentration in the Eldrich diorite clearly distinguishes this diorite from the Méritens quartz-diorite. Ni concentrations within the Eldrich diorite are at the low end of concentrations for Méritens quartz-diorite, and Eu concentrations are slightly higher relative to the Méritens quartz-diorite. The pattern of chondrite normalized REE for the Eldrich diorite is relatively flat and less fractionated than the pattern for Méritens quartz-diorite. This difference is reflected in their distinctive La/Yb ratios. The Eldrich diorite is also depleted in Th, Hf, Zr and La relative to andesites of the Noranda cauldron. The crosscutting relationships and distinctive geochemistry indicate that the Eldrich diorite did not have extrusive equivalents within the cauldron. The Eldrich diorite may correlate with the numerous mafic dikes that cut the volcanic rocks of the Noranda cauldron. Figure D.1F shows the state of the Flavrian pluton after intrusion of the Eldrich diorite and late trondhjemite.

Late trondhjemite occurs in the central part of the Flavrian pluton. It occupies about 30% of the pluton's surface and is characterized by a well-developed homogeneous, coarse-grained granitic texture. Abundant irregular-shaped mafic inclusions occur throughout the late trondhjemite. Late trondhjemite is mainly composed of plagioclase and quartz, with plagioclase commonly showing oligoclase cores and clear albite rims. The amphibole is generally actinolite and accessory phases include epidote, chlorite, magnetite, stilpnomelane and zircon. Late trondhjemite clearly transects both tonalite and Méritens quartz-diorite in the northwest part of the pluton. The contact zone is composed of late trondhjemite

matrix breccia, in which the late trondhjemite matrix hosts angular inclusions of andesite, tonalite and rarely early trondhjemite. Late trondhjemite, dated by U/Pb in zircon, gives a preliminary discordant age of 2679 Ma, as well as ages of 2700 Ma and 2712 Ma interpreted to represent ages of inherited zircons. The 2679 Ma age suggests that late trondhjemite was clearly intruded later than early trondhjemite (2700 Ma).

Late trondhjemite is enriched in Fe_2O_3^* , MnO and P_2O_5 and depleted in SiO_2 relative to pink trondhjemite, coarse-grained trondhjemite and granophyre. It is compositionally similar to trondhjemite porphyry, but the late trondhjemite's slightly lower concentrations of P_2O_5 and MgO may distinguish it from trondhjemite porphyry. This distinction is supported by the late trondhjemite's enrichments in Co, Cu and Zn and depletions in Nb, Y, Th and REE (except Eu) compared to early trondhjemite. The late trondhjemite's lower Th and La concentrations clearly distinguish it from early trondhjemite on graphs of compatible vs incompatible and incompatible vs incompatible elements. A comparison of REE patterns for late trondhjemite and the Lac Dufault granodiorite indicates that the patterns are clearly different, with the Lac Dufault granodiorite showing a significantly more fractionated pattern than the Flavrian pluton's late trondhjemite. La/Yb ratios for the Lac Dufault granodiorite are considerably higher than those of late trondhjemite. Consequently, the late trondhjemite phase of the Flavrian pluton cannot be correlated with the Lac Dufault granodiorite. The distinctive geochemistry of late trondhjemite supports field investigations and geochronological data identifying the late trondhjemite as a

separate phase of the pluton, probably derived from a separate source. Consequently intrusion of late trondhjemite postdates the main VHMS episode of the Noranda cauldron.

Geochemical evolution

The geochemical evolution of the Flavrian pluton from Méritens quartz-diorite to granophyre is characterized by a general enrichment in SiO_2 , Na_2O , Y, Nb, Zr, Hf, Ta, Th, U and REE and relative depletion in Al_2O_3 , Fe_2O_3^* , MnO, MgO, CaO, Co, Sc, V and Sr. La/Yb ratios remained relatively constant and Eu was depleted as the more differentiated phases were introduced into the pluton, with variations occurring in the silica-rich phases. The pluton evolved through episodic injection of magma into preferentially oriented fractures and faults that produced complex dike-fed sill geometries.

Important variations occur in the geochemical trends of the various phases of the Flavrian pluton. Interaction between what is now represented by Méritens quartz-diorite and early trondhjemite caused significant scatter in the trends of most elements except Th, and to a lesser extent Ta and Nb. This interaction likely occurred by magma mixing and partial assimilation of Méritens quartz-diorite by trondhjemite. Variations in incompatible element concentrations and La/Yb ratios for coarse-grained trondhjemite were likely caused by the separation of an aqueous fluid phase from the trondhjemite magma through boiling. In addition, intrusion of granophyre caused important increases in incompatible elements relative to the other early

trondhjemite phases. Granophyre is interpreted as a late-stage, high SiO_2 -, Na_2O - and incompatible element-enriched phase that either quenched due to rapid cooling or crystallized at eutectic conditions. The distinct geochemistry of late trondhjemite supports field investigations and geochronological data indicating the late trondhjemite to be a separate late phase of the pluton produced from a separate magma. However, chondrite-normalized REE patterns suggest that late trondhjemite is not equivalent to the Lac Dufault granodiorite, as was previously suggested by Kennedy (1984).

A broad negative correlation occurs between compatible and incompatible elements for Méritens quartz-diorite to early trondhjemite. Granophyre is clearly distinguished by its relative enrichment in incompatible elements, and may represent a late-stage differentiate of trondhjemite. Therefore, Méritens quartz-diorite, tonalite, early trondhjemite and granophyre are probably linked genetically. Late trondhjemite shows a distinct depletion in incompatible elements suggesting it was related to a different magmatic source. Variation diagrams of incompatible elements generally show large variations in granophyre and a crude positive correlation for Méritens quartz-diorite with early trondhjemite. Late trondhjemite is clearly distinguished from all other phases. The general negative correlation between Eu/Eu^* and Th suggests that feldspar crystallization played an important role in the differentiation of the pluton. Much of the fractionation probably occurred in a deeper source area because large compositional differences occur between different sills with sharp

contacts. Batches of fractionated magma would then be injected from a deep reservoir into the subvolcanic chamber.

Comments on the timing of gold mineralization within the Flavrian pluton

Economic mineralization at the Pierre Beauchemin mine was clearly associated with shears and fractures developed in and near the Eldrich diorite dike within the Eldrich Fault zone. The fault is interpreted to have occurred in response to a WNW-ESE compression, and the distribution of gold is clearly controlled by structures related to this fault. Gold-bearing veins at Pierre Beauchemin are generally located in or associated with areas that have undergone some degree of dilation, most of which was created by a change in orientation of shear zones due to competency contrasts between the dikes and their host granitoid. Two types of ore shoots, both trending in approximately the same direction are observed at the Pierre Beauchemin mine: (1) diorite dike-associated shoots, and (2) granitoid-associated shoots. Variations in the plunges of ore shoots is interpreted to have resulted from refraction of shears due to competency contrasts between diorite and granitoid host rocks.

Crosscutting relationships suggest that albitization (and possibly a phase of hematitization) preceded or was coeval with gold precipitation associated with pyritization and carbonatization. The intimate association between specularite-, magnetite- and pyrite-rich ore was also observed at the Elder deposit (Trudel et al., 1991) and the Silidor deposit (Gaulin, 1992; Carrier, 1994). The presence of pyrite, magnetite, specularite and gold in the ore at Pierre Beauchemin suggests that a

combination of oxidizing and reduced fluids may have been involved in the mineralizing event. Carrier (1994) concluded that the Silidor gold deposit occurred during a NE-SW compression between 2630 and 2580 Ma. Carrier's conclusion is based on detailed structural analysis and a Pb isotope date of 2562 ± 12 Ma by Carignan and Gariépy (1993). However, it is not clear whether the 2562 ± 12 Ma age represents the age of gold deposition or a complete resetting of the U-Pb system, 140 Ma. after the intrusion of the host tonalite Carignan and Gariépy (1993).

Observations presented in CHAPTER 5 clearly indicate that gold mineralization at the Pierre Beauchemin mine occurred after the emplacement of the Eldrich diorite. In addition, the intimate relation between the Eldrich Fault and gold mineralization clearly demonstrates that the distribution of gold is controlled by the fault. The WNW-ESE compression, interpreted to have induced faulting at Pierre Beauchemin, may correlate with the late phase of compression associated with the Kenoran orogeny (see Section 1.1.3). This compression is interpreted to have occurred during the late stages or immediately following the Main Timiskaming period (Corfu, 1993). The Main Timiskaming period, which includes deposition of Timiskaming-type alluvial sediments and alkaline volcanism, is dated between 2681 and 2676 Ma (Corfu, 1993) and is interpreted to mark the emergence of the continent. Continental emergence is consistent with the conclusions of Kennedy (1984), who suggested from oxygen isotopic data, that the Pierre Beauchemin deposit was formed by a significant component of meteoric fluids. Consequently, Kennedy's study suggests that gold mineralization occurred during or after continental emergence between 2681 and

2676 Ma. Several other mesothermal gold deposits have been attributed to this period (Spooner and Barrie, 1993).

Kennedy (1984) suggested that gold mineralization in the Flavrian pluton was associated with intrusion of the late trondhjemite. The tentative age of the late trondhjemite is 2679 Ma, consistent with the period marked by continental emergence and the availability of meteoric fluids. According to Kennedy (1984), gold would have been concentrated in "skarn-like" systems near the intrusion's contact. Because gold is associated with pyrite, magnetite and hematite, as well as with widespread albitization and carbonatization, high temperature "skarn-associated" fluids may have played a role in the formation of the deposit. However, epidote, a typical skarn mineral, is clearly overprinted by alteration associated with gold mineralization at the Pierre Beauchemin deposit. In addition, gold-rich veins are found within late trondhjemite, near its contact with late trondhjemite matrix breccia; suggesting that gold mineralization occurred after intrusion of the late trondhjemite. Consequently, based on the observations presented above, the distribution of ore lenses at Pierre Beauchemin is interpreted to have been associated with faults formed in response to a WNW-ESE compression that occurred after 2681 Ma.

Conclusions

- (1) The Flavrian pluton is a composite sill-shaped pluton emplaced at high crustal levels during asymmetric subsidence of the Noranda cauldron.

- (2) Ascending magma pulses were emplaced episodically in fractures and faults, causing internal pressure variations and resulting in a dike-fed sill geometry.
- (3) Homogeneous tonalite may have formed by differentiation of Méritens quartz-diorite; whereas heterogeneous tonalite probably formed by the interaction of early trondhjemite and Méritens quartz-diorite. The early trondhjemite matrix breccias clearly indicate that part of the early trondhjemite intruded a solidified Méritens quartz-diorite. Scatter in the geochemical data within heterogeneous tonalite is attributed to interaction between what is now represented by Méritens quartz-diorite and early trondhjemite.
- (4) The coarse-grained trondhjemite is characterized by a breccia texture interpreted to have resulted from major pressure variations that induced boiling and caused the separation of a free aqueous fluid phase from the trondhjemite magma. The aqueous fluid probably altered early trondhjemite; causing the large variations in incompatible element concentrations.
- (5) Field relationships along with distinctive texture and geochemistry suggest that granophyre is a late-stage, SiO_2 , Na_2O and incompatible element-enriched differentiate of trondhjemite.
- (6) Crosscutting relationships, distinct geochemistry and a discordant U-Pb zircon date suggest that late trondhjemite is a separate intrusion that was intruded at

2679 Ma; 20 Ma younger than early trondhjemite. Therefore the intrusion of late trondhjemite postdates the formation of VHMS deposits within the Noranda cauldron. In addition, REE patterns indicate that late trondhjemite cannot be correlated with the Lac Dufault granodiorite.

- (7) Méritens quartz-diorite, tonalite, early trondhjemite and granophyre are probably linked genetically; whereas late trondhjemite was related to a different magmatic source.
- (8) Similar geochemical signatures for the Méritens quartz-diorite and andesites of the Noranda cauldron suggest that quartz-diorite is an intrusive equivalent of andesite. Similar conclusions can be drawn for early trondhjemite and rhyolite from the Noranda cauldron. However, compositional differences between early trondhjemite and Cycle 4 rhyolite suggest that the link between the chamber and the overlying volcanic rocks terminated before or during the onset of Cycle 4 volcanism. The chemical compositions of granophyre, Eldrich diorite and late trondhjemite indicate that these phases did not have extrusive equivalents within the Noranda cauldron.
- (9) Crosscutting relationships and geochemical evidence indicate that development of the Noranda cauldron, and its associated VHMS deposits, is constrained to an interval of time that began with intrusion of the Méritens quartz-diorite and ended before complete emplacement of the phases that compose the early

trondhjemite. The magmatic brecciation texture characteristic of coarse-grained trondhjemite may represent a link between boiling of the intrusive phase and VHMS mineralization.

- (10) The distribution of ore at the Pierre Beauchemin gold mine is associated with faults at the contact between incompetent diorite dikes and the competent host granitoid rocks. Shear, vein and ore shoot refraction is caused by the competency differences of the host rocks. Mineralization is interpreted to have occurred in response to a WNW-ESE compression after 2681 Ma.

REFERENCES

Anderson, E.M., 1951. *The Dynamics of Faulting*. Oliver and Boyd, Edinburg, 206

p.

Arth, J.G. and Hanson, G.N., 1972. Quartz diorites derived by partial melting of eclogite of amphibolite at mantle depths. *Contributions to Mineralogy and Petrology*, v. 37, p. 161-174.

Arth, J.G. and Hanson, G.N., 1975. Geochemistry and origin of the early Precambrian crust of north-eastern Minnesota. *Geochimica et Cosmochimica Acta*, v. 39, p. 325-362.

Arth, J.G., Barker, F., Peterman, Z.E. and Friedman, I., 1978. Geochemistry of the gabbro-diorite-tonalite-trondhjemite suite of southwest Finland and its implications for the origin of tonalitic and trondhjemitic magmas. *Journal of Petrology*, v. 19, p. 289-316.

Babineau, L., 1985. *Géologie de la région de La Motte, Abitibi: Québec*. Ministère de l'Énergie et des Ressources du Québec, DPV 83-11, p. 105-106.

Bard, J.P., 1980. *Microtexture des Roches Magmatiques et Métamorphiques*. Masson, Paris, 192 p.

Barker, F., Arth, J.G., Peterman, Z.E. and Friedman, I., 1976. The 1.7- 1.8-b.y. old trondhjemites of southwestern Colorado and northern New Mexico: geochemistry and depths of genesis. *Geological Society of America Bulletin*, v. 87, p. 189-198.

Barker, F., Arth, J.G. and Millard, H.T., Jr, 1979. Archean trondhjemites of the southwestern Big Horn Mountains, Wyoming: a preliminary report. *In* F. Barker, (ed.), *Trondhjemites, Dacites and Related Rocks*. Elsevier, Amsterdam, p. 401-414.

Barrett, T.J., MacLean, W.H., Cattalani, S., Hoy, L. and Riverin, G., 1991. Massive sulfide deposits of the Noranda area, Quebec. III. The Ansil mine. *Canadian Journal of Earth Sciences*, v. 28, p. 1699-1730.

Bateman, R., 1984. On the role of diapirism in the segregation, ascent and final emplacement of granitoid magmas. *Tectonophysics*, v. 110, p. 211-231.

Bateman, R., 1985. Aureole deformation by flattening around a diapir during in situ ballooning: the Cannibal Creek granite. *Journal of Geology*, v. 93, p. 293-310.

Belkibir, A., Robert, F., Vu, L. and Hubert, C., 1994. The influence of dikes on auriferous shear zone development within granitoid intrusions: the Bourlamaque pluton, Val d'Or district. *Canadian Journal of Earth Sciences*, v. 30, p. 1924-1933.

Bellefleur, G., 1992. Contribution des méthodes de potentiel à la cartographie géologique et à la structure profonde dans le Groupe de Blake River, Abitibi. M.Sc.A. thesis, École Polytechnique, Montréal, 101 p.

Behr, S.H., Dugas, J. and Emo, W.B., 1958. Part of western Duprat Township, Quebec. Department of Mines, Preliminary Report 368.

Best, M.G., 1982. Igneous and Metamorphic Petrology. W.H. Freeman and Company, New York, 630 p.

Billings, M.P., 1945. Mechanics of igneous intrusion in New Hampshire. American Journal of Science, v. 243a, p. 40-74.

Boivin, P., 1974. Pétrographie, stratigraphie et structure de la ceinture de "schistes verts" de Noranda dans les cantons de Hébécourt, de Duparquet et de Destor, Québec, Canada. Université de Clairmont-Ferrand, Clermont, France, 133 p.

Bott, M.H.P., 1959. The mechanics of oblique slip faulting. Geological Magazine, v. 96, p. 109-117.

Bouchard, M., 1980. Région de Cadillac-Malartic. Ministère de l'Énergie et des Ressources du Québec, DPV-791.

Buddington, A.F., 1959. Granite emplacement with special reference to North America. *Geological Society of America Bulletin*, v. 70, p. 671-747.

Campbell, I.H., Franklin, J.M., Gorton, M.P., Hart, T.R. and Scott, S.D., 1982. The role of subvolcanic sills in the generation of massive sulfide deposits. *Economic Geology*, V. 77, p. 2248-2253.

Camiré, G. and Watkinson, D.H., 1990. Volcanic stratigraphy and structure in the Hunter Creek Fault area, Rouyn-Noranda, Quebec. *Canadian Journal of Earth Sciences*, v. 27, p. 1348-1358.

Card, K.D., 1990. A review of the Superior Province of the Canadian Shield, a product of Archean accretion. *Precambrian Research*, v. 48, p. 99-156.

Carignan, J. and Gariépy, C., 1993. Pb Isotope Geochemistry of the Silidor and Launay Gold Deposits: Implications for the Source of Archean Au in the Abitibi Subprovince. *Economic Geology*, v. 88, p. 1722-1730.

Carrier, A., 1994. *Évolution Structurale et Métallogénique du Gisement Aurifère Silidor, Abitibi, Québec*. M.Sc. thesis, Université du Québec à Montréal, Montréal, 272 p.

Castro, A., 1985. The Central Extremadura Batholith: geotectonic implications (European Hercynian belt) - an outline. *Tectonophysics*, v. 120, p. 57-68.

Castro, A., 1986. Structural pattern and ascent model in the Central Extremadura Batholith, Hercynian belt, Spain. *Journal of Structural Geology*, v. 8, no. 6, p. 633-645.

Castro, A., 1987. On granitoid emplacement and related structures. A review. *Geologische Rundschau*, v. 76, no. 1, p. 101-124.

Castro, A., 1990. Magma mixing in the subvolcanic environment: petrology of the Genera interaction zone near Seville, Spain. *Contributions to Mineralogy and Petrology*, v. 98, p. 9-26.

Cathles, L.M., 1993. Oxygen Isotope Alteration in the Noranda Mining District, Abitibi Greenstone Belt, Quebec. *Economic Geology*, v. 88, p. 1483-1511.

Chouteau, M. and Deschamps, F., 1989. Geometric constraints of the Blake River Group and surrounding terranes in the Noranda region, Abitibi, from gravity interpretation: Transect report and update proposal, the Abitibi-Grenville LITHOPROBE project, Ecole Polytechnique, Montreal, Quebec, p. 97-101.

Clarke, D.B., 1992. Granitoid Rocks. T.H. van Andel (ed.), Chapman and Hall, London, 283 p.

Clemens, J.D. and Mawer, C.K., 1992. Granitic magma transport by fracture propagation. *Tectonophysics*, v. 204, p. 339-360.

Coleman, R.G. and Peterman, Z.E., 1975. Oceanic plagiogranite. *Journal of Geophysical Research*, v. 80, p. 1099-1108.

Cooke, H.C., James, W.F. and Mawdsley, J.B., 1931. Geology and ore deposits of Rouyn-Harricana region, Quebec. *Geological Survey of Canada, Memoir 166*, 314 p.

Corfu, F., Krogh, T.E., Kwok, Y.Y. and Jensen, L.S., 1989. U-Pb zircon geochronology in the southwestern Abitibi greenstone belt, Superior Province. *Canadian Journal of Earth Sciences*, v. 26, p. 1747-1763.

Corfu, F., 1993. The evolution of the southern abitibi greenstone belt in light of precise U-Pb geochronology. *Economic Geology*, v. 88, p. 1323-1340.

Coward, M.P., 1981. Diapirism and gravity tectonics: Report of a tectonic studies group conference held at Leeds University, 25-26 March 1980. *Journal of Structural Geology*, v. 3, no. 1, p. 89-95.

Davies, B.F., 1982. Pan-African granite intrusion in response to tectonic volume changes in a ductile shear zone from northern Saudi Arabia. *Journal of Geology*, v. 90, p. 467-483.

de Rosen-Spence, A.P., 1969. Genèse des roches à cordiérite-anthophyllite des gisements cupro-zincifères de la région de Rouyn-Noranda, Québec. *Canadian Journal of Earth Sciences*, v. 9, p. 1339-1345.

de Rosen-Spence, A.P., 1976. Stratigraphy, development and petrogenesis of the central Noranda volcanic pile, Noranda, Quebec. Ph.D. thesis, University of Toronto, Toronto, 166 p.

Desrochers, J.P. and Hubert, C., 1996. Structural evolution and early accretion of the Malartic Composite Block, southern Abitibi greenstone belt, Quebec, Canada. *Canadian Journal of Earth Sciences*, v. 33, p. 1556-1569.

Desrochers, J.P., Hubert, C., Ludden, J.N. and Pilot, P., 1993. Accretion of Archean oceanic plateau fragments in the Abitibi greenstone belt, Canada. *Geology*, v. 21, p. 451-454.

Dimroth, E., Imreh, L., Rocheleau, M. and Goulet, N., 1982. Evolution of the south central segment of the Archean Abitibi belt, Quebec. Part I: Stratigraphy and paleogeographic model. *Canadian Journal of Earth Sciences*, v. 19, p. 1729-1758.

Dimroth, E., Imreh, L., Rocheleau, M. and Goulet, N., 1983a. Evolution of the south central segment of the Archean Abitibi Belt, Quebec. Part II: Tectonic evolution and geomechanical model. *Canadian Journal of Earth Sciences*, v. 20, p. 1355-1373.

Dimroth, E., Imreh, L., Cousineau, P., Leduc, M. and Sanschagrín, Y., 1985. Paleogeographic analysis of mafic submarine flows and its use in the exploration for massive sulphide deposits. *In* L.D. Ayres, P.C. Thurston, K.D. Card and W. Weber (eds.), *Evolution of Archean Supracrustal Sequences*. Geological Association of Canada, Special Paper 28, p. 203-220.

Dugas, J., 1960. Descriptive notes to accompany the geological compilation of the northwest quarter of Beauchastel Township. Quebec Department of Mines, Publication S-51, 10 p.

Dugas, J., 1965. Descriptive notes to accompany the compilation of the geology of the northwest quarter of Beauchastel Township. Quebec Department of Natural Resources, Publication S-90, 7 p.

Dzurisin, D. and Yamashita, K.M., 1987. Vertical surface displacements at Yellowstone caldera, Wyoming, 1976-1986. *Journal of Geophysical Research*, v. 92, no. B13, p. 13753-13766.

Dzurisin, D., Yamashita, K.M. and Kleinman, J.W., 1994. Mechanisms of crustal uplift and subsidence at the Yellowstone caldera, Wyoming. *Bulletin of Volcanology*, v. 56, p. 261-270.

Eisenstadt, G. and De Paor, D.G., 1987. Alternative model of thrust-fault propagation. *Geology*, v. 15, p. 630-633.

Feng, R. and Kerrich, R., 1990. Geobarometry, differential block movements, and crustal structure of the southwest Abitibi greenstone belt, Canada. *Geology*, v. 18, p. 870-873.

Feng, R., Fan, J. and Kerrich, R., 1993. Noble metal abundances and characteristics of six granitic magma series, Archean Abitibi belt, Pontiac Subprovince: Relationships to metallogeny and overprinting of mesothermal gold deposits. *Economic Geology*, v. 88, p. 1376-1401.

Flynn, R.T. and Burnham, C.W., 1978. An experimental determination of rare earth partition coefficients between a chloride containing vapor phase and silica melts. *Geochimica et Cosmochimica Acta*, v. 42, p. 685-701.

Foster, M.E. and Huddleston, P.J., 1986. "Fracture cleavage" in the Duluth complex, northeastern Minnesota. *Geological Society of America Bulletin*, v. 97, p. 85-96.

Franklin, J.M., 1992. Volcanic-associated massive sulphide deposits. In S.E. Ho, F. Robert and D.I. Groves (eds.), *Gold and Base-Metal Mineralization in the Abitibi Subprovince, Canada, with Emphasis on the Quebec Segment*. University of Western Australia, Publication 24, p. 211-241.

Galley, A.G., 1994. Geology of the Ansil Cu-Zn massive sulfide deposit, Rouyn-Noranda, Quebec, Canada. Ph.D. thesis, Carlton University, Ottawa, 385 p.

Galley, A.G., 1996. Geochemical characteristics of subvolcanic intrusions associated with Precambrian massive sulfide districts. *In* D.A. Wyman (ed.), Trace Element Geochemistry of Volcanic Rocks: Application for Massive Sulfide Exploration. Geological Association of Canada, Short Course Notes Volume 12, p. 239-278.

Gaulin, R., 1992. Métallogénie de la mine Silidor, Abitibi, Québec, Ministère de l'Énergie et des Ressources, Report MB 92-17, 51 p.

Gaulin, R. and Trudel, P., 1990. Caractéristiques pétrographiques et géochimiques de la minéralisation aurifère à la mine Elder, Abitibi, Québec. *Canadian Journal of Earth Sciences*, v. 27, p. 1637-1650.

Gauthier, N., Rocheleau, M., Kelly, D. and Gagnon, Y., 1990. Controls on the distribution of gold mineralization within the Cadillac Tectonic Zone, Rouyn-Beauchastel segment, Abitibi belt, Quebec. *In* M. Rive, P. Verpaelst, Y. Gagnon, J.M. Lulin, G. Riverin and A. Simard (eds.), The Northwestern Quebec Polymetallic Belt: A Summary of 60 Years of Mining Exploration. Canadian Institute of Mining and Metallurgy, Special Volume 43, p. 185-198.

Gélinas, L., Trudel, P. and Hubert, C., 1984. Chemostratigraphic division of the Blake River Group, Rouyn-Noranda area, Abitibi, Quebec. *Canadian Journal of Earth Sciences*, v. 21, p. 220-231.

Gibson, H.L., Walker, S.D. and Coad, P.R., 1984. Surface geology and volcanogenic base metal massive sulphide deposits and gold deposits of Noranda and Timmins. Geological Association of Canada, Field trip 14, 124 p.

Gibson, H.L. and Lichtblau, A.P., 1986. Subaqueous rhyolite flows of the Central Mine Sequence, Noranda, Quebec. Geological Association of Canada-Mineralogical association of Canada, Program with Abstracts, v. 11, 72 p.

Gibson, H.L. and Watkinson, D.H., 1990. Volcanogenic massive sulphide deposits of the Noranda cauldron and shield volcano, Quebec. In M. Rive, P. Verpaelst, Y. Gagnon, J.M. Lulin, G. Riverin and A. Simard (eds.), *The Northwestern Quebec Polymetallic Belt: A Summary of 60 Years of Mining Exploration*. Canadian Institute of Mining and Metallurgy, Special Volume 43, p. 119-132.

Gibson, H.L., Watkinson, D.H., Watkins, J.J., Labrie, M. and Doiron G., 1993. Volcanological reconstruction of the Corbet breccia pile, and Cu-Zn massive sulfide deposit, Noranda, Quebec. *Exploration and Mining Geology*, v. 2, no. 2, p. 1-16.

Goldie, R.J., 1976. *The Flavrian and Powell Plutons, Noranda area, Quebec*. Ph.D. thesis, Queen's University, Kingston, 352 p.

Goldie, R.J., 1978. Magma mixing in the Flavrian pluton, Noranda area, Quebec. *Canadian Journal of Earth Sciences*, v. 15, p. 132-144.

Goldie, R.J., 1979a. Consanguineous Archean intrusive and extrusive rocks, Noranda: chemical similarities and differences. *Precambrian Research*, v. 9, p. 275-287.

Goldie, R.J., 1979b. Metamorphism of the Flavrian and Powell plutons, Noranda area, Quebec. *Journal of Petrology*, v. 20, p. 227-238.

Goldie, R.J., 1991. Comment on "Geobarometry, differential block movements, and crustal structure of the southwestern Abitibi greenstone belt, Canada". *Geology*, v. 18, p. 861-862.

Goodwin, A.M. and Ridler, R.H., 1970. The Abitibi orogenic belt. Symposium on Basins and Geosynclines of the Canadian Shield. Geological Survey of Canada, Paper 70-40, p. 1-24.

Goodwin, A.M. and Smith, E.M., 1980. Chemical discontinuities in Archean volcanic terrains and the development of Archean Crust. *Precambrian Research*, v. 10, p. 301-311.

Goulet, N., 1978. Stratigraphy and structural relationship across the Cadillac-Larder Lake Fault, Rouyn-Beauchastel area, Quebec. Ph.D. thesis, Queen's University, Kingston. Ministère des Richesses naturelles du Québec, DPV-602, 155 p.

Gromet, L.P. and Silver, L.T., 1983. Rare earth element distributions among minerals in a granodiorite and their petrogenetic implications. *Geochimica et Cosmochimica Acta*, v. 47, p. 925-939.

Guineberteau, B., Bouchez, J.L. and Vignerisse, J.L., 1987. The Mortagne granite pluton (France) emplaced by pull-apart along a shear zone: Structural and gravimetric arguments and regional implication. *Geological Society of America Bulletin*, v. 99, p. 763-770.

Gussow, W.C., 1937. Petrogeny of the major acid intrusives of the Rouyn-Bell River area of northwestern Quebec. *Trans. of the Royal Society of Canada, Sec IV*, p. 129-161.

Hancock, P.L., 1985. Brittle microtectonics: principles and practice. *Journal of Structural Geology*, v. 7, p. 437-457.

Hodgson, C.J., 1989a. The structure of shear-related, vein-type gold deposits: a review. *Ore Geology Review*, v. 4, p. 231-273.

Hodgson, C.J., 1989b. Patterns of mineralization. *In* J. Bursnall (ed.), *Mineralization and Shear Zones*. Geological Association of Canada, Short Course Notes, v. 6, p. 51-88.

Hoek, J.D., 1992. A classification of dyke-fracture geometry with examples from Precambrian dyke swarms in the Vestfold Hills, Antarctica. *Geologische Rundschau*, v. 80 no. 2, p. 233-248.

Hogg, W.A., 1960. Descriptive notes to accompany the compilation of the geology of the southwest quarter of Duprat Township. Quebec, Department of Mines, Publication S-54, 8 p.

Honsberger, A.H., 1954. Report on Eldrich Mines Ltd., Duprat Township, Québec. Mine Internal Report.

Hoy, L.D., 1993. Regional evolution of hydrothermal fluids in the Noranda district, Quebec: Evidence from $\delta^{18}\text{O}$ values from volcanogenic massive sulfide deposits. *Economic Geology*, v. 88, p. 1526-1541.

Hubert, C., 1990. Geological framework, evolution and structural setting of gold and base metal deposits of the Abitibi greenstone belt, Canada. *In* S.E. Ho, F. Robert and D.I. Groves (eds.), *Gold and Base-Metal Mineralization in the Abitibi Subprovince, Canada, with Emphasis on the Quebec Segment*. University of Western Australia, Geology Dept., Key Centre, Publication 24, p. 53-63.

Hubert, C., Trudel, P. and Gélinas, L., 1984. Archean wrench fault tectonics and structural evolution of the Blake River Group, Abitibi Belt, Quebec. *Canadian Journal of Earth Sciences*, v. 21, p. 1024-1032.

Hughes, C.J., 1973. Spilites, keratophyres, and the igneous spectrum. *Geological Magazine*, v. 109 (6), p. 513-527.

Humphris, S.E., 1984. The mobility of the rare earth elements in the crust. *In* Rare earth element geochemistry. P. Henderson (ed.), Elsevier, Amsterdam, p. 317-342.

Hutton, D.H.W., 1988. Igneous emplacement in a shear-zone termination: The biotite granite at Stontian, Scotland. *Geological Society of America Bulletin*, v. 100, p. 1392-1399.

Hutton, D.H.W., Dempster, T.J., Brown, P.E. and Becker, S.D., 1990. A new mechanism of granite emplacement: intrusion in active extensional shear zones. *Nature*, v. 343, p. 452-455.

Ida, Y. and Kumazawa, M., 1986. Ascent of magma in a deformable vent. *Journal of Geophysical Research*, v. 91, no. B9, p. 9297-9301.

Irvine, T.N. and Baragar, W.R.A., 1971. A guide to the classification of the common volcanic rocks. *Canadian Journal of Earth Sciences*, v. 8, p. 523-548.

Jensen, L.S., 1985. Stratigraphy and petrogenesis of Archean metavolcanic sequences, southwestern Abitibi Subprovince, Ontario. *In* L.D. Ayres, P.C. Thurston, K.D. Card and W. Weber (eds.), *Evolution of Archean Supracrustal Sequences*. Geological Association of Canada, Special Paper 28, p. 65-87.

Jolly, W.T., 1980. Development and degradation of Archean lavas, Abitibi area, Canada, in light of major element geochemistry. *Journal of Petrology*, v. 21, p. 323-363.

Johnson, D.J., 1992. Dynamics of magma storage in the summit reservoir of Kilauea volcano, Hawaii. *Journal of Geophysical Research*, v. 97, no. B2, p. 1807-1820.

Kalogeropoulos, S.I. and Scott, S.D., 1989. Mineralogy and geochemistry of an Archean tuffaceous exhalite: the Main Contact Tuff, Millenbach mine area, Noranda, Quebec. *Canadian Journal of Earth Sciences*, v. 26 p. 88-105.

Kay, R.W. and Senechal, R.G., 1976. The rare earth geochemistry of the Troodos ophiolite complex. *Journal of Geophysical Research*, v. 81, p. 964-970.

Kennedy, L.P., 1984. The geology and geochemistry of the Archean Flavrian pluton, Noranda, Quebec. Ph.D. thesis, University of Western Ontario, London Ontario, 499 p.

Kennedy, L.P. and Kerrich, R., 1982. Transition from marine to meteoritic hydrothermal regimes in an emerging Archean intrusive complex: ^{18}O evidence from the Flavrian pluton, Noranda. *American Geophysical Union (EOS)*, v. 63, no. 45, p. 128 (abstract).

Kerr, D.J. and Mason, R., 1990. A re-appraisal of the geology and ore deposits of the Horne mine complex at Rouyn-Noranda, Quebec. *In* M. Rive, P. Verpaelst, Y. Gagnon, J.M. Lulin, G. Riverin and A. Simard (eds.), *The Northwestern Quebec Polymetallic Belt: A Summary of 60 Years of Mining Exploration*. Canadian Institute of Mining and Metallurgy, Special Volume 43, p. 153-165.

Kerr, D.J. and Gibson, H.L., 1993. A comparison of the Horne massive sulphide deposit and intracauldron deposits of the Mine Sequence, Noranda, Quebec. *Economic Geology*, v. 88, p. 1419-1442.

Kindle, E.D., 1941. Northeast part, Beauchastel Township, Témiscamingue County, Quebec. *Geological Survey of Canada, Paper 41-7*, 5 p.

Kinnaird, J. and Bowden, P., 1987. African anorogenic alkaline magmatism and mineralization -a discussion with reference to the Niger-Nigerian Province. *Geological Journal*, v. 22, Thematic Issue, p. 297-340.

Knukey, M.J. and Watkins, J.J., 1982. The Geology of the Corbet massive sulphide deposit, Noranda District, Quebec, Canada. *In* R.W. Hutchinson, C.D. Spence and

J.M. Franklin (eds.), *Precambrian Sulphide Deposits*. Geological Association of Canada, Special Paper 25, p. 297-317.

Laflèche, M.R., 1991. *Pétrologie et Géochimie des éléments traces du magmatisme Archéens de la partie sud de la ceinture volcano-plutonique de l'Abitibi, Québec*. Doctoral thesis, Université de Montpellier II, Montpellier, France, 196 p.

Laflèche, M.R., Dupuy, C. and Bougault, H., 1992. *Geochemistry and petrogenesis of Archean mafic volcanic rocks of the southern Abitibi Belt, Quebec*. *Precambrian Research*, v. 57, p. 207-241.

Lagraa, K., 1994. *Pétrographie et géochimie des dykes de diorites du Groupe de Blake River, Abitibi, P.Q.* M.Sc thesis., Université de Montréal, Montreal, 81 p.

LeMaître, R.W., 1989. *A Classification of Igneous Rocks and Glossary of Terms*. R.W. LeMaître (ed.), Blackwell, Oxford, 193 p.

L'Espérance, R.L., 1950. *Northeast part of Duprat Township, Quebec*. Quebec Department of Mines, Preliminary Report 241, 12 p.

L'Espérance, R.L., 1951. *The geology of Duprat Township and some adjacent areas, northwestern Quebec*. Ph.D. thesis, McGill University, Montreal.

L'Espérance, R.L., 1952. Southeast quarter of Duprat Township, Quebec. Quebec Department of Mines, Preliminary Report 273, 15 p.

Lichtblau, A.P. and Dimroth, E., 1980. Stratigraphy and facies at the south margin of the Archean Noranda caldera, Noranda, Quebec. Geological Survey of Canada, Current Research, Paper 80-1A, p. 69-76.

Lowenstern, J.B., Clynne, M.A. and Bullen, T.D., 1997. Comagmatic A-type granophyre and rhyolite from the Alid volcanic center, Eritrea, Northeast Africa. *Journal of petrology*, v. 38, no.12, p. 1707-1721.

Ludden, J., Hubert, C. and Gariépy, C., 1986. The tectonic evolution of the Abitibi greenstone belt of Canada. *Geological Magazine*, 123, p. 153-166.

Lulin, J.-M., 1990. Une Analyse du Développement Minier du Nord-Ouest Québécois. *In* M. Rive, P. Verpaelst, Y. Gagnon, J.M. Lulin, G. Riverin and A. Simard (eds.), *The Northwestern Quebec Polymetallic Belt: A Summary of 60 Years of Mining Exploration*. Canadian Institute of Mining and Metallurgy, Spec. Volume 43, p. 17-34.

McCarthy, J. and Thompson, G.A., 1988. Seismic imaging of extending crust with emphasis on the western United States. *Geological Society of America Bulletin*, v. 100, p. 1361-1374.

Mackenzie, G.S., 1941. Halliwell Mine map-area, Quebec. Quebec Department of Mines, Geological Report 7, 27 p.

MacLean, W.H., 1988. Rare earth element mobility at constant inter-REE ratios in the alteration zone at the Phelps Dodge massive sulphide deposit, Matagami, Quebec. *Mineralium Deposita*, v. 23, p.231-238.

Méthot, Y., 1987. Pétrographie et géochimie du minerai et de l'altération reliée au gîte aurifère Eldrich, Abitibi, Québec. M.Sc. thesis, École Polytechnique de Montréal, Montréal, 231 p.

Mortensen, J.K., 1987. Preliminary U-Pb zircon ages for volcanic and plutonic rocks of the Noranda-Lac Abitibi area, Abitibi Subprovince, Quebec. *In* Current Research, Part A, Geological Survey of Canada, Paper 87-1A, p. 581-590.

Mortensen, J.K., 1993. U-Pb geochronology of the eastern Abitibi Subprovince. Part 2: Noranda-Kirkland Lake area. *Canadian Journal of Earth Sciences*, v. 30, p. 29-41.

Myers, J.S., 1975. Cauldron subsidence and fluidization: mechanisms of intrusion of the Coastal Batholith of Peru into its own volcanic ejecta. *Geological Society of America Bulletin*, v. 86, p. 1209- 1220.

Newhouse, W.H., 1942. Structural features associated with the ore deposits described in this volume. *In* W.H. Newhouse (ed.), *Ore Deposits as Related to Structural Features*. Princeton University Press, Princeton, N.J., p. 9-53.

Norrish, K. and Hutton, J.T., 1969. An accurate X-ray spectrographic method for the analysis of a wide range of geological samples. *Geochimica et Cosmochimica Acta*, v. 33, p. 431-453.

Ojakangas, R.W., 1985. Review of Archean clastic sedimentation, Canadian Shield: major felsic volcanic contributions to turbidite and alluvial fan-fluvial associations. *In* L.D. Ayres, P.C. Thurston, K.D. Card and W. Weber (eds.), *Evolution of Archean Supracrustal Sequences*. Geological Association of Canada, Special Paper 28, p. 23-48.

Paradis, S., 1984. Le pluton de Flavrian: Évolution pétrologique et relation avec les roches volcaniques du groupe de Blake River, Abitibi, Québec. M.Sc. thesis, Université de Montréal, Montréal, Québec, 196 p.

Paradis, S., 1990. Stratigraphy, volcanology and geochemistry of the New-Vauze-Norbec area, central Noranda volcanic complex, Quebec, Canada. Ph.D. thesis, Carleton University, Ottawa, 453 p.

Paradis, S., Ludden J. and Gélinas L., 1988. Evidence for contrasting compositional spectra in comagmatic intrusive and extrusive rocks of the late Archean Blake River

Group, Abitibi, Quebec. *Canadian Journal of Earth Sciences*, v. 25, no. 1, p. 134-144.

Paterson, S.R. and Fowler, T.K., 1993. Re-examining pluton emplacement processes. *Journal of Structural Geology*, v. 15, no. 2, p. 191-206.

Péloquin, A.S. and Verspaelst, P., 1989. Groupe de Blake River, Région de Rouyn-Noranda, Québec: Corrélation au nord et au sud de la faille Hunter Creek. *Geological Association of Canada/Mineralogical Association of Canada, Program with Abstracts*, v. 14, p. A37.

Péloquin, S., Potvin, R., Paradis, S., Laflèche, M.R., Verspaelst, P. and Gibson H.L., 1990. The Blake River Group, Rouyn-Noranda Area, Quebec: A stratigraphic synthesis. *In* M. Rive, P. Verspaelst, Y. Gagnon, J.M. Lulin, G. Riverin and A. Simard (eds.), *The Northwestern Quebec Polymetallic Belt: A Summary of 60 Years of Mining Exploration*. Canadian Institute of Mining and Metallurgy, Special Volume 43, p. 107-118.

Péloquin, S., Ludden, J. and Hubert, C., 1994. Magmatic systems in Late Archean volcanic basins: implications for Noranda-type VMS. *Geological Association of Canada/Mineralogical Association of Canada, Program with Abstracts*, v. 19, A87.

Péloquin, A.S., Verpaelst, P. and Ludden, J.N., 1996. Spherulitic rhyolites of the Archean Blake River Group, Canada: Implications for stratigraphic correlation and volcanogenic massive sulfide exploration. *Economic Geology*, v. 91, p. 343-354.

Picard, S., 1990. Le gisement Silidor. *In* M. Rive, P. Verpaelst, Y. Gagnon, J.M. Lulin, G. Riverin and A. Simard (eds.), *The Northwestern Quebec Polymetallic Belt: A Summary of 60 Years of Mining Exploration*. Canadian Institute of Mining and Metallurgy, Special Volume 43, p. 175-183.

Pitcher, W.S., 1979. The nature, ascent and emplacement of granitic magmas. *Journal of the Geological Society of London*, v. 136, p. 627-662.

Pitcher, W.S., 1987. Granites and yet more granites forty years on. *Geologische Rundschau*, v. 76, no. 1, p. 51-79.

Pitcher, W.S. and Berger, A.R., 1972. The Rosses Centered Complex: an example of cauldron subsidence. *In* L.U. Sitter (ed.), *The Geology of Donegal: A Study of Granite Emplacement and Unroofing*, Wiley-Interscience, London, p. 196-200.

Poulsen, K.H. and Robert, F., 1989. Shear zones and gold: Practical examples from the southern Canadian Shield. *In* J. Bursnall (ed.), *Mineralization and Shear Zones*. Geological Association of Canada, Short Course Notes, v. 6., p. 239-266.

Powell, W.G., Carmichael, D.M. and Hodgson, C.J., 1993. Thermobarometry in a subgreenschist to greenschist transition in metabasites of the Abitibi greenstone belt, Superior Province, Canada. *Journal of Metamorphic Geology*, v. 11, p. 165-178.

Ramsay, J.G., 1982. Rock ductility and its influence on the development of tectonic structures in mountain belts. *In* K.J. Hsü (ed.), *Mountain Building Processes*. Academic Press, London, p. 111-127.

Ramsay, G.J., 1989. Emplacement Kinematics of a granite diapir: the Chindamora batholith, Zimbabwe. *Journal of Structural Geology*, v. 11, no. 1, p. 191-209.

Richard, M., Hubert, C., Brown, A.C. and Sirois, R., 1990. The Pierre Beauchemin gold mine: a structurally controlled deposit within a subhorizontal layered composite granitoid. *In* M. Rive, P. Verpaelst, Y. Gagnon, J.M. Lulin, G. Riverin and A. Simard (eds.), *The Northwestern Quebec Polymetallic Belt: A Summary of 60 Years of Mining Exploration*. Canadian Institute of Mining and Metallurgy, Special Volume 43, p. 211-219.

Richard, M., Hubert, C. and Brown, A.C., 1991. Archean granitoid-hosted gold deposits of the Abitibi greenstone belt, Quebec: An example from the Pierre Beauchemin mine. *In* E.A. Ladeira (ed.), *Proceedings of the Symposium Brazil Gold '91. The Economics, Geology, Geochemistry and Genesis of Gold Deposits*, Rotterdam, p. 551-556.

Richard, M., Hubert, C., Brown, A.C., 1993. Subvolcanic Intrusions and Exploration for Volcanic Rock-Associated Massive Sulfide Deposits. *In* S.B. Romberger and D.I. Fletcher (eds.), *Integrated Methods in Exploration and Discovery*. Society of Economic Geologist Conference, Program and Extended Abstract, Denver, Colorado, April 17-20, p. AB 93.

Rive, M., Pinston, H. and Ludden, J.N., 1990. Characteristics of Late Archean rocks from the Abitibi and Pontiac Subprovinces, Superior Province, Canada. *In* M. Rive, P. Verpaelst, Y. Gagnon, J.M. Lulin, G. Riverin and A. Simard (eds.), *The Northwestern Quebec Polymetallic Belt: A Summary of 60 Years of Mining Exploration*. Canadian Institute of Mining and Metallurgy, Special Volume 43, p. 65-76.

Riverin, G. and Hodgson, C.J., 1980. Wall-rock alteration at the Millenbach Cu-Zn Mine, Noranda, Quebec. *Economic Geology*, v. 75, p. 424-444.

Riverin, G., Labrie, M., Salmon, B., Cazavant, A., Asselin, R. and Gagnon, M., 1990. The geology of the Ansil Deposit, Rouyn-Noranda, Quebec. *In* M. Rive, P. Verpaelst, Y. Gagnon, J.M. Lulin, G. Riverin and A. Simard (eds.), *The Northwestern Quebec Polymetallic Belt: A Summary of 60 Years of Mining Exploration*. Canadian Institute of Mining and Metallurgy, Special Volume 43, p. 143-151.

Robert, F., 1989. Internal structure of the Cadillac tectonic zone southeast of Val d'Or, Abitibi greenstone belt, Québec. *Canadian Journal of Earth Sciences*, v. 26, p. 2661-2675.

Robert, F., 1990. Structural setting and control of gold-quartz veins of the Val d'Or area, southeastern Abitibi Subprovince. *In* S.E. Ho, F. Robert and D.I. Groves (eds.), *Gold and Base-Metal Mineralization in the Abitibi Subprovince, Canada, with Emphasis on the Quebec Segment*. University of Western Australia, Geol. Dept. Key Centre Publication 24, p. 167-209.

Robert, F., 1991. Gold metallogeny of greenstone belts: considerations from the eastern Abitibi Subprovince, Canada. *In* E.A., Ladeira (ed.), *Proceedings of the Symposium Brazil Gold '91. The Economics, Geology, Geochemistry and Genesis of Gold Deposits*, Rotterdam, p. 31-47.

Robinson, W.G., 1943. Région du lac Flavrian, Cantons de Beauchastel et Duprat, Comtés de Témiscamingue et d'Abitibi. Ministère des Mines, Province de Québec, *Rapport Géologique* 13, 23 p.

Ryan, M.P., 1987. Neutral buoyancy and the mechanical evolution of magmatic systems. *In* B.O. Mysen (ed.), *Magmatic Processes: Physicochemical Principles*. The Geochemical Society, Special Publication Number 1, p. 259-287.

Ryan, M.P., 1988. The Mechanics and Three-Dimensional Internal Structure of Active Magmatic Systems: Kilauea Volcano, Hawaii. *Journal of Geophysical Research*, v. 93, no. B5, p. 4213-4248.

Sansfacon, R., and Hubert, C., 1990. The Malartic gold district, Abitibi belt, Quebec: Geological setting, structure and timing of gold emplacement at Malartic Gold fields, Barnat, East Malartic, Canadian Malartic and Sladen mines. *In* M. Rive, P. Verpaelst, Y. Gagnon, J.M. Lulin, G. Riverin and A. Simard (eds.), *The Northwestern Quebec Polymetallic Belt: A Summary of 60 Years of Mining Exploration*. Canadian Institute of Mining and Metallurgy, Special Volume 43, p. 221-235.

Schwerdtner, W.M., Stott, G.M. and Sutcliffe, R.H., 1983. Strain patterns of crescentic granitoid plutons in the Archean greenstone terrain of Ontario. *Journal of Structural Geology*, v. 5, no. 4, p. 419- 430.

Schwerdtner, W.M., 1990. Structural tests of diapir hypotheses in Archean crust of Ontario. *Canadian Journal of Earth Sciences*, v. 27, p. 387-402.

Sibson, R., 1987. Earthquake rupturing as a mineralizing agent in hydrothermal systems. *Geology*, v. 15, p. 701-704.

Sibson, R., 1989. Earthquake faulting as a structural process. *Journal of Structural Geology*, v. 11, p. 1-14.

Spence, C.D., 1967. The Noranda Area. Canadian Institute of Mining and Metallurgy, Centennial Field Excursion Guidebook, p. 36-39.

Spence, C.D. and de Rosen-Spence, A.F., 1975. The place of sulfide mineralization in the volcanic sequence at Noranda, Quebec. *Economic Geology*, v. 70, p. 90-101.

Spooner, E.T.C. and Barrie, C.T., 1993. A Special Issue devoted to Abitibi ore deposits in a modern context. *Economic Geology*, v. 88, p. 1307-1322.

Stephansson, O. and Johnson, K., 1976. Granite diapirism in the Rum Jungle area, northern Australia. *Precambrian Research*, v. 3, p. 159-185.

Stix, J. and Gorton, M., 1993. Replenishment and crystallization in epicontinental silicic magma chambers: evidence from the Bandelier magmatic system. *Journal of Volcanology and Geothermal Research*, v. 55, p. 201-215.

Sun, S.S., 1982. Chemical composition and origin of the Earth's primitive mantle. *Geochimica et Cosmochimica Acta*, vol.46, p.179-192.

Sutcliffe, R.H., Barrie, C.T., Burrows, D.R. and Beakhouse, G.P., 1993. Plutonism in the Southern Abitibi Subprovince: A Tectonic and Petrogenetic Framework. *Economic Geology*, v. 88, p. 1359-1375.

Sylvester, A.G., Oertel, G., Nelson, C.A. and Christie, J.M., 1978. Papoose Flat pluton: a granitic blister in the Inyo Mountains. *Geological Society of America Bulletin*, v. 89, p. 1205-1219.

Tagliamonte, F.P., 1979. Report on Win-Eldrich Mines Ltd., Duprat Township gold property. Unpublished internal report, 33 p.

Tait, S., Jaupart, C. and Vergnolle, S., 1989. Pressure, gas content and eruption periodicity of a shallow, crystallising magma chamber. *Earth and Planetary Science Letters*, v. 92, p. 107-123.

Tourigy, G., 1984. Géologie structurale et métamorphisme des roches précambriennes du Groupe de Kewagama dans la région de Cadillac-Malartic, Abitibi, Québec. M.Sc. Thesis, University of Montreal, Montreal.

Treagus, S.H., 1988. Strain refraction in layered systems. *Journal of Structural Geology*, v. 10, p. 517-527.

Trudel, P., 1978. Géologie de la région de Cléricky, Abitibi-Ouest. Ministère des Richesses naturelles du Québec, Geological Report, DP-0598, 152 p.

Trudel, P., Méthot, Y. and Perrault, G., 1989. Géochimie de la minéralisation aurifère à la mine Eldrich, région de Rouyn-Noranda, Québec, Canada. *Journal of Geochemical Exploration*, v. 32, p. 415-428.

Trudel, P., Gaulin, R., Hoy, L. and Lao, K., 1991. Géologie de la mine Elder, canton de Beauchastel, région de Rouyn-Noranda. Ministère de l'Énergie et des Ressources du Québec, Report MB 91-09, 139 p.

Ujike, O., 1985. Geochemistry of Archean alkalic volcanic rocks from the Crystal Lake area, east of Kirkland lake, Ontario, Canada. *Earth and Planetary Science Letters*, v. 73, p. 333-344.

Verpaelst, P., adam, E., Barnes, A., Dion, D-J., Milkereit, B., Peloquin, S. and Riverin, G., 1991. High-resolution seismic reflection profile of line 21, Blake River Group, Abitibi Subprovince, Quebec. Lithoprobe Abitibi-Grenville Project, Abstract, Workshop III.

Walker, G.P.L., 1989. Gravitational (density) controls on volcanism, magma chambers and intrusion. *Australian Journal of Earth Sciences*, v. 36, p. 149-165.

Watkins, J.J., 1980. The geology of the Corbet Cu-Zn deposit and the environment of ore deposition in the Central Noranda area. M.Sc. thesis, Queen's University, Kingston, 130 p.

Wilson, M.E., 1941. Noranda District, Quebec. Canadian Geological Survey, Memoir 229, p. 162.

Wong, L., Davies, D.W., Krough, T.E. and Robert, F., 1991. U-Pb zircon and rutile chronology of Archean greenstone formation and gold mineralization in the Val d'Or region, Quebec. *Earth and Planetary Science Letters*, v. 104, p. 325-336.

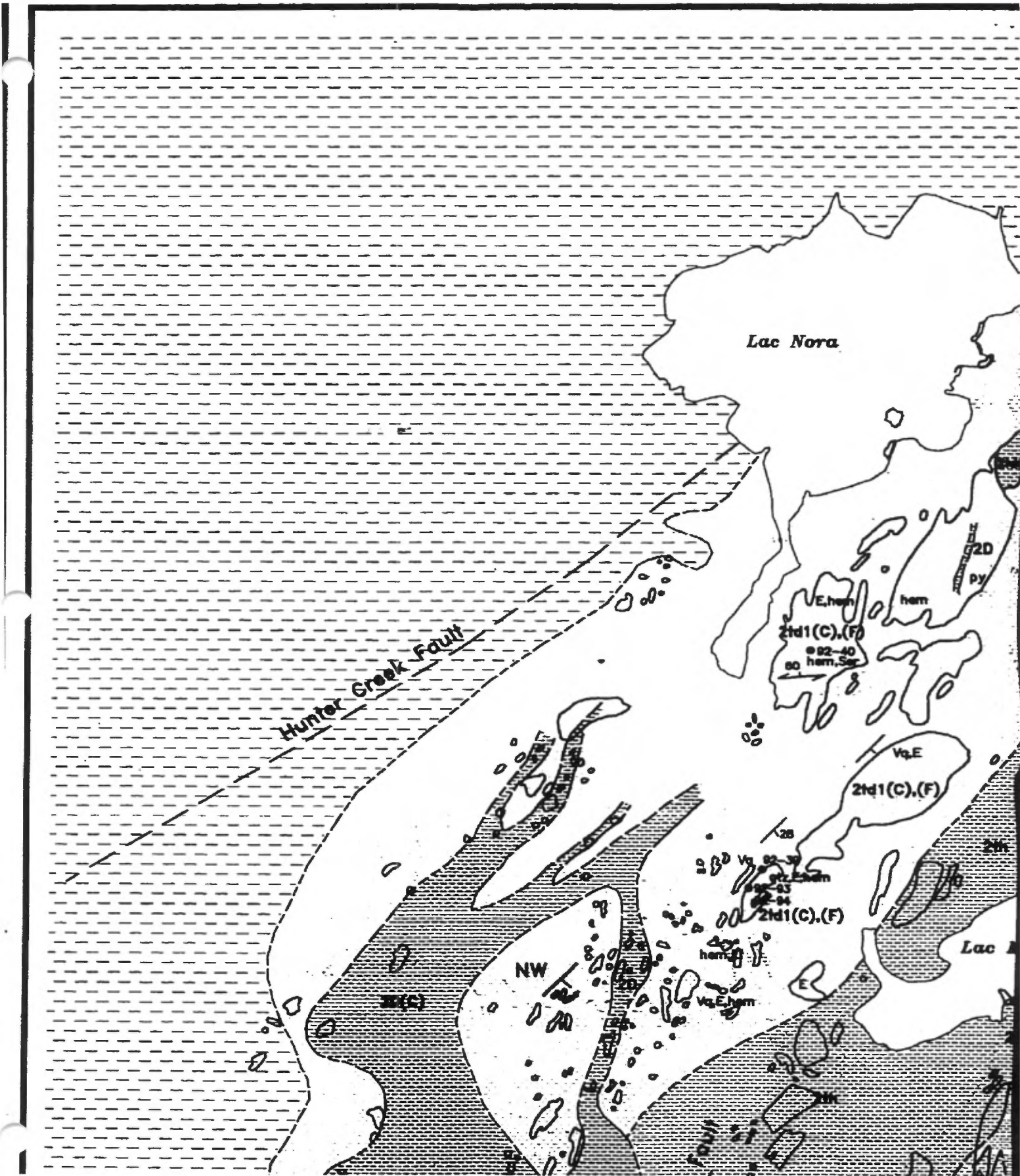
Zweng, P.L., Mortensen, J.K. and Dalrymple, G.B., 1993. Thermochronology of the Camflo gold deposit, Malartic, Québec: Implications for magmatic underplating and the formation of gold-bearing quartz veins. *Economic Geology*, v. 88, p. 1700-1721.

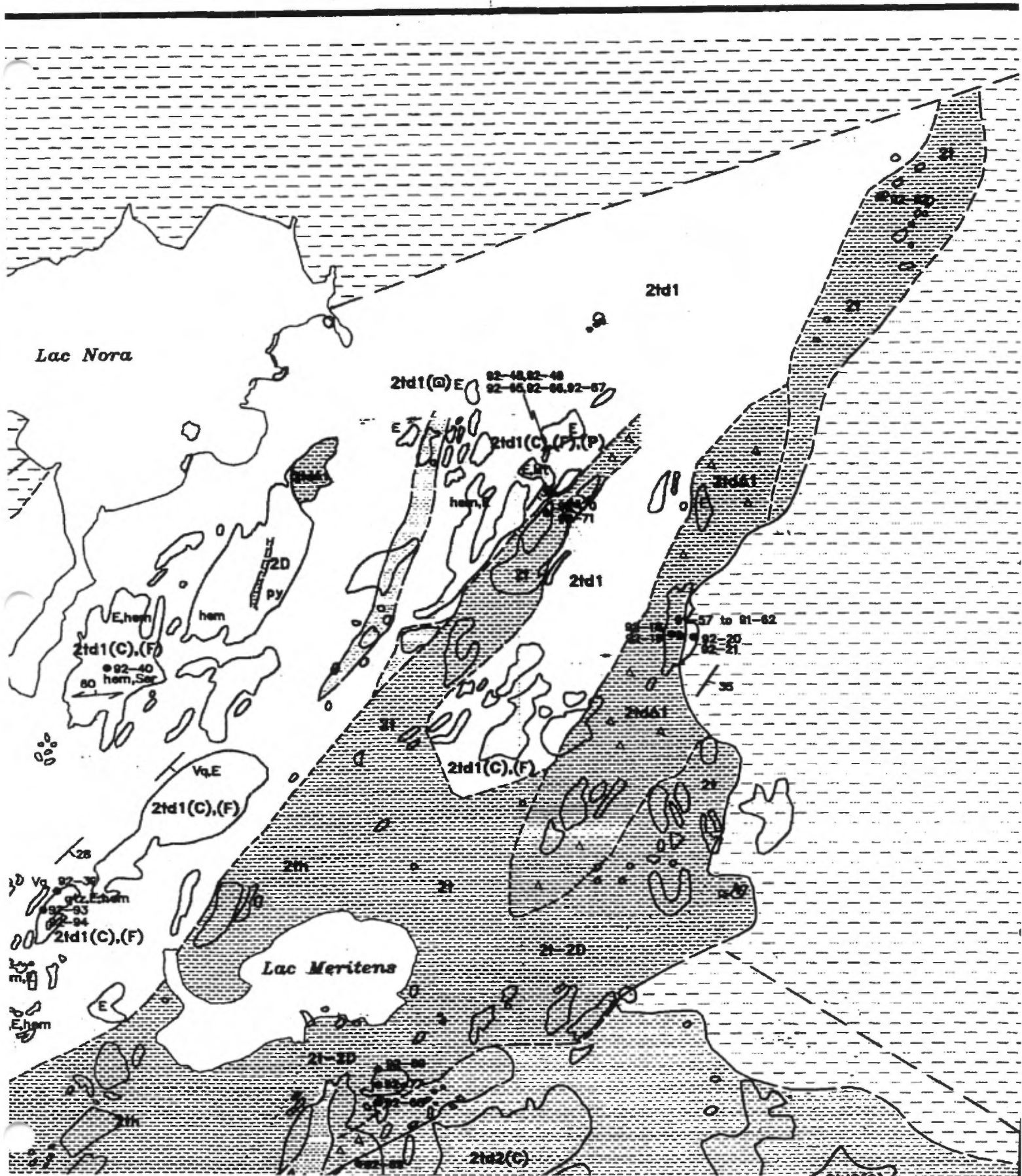
NOTE TO USERS

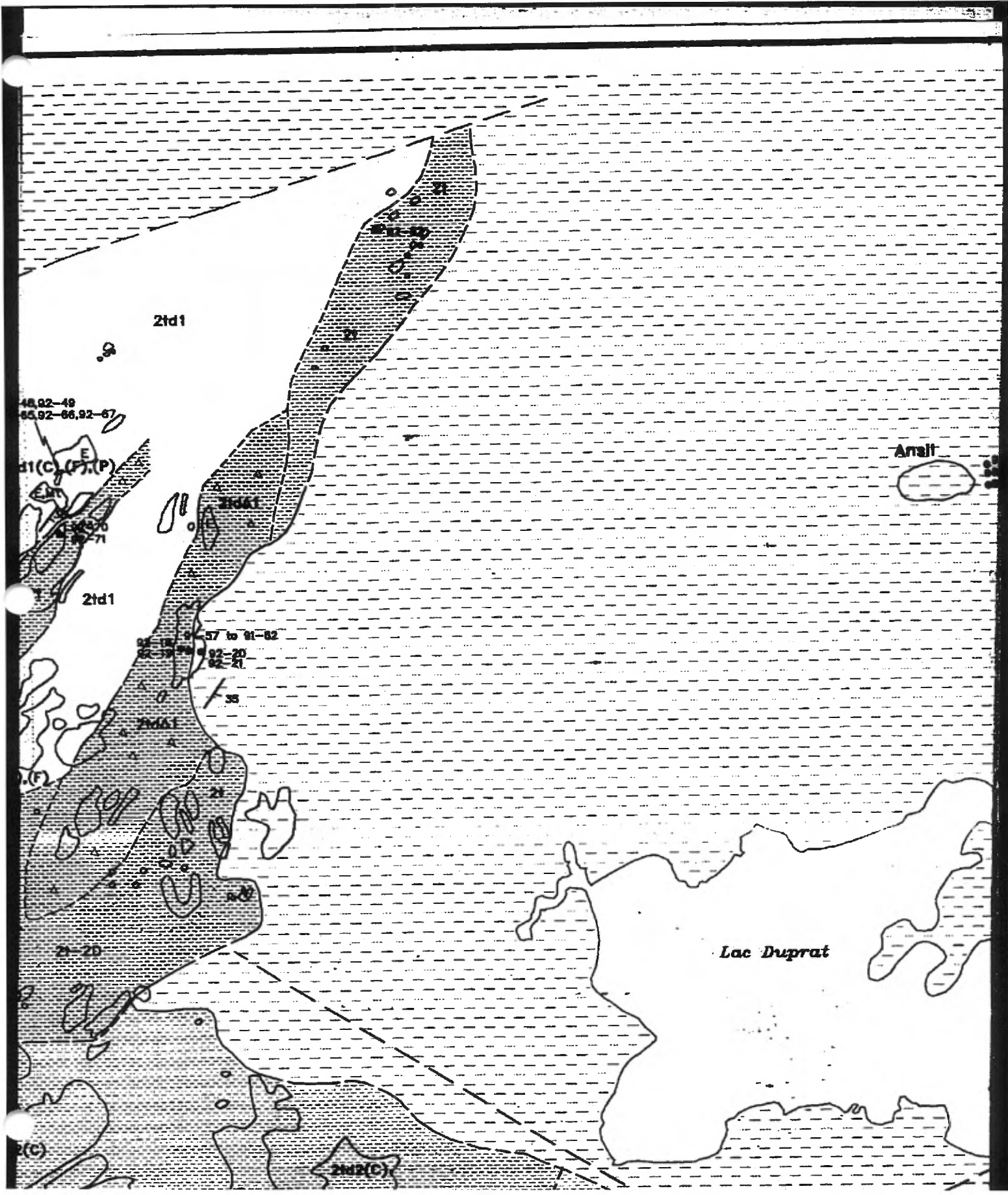
**Oversize maps and charts are microfilmed in sections in
the following manner:**

**LEFT TO RIGHT, TOP TO BOTTOM, WITH
SMALL OVERLAPS**

UMI



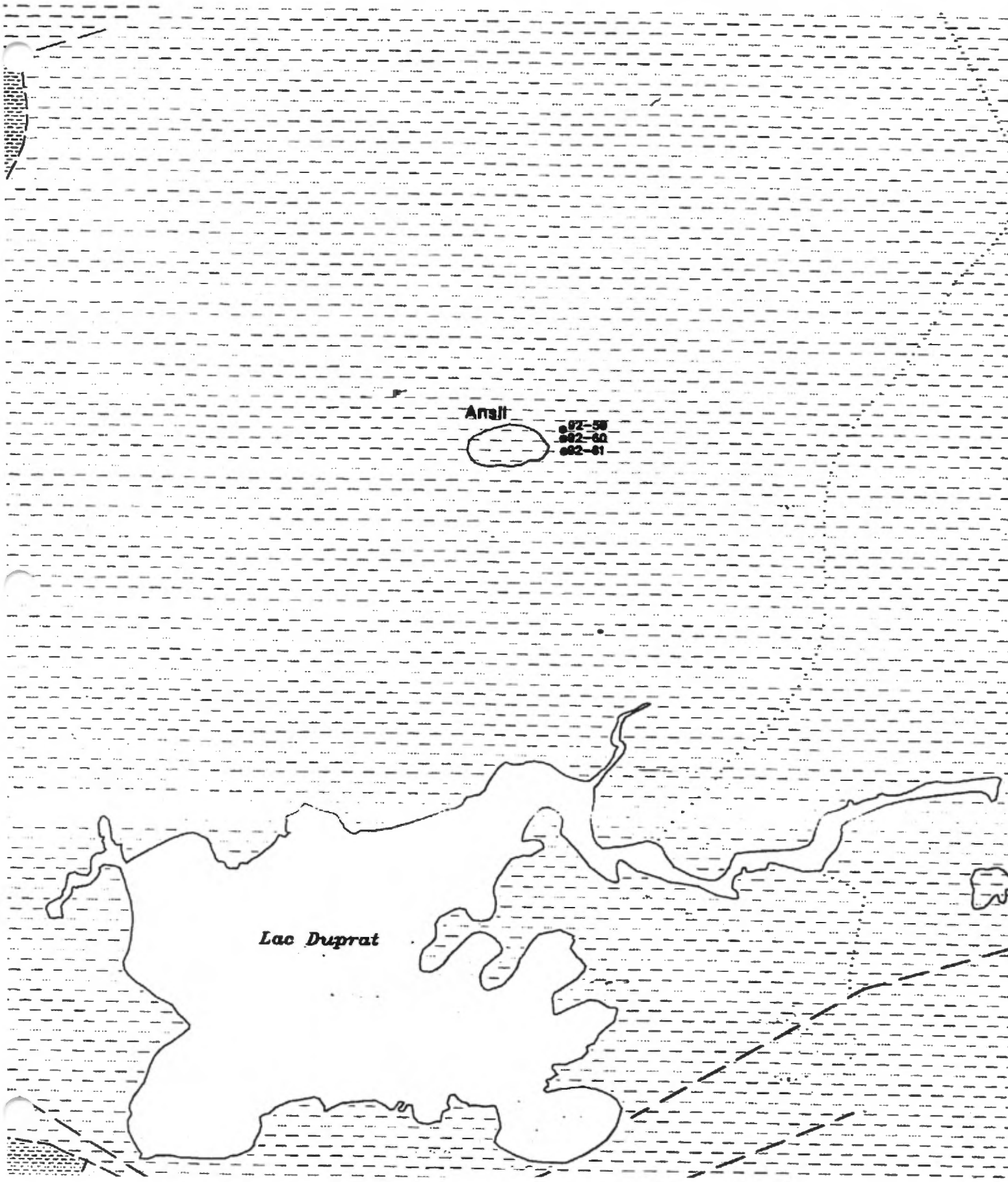




Anall

682-58
682-60
682-61

Lac Duprat



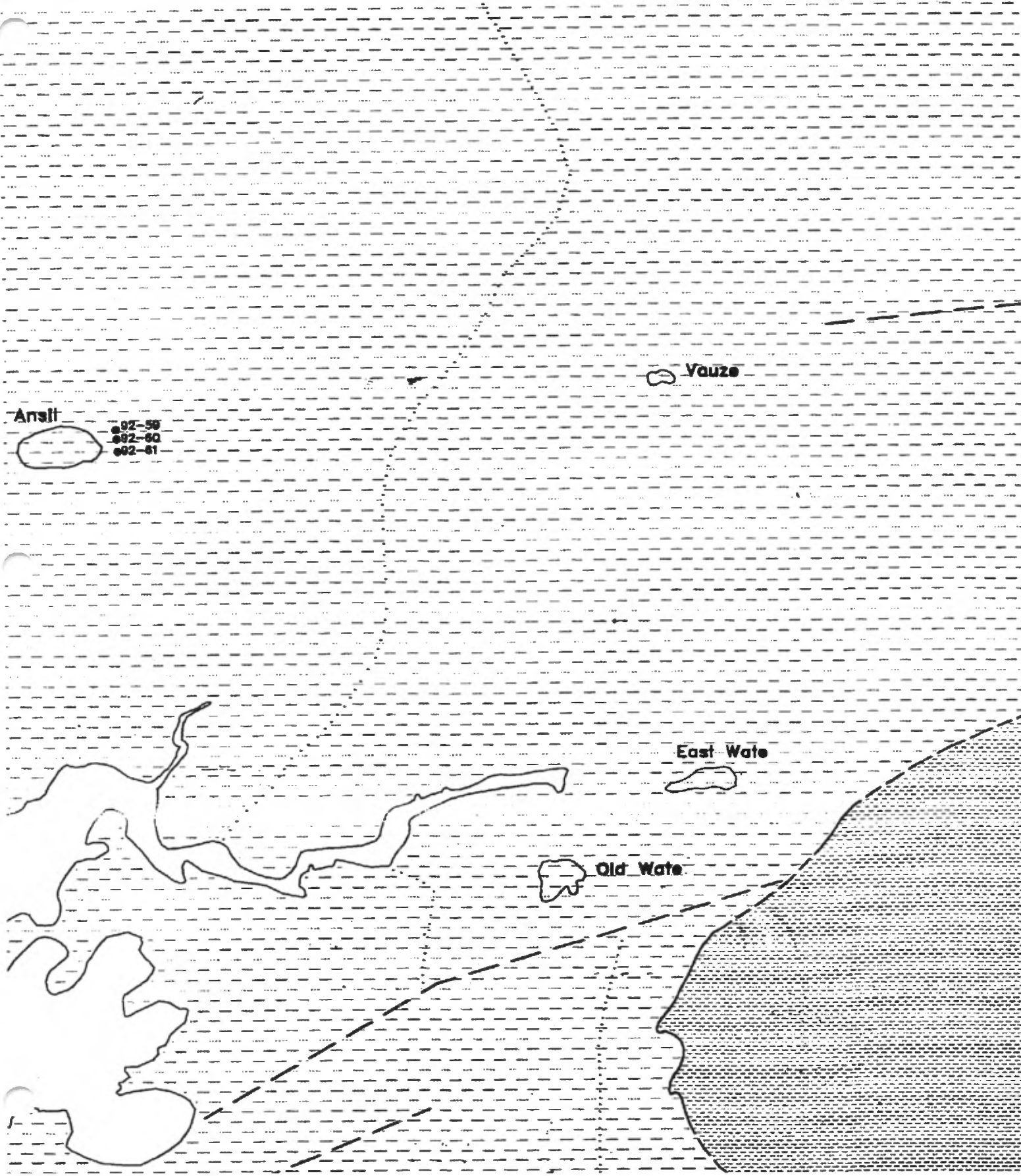
Ansil

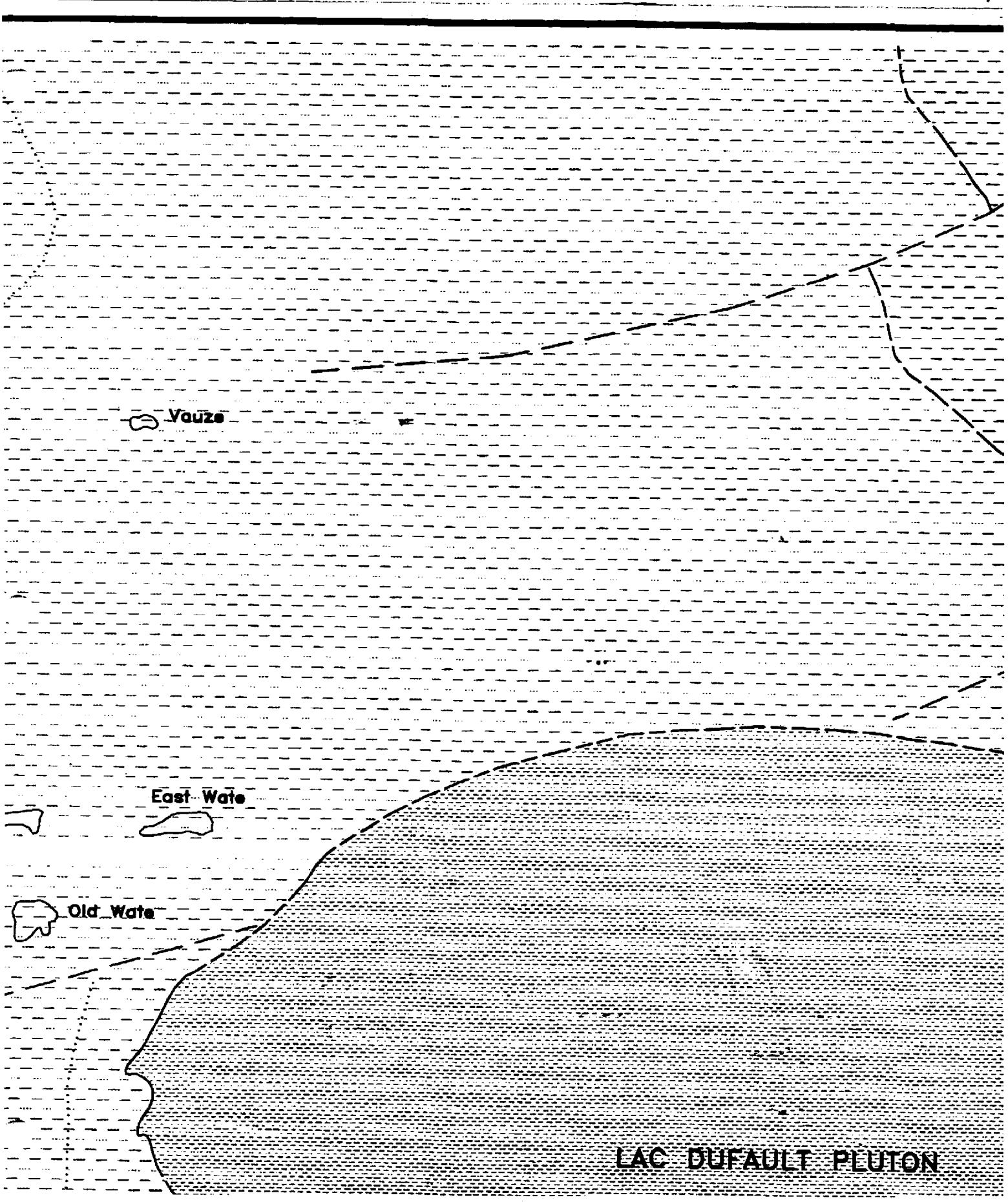
02-59
02-60
02-61

Vauze

East Wate

Old Wate



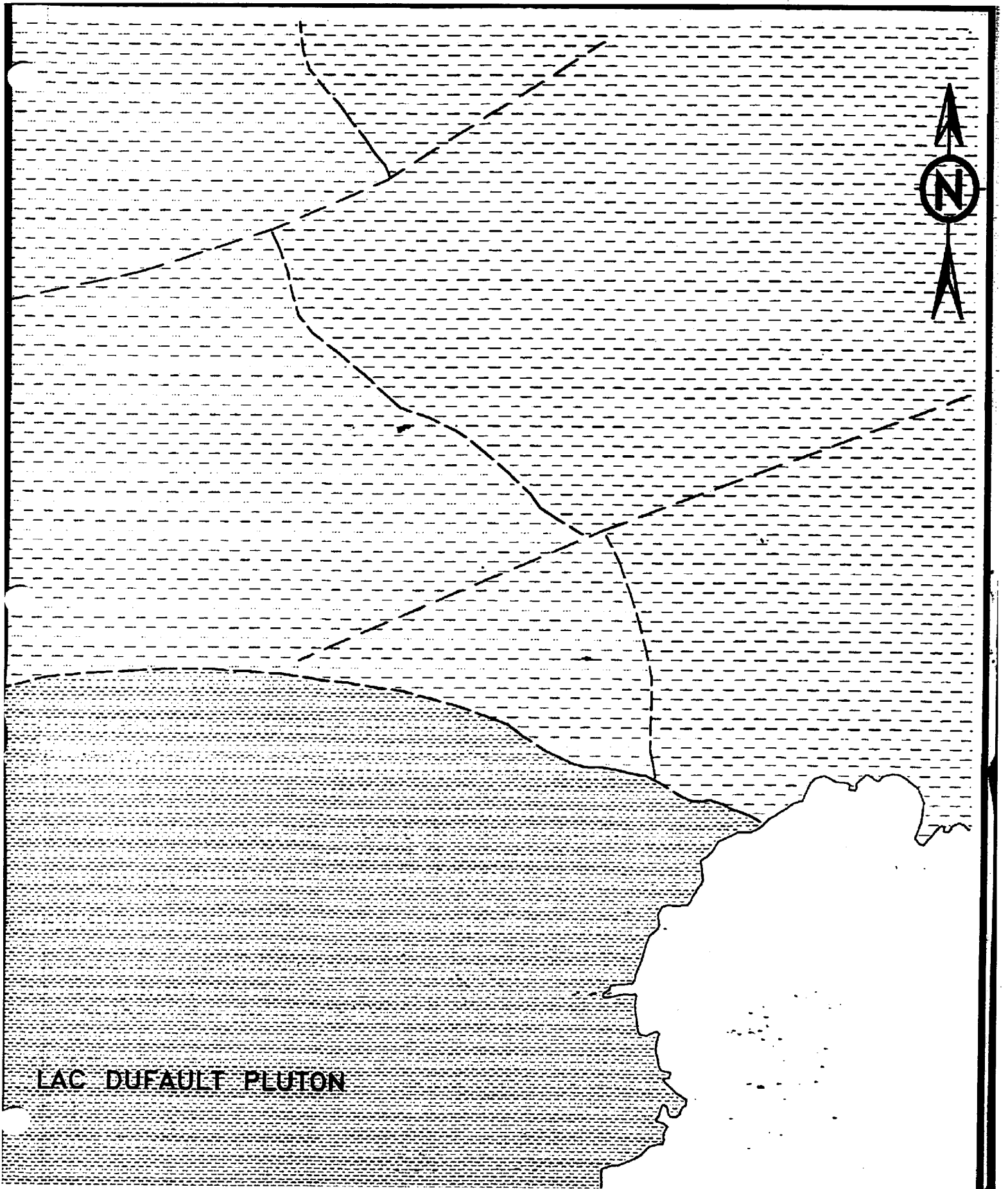


Vauze

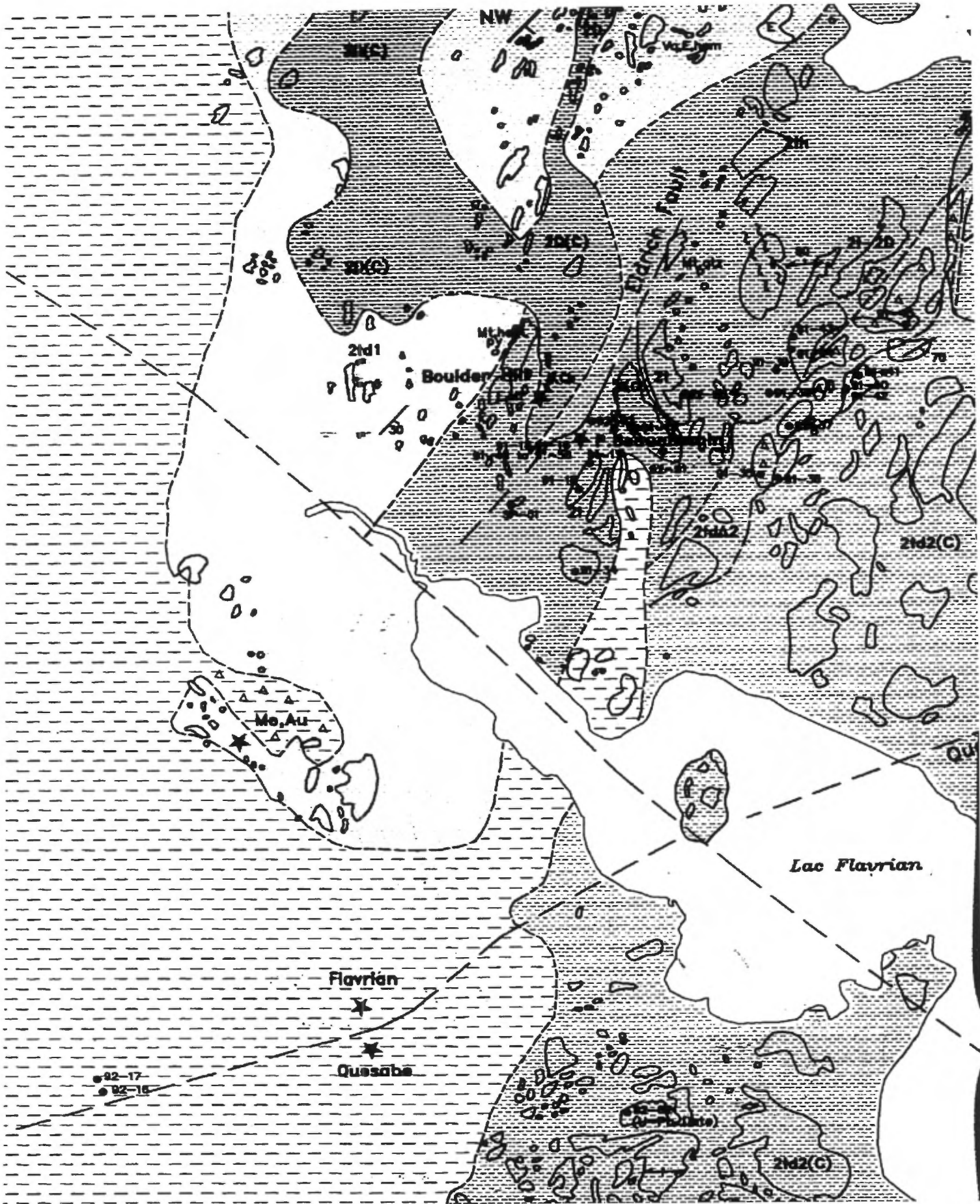
East Water

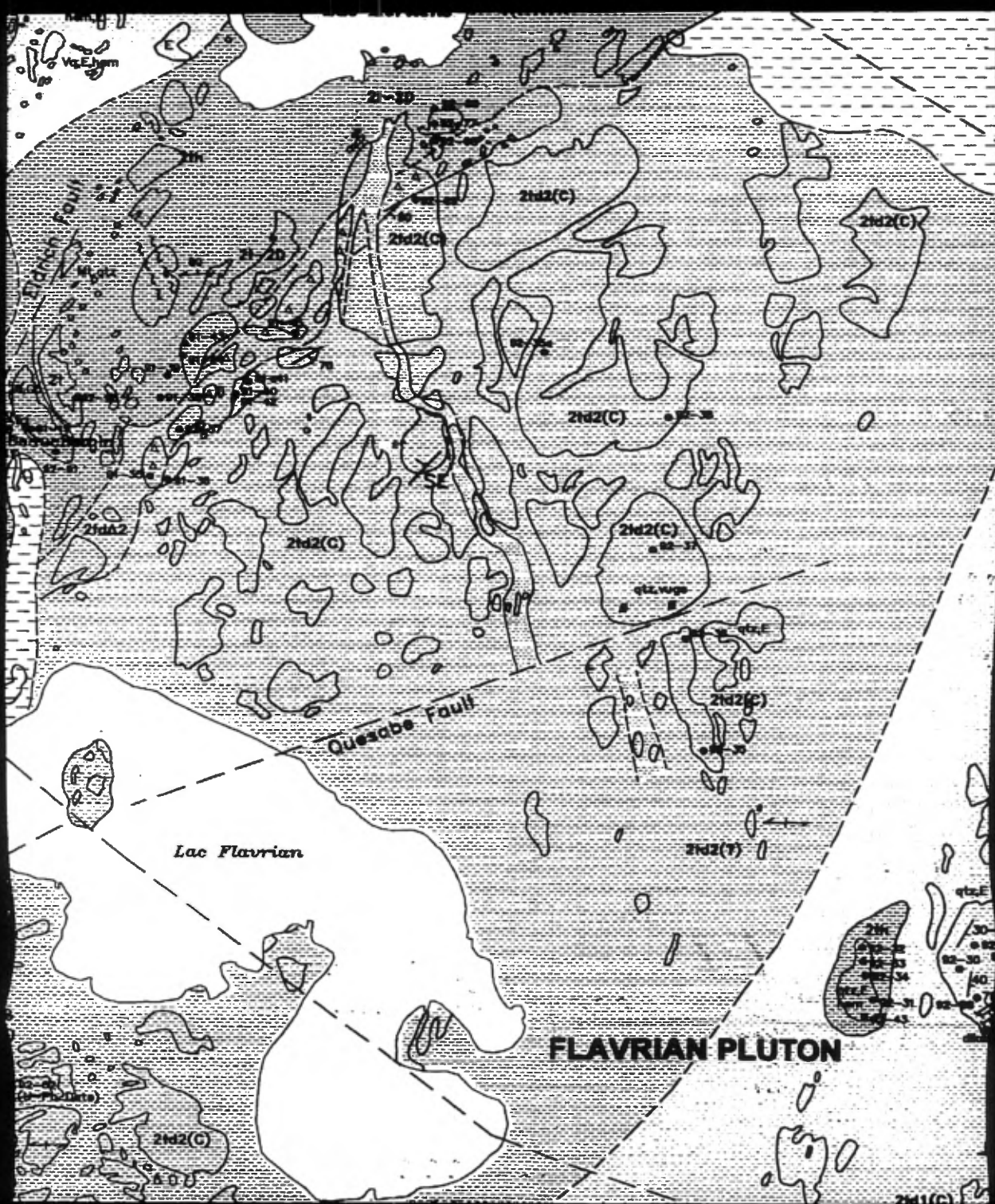
Old Water

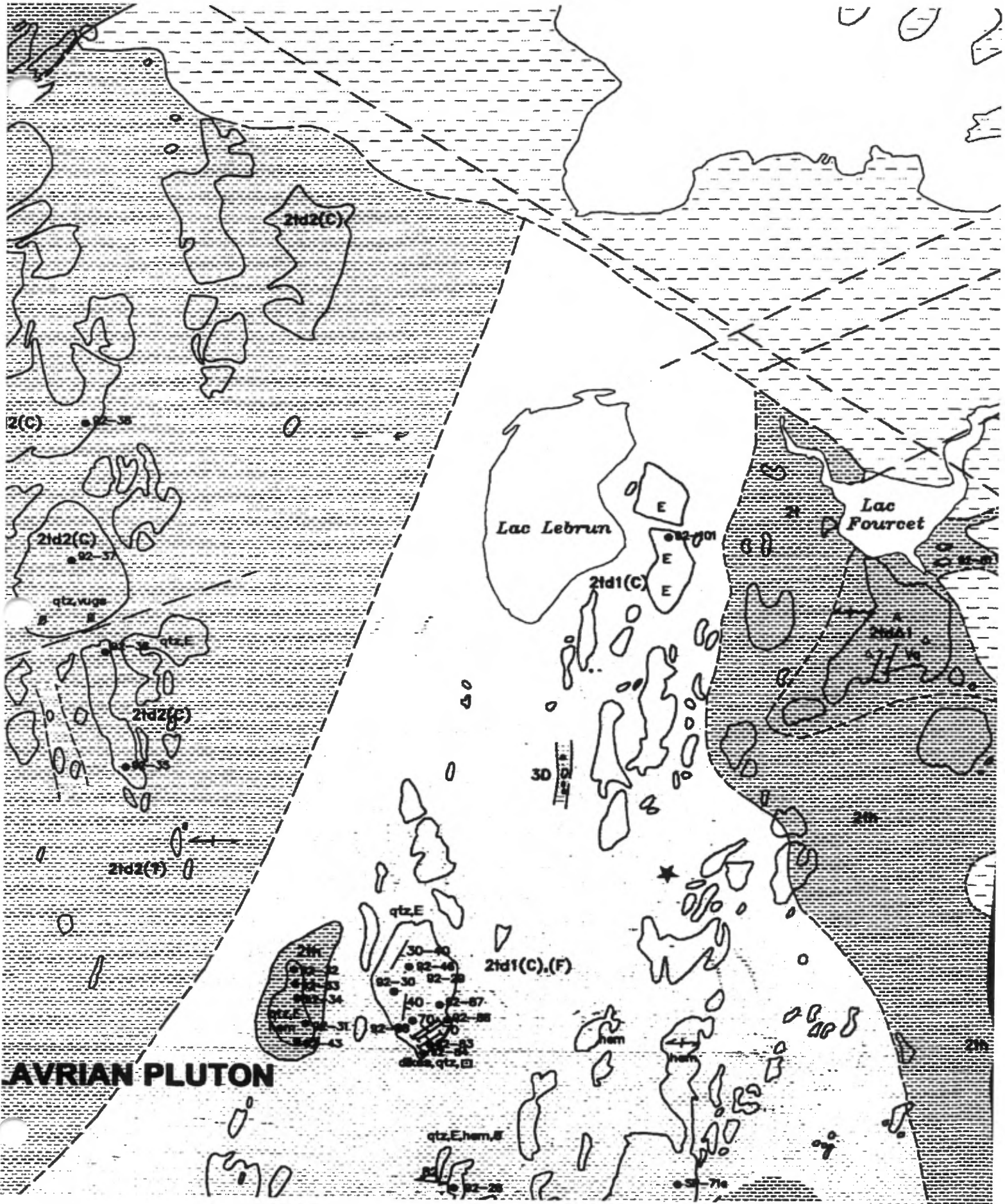
LAC DUFALT PLUTON



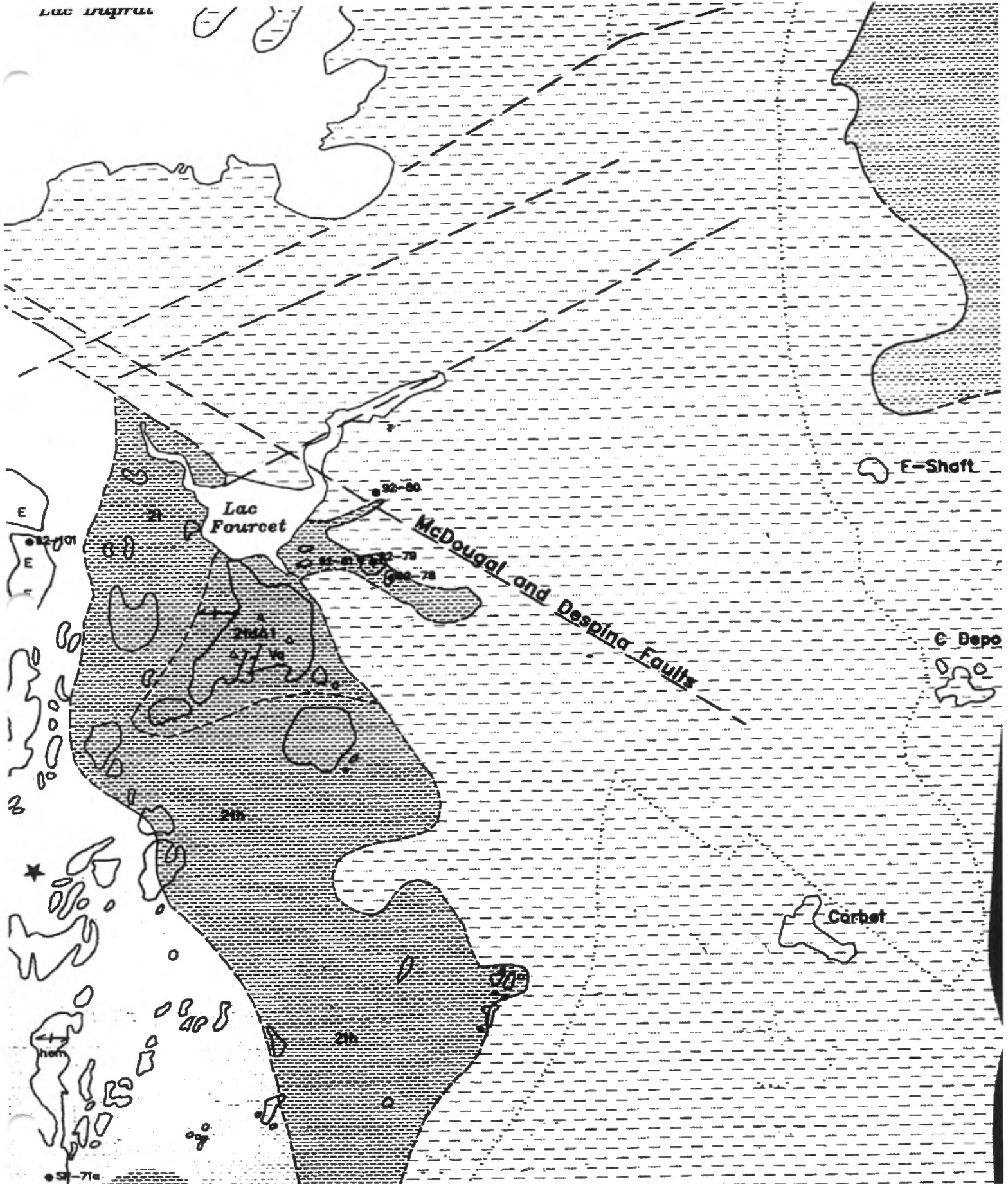
LAC DUFAULT PLUTON







Lac Fourcet



E-Shaft

McDougal and Despinas Faults

C Depo

Corbet

32-71a

LAC DUFAULT

E-Shaft

C Deposits

Bluff

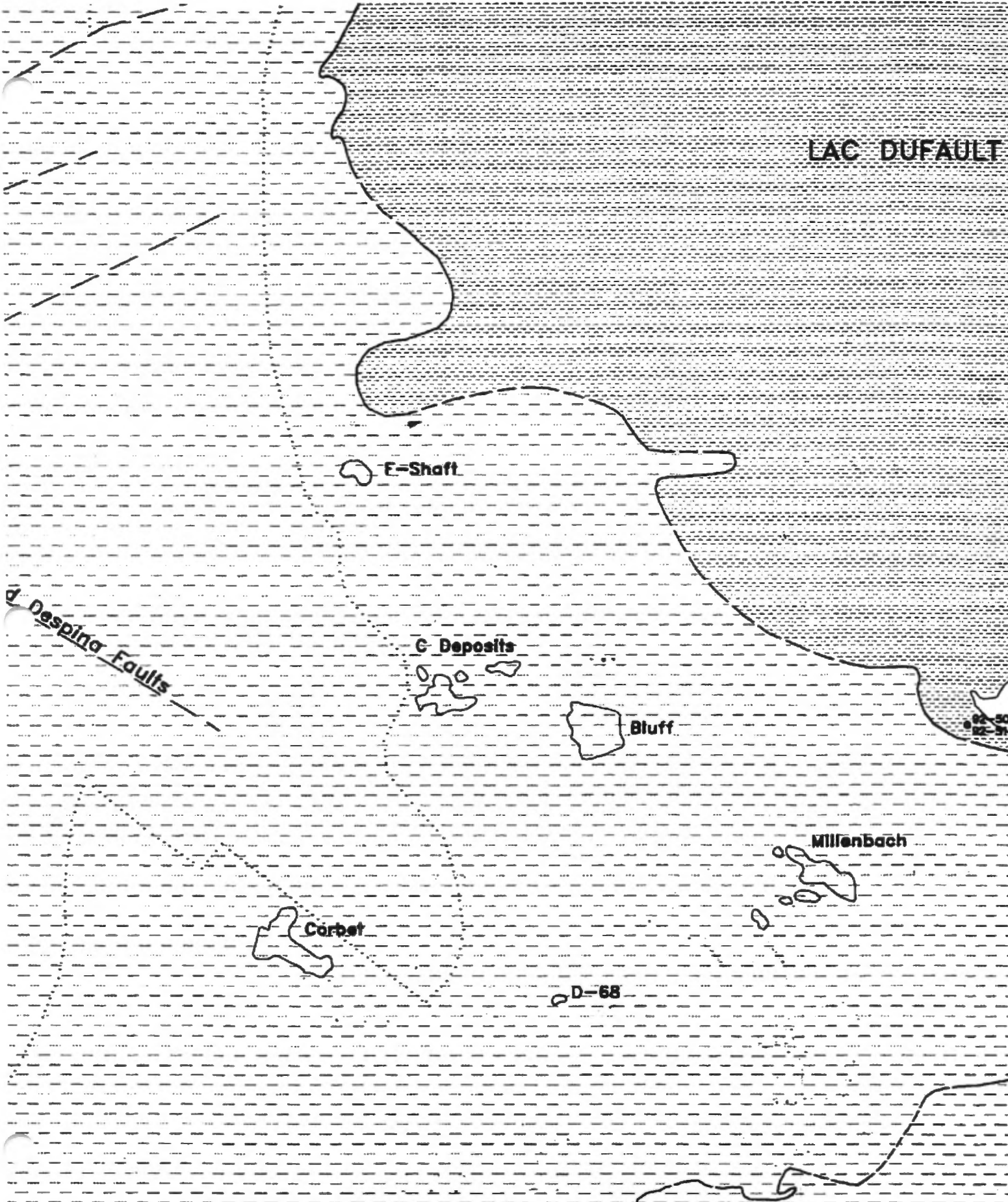
Millenbach

Corbet

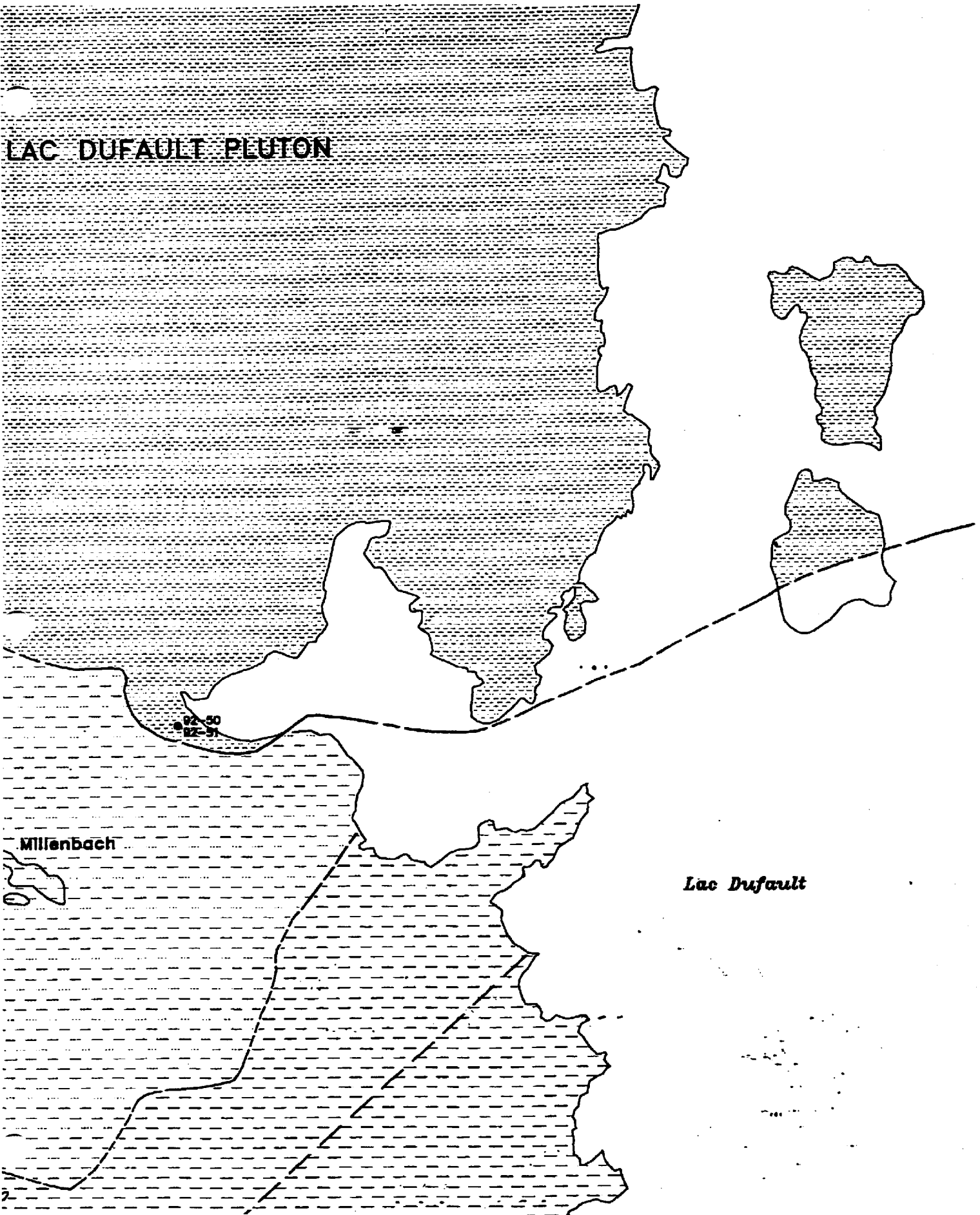
D-68

Despina Faults

92-50
92-51



LAC DUFAULT PLUTON



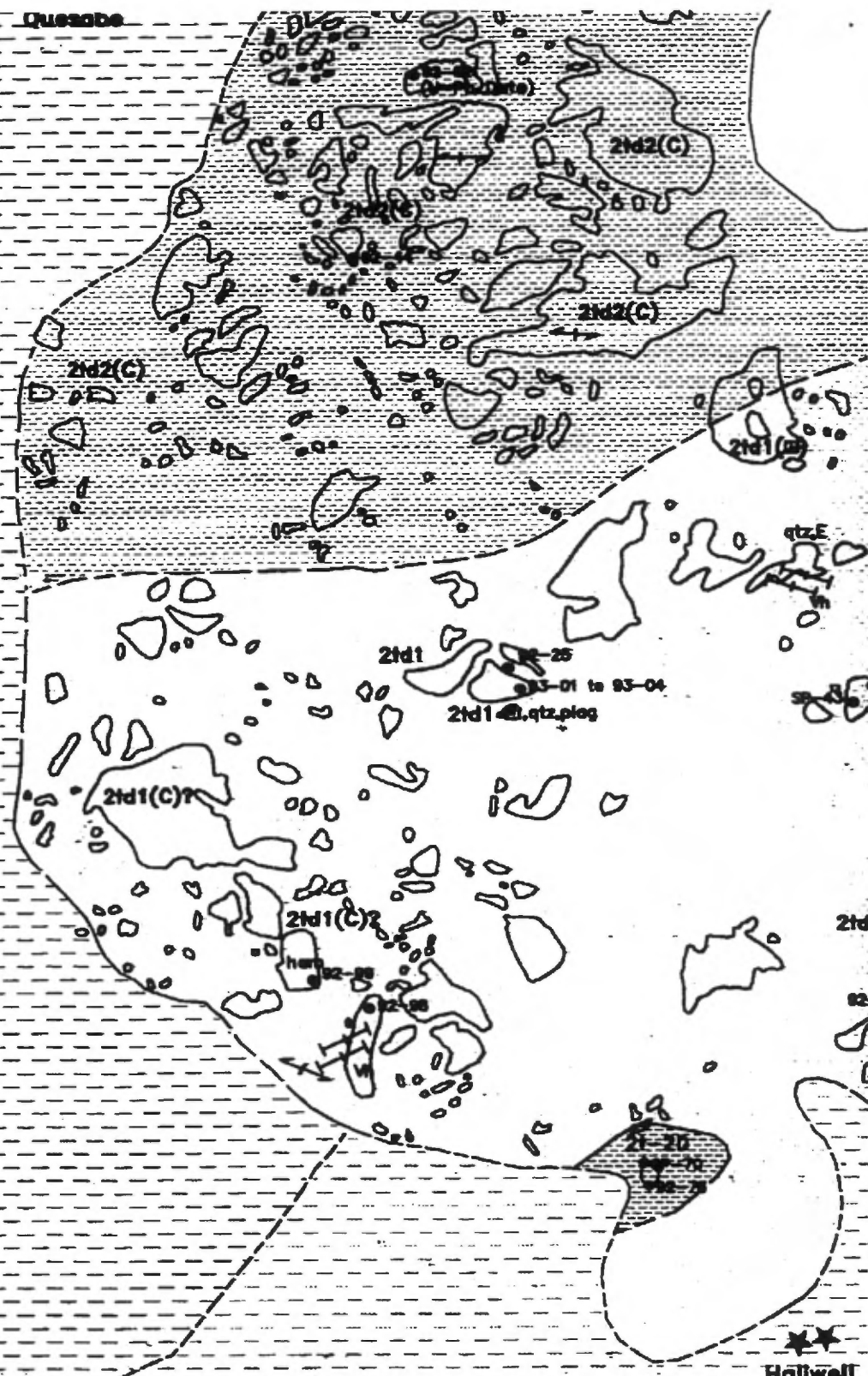
Millenbach

Lac Dufault

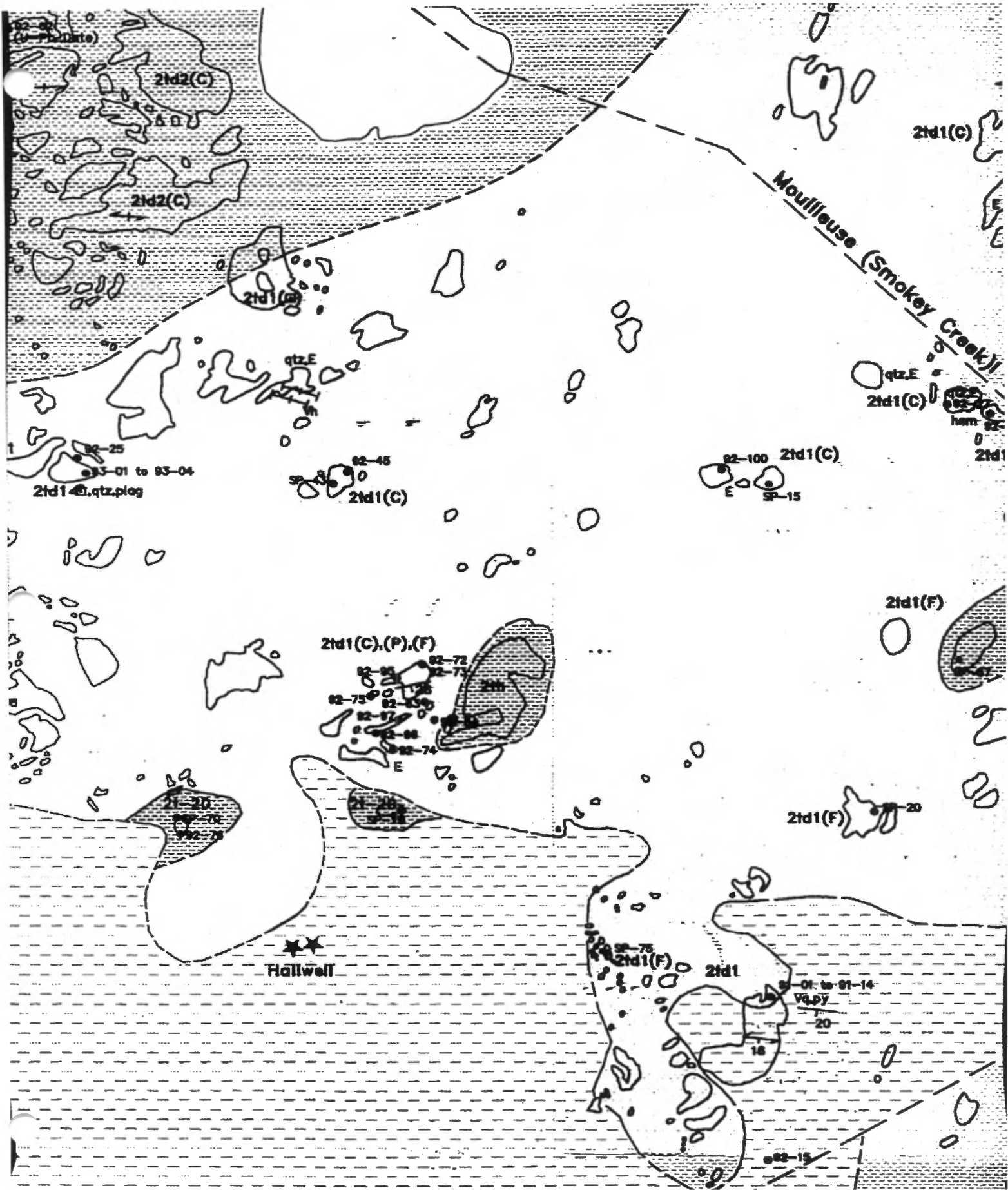
82-56
87-97

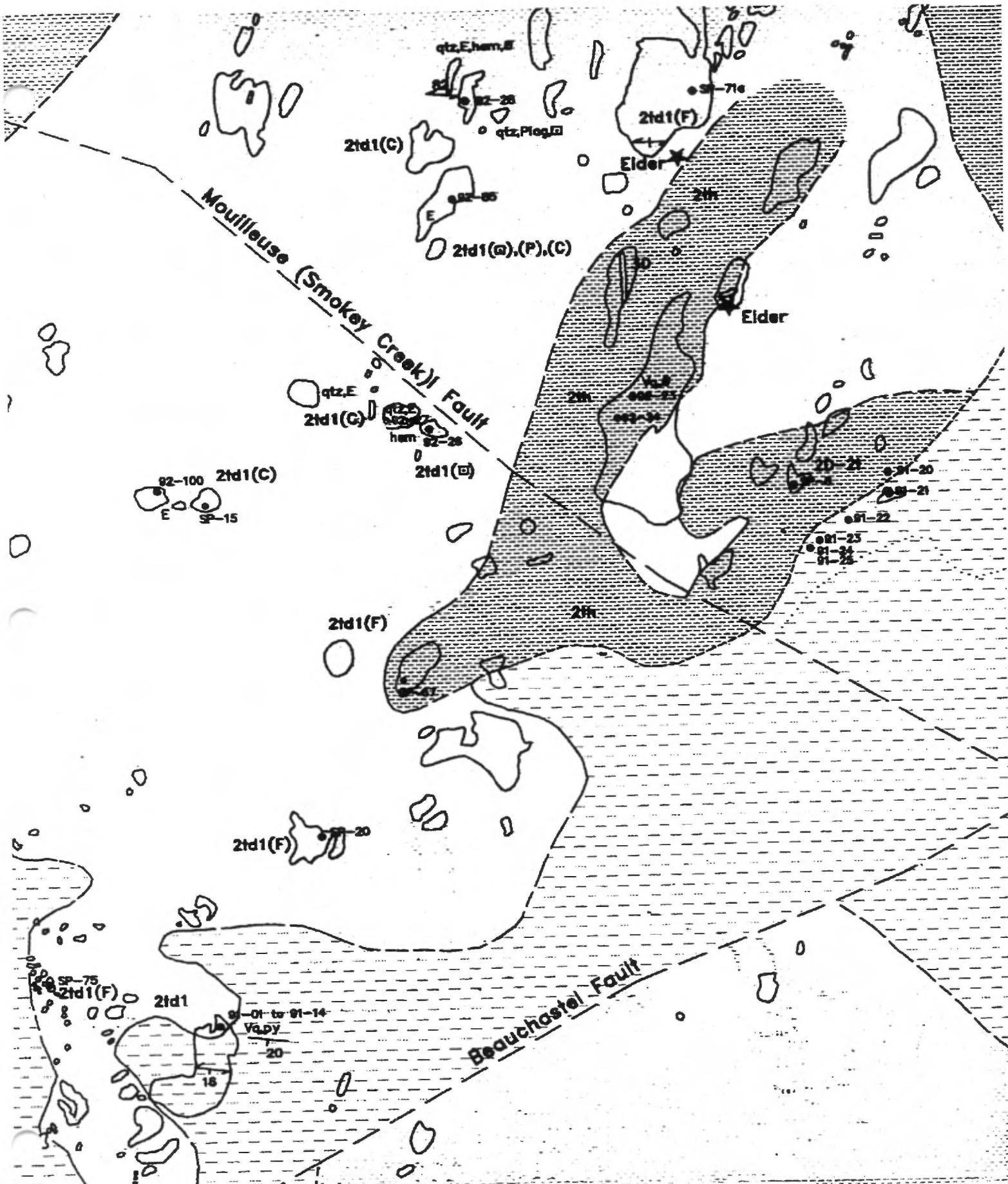
92-17
92-16

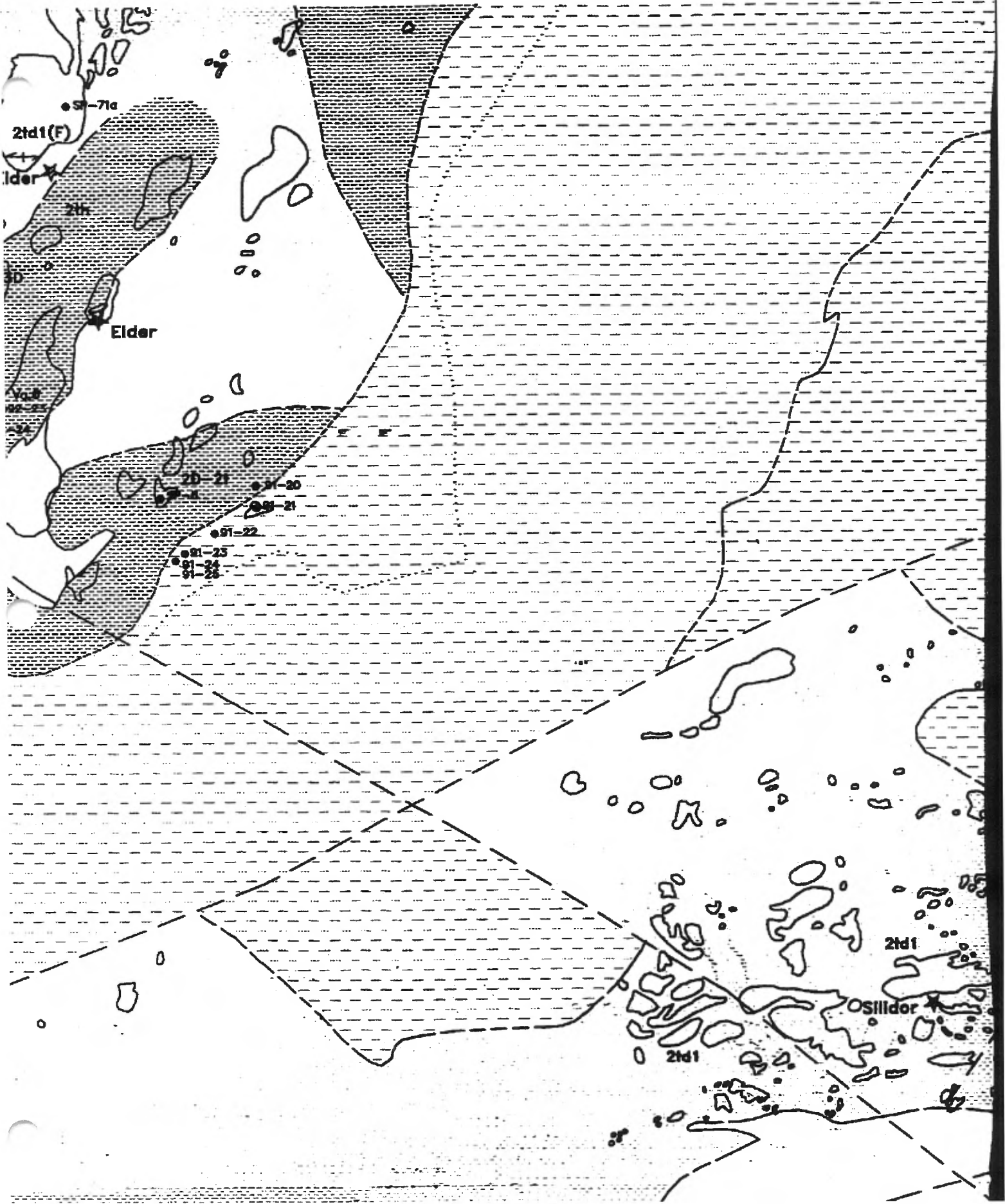
Queasbe

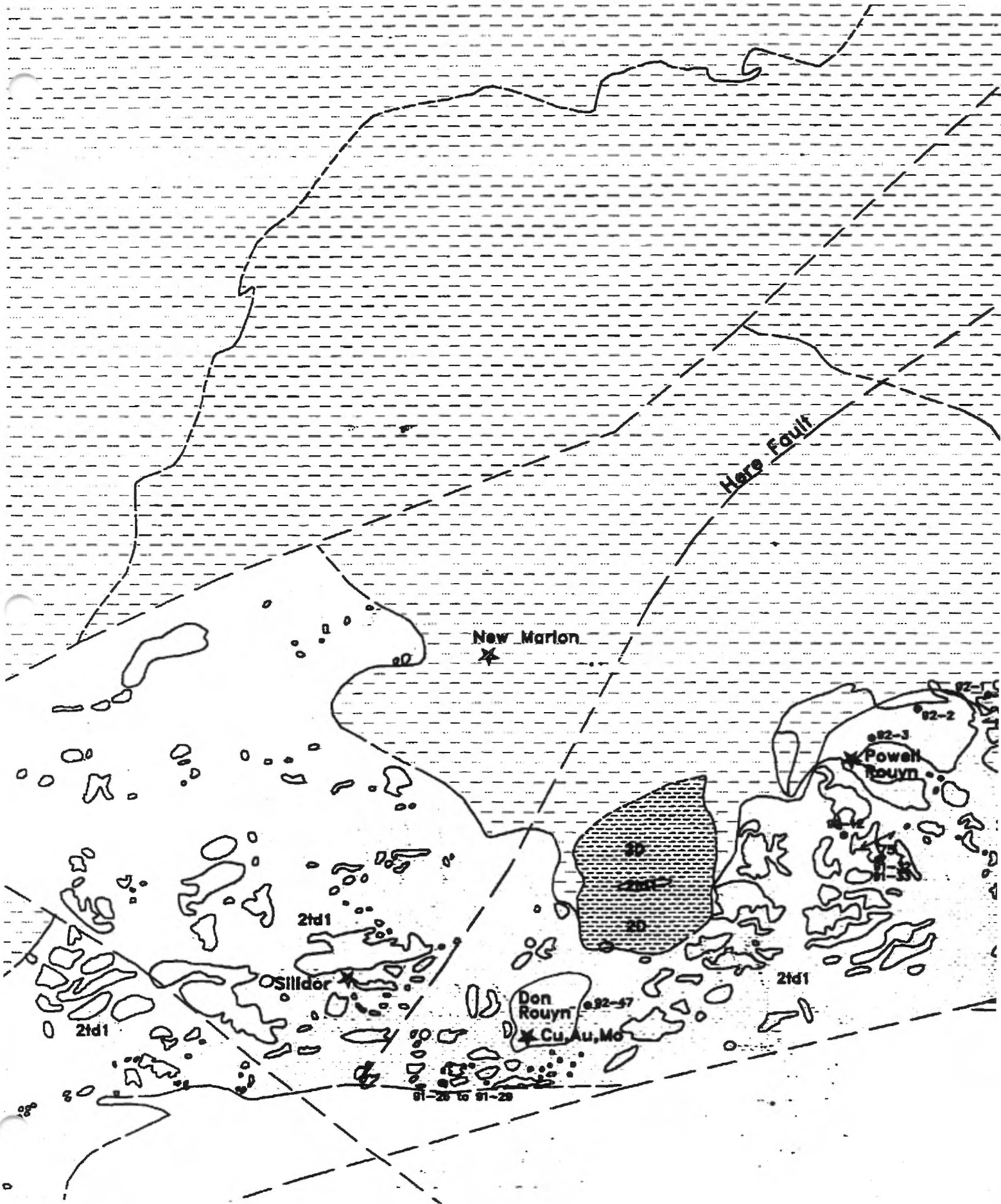


Hallwell









Here Fault

New Marlon

Powell Rouyn

Don Rouyn
Cu, Au, Mo

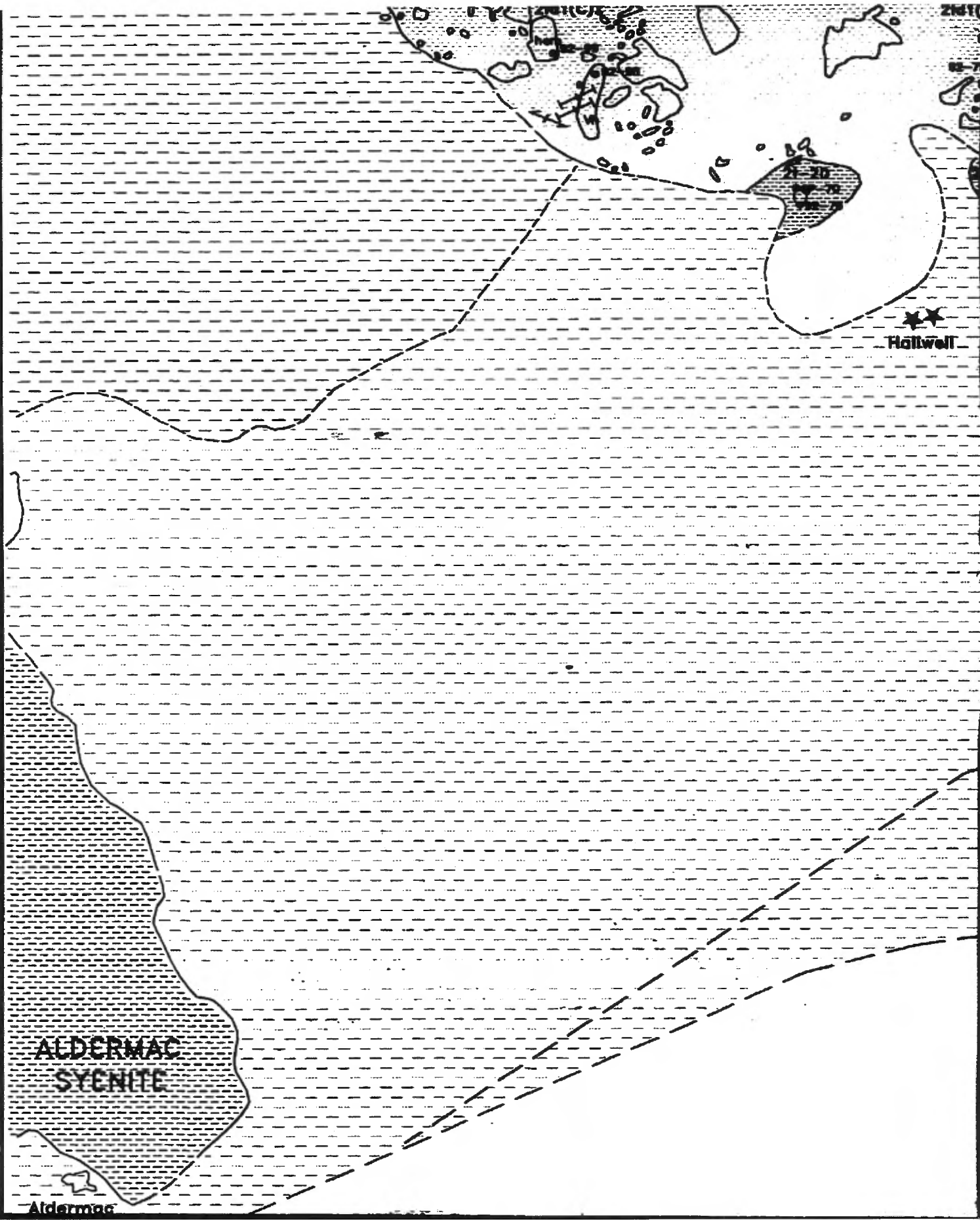
21d1

21d1

21d1

91-28 to 91-29

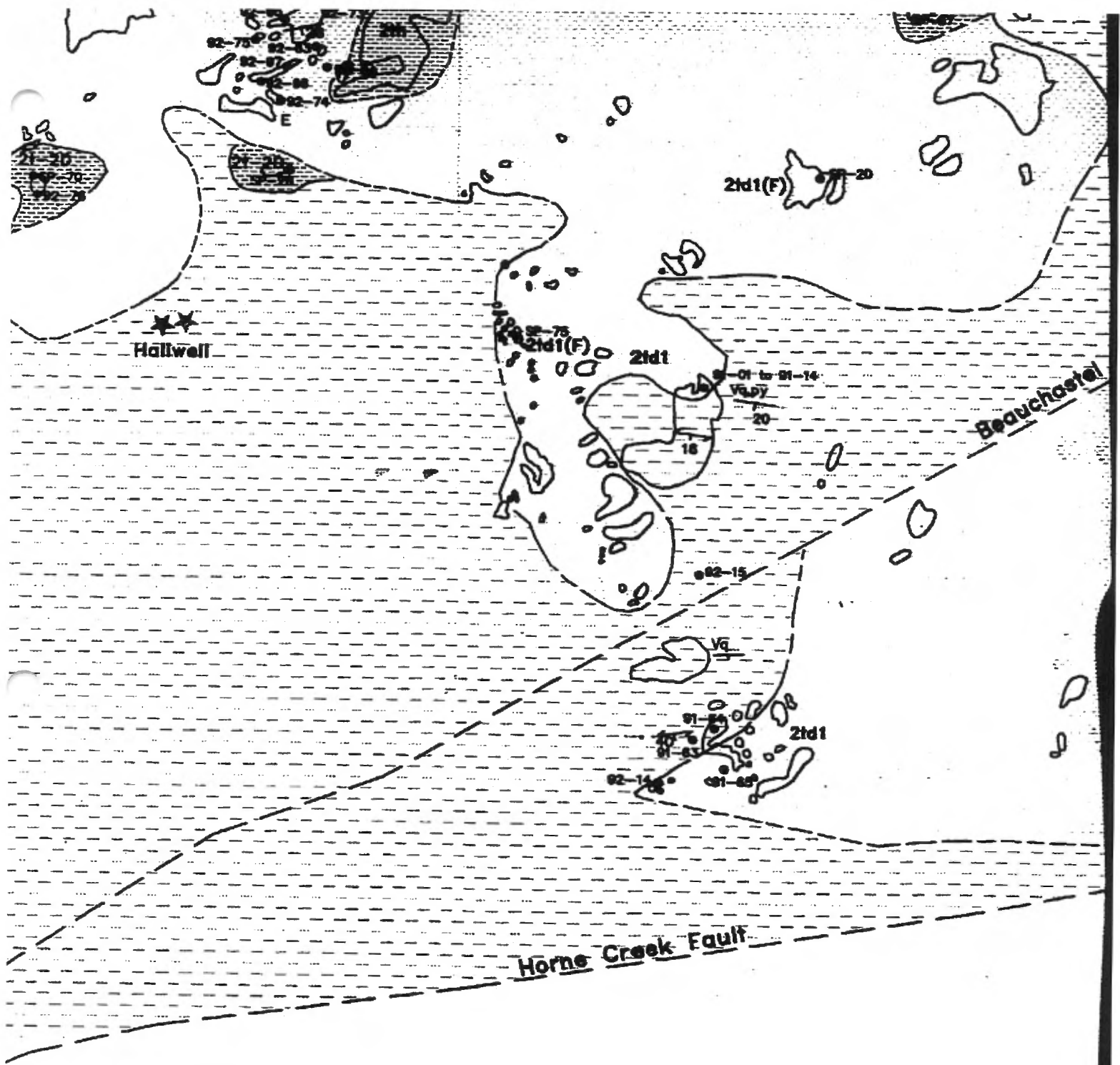


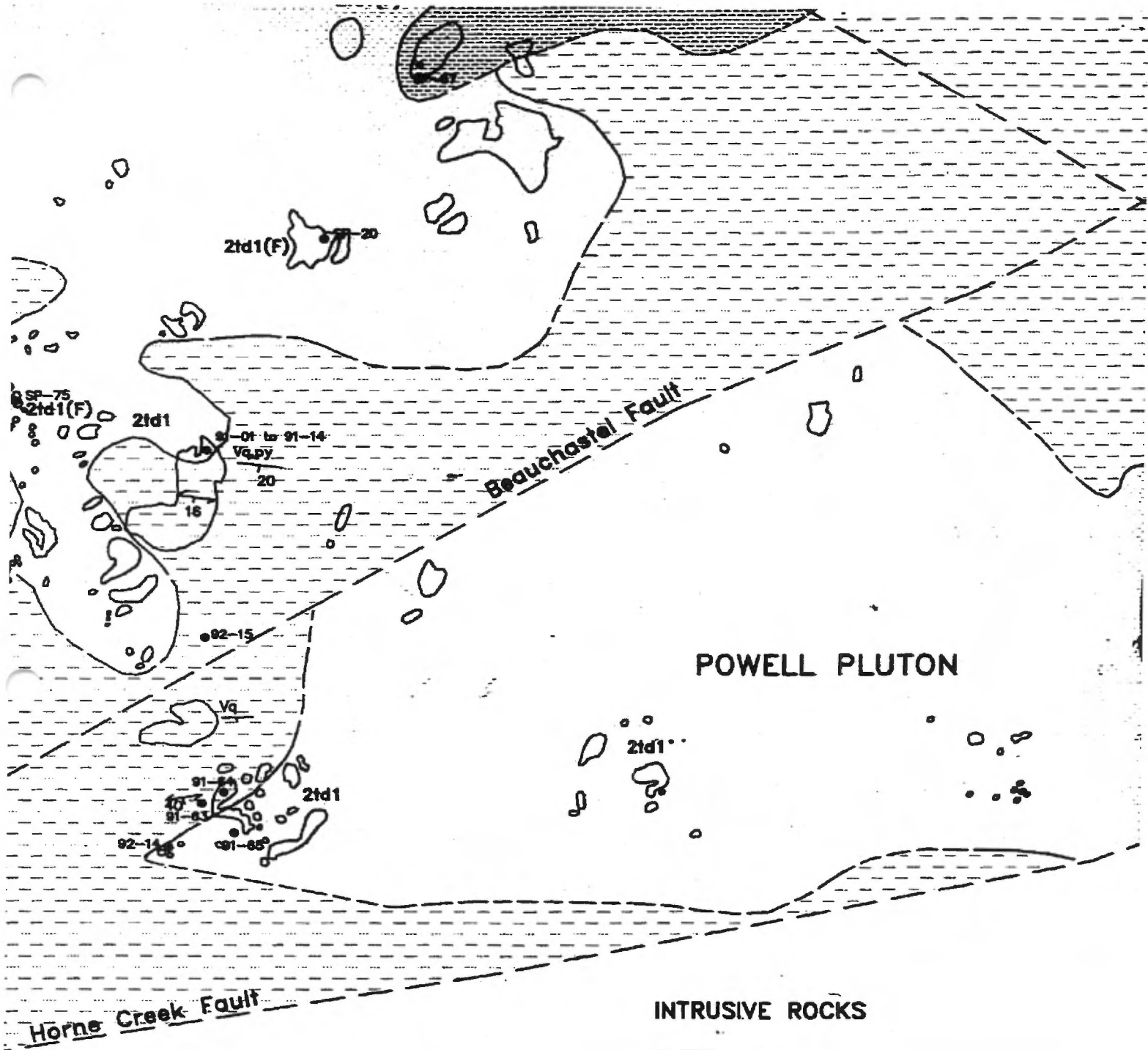


Hallwell

ALDERMAC
SYENITE

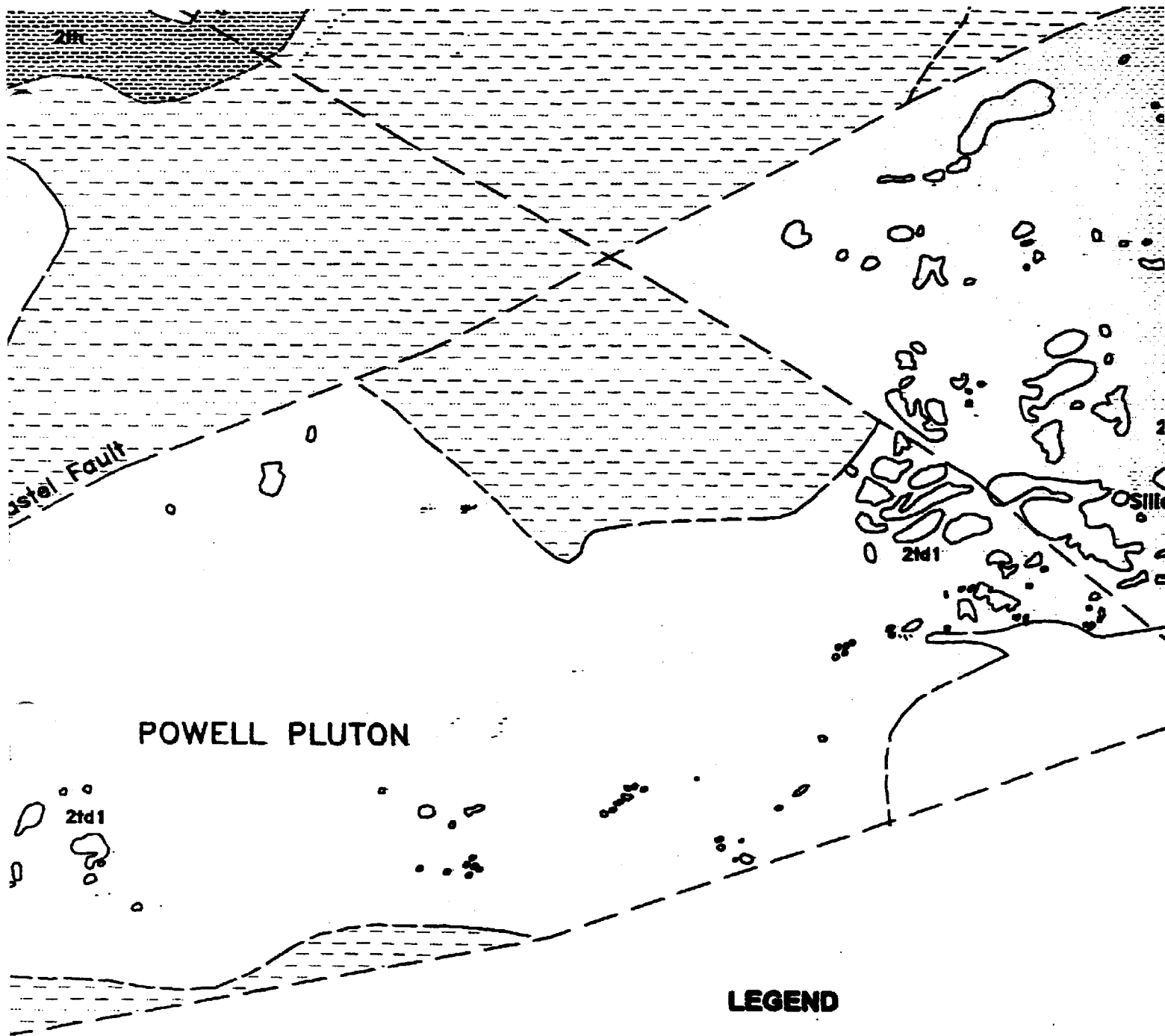
Aldermac





INTRUSIVE ROCKS

- 3D Diabase
- 2tdA2 Late trondhjemite matrix breccia
- 2td2 Late trondhjemite
- 2D Diorite
- 2tdA1 Early trondhjemite matrix breccia



POWELL PLUTON

LEGEND

INTRUSIVE ROCKS

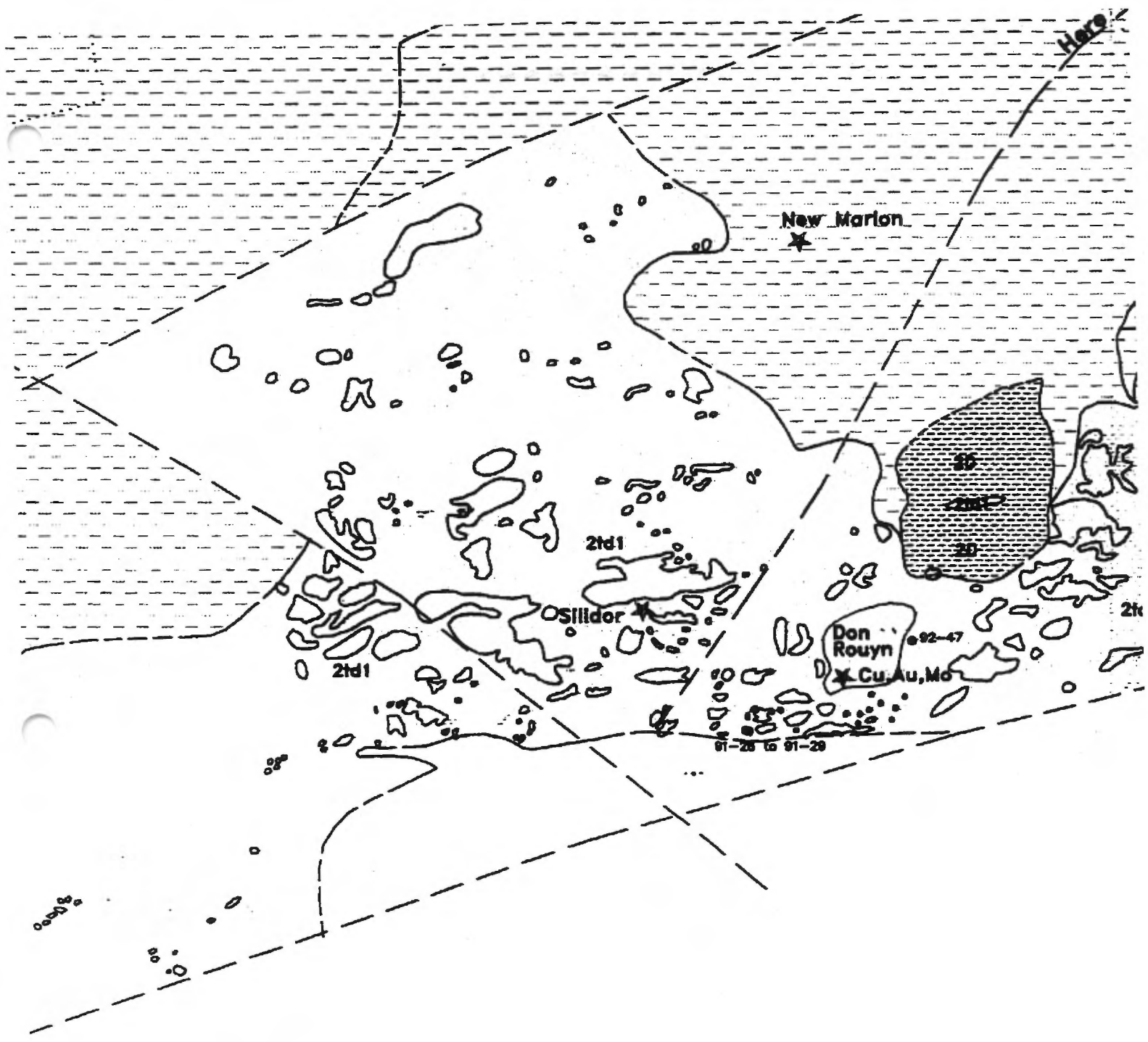
- 3D Diabase
- 2Hd2 Late trondhjemite matrix breccia
- 2Hd1 Late trondhjemite
- 2D Diorite
- 2Hd1 Early trondhjemite matrix breccia

TEXTURES

- (F) Fine
- (C) Coarse
- (P) Pink
- (@) Porphyritic
- Δ Breccia

STRUCTURES

--- Contact (Pluton and Host)



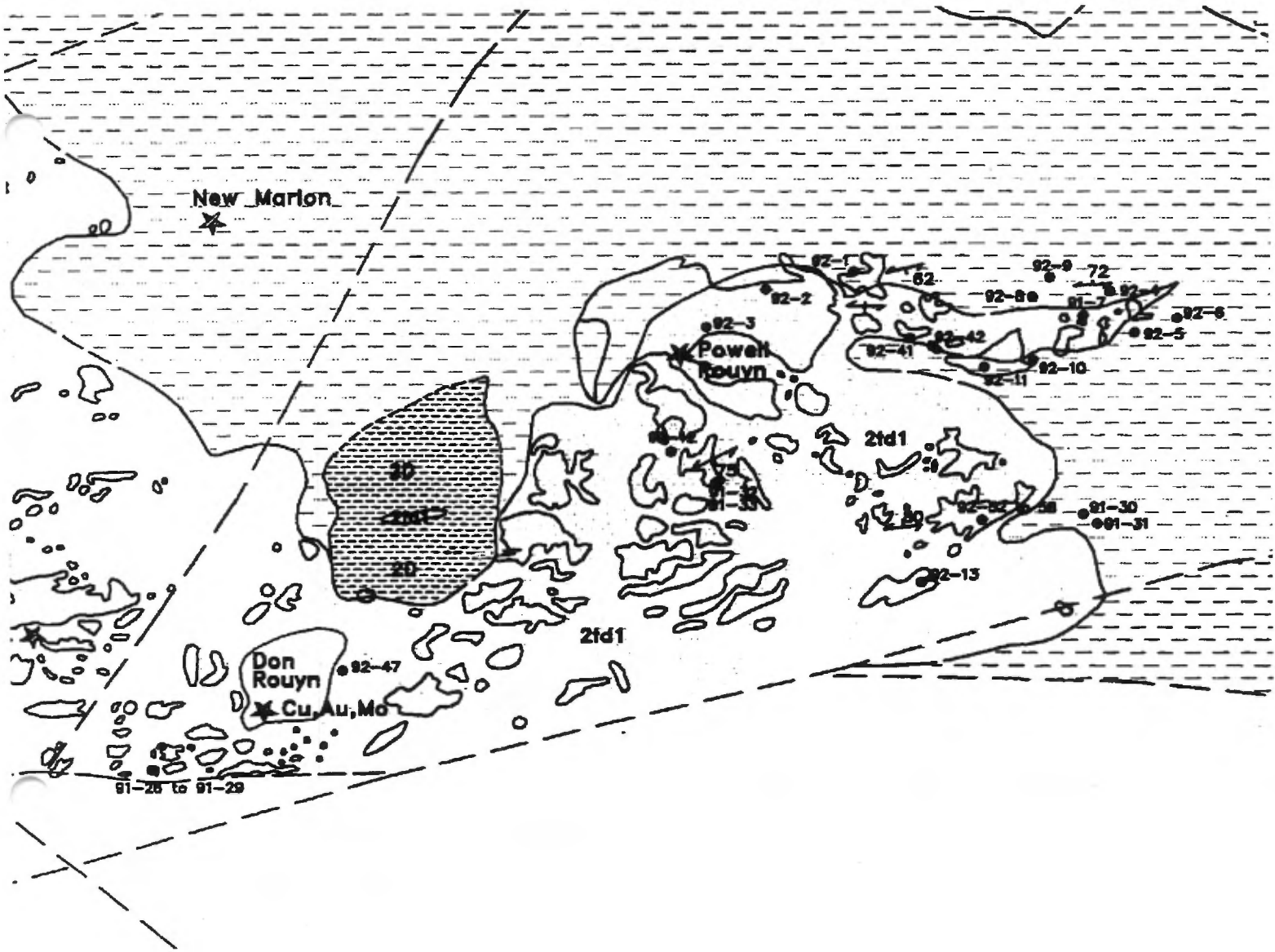
LEGEND

TEXTURES

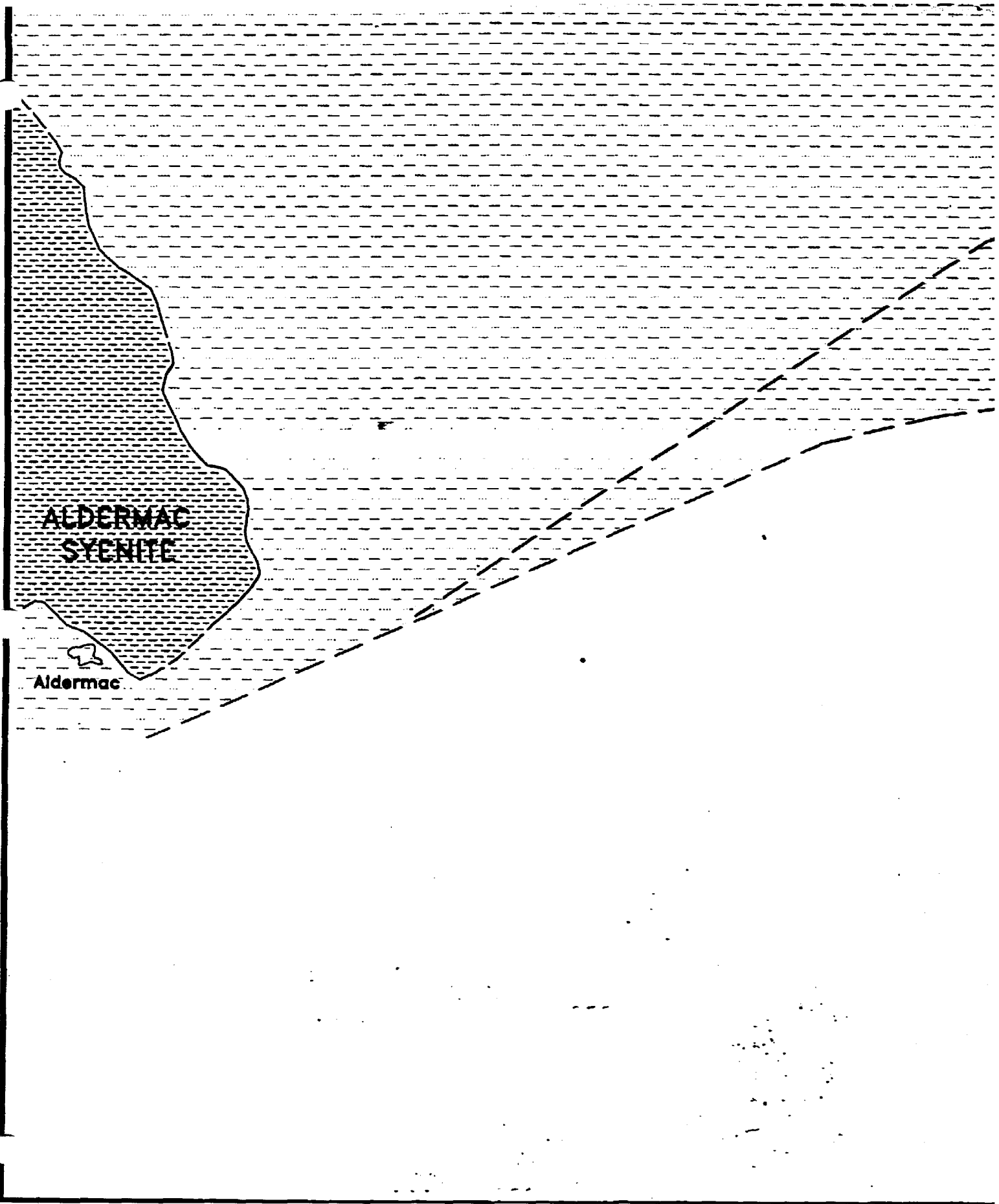
- (F) Fine
- (C) Coarse
- (P) Pink
- (□) Porphyritic
- △ Breccia

MINERALS

- hem Hematite
- Cb Carbonate
- ☞ Chlorite

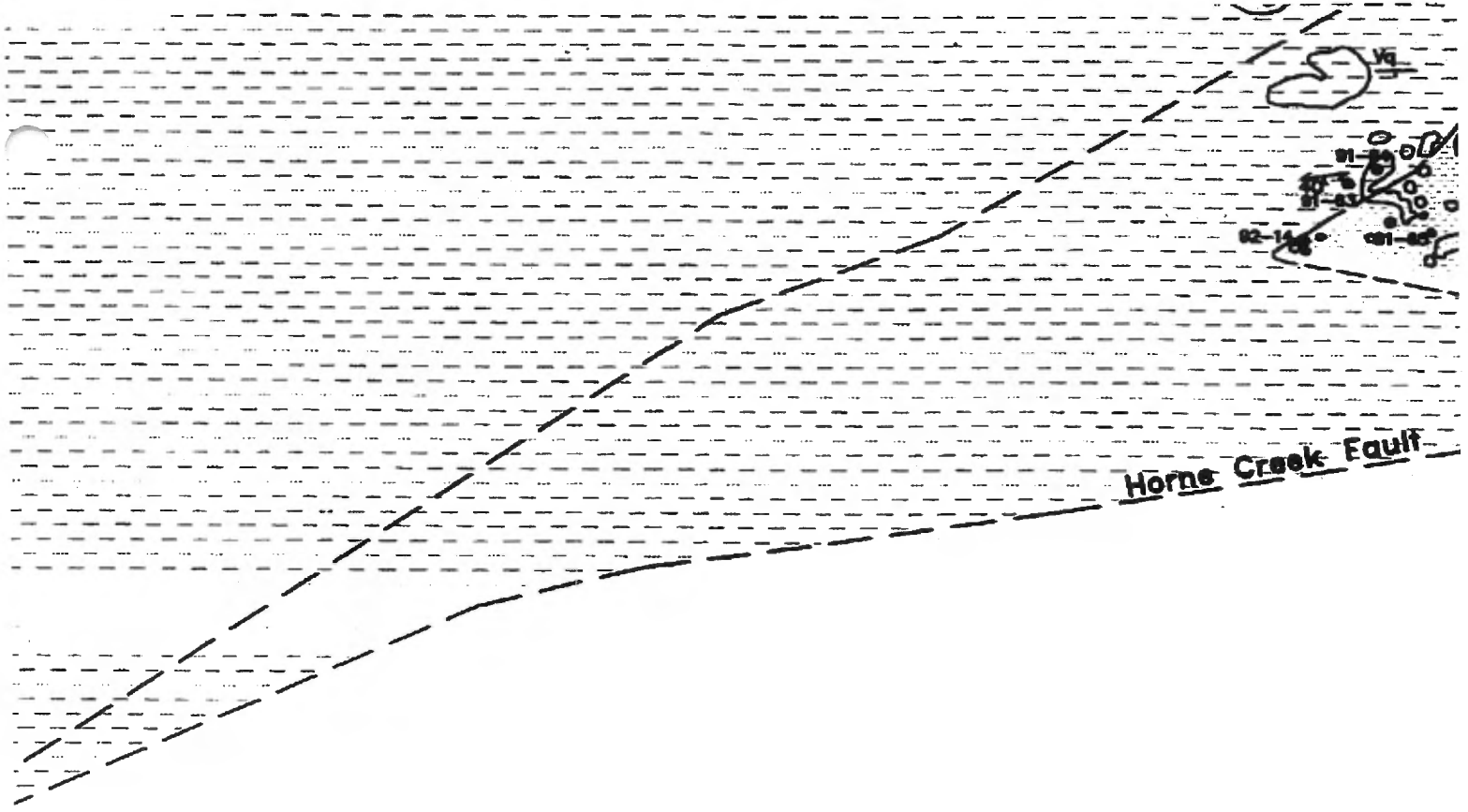






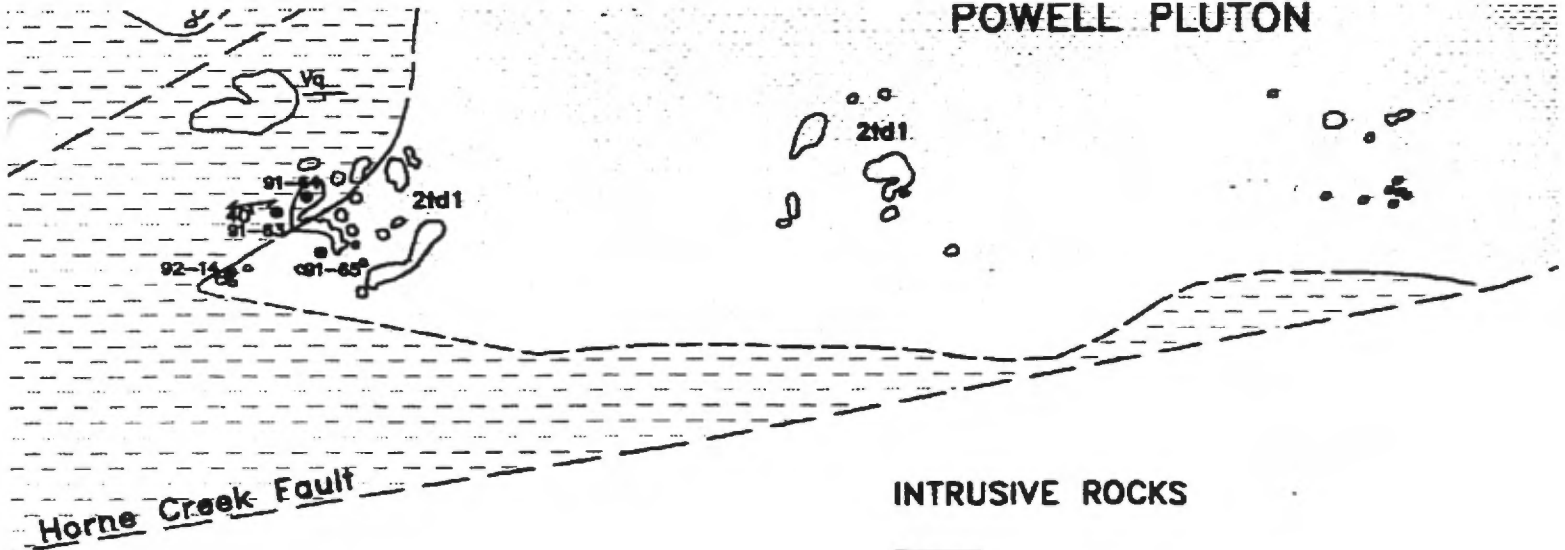
**ALDERMAC
SYENITE**


Aldermac






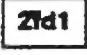





Horne Creek Fault




POWELL PLUTON



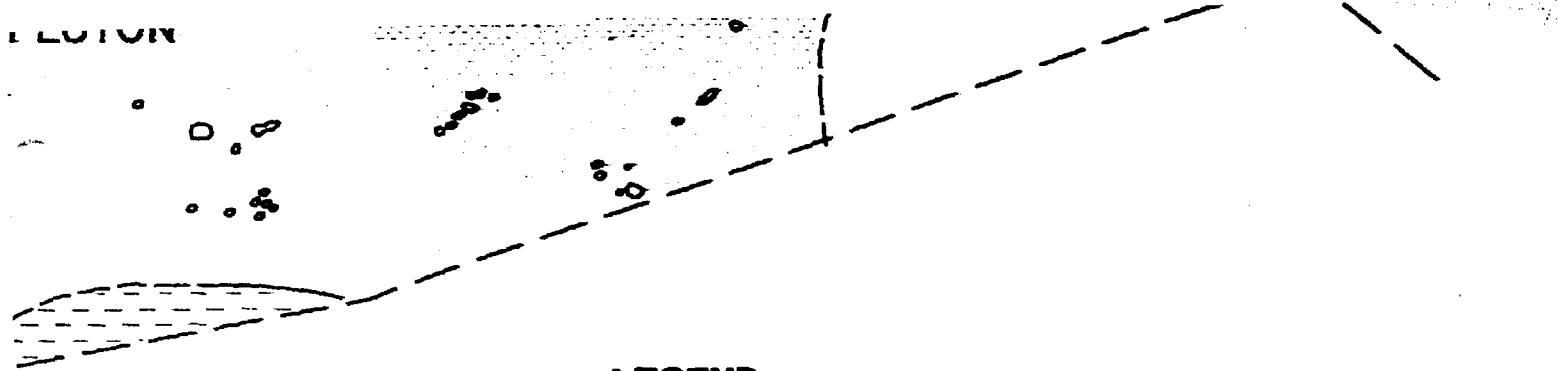
INTRUSIVE ROCKS

-  **3D** Diabase
-  **2td2** Late trondhjemite matrix breccia
-  **2td1** Late trondhjemite
-  **2td3** Diorite
-  **2td4** Early trondhjemite matrix breccia
-  **2td5** Early trondhjemite
-  **2td6** Hybrid rocks
-  **2td7** Tonalite
-  Meritens quartz-diorite + tonalite

VOLCANIC ROCKS

-  Post cauldron sequence (cycle 4)
-  Cauldron sequence (Mine sequence - including Sub-cycles 1 and 2)
-  Pre cauldron sequence (cycles 1 and 2)

ELEVATION



LEGEND

CS

hemite matrix breccia

hemite

hemite matrix breccia

hemite

CS

quartz-diorite + tonalite

on sequence (cycle 4)

quence (Mine sequence - cycle 3)
cycles 1 and 2

n sequence (cycles 1 and 2)

TEXTURES

- (F) Fine
- (C) Coarse
- (P) Pink
- (a) Porphyritic
- △ Breccia

STRUCTURES

- Contact (Strike and Dip)
- Spaced cleavage
- Strike and Dip of vein
- Shear
- Fault

91-94 Sample Location

MINERALS

- Hematite
- Carbonate
- Chlorite
- Hematite veinlet
- Pyrite
- Magnetite
- Quartz
- Quartz vein
- Epidote
- Sericite
- Actinolite
- Plagioclase
- Cu : Copper
- Mo : Molybdenite
- Au : Gold

MINERALS

hem	Hematite
Cb	Carbonate
Ch	Chlorite
Vh	Hematite veinlet
Py	Pyrite
Mt	Magnetite
Qtz	Quartz
Vq	Quartz vein
E	Epidote
Ser	Sericite
Act	Actinolite
Plag	Plagioclase

★ Cu : Copper

Mo : Molybdenite

★ Au : Gold

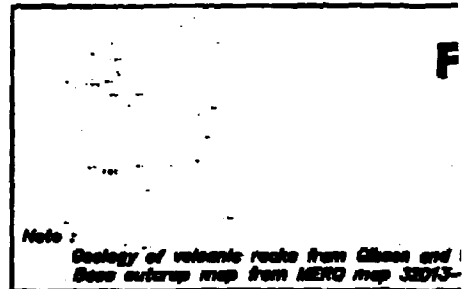
and Dip)

of vein

1 km

0

1 : 20





FLAVRIAN PLUTON GEOLOGY

Scale 1 : 20000

Mike Richard (1994)

Note :

Geology of volcanic rocks from Gibben and Widdowson (1980) and Gibben et al. (1993)
Base outcrop map from MERG map 32D13-0404

APPENDIX II. Work Completed on Samples.

Sample number	Location	Description	Thin section	Major element	Trace element	REE
•91-01	•Flavrian south	•quartz veins	X			
•91-02	•Flavrian south	•tonalite				
•91-03	•Flavrian south	•tonalite				
•91-04	•Flavrian south	•andesite				
•91-05	•Flavrian south	•quartz veins	X			
•91-06	•Flavrian south	•tonalite				
•91-07	•Flavrian south	•andesite				
•91-08	•Flavrian south	•diorite	X			
•91-09	•Flavrian south	•tonalite	X			
•91-10	•Flavrian south	•plagioclase porphyritic andesite	X			
•91-11	•Flavrian south	•felsic dike	X			
•91-12	•Flavrian south	•contact between felsic dike and andesite	X			
•91-13	•Flavrian south	•dike	X			
•91-14	•Flavrian south	•felsic dike	X			
•91-15	•Pierre Beauchemin mine	•mafic volcanic rocks				
•91-16	•Pierre Beauchemin mine	•contact between andesite and tonalite				
•91-17	•Pierre Beauchemin mine	•chlorite veins in tonalite				
•91-18	•Pierre Beauchemin mine	•quartz vein				
•91-19	•near Pierre Beauchemin mine	•vein or dike in diorite	X			
•91-20	•Flavrian southeast near Elder	•felsic dike				
•91-21	•Flavrian southeast near Elder	•andesite				
•91-22	•Flavrian southeast near Elder	•rhyolite				
•91-23	•Flavrian southeast near Elder	•rhyolite				
•91-24	•Flavrian southeast near Elder	•rhyolite	X			
•91-25	•Flavrian southeast near Elder	•rhyolite or tonalite				
•91-26	•near Silidor	•chlorite tonalite	X			
•91-27	•near Silidor	•trondjemite	X			
•91-28	•near Silidor	•felsic dike	X			
•91-29	•near Silidor	•felsic dike	X			
•91-30	•Powell southeast	•rhyolite	X			
•91-31	•Powell southeast	•mafic dike				
•91-32	•Powell south	•felsic dike of type 1	X			
•91-33	•Powell south	•dike type 2 mafic?				
•91-34	•near Pierre Beauchemin	•quartz-chlorite vein + actinolite?				

Sample number	Location	Description	Thin section	Major element	Trace element	REE
•91-35	•Flavrian northwest near Pierre Beauchemin	•late trondhjemite matrix breccia				
•91-36	•Flavrian northwest near Pierre Beauchemin	•aplite dike	X			
•91-37	•Flavrian northwest near Pierre Beauchemin	•aplite dike				
•91-38	•Flavrian northwest near Pierre Beauchemin	•aplite dike				
•91-39	•Flavrian northwest near Pierre Beauchemin	•diabase				
•91-40	•Flavrian northwest near Pierre Beauchemin	•aplite dike				
•91-41	•Flavrian northwest near Pierre Beauchemin	•aplite dike				
•91-42	•Flavrian northwest near Pierre Beauchemin	•late trondhjemite				
•91-43	•Flavrian northwest near Pierre Beauchemin	•aplite dike				
•91-44	•Flavrian northwest near Pierre Beauchemin	•aplite dike				
•91-45	•Flavrian northwest near Pierre Beauchemin	•aplite dike	X			
•91-46	•Pierre Beauchemin mine	•fault breccia				
•91-47	•Pierre Beauchemin mine	•contact between tonalite and early trondhjemite dike				
•91-48	•Pierre Beauchemin mine	•early trondhjemite dike				
•91-49	•Pierre Beauchemin mine	•contact between quartz vein and lamprophyre				
•91-50	•Pierre Beauchemin mine	•tonalite				
•91-51	•Pierre Beauchemin mine	•lamprophyre				
•91-52	•Pierre Beauchemin mine	•tonalite				
•91-53	•Pierre Beauchemin mine	•aplite dike				
•91-54	•Pierre Beauchemin mine	•early trondhjemite dike				

Sample number	Location	Description	Thin section	Major element	Trace element	REE
•91-55	•Pierre Beauchemin mine	•contact between tonalite and early trondhjemite dike				
•91-56	•Pierre Beauchemin mine	•tonalite				
•91-57	•Flavrian northeast	•mafic volcanic rocks				
•91-58	•Flavrian northeast	•early trondhjemite matrix breccia with mafic and felsic dikes??				
•91-59	•Flavrian northeast	•late vein in andesite	X			
•91-60	•Flavrian northeast	•mafic volcanic rocks				
•91-61	•Flavrian northeast	•aplite dike				
•91-62	•Flavrian northeast	•chlorite dike	X			
•91-63	•Powell west	•mafic tonalite	X			
•91-64	•Powell west	•mafic volcanic rocks	X			
•91-65	•Powell west	•mafic tonalite	X			
•92-01	•Powell east	•rhyolitic dike	X			
•92-02	•north of Powell-Rouyn mine	•sheared and altered tonalite	X			
•92-03	•Powell-Rouyn	•felsic dike				
•92-04	•Powell-Rouyn mine east	•rhyolitic dike	X			
•92-05	•near Powell-Rouyn mine east	•rhyolitic volcanic rocks	X			
•92-06	•near Powell-Rouyn mine east	•felsic pyroclastic	X			
•92-07	•Powell	•Powell quartz-diorite	X			
•92-08	•Powell	•sheared mafic dike within Quemont rhyolite				
•92-09	•Powell area	•diorite dike in Quemont rhyolite	X			
•92-10	•Powell, Quemont area	•sheared rhyolite	X			
•92-11	•Powell, Quemont area	•schistose mafic dike				
•92-12	•Powell pluton	•flow banded dike	X			
•92-13	•Powell pluton	•diabase?	X			
•92-14	•Powell southwest	•altered tonalite	X			
•92-15	•Powell west	•volcanic rocks near Beauchastel fault	X			
•92-16	•Flavrian west, Quesabe fault	•volcanic or tectonic breccia?	X			
•92-17	•Flavrian west, Quesabe fault	•volcanic or tectonic breccia?	X			
•92-18	•Flavrian east	•homogeneous tonalite	X			
•92-19	•Flavrian east	•quartz-epidote cavity				
•92-20	•Flavrian east contact	•volcanic rocks				
•92-21	•Flavrian east contact	•volcanic rocks				
•92-22	•Dalembert shear		X			
•92-23	•Flavrian southeast, Elder area	•heterogeneous tonalite				
•92-24	•Flavrian southeast, Elder area	•banded texture in hybrid rocks	X			

Sample number	Location	Description	Thin section	Major element	Trace element	REE
•92-25	•Flavrian southwest	•porphyritic trondhjemite	X			
•92-26	•Flavrian south	•quartz-gabbro inclusion within early trondhjemite	X			
•92-27	•Flavrian south	•early trondhjemite	X			
•92-28	•Flavrian central	•early trondhjemite	X			
•92-29	•Flavrian central	•microgranitic early trondhjemite	X			
•92-30	•Flavrian central	•coarse early trondhjemite	X			
•92-31	•Flavrian central	•coarse rhyolite?	X			
•92-32	•Flavrian central	•early trondhjemite (fabric)	X			
•92-33	•Flavrian central	•early trondhjemite (fabric)	X			
•92-34	•Flavrian central	•early trondhjemite	X			
•92-35	•Flavrian central	•late trondhjemite				
•92-35a	•Flavrian central	•late trondhjemite				
•92-36	•Flavrian central	•early trondhjemite in late trondhjemite	X			
•92-37	•Flavrian central	•early trondhjemite inclusion within late trondhjemite	X			
•92-38	•Flavrian central	•transitional (metamorphosed) rock at contact between early and late trondhjemite	X			
•92-39	•Flavrian northwest	•contact between coarse and fine early trondhjemite				
•92-40	•Flavrian northwest	•altered late trondhjemite	X			
•92-41	•Powell east	•altered tonalite?	X			
•92-42	•Powell east	•altered tonalite?	X			
•92-43	•Flavrian northwest, near Pierre Beauchemin	•chlorite or amphibole vein in tonalite	X			
•92-44	•Flavrian southwest	•late trondhjemite	X			
•92-45	•Flavrian south	•early trondhjemite	X			
•92-46	•Flavrian central	•early trondhjemite				
•92-47	•Don Rouyn	•molybdenite	X			
•92-48	•Flavrian northwest	•epidote patch	X			
•92-49	•Flavrian northwest	•epidote vein				
•92-50	•lac Dufault	•lac Dufault	X			
•92-51	•lac Dufault	•lac Dufault	X			
•92-52	•Powell east	•Brownlee north?	X			
•92-53	•Powell east	•altered tonalite	X			
•92-54	•Powell east	•rhyolitic matrix	X			
•92-55	•Powell east	•mafic inclusion	X			
•92-56	•Powell east	•rhyolite feeder dike?	X			
•92-57	•Powell east	•latest mafic dikes	X			
•92-58	•Powell east	•Brownlee south?	X			
•92-59	•Ansil, underground	•fault	X			
•92-60	•Ansil, underground	•felsic dike	X			
•92-61	•Ansil, underground	•felsic dike	X			
•92-62	•Flavrian central	•late trondhjemite	X (date)			

Sample number	Location	Description	Thin section	Major element	Trace element	REE
•92-63	•Flavrian south	•fine grained felsic trondhemite				
•92-64	•Flavrian south	•pegmatite in microgranite or granophyre				
•92-65	•Flavrian northeast	•magnetic early trondhemite	X	X	X	X
•92-66	•Flavrian northeast	•coarse early trondhemite	X	X	X	X
•92-67	•Flavrian northeast	•granophyre	X	X	X	X
•92-68	•Flavrian northwest	•Méritens	X	X	X	X
•92-69	•Flavrian northwest	•late trondhemite	X	X	X	X
•92-70	•Flavrian northeast	•spotted heterogeneous tonalite?	X	X	X	X
•92-71	•Flavrian northeast	•homogeneous tonalite	X	X	X	X
•92-72	•Flavrian south	•microgranite	X	X	X	X
•92-73	•Flavrian south	•hematitic early trondhemite	X	X	X	X
•92-74	•Flavrian south	•actinolite vein				
•92-75	•Flavrian south	•deformed early trondhemite				
•92-76	•Flavrian south	•coarse gabbro	X	X	X	X
•92-77	•Flavrian south	•homogeneous tonalite (Méritens?)	X	X	X	X
•92-78	•Flavrian east, lac Fourcet	•Méritens quartz-gabbro	X	X	X	X
•92-79	•Flavrian east, lac Fourcet	•rhyolite breccia				
•92-80	•Flavrian east, lac Fourcet	•quartz-plagioclase porphyry dike				
•92-81	•Flavrian east, lac Fourcet	•Méritens quartz-gabbro	X	X	X	X
•92-82	•Flavrian north	•tonalite with mafic inclusion	X	X	X	X
•92-83	•Flavrian south	•quartz-plagioclase porphyry inclusion in early trondhemite	X	X	X	X
•92-84	•Flavrian south	•contact between quartz-plagioclase porphyry inclusion and host				
•92-85	•Flavrian south	•coarse early trondhemite	X	X	X	X
•92-86	•Flavrian central	•hematitic, coarse and granophyric early trondhemite	X	X	X	X
•92-87	•Flavrian central	•coarse early trondhemite	X	X	X	X
•92-88	•Flavrian central	•quartz-plagioclase porphyry inclusion within coarse early trondhemite	X	X	X	X
•92-89	•Flavrian north, lac Méritens	•Méritens quartz-gabbro				
•92-90	•Pierre Beauchemin	•homogeneous tonalite	X	X	X	X
•92-91	•Pierre Beauchemin	•Eldrich diorite	X	X	X	X
•92-92	•Pierre Beauchemin	•epidote alteration				
•92-93	•Flavrian northwest	•microgranitic early trondhemite or granophyre	X	X	X	X

Sample number	Location	Description	Thin section	Major element	Trace element	REE
•92-94	•Flavrian northwest	•coarse early trondhjemite	X	X	X	X
•92-95	•Flavrian south	•coarse early trondhjemite	X	X	X	X
•92-96	•Flavrian south	•granophyre	X	X	X	
•92-97	•Flavrian south	•quartz vein				
•92-98	•Flavrian southwest	•coarse early or late trondhjemite	X	X	X	X
•92-99	•Flavrian southwest	•coarse early or late trondhjemite				
•92-100	•Flavrian south	•coarse early trondhjemite	X	X	X	X
•92-101	•Flavrian east, lac Lebrun	•coarse early trondhjemite	X	X	X	X
•93-01	•Flavrian southwest	•porphyritic trondhjemite				
•93-02	•Flavrian southwest	•porphyritic trondhjemite		X	X	X
•93-02a	•Flavrian southwest	•porphyritic trondhjemite	X	X	X	X
•93-03	•Flavrian southwest	•microgranitic trondhjemite				
•93-04	•Flavrian southwest	•microgranitic trondhjemite				
•93-05	•Flavrian southwest	•fabric in early trondhjemite				
•SP-8	•Flavrian southeast, Elder area	•tonalite?	X	X	X	X
•SP-15	•Flavrian south	•coarse early trondhjemite	X	X	X	X
•SP-20	•Flavrian south	•granophyre	X	X	X	
•SP-43	•Flavrian southwest	•early trondhjemite	X	X	X	
•SP-51	•Flavrian northwest	•tonalite	X	X	X	X
•SP-67	•Flavrian south contact area	•tonalite or trondhjemite?	X	X	X	
•SP-71a	•Flavrian south	•tonalite?	X	X	X	
•SP-75	•Flavrian south	•coarse early trondhjemite	X	X	X	X
•AN-74 1602m	•Ansil drilling	•homogeneous tonalite	X			
•AN-74 1593m	•Ansil drilling	•heterogeneous tonalite	X			
•AN-79 1577	•Ansil drilling	•tonalite or early trondhjemite?	X			
•AN-79 1602m	•Ansil drilling		X			
•AN-497 367.5m	•Ansil drilling	•tonalite	X			
•AN-498 366m	•Ansil drilling	•tonalite	X			
•AN-499 341m	•Ansil drilling	•heterogeneous tonalite	X			

APPENDIX III. Mineralogy Table.

sample	rock name	qtz	plag.	horn.	ep.	chl.	act.	ser.	carb.	stilp.	sph.	rut.	ap.	zr.	opa.	textures and comments
92-76	gabbro	5%	60%	34%	X	X		X	X				tr.	tr.	1%	plag. altered to chl., ep. and ser. qtz-ser.-carb. alteration of matrix carb. exsolution in act. (poikilitic)
92-68	qtz-diorite	20%	58%	20%	X	X		tr.							2%	xenomorphic qtz plag. altered to ep. and chl. zoned plag. sph. replacing opa. ep. veinlets
92-70	tonalite	40%	40%	20%	X	X	X	tr.	tr.	X				tr.	tr.	plag. altered to chl., ser. and carb. granophyric texture (qtz-plag.) spotted texture (chl., stilp., plag.) crystallization sequence: plag.-horn.-qtz qtz-ep. veinlets act. after horn.
92-71	tonalite	30%	45%	25%*										tr.	tr.	xenomorphic qtz plag. altered to ser. and ep. subophitic to ophitic texture
92-77	tonalite	35%	45%	20%		X		X	X	X			tr.	tr.	tr.	zoned plag. stilp. after amph. opa. after amph. amph. acicular graphic/granophyric qtz
92-78	tonalite	27%	60%		X	13%			X						tr.	ep.-chl.-carb. secondary ep. and qtz alteration of plag.
92-81	tonalite	35%	45%		X	X	20%*	X						tr.	tr.	chl.-ep.-ser. (tr.) after plag. qtz-plag. intergrowth qtz after amph. (act.?) ep. disseminated throughout
92-82	tonalite	10%	60%		X		30%*	X						tr.	tr.	clots of plag.-amph.-opa.-qtz (tr.) surrounded by plag.-qtz matrix ep. and ser. alteration

X: associated to other mineral (e.g. plag. contains ep. and chl.)

*: type of amphibole not differentiated

abbreviations: qtz = quartz, plag. = plagioclase, horn. = hornblende, chl. = chlorite, act. = actinolite, ser. = sericite, carb. = carbonate, stilp. = stilpnomelane, sph. = sphene, rut. = rutile, ap. = apatite, zr. = zircon, opa. = opaques (magnetite [mt.], ilmenite, pyrite, hematite), gran. = granular, euh. = euhedral, anh. = anhedral, int. = interstitial, xen. = xenomorphic, frag. = fragment, alt. = altered, tr. = trace.

sample	rock name	qtz	plag.	horn.	ep.	chl.	act.	ser.	carb.	stilp.	sph.	rut.	ap.	zr.	opa.	textures and comments
92-83	inclusion	44%	50%		X	X	5%*			tr						textural variability sharp contacts between amph. and plag. but rounded with qtz (late qtz?) ep. and chl. after plag.
92-88	inclusion	50%	47%		X		3%*								tr.	unidentified tr. mineral associated with opa. all? plag. porphyritic matrix of qtz-plag. intergrowth epidotization of plag. plag. weakly zoned
92-90	tonalite?	30%	48%				20%*								2%	amph. occurs as small irregular zones to euhedral crystals. ep. after plag. dark green pleochroic amph. qtz-plag. intergrowth
SP-8	tonalite	25% xen.	58% euh. alt.			X	15%*		X						2%	ep. after plag. act. shows disturbed poikilitic (plag.) surface, chl. after amph.
SP-51- 82	trondhjemite	40% xen.	38% euh.		1%	X	20%	X	tr.		1% euh.			tr.		granophytic intergrowth ser. after plag. not intense. spectacular sph. crystals. all?
SP-67- 82	tonalite	20% xen.	57%		X	X	20%	X							3%	qtz-plag. intergrowth plag. and act. are intensely altered. ep. and ser. after plag. chl. and ep. after amph.
92-65	early trondhjemite	40%	56%		1%	1%	tr.				1%				1%	qtz-plag. intergrowth granitic texture clots of ep.-mt.-chl.-act. ep.-mt.-qtz veinlets
92-66	early trondhjemite	48%	55%		X	X	X		tr.		tr.			tr.		act.-ep.-chl. = 2% ep. after plag. and act. local qtz-plag. intergrowth

X: associated to other mineral (e.g. plag. contains ep. and chl.)

*: type of amphibole not differentiated

abbreviations: qtz = quartz, plag. = plagioclase, horn. = hornblende, chl. = chlorite, act. = actinolite, ser. = sericite, carb. = carbonate, stilp. = stilpnomelane, sph. = sphene, rut. = rutile, ap. = apatite, zr. = zircon, opa. = opaques (magnetite [mt.], ilmenite, pyrite, hematite), gran. = granular, euh. = euhedral, anh. = anhedral, int. = interstitial, xen. = xenomorphic, frag. = fragment, alt. = altered, tr. = trace.

sample	rock name	qtz	plag.	horn.	ep.	chl.	act.	ser.	carb.	stilp.	sph.	rut.	ap.	zr.	opa.	textures and comments	
92-73	early trondhjemite	55%	44%		tr.	tr.		X								coarse grained granitic texture ep. + chl. = 1% competitive growth of qtz and plag. ep. surrounds mt. chl. and ep. occur at grain boundaries ep. and ser. after plag. (not intense)	
92-85	early trondhjemite	47%	48%		X	X	5%	X		X					X	chl.-stilp. and mt. occur in small clots. ser.-ep. after plag. act.-ep.-chl.-stilp. total 5%	
92-86	early trondhjemite	50%	47%			1%	2%	X				tr.			tr.	ser.-chl. after plag. coarse grained granitic and granophyric texture.	
92-87	early trondhjemite	42%	53%		X	X	X	X				X				ser.-ep. after plag. plag. are zoned magmatic brecciation texture coarse grained granitic texture ep.-chl.-act. = 5%	
92-94	early trondhjemite	45%	50%		X	X	X					X			tr.	zoned plag. ep. after plag. act.-ep.-chl. = 5%	
92-95	early trondhjemite	60% frag. 2 mm	37% euh. 1.8 mm					1%			tr.	tr.				tr.	magmatic brecciation texture minor qtz-plag. intergrowth mafic minerals form clotted texture qtz shows minor internal deformation ser. associated with late micro-shears mt. poikilitic within ep. ser. after plag. clots consist of ep.-mag-ser. alb. after quartz

X: associated to other mineral (e.g. plag. contains ep. and chl.)

*: type of amphibole not differentiated

abbreviations: qtz = quartz, plag. = plagioclase, horn. = hornblende, chl. = chlorite, act. = actinolite, ser. = sericite, carb. = carbonate, stilp. = stilpnomelane, sph. = sphene, rut. = rutile, ap. = apatite, zr. = zircon, opa. = opaques (magnetite [mt.], ilmenite, pyrite, hematite), gran. = granular, euh. = euhedral, anh. = anhedral, int. = interstitial, xen. = xenomorphic, frag. = fragment, alt. = altered, tr. = trace.

sample	rock name	qtz	plag.	horn.	ep.	chl.	act.	ser.	carb.	stilp.	sph.	rut.	ap.	zr.	opa.	textures and comments
92-100	early trondhjemite	54% xen. frag. up to 5 mm	45% euh. up to 3.5 mm		X	X (blue)	X	X					tr. euh.			magmatic brecciation texture ep. and chl. after amph. corroded, resorbed contacts between individual qtz crystals. mafic minerals form clots
92-101	early trondhjemite	42% xen. frag.	55% euh.			X	3%									brecciated magmatic texture plag. is zoned and altered (ser.) deformed qtz coarse grained
SP-20	granophyre	44%	44%		1%	X	1% up to 2 mm	X			tr.			X		granophyric intergrowth ser. after plag. relict zoning of plag. chl. after act.
SP-43-82	granophyre	43% 0.3 to 2 mm	42%		2%	tr.					tr.					granophyric zones vary in size ep. group mineral could be all.
92-96	granophyre	44%	44%		2%	X								tr.		granophyric intergrowth of qtz and plag. The areas of intergrowth are in optical continuity with anhedral qtz crystals. patches of ep. interstitial to qtz-plag. intergrowth and also as veinlets.
SP-75	granophyre	60%	40%		X		X		X						tr.	20% of qtz occurs as microqtz brecciated texture (not magmatic), fragments show granophyric texture ep.-act.-carb.-qtz veinlets ser. late associated to micro-fractures
92-91	Eldrich diorite	5%	55% alt.	44%*	X gran.	X									1%	intense epidotization of plag. skeletal opa.

X: associated to other mineral (e.g. plag. contains ep. and chl.)

*: type of amphibole not differentiated

abbreviations: qtz = quartz, plag. = plagioclase, horn. = hornblende, chl. = chlorite, act. = actinolite, ser. = sericite, carb. = carbonate, stilp. = stilpnomelane, sph. = sphene, rut. = rutile, ap. = apatite, zr. = zircon, opa. = opaques (magnetite [mt.], ilmenite, pyrite, hematite), gran. = granular, euh. = euhedral, anh. = anhedral, int. = interstitial, xen. = xenomorphic, frag. = fragment, alt. = altered, tr. = trace.

sample	rock name	qtz	plag.	horn.	ep.	chl.	act.	ser.	carb.	stilp.	sph.	rut.	ap.	zr.	opa.	textures and comments	
92-69	late trondhemite	45%	46% euh.	8%	1%									tr.		granitic texture crystallization of plag.-amph.-qtz (in this order) zoned plag.	
92-62	late trondhemite	50%	43%	5%	X	X		X				tr.		tr.	tr.	granitic texture ser. after plag. amph. altered to qtz-ep.-chl.	
92-35	late trondhemite	45%	50%		X	X	7%	X		X				tr.	tr.	coarse granitic texture	
92-35a	late trondhemite	50%	45%		X	X	5%	X		X				tr.	tr.	coarse granitic texture	
92-44	late trondhemite	44%	50%	6%	X							tr.			tr.	granitic texture with local qtz-plag. intergrowth zoned plag.ep. after amph.	
93-02	trondhemite porphyry	40%	50%		X	X	5%	X		tr.	tr.			tr.	tr.	qtz- alb. phenocrysts minor magmatic brecciation	
93-02a	trondhemite porphyry	45%	50%		X	X	3%	X		tr.	tr.			tr.	tr.	qtz- alb. phenocrysts minor magmatic brecciation	
AN-74 (1593m)	tonalite	30% anh.	60% euh., alt. .2 to .6 mm		3%	3%	4%	X	X							tr.	interstitial qtz ep.-act.-chl. replace acicular amph. carb.-ser. after plag. local granophyric intergrowth ep. veinlets
AN-74 (1602m)	tonalite	20% anh., int.	50% euh., alt. 0.3 mm		X	10%	15%									tr.	interstitial qtz contains plag intergrowth chl.-act. replace amph. ep.-ser. after plag. opa. show a pseudomorph habit

X: associated to other mineral (e.g. plag. contains ep. and chl.)

*: type of amphibole not differentiated

abbreviations: qtz = quartz, plag. = plagioclase, horn. = hornblende, chl. = chlorite, act. = actinolite, ser. = sericite, carb. = carbonate, stilp. = stilpnomelane, sph. = sphene, rut. = rutile, ap. = apatite, zr. = zircon, opa. = opaques (magnetite [mt.], ilmenite, pyrite, hematite), gran. = granular, euh. = euhedral, anh. = anhedral, int. = interstitial, xen. = xenomorphic, frag. = fragment, alt. = altered, tr. = trace.

sample	rock name	qtz	plag.	horn.	ep.	chl.	act.	ser.	carb.	stilp.	sph.	rut.	ap.	zr.	opa.	textures and comments
AN-79 (1577m)	tonalitic granophyre	42%	43% euh. 1 mm		3%	5%	7%								tr.	qtz-plag. granophyric intergrowth carb. veinlets opa. needles (0.1 mm) occur in groundmass
AN-79 (1652m)	tonalite	20%	70% euh. 0.3 mm		3%	3%	4%									interstitial qtz (optical continuity) chl.-act.-ep. -ep. form clots (2 mm) 0.1 mm qtz grains associated to mafic clots
A-497 (3675m)	tonalite	35% anh., int.	45% euh. up to 2 mm		6%	7%	7%									medium to coarse grained, granophyric intergrowth common surrounding plag. crystals clots of chl.-ep.-act.-op (mt.) are 2 mm in diameter chl.-ep.-act. pseudomorph mafic acicular zoned plag.
A-498 (366m)	tonalite	25% anh., int.	65% euh. 0.5 mm			5%	5%	X	tr.		tr.				tr.	medium grained interstitial texture (blue chl.) mafic minerals occur both in clots and pseudomorph acicular amph. ep. veinlets crosscut sample
A-499 (341m)	tonalite	40% anh., int.	45% euh.		3%	6%	6%									chl.-act.-ep. pseudomorph 2 mm acicular amph. crystals and occur at grain boundaries variably textured: areas of variable grain size. Irregular shaped qtz-poor zones are surrounded by qtz-rich matrix

X: associated to other mineral (e.g. plag. contains ep. and chl.)

*: type of amphibole not differentiated

abbreviations: qtz = quartz, plag. = plagioclase, horn. = hornblende, chl. = chlorite, act. = actinolite, ser. = sericite, carb. = carbonate, stilp. = stilpnomelane, sph. = sphene, rut. = rutile, ap. = apatite, zr. = zircon, opa. = opaques (magnetite [mt.], ilmenite, pyrite, hematite), gran. = granular, euh. = euhedral, anh. = anhedral, int. = interstitial, xen. = xenomorphic, frag. = fragment, alt. = altered, tr. = trace.

APPENDIX IV. Geochemical data

	92-44	92-76	SP-70	92-91	FL-3	SP-28	92-68	SP-8
SiO ₂	-	48.9	52.14	53.28	53.88	56.33	59.15	61.61
TiO ₂	-	1.24	0.99	1.58	0.93	0.95	1.72	1.52
Al ₂ O ₃	-	19.79	15.13	15.98	16.57	16.58	14.93	14.82
Fe ₂ O ₃ *	-	10.59	13.25	11.25	10.92	7.32	8.85	7.97
FeO	-	-	-	-	-	-	-	-
MnO	-	0.15	-	0.19	-	-	0.07	0.1
MgO	-	3.9	6.84	4.65	4.75	4.63	2.48	2.28
CaO	-	10.93	8.68	8.22	7.53	8.55	7.87	5.63
Na ₂ O	-	2.5	1.79	3.45	3.63	3.63	4.07	4.69
K ₂ O	-	0.33	0.14	0.48	0.53	0.25	0.21	0.36
P ₂ O ₅	-	0.09	0.21	0.25	0.44	0.15	0.4	0.47
Total	-	98.42	99.17	99.33	99.18	98.39	99.75	99.45
LOI	-	2.45	2.24	1.71	-	1.82	0.95	1.31
Cr	-	23	122.82	70	14.03	89.64	5	-
Ni	-	34.96	88.97	24.65	25	44.36	3.13	2.18
Co	-	31	40.84	27	-	22.3	12	-
Sc	-	29.3	33.33	34.01	20.45	24.6	18.26	-
V	-	383	376.85	235	-	205.62	135	122
Cu	-	105.37	8.68	15.69	93	-	5.311	3.89
Zn	-	70.37	91.84	81.77	72	17.52	47.21	20.26
W	-	-	-	-	-	-	-	-
As	-	1	-	-	-	-	0.7	-
Sb	-	-	-	-	-	-	0.08	-
Au	-	4	-	8	-	-	16	-
K	-	2739	-	3985	-	-	1743	2988
Rb	-	6.81	7.29	5.93	13.4	11.5	3.37	4.36
Cs	-	-	-	-	-	-	0.5	-
Ba	-	86	58.39	91	-	134.91	81	-
Sr	-	230.99	159.59	195.36	248.7	255.17	195.36	182.56
Ga	-	-	-	-	-	-	-	-
Ta	-	0.1	0.1	0.26	0.6	0.42	0.37	-
Nb	-	4.37	4.41	5.96	8	5.07	10.1	11.52
Hf	-	0.9	1.45	2	1.48	2.7	3.4	-
Zr	-	42.25	61.05	81.76	71	113.11	151	150.26
Ti	-	7434	-	9472	-	-	10311	9112
Y	-	11.95	14.25	20.83	18.3	16.29	37.17	52.78
Th	-	-	0.63	0.5	0.83	1.24	1.1	-
U	-	0.14	0.6	0.14	0.25	1.06	0.35	-
La	-	5.1	6.27	7.5	8.45	11.44	12.3	-
Ce	34	11	13.43	16	19.53	24.72	30	-
Nd	-	7	7.49	12	11.77	13.18	19	-
Sm	7.67	1.81	1.79	3.26	2.79	4.39	5.59	-
Eu	-	0.64	0.73	1.15	1.06	1.07	1.75	-
Tb	-	0.35	0.36	0.47	0.47	0.49	0.85	-
Ho	-	-	0.47	-	0.56	-	-	-
Tm	-	0.2	0.2	-	0.23	0.31	0.61	-
Yb	5.3	1.3	1.4	2.2	1.78	1.54	3.5	-
Lu	0.83	0.14	0.27	0.36	0.28	0.26	0.48	-

Total iron as Fe₂O₃*

Oxide concentrations in weight %

Trace elements in ppm

Au concentrations in ppb

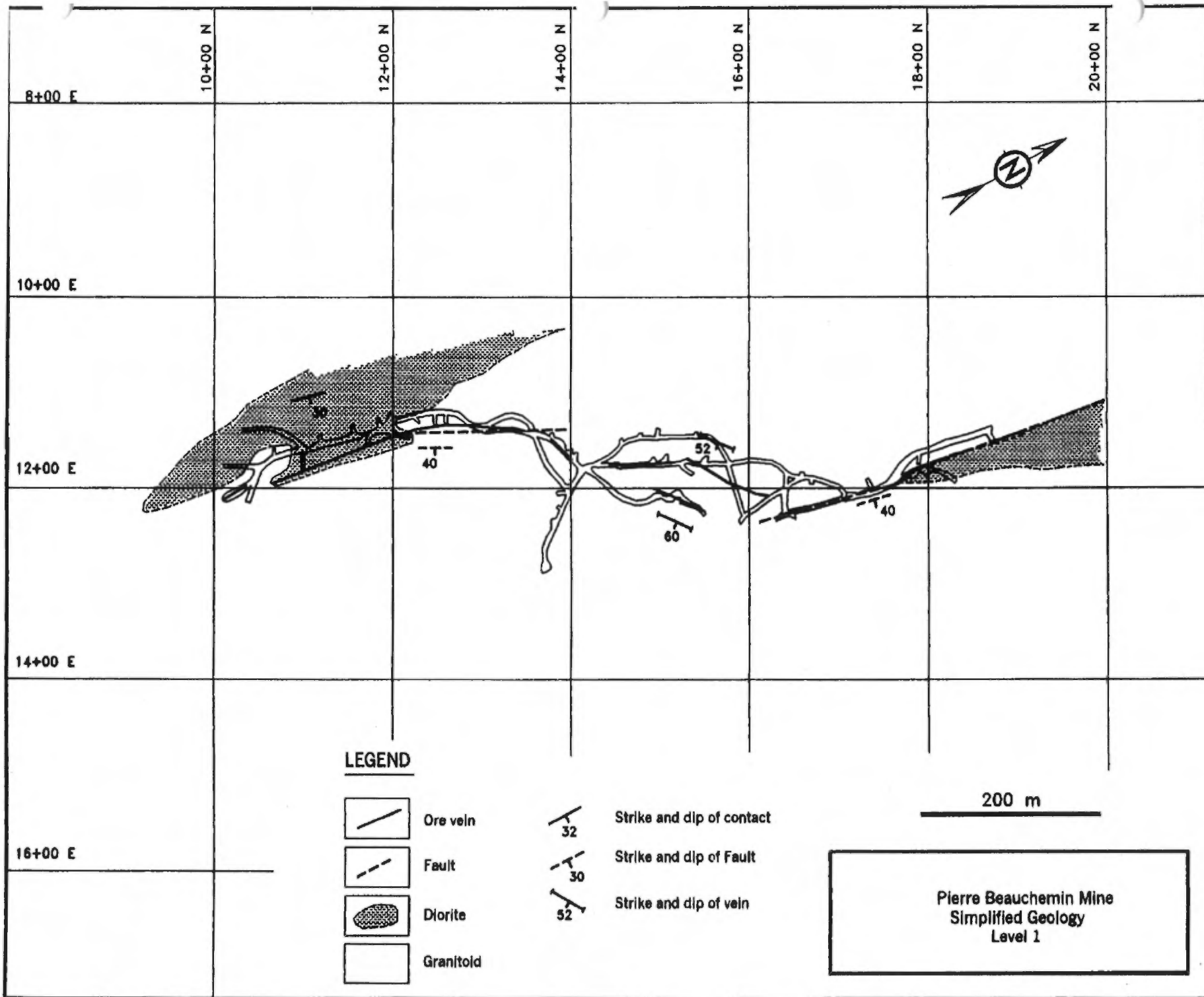
	92-90	92-71	92-78	92-77	SP-51-82	92-81	SP-67	92-70
SiO ₂	61.66	62.1	63.45	65.4	65.6	65.9	66.04	66.05
TiO ₂	1.03	1.03	1.14	0.58	0.75	1.03	0.86	0.63
Al ₂ O ₃	15.27	15.21	14.62	13.33	14.15	14.33	14.4	14.63
Fe ₂ O ₃ *	9.19	8.46	8.01	10.58	8.63	6.84	6.18	7.8
FeO	-	-	-	-	-	-	-	-
MnO	0.1	0.1	0.14	0.18	0.08	0.14	0.06	0.12
MgO	1.5	1.34	1.89	0.29	2.93	1.75	1.37	0.72
CaO	5.23	5.7	3.77	4.24	1.5	3.87	6.07	3.94
Na ₂ O	4.9	4.76	4.26	4.64	3.48	4.79	4.01	4.49
K ₂ O	0.43	0.58	0.28	0.41	0.7	0.39	0.72	0.84
P ₂ O ₅	0.38	0.37	0.3	0.14	0.21	0.27	0.24	0.18
Total	99.69	99.65	97.86	99.79	98.03	99.31	99.95	99.4
LOI	0.83	0.76	2.54	0.82	2.56	1.41	0.74	1.17
Cr	4	4	4	4	5	6	-	4
Ni	0.45	4.6	3.08	1.8	1.17	4.17	3.2	1.74
Co	9	9	10	1	10	10	-	6
Sc	25.63	25.1	19.4	39.83	17.4	18.26	-	19.89
V	37	22	80	15	21	75	58	16
Cu	16.25	2.96	7.35	11.12	3.22	2.4	3.96	3.58
Zn	24.98	36.8	47.97	41.53	33.57	46.12	10.86	42.73
W	-	-	-	-	-	-	2	-
As	-	-	0.6	-	-	1.6	-	-
Sb	-	-	-	-	0.12	0.13	-	-
Au	8	-	10	8	13	5	-	-
K	3570	4815	2324	3404	5811	3238	5977	6973
Rb	6.72	9.46	4.85	4.51	14.33	4.06	11.11	13.72
Cs	-	-	-	0.7	-	-	-	-
Ba	135	141	130	113	274	135	-	247
Sr	173.68	168.49	145.62	145.84	86.95	156.8	158.84	158.39
Ga	-	-	-	-	-	-	-	-
Ta	0.57	0.4	0.58	0.61	0.54	0.53	-	0.61
Nb	11.51	11.3	13.06	13.18	11.27	12.09	15.05	14.2
Hf	6	4.2	4.7	3.9	7.4	5	-	8.3
Zr	246.29	152.72	204.78	132.28	318.53	214.99	254.57	194.28
Ti	6175	6175	6834	3477	4496	6175	5156	3777
Y	47.05	46.47	41.6	45.73	46.45	39.42	52.94	49.57
Th	2.2	1.8	2.7	2.4	2.8	2.6	-	2.4
U	0.43	0.51	0.61	0.55	0.94	0.58	-	0.37
La	22.8	21.4	18.4	17.3	18	18.3	-	19.4
Ce	50	51	44	39	40	40	-	45
Nd	29	31	26	23	24	22	-	26
Sm	8.49	8.08	6.75	6.93	6.72	6.82	-	8
Eu	2.47	2.38	1.38	2.19	1.67	1.51	-	2.28
Tb	1.3	1.23	0.98	1.17	1.1	1	-	1.18
Ho	-	-	-	-	-	-	-	-
Tm	0.6	0.6	0.54	0.65	0.76	0.57	-	0.71
Yb	5	4.8	4.4	5	5.4	4.2	-	5
Lu	0.72	0.65	0.58	0.68	0.9	0.56	-	0.73

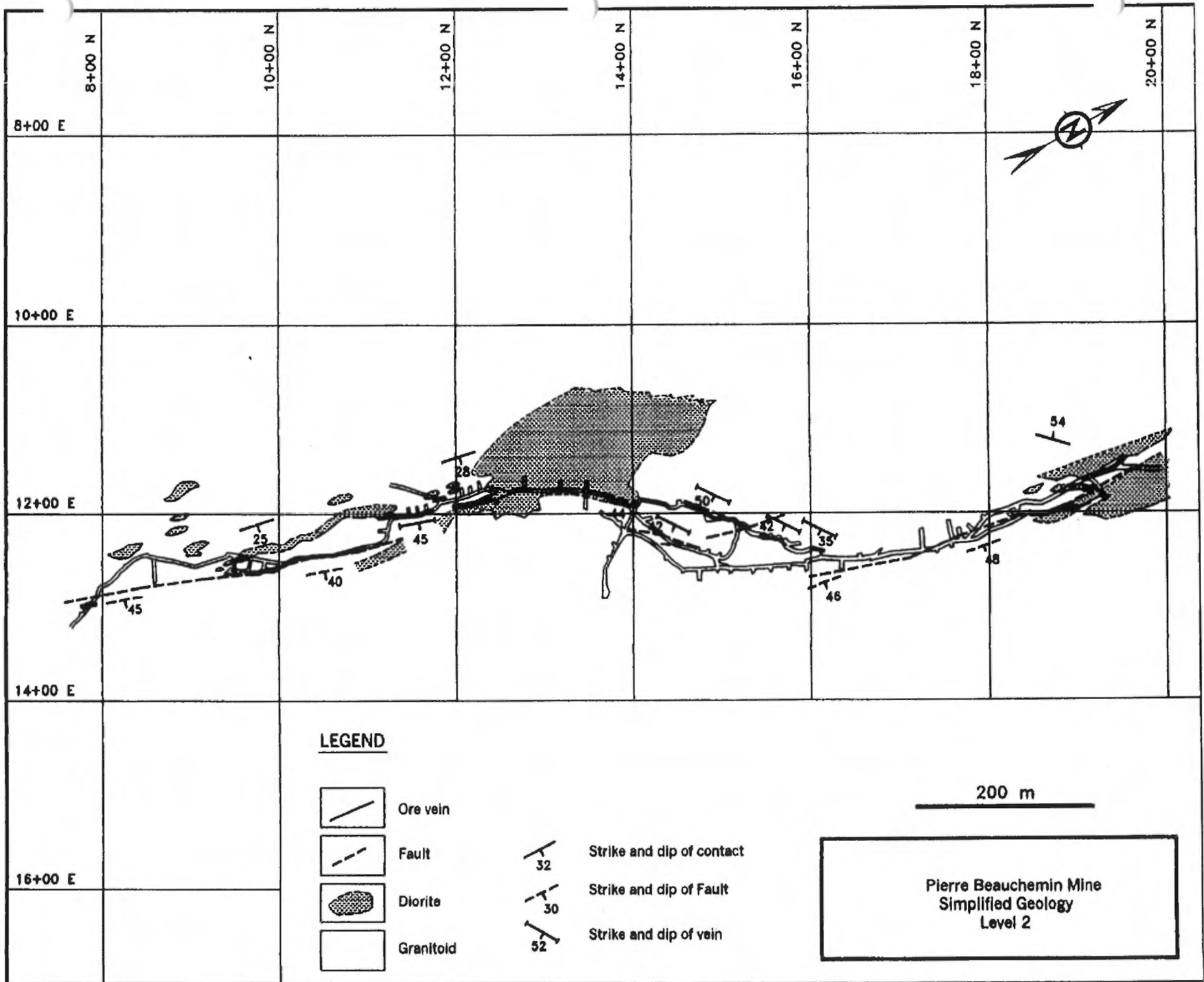
	92-82	92-83	92-88	93-02	92-69	92-44a	93-02a	92-35
SiO ₂	67.23	67.57	68.52	70.73	72.87	73.18	73.4	73.9
TiO ₂	0.71	0.61	0.88	0.47	0.38	0.3	0.35	0.33
Al ₂ O ₃	14.35	14.65	14.43	13.26	12.89	12.45	12.31	13.1
Fe ₂ O ₃ *	6.7	5.67	4.23	4.6	4.32	4.62	3.83	3.95
FeO	-	-	-	-	-	-	-	-
MnO	0.1	0.08	0.04	0.06	0.06	0.08	0.06	0.03
MgO	1.04	0.95	1.2	0.78	0.49	0.49	0.53	0.34
CaO	3.37	3.64	4.68	2.72	2.22	2.37	2.18	1.65
Na ₂ O	5.89	4.69	5.22	4.63	4.39	4.6	5.1	4.88
K ₂ O	0.46	0.98	0.24	1.21	0.87	0.59	0.26	1.07
P ₂ O ₅	0.22	0.13	0.14	0.1	0.06	0.07	0.08	0.06
Total	100.07	98.97	99.58	98.56	98.55	98.75	98.1	99.31
LOI	0.55	1.07	0.64	1.09	1.11	0.96	0.93	0.85
Cr	4	6	6	11.5	2	6.6	13.8	2
Ni	2.04	7.85	8.06	12	3.71	9	9	5.65
Co	5	8	6	5.5	4	3	3.8	4
Sc	18.56	15.6	14.54	9.7	8.88	8.9	7.5	9.26
V	16	56	80	-	19	11	-	23
Cu	2.6	19.4	2.03	9	25.26	11	6	13.42
Zn	25.02	40.38	20.34	26	34.1	38	23	36.4
W	-	-	-	-	-	-	-	-
As	-	-	0.7	-	-	-	-	0.07
Sb	-	-	-	-	-	-	-	-
Au	-	3	-	-	-	-	-	3
K	3819	8135	1992	10045	7222	4898	2158	8882
Rb	5.59	16.83	2.8	3	20.86	18	24	22.19
Cs	-	0.6	0.6	0.2	0.7	0.2	-	-
Ba	191	386	213	387	206	183	213	360
Sr	128.93	100.38	121.79	94	83.77	116	110	102.64
Ca	-	-	-	20	-	19	17	-
Ta	0.6	1.22	1.24	1.2	0.8	0.6	0.9	0.74
Nb	15.05	28.9	24.03	18	19.14	9	20	16.02
Hf	4.7	5.3	7.4	7.1	7.9	6.9	7.1	7.6
Zr	181.62	159.75	264.7	256	323.32	350	245	262.37
Ti	4256	3657	5276	2818	2278	1799	2098	1978
Y	61.73	108.68	88.65	87	54.14	42	96	62.2
Th	2.1	2.4	3	3.4	1.4	1.1	3.5	3
U	0.34	0.52	0.85	1	0.28	0.3	0.8	0.52
La	18.7	27.3	27.6	27.1	12.6	11.8	31.8	20.8
Ce	47	67	66	60	28	28	64	45
Nd	33	45	45	31	19	16	35	25
Sm	9.7	13.93	12.23	7.85	6.23	4.01	7.72	8.13
Eu	1.88	1.36	1.62	1.13	1.5	1.65	1.12	1.27
Tb	1.6	2.52	2.08	1.8	1.09	0.9	1.6	1.33
Ho	-	-	-	-	-	-	-	-
Tm	0.97	1.49	1.35	-	0.79	-	-	0.86
Yb	5.8	11.5	9.84	7.98	6.1	3.92	7.1	7.18
Lu	0.85	1.58	1.44	1.24	0.86	0.61	1.08	1.05

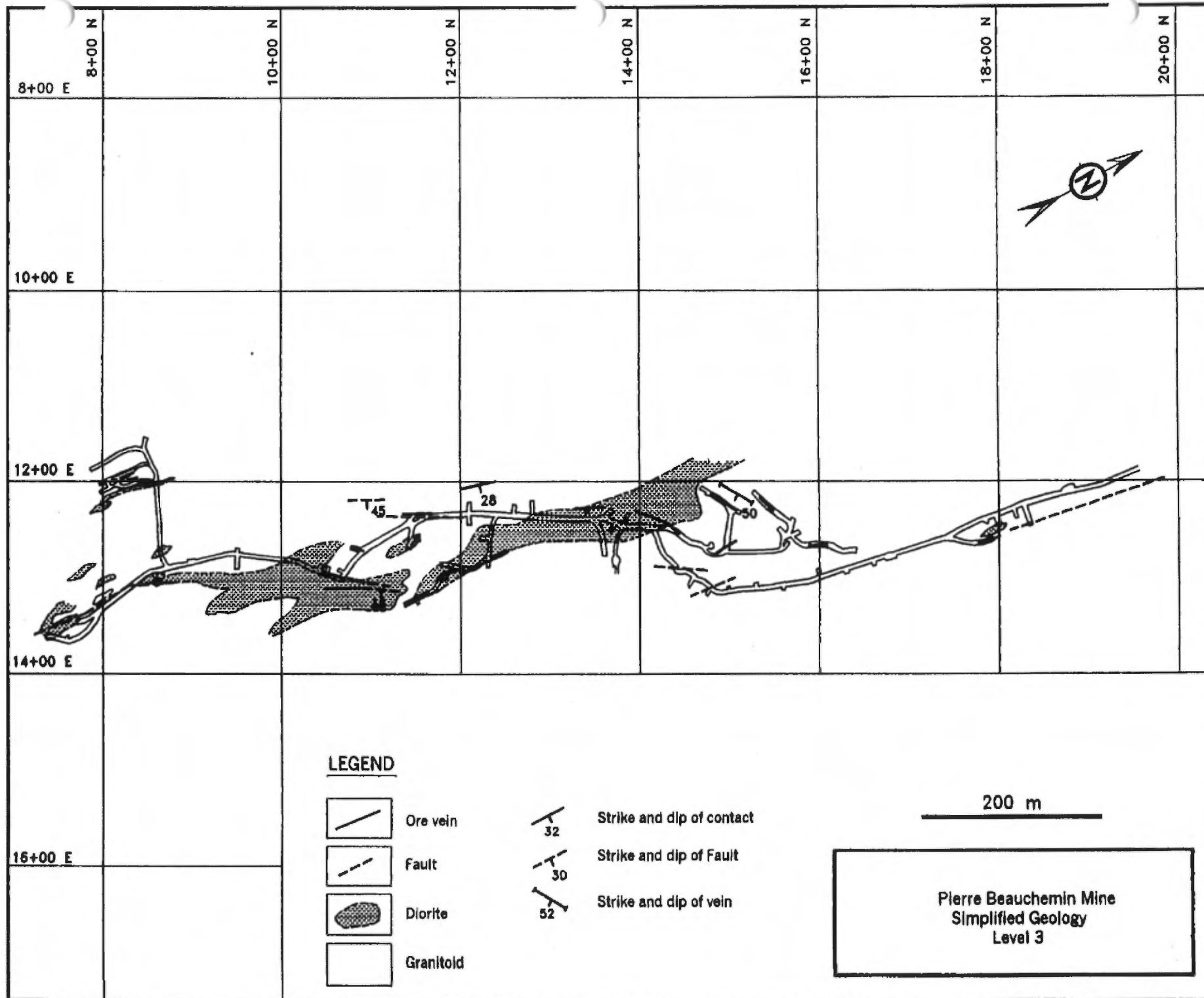
	92-35a	92-98	SP-20	92-62	92-87	92-101	92-85	SP-15
SiO ₂	74	74.27	74.45	75	75.22	75.42	75.63	75.8
TiO ₂	0.34	0.31	0.35	0.27	0.32	0.32	0.28	0.28
Al ₂ O ₃	13.01	12.79	12.67	12.26	13.12	12.85	12.26	12.6
Fe ₂ O ₃ *	3.56	3.78	3.21	4.06	1.78	1.78	3.27	1.11
FeO	-	-	-	-	-	-	-	-
MnO	0.04	0.03	0.01	0.06	0.01	0.01	0.02	-
MgO	0.34	0.45	0.67	0.35	0.55	0.56	0.34	1.12
CaO	2.31	2.81	3.38	2.24	3.63	4.01	1.87	3.12
Na ₂ O	4.96	4.31	4.06	4.2	4.91	4.51	4.23	4.84
K ₂ O	0.53	0.26	0.23	0.62	0.33	0.21	1.5	0.33
P ₂ O ₅	0.06	0.05	0.06	0.06	0.06	0.06	0.05	0.05
Total	99.15	99.06	99.09	99.12	99.93	99.73	99.45	99.25
LOI	0.73	1.04	0.97	1	0.58	0.73	0.87	0.67
Cr	-	4	-	3	3	4	-	4
Ni	4.88	3.9	3.36	3.42	3.25	4.54	3.38	2.95
Co	-	3	-	3	1	1	-	1
Sc	-	8.99	-	8.72	9.3	9.89	-	8.06
V	-	13	-	17	17	-	29	-
Cu	19.15	2.07	0.6	9.88	2.11	1.97	6.09	0.69
Zn	20.29	17.21	12.13	38.05	9.35	11.21	17.71	10.21
W	-	-	-	-	-	-	-	-
As	-	-	-	0.5	-	-	-	-
Sb	-	-	-	-	-	-	-	-
Au	-	-	-	6	3	-	-	3
K	4400	2158	1909	5147	2739	1743	12452	2739
Rb	7.82	5.69	2.67	15.4	2.95	3.66	23.06	4.86
Cs	-	-	-	-	0.4	-	-	0.3
Ba	-	141	-	182	157	114	-	137
Sr	88.43	139.22	138.73	110.69	121.55	145.76	80.79	120.41
Ga	-	-	-	-	-	-	-	-
Ta	-	1.12	-	0.39	0.76	0.91	-	1.02
Nb	15.92	23.19	17.31	11.1	19.09	21.79	20.18	22.33
Hf	-	8.1	-	7.3	7.7	7.7	-	7.5
Zr	239.95	281.01	327	273.48	263.57	249.19	272.95	266.32
Ti	2038	1858	2098	1619	1918	1918	1679	1679
Y	60.03	80.6	52.23	40.25	75.91	83.7	76.72	87.44
Tb	-	3.2	-	1.4	3.5	3	-	2.8
U	-	0.64	-	0.35	0.6	0.7	-	0.61
La	-	26.5	-	13.8	15.4	24.1	-	38.9
Ce	-	59	-	26	39	58	-	87
Nd	-	35	-	17	29	35	-	50
Sm	-	11.36	-	5.6	9.9	10.63	-	14.64
Eu	-	1.7	-	1.81	1.81	1.68	-	2.4
Tb	-	2	-	0.91	1.77	1.85	-	2.24
Ho	-	-	-	-	-	-	-	-
Tm	-	1.08	-	0.48	1.16	1.16	-	1.12
Yb	-	8.61	-	4.53	8.23	9.2	-	9.5
Lu	-	1.27	-	0.67	1.22	1.35	-	1.25

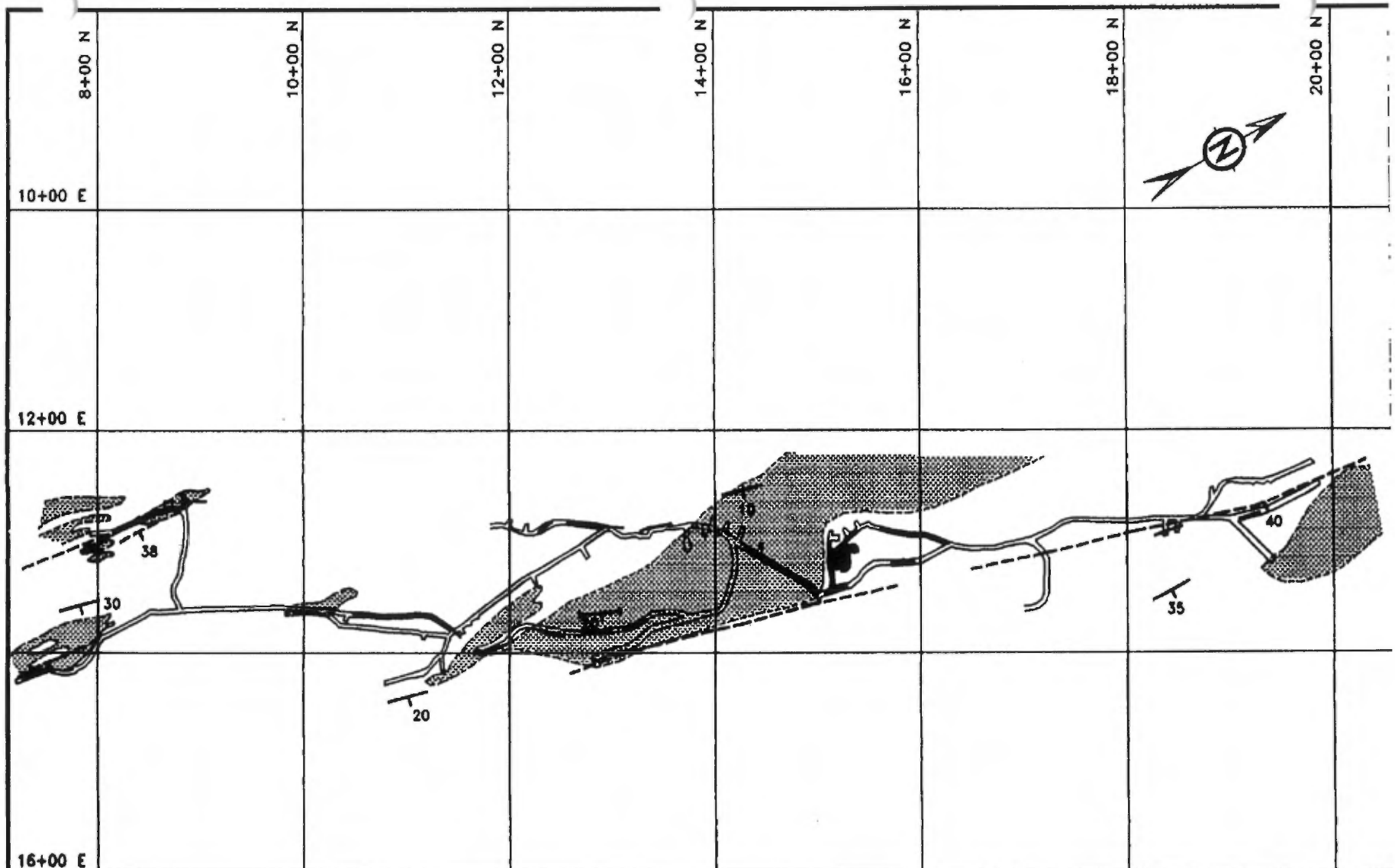
	SP-75	92-65	92-45	92-86	92-66	92-96	SP-43	92-100
SiO ₂	76.13	76.92	76.99	77.04	77.15	77.42	77.46	77.62
TiO ₂	0.25	0.16	0.26	0.14	0.18	0.14	0.13	0.24
Al ₂ O ₃	11.96	11.62	12.22	12.06	11.97	11.95	11.82	12.32
Fe ₂ O ₃ *	2.29	2.9	0.62	2.96	1.82	1.7	2.05	1.09
FeO	-	-	-	-	-	-	-	-
MnO	0.01	0.03	-	0.02	0.02	-	-	-
MgO	0.68	0.1	1.39	0.22	0.22	0.11	0.37	0.3
CaO	2.95	1.5	2.71	0.56	2.25	2.47	3.18	2.41
Na ₂ O	3.98	5.04	4.77	4.78	5.37	5.04	4.12	5.22
K ₂ O	0.47	0.57	0.37	1.72	0.11	0.1	0.26	0.26
P ₂ O ₅	0.04	0.03	0.05	0.03	0.03	0.02	0.02	0.04
Total	98.76	98.87	99.38	99.53	99.12	98.95	99.41	99.5
LOI	1.3	0.48	0.68	0.67	0.72	0.51	0.88	0.46
Cr	4	3	-	-	4	-	-	3
Ni	3.66	2.98	4.45	3.44	1.77	5.6	1.74	2.81
Co	1	1	-	-	1	-	-	1
Sc	10.06	8.4	-	-	9.15	-	-	6.97
V	14	-	-	-	-	-	-	-
Cu	2.02	3.02	0.75	18.44	1.54	1.22	0.54	3.71
Zn	13.23	25.97	9.58	28.65	40.28	11.07	10.13	10.74
W	-	-	-	-	-	-	-	-
As	-	-	-	-	-	-	-	-
Sb	-	-	-	-	-	-	-	-
Au	3	-	-	-	3	-	-	4
K	3902	4732	3071	14278	913	830	2158	2158
Rb	12.03	7.74	6.02	21.94	1.48	1.75	5.01	2.32
Cs	0.3	0.6	-	-	-	-	-	-
Ba	266	252	-	-	102	-	-	176
Sr	140.61	70.55	116.48	29.1	76.05	53.75	105.07	91.21
Ga	-	-	-	-	-	-	-	-
Ta	0.74	0.95	-	-	0.8	-	-	0.89
Nb	16.73	19.94	18.79	21.54	19.72	29.79	24.24	18.85
Hf	7.9	7.1	-	-	8.3	-	-	8.7
Zr	328.98	254.71	221.85	217.7	306.76	304.71	327.9	306.33
Ti	1499	959	1559	839	1079	839	779	1439
Y	58.22	64.39	65.26	103.42	79.5	110.55	101.24	68.34
Th	3.7	3.6	-	-	4.3	-	-	3
U	1.11	0.69	-	-	0.56	-	-	0.68
La	25.1	28.6	-	-	35	-	-	5.1
Ce	56	64	-	-	72	-	-	16
Nd	29	36	-	-	42	-	-	18
Sm	8.47	10.04	-	-	11.17	-	-	7.79
Eu	1.43	1.74	-	-	2.15	-	-	1.7
Tb	1.36	1.6	-	-	1.87	-	-	1.51
Ho	-	-	-	-	-	-	-	-
Tm	0.77	0.85	-	-	1.1	-	-	0.97
Yb	6.7	7.02	-	-	8.83	-	-	7.7
Lu	0.95	1.06	-	-	1.31	-	-	1.03

	92-67	92-72	92-95	92-73	SP-71a	92-94	92-93
SiO ₂	77.86	78.05	78.21	78.39	78.57	78.67	78.73
TiO ₂	0.12	0.12	0.13	0.14	0.13	0.18	0.13
Al ₂ O ₃	11.87	12.16	11.65	11.59	11.89	11.68	12.01
Fe ₂ O ₃ *	1.58	2.26	1.74	2.91	-	1.47	1.26
FeO	-	-	-	-	2.63	-	-
MnO	-	0.01	-	0.02	-	0.01	0.02
MgO	0.22	0.42	0.81	-	0.7	0.16	0.07
CaO	1.63	0.22	1.34	0.81	0.13	2.22	1.1
Na ₂ O	5.46	5.75	4.57	5	5.28	5.1	5.93
K ₂ O	0.12	0.34	0.34	1.06	0.18	0.18	0.1
P ₂ O ₅	0.02	0.02	0.01	0.02	0.02	0.03	0.02
Total	98.88	99.35	98.8	99.94	99.82	99.7	99.37
LOI	0.66	0.59	0.98	0.48	0.77	0.52	0.34
Cr	4	3	3	4	-	3	3
Ni	2.94	4.83	3.45	3.38	3.55	2.39	2.83
Co	1	1	1	1	-	1	1
Sc	6.16	6.27	7.24	6.86	-	7.6	7.08
V	-	-	-	-	-	-	-
Cu	-	-	0.24	2.01	-	1.33	1.01
Zn	17.02	15.65	9.77	21.89	21.73	12.96	13.57
W	-	-	-	-	-	-	-
As	-	-	-	-	-	-	0.04
Sb	-	-	-	-	-	-	-
Au	-	-	-	-	-	-	3
K	996	2822	2822	8799	1494	1494	830
Rb	2.03	5.95	8.63	10.8	17.04	2.65	1.81
Cs	-	0.7	-	-	-	0.6	0.5
Ba	62	102	108	328	-	234	232
Sr	58.77	22.46	56.33	41.03	40	85.12	82.03
Ga	-	-	-	-	-	-	-
Ta	1.48	2.74	1.8	1.77	-	0.79	1.46
Nb	25.19	54.79	34.66	34.06	39.58	17.89	23.43
Hf	8.6	13	10	8.3	-	7.7	9.6
Zr	267.96	315.1	263.92	253.76	343.68	279.92	284.06
Ti	719	719	779	839	779	1079	779
Y	81.17	165.19	137.26	96.03	102.76	69.39	96.08
Th	5.5	8	6.1	4.7	-	3.6	6
U	1.09	1.46	1.3	0.84	-	0.8	1.21
La	46.3	46.7	47.5	35.4	-	33.9	48.7
Ce	92	94	108	72	-	68	105
Nd	47	60	65	45	-	36	58
Sm	12.05	18.21	19.44	13.3	-	10.89	16.14
Eu	1.31	1.31	1.34	1.65	-	1.67	1.2
Tb	2.06	4.23	3.52	2.06	-	1.63	2.64
Ho	-	-	-	-	-	-	-
Tm	1.13	2.33	1.95	1.1	-	0.86	1.4
Yb	9.02	18.7	15.4	11.9	-	7.84	12
Lu	1.37	2.62	2.2	1.74	-	1.02	1.8


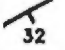

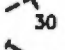


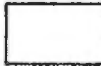









LEGEND

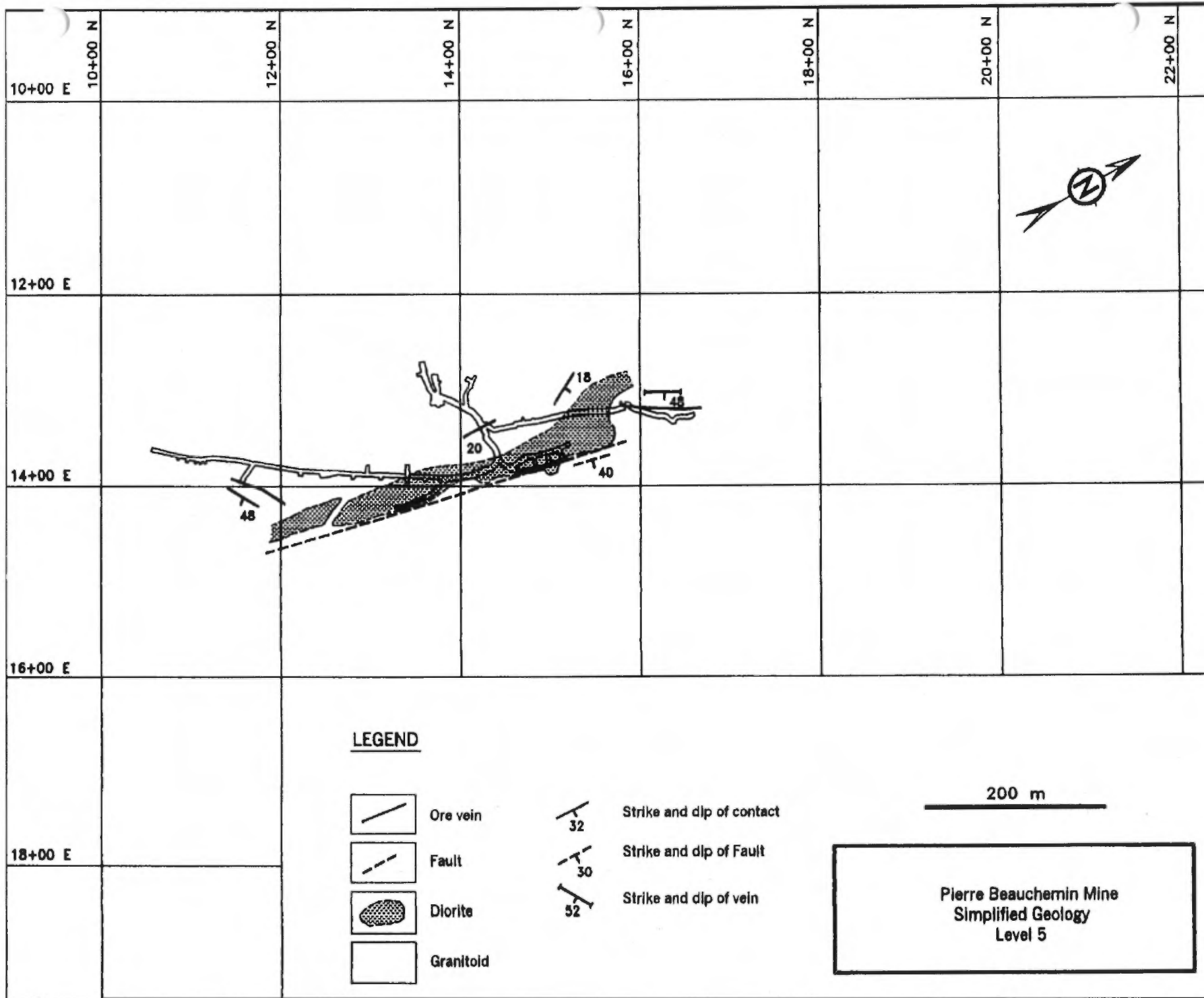
- | | | | |
|---|-----------|--|---------------------------|
|  | Ore vein |  | Strike and dip of contact |
|  | Fault |  | Strike and dip of Fault |
|  | Diorite |  | Strike and dip of vein |
|  | Granitoid | | |

200 m



Pierre Beauchemin Mine
Simplified Geology
Level 4

18+00 E



10+00 E

10+00 N

12+00 N

14+00 N

16+00 N

18+00 N

20+00 N

22+00 N





12+00 E


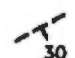

14+00 E

16+00 E

18+00 E

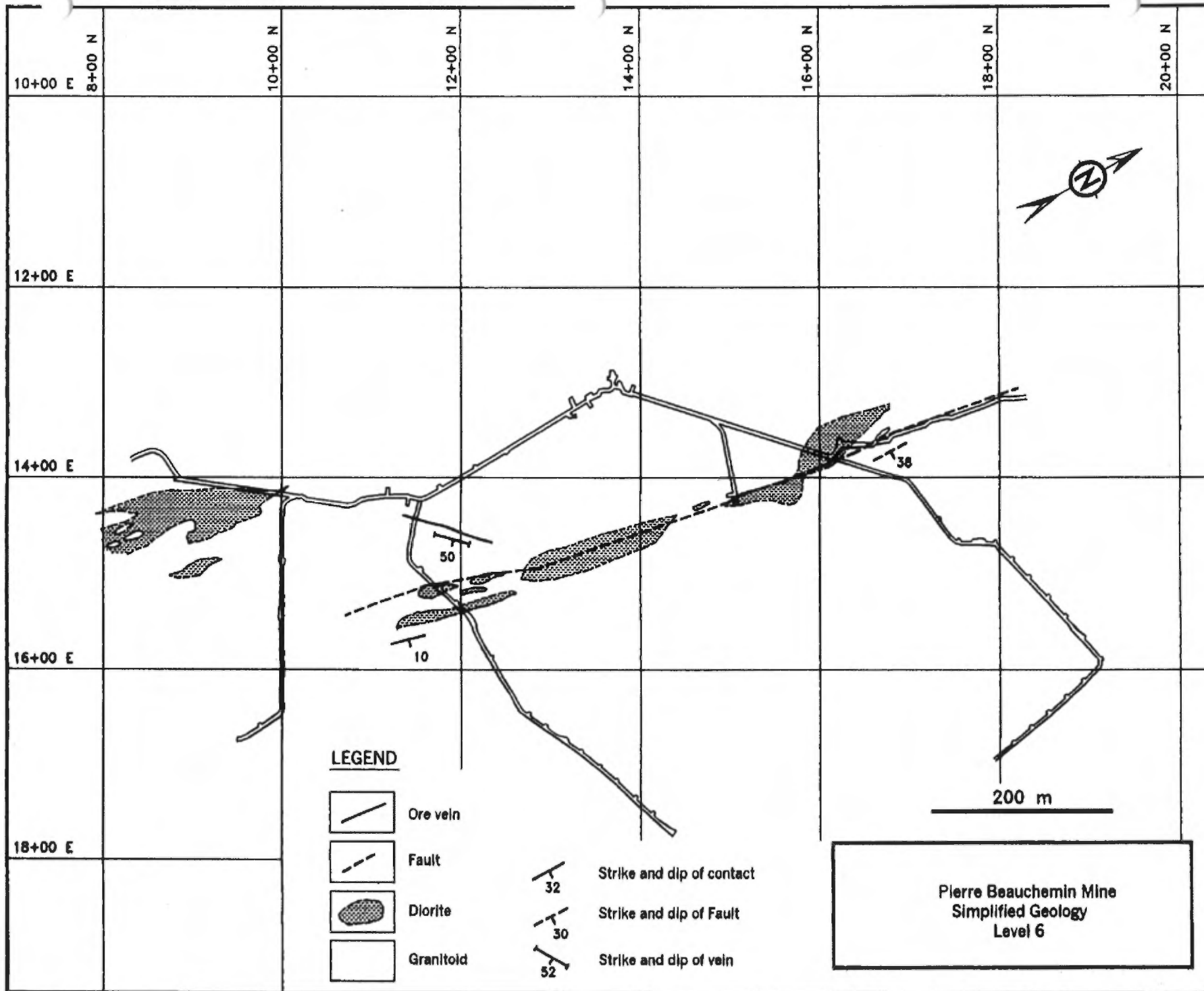
LEGEND

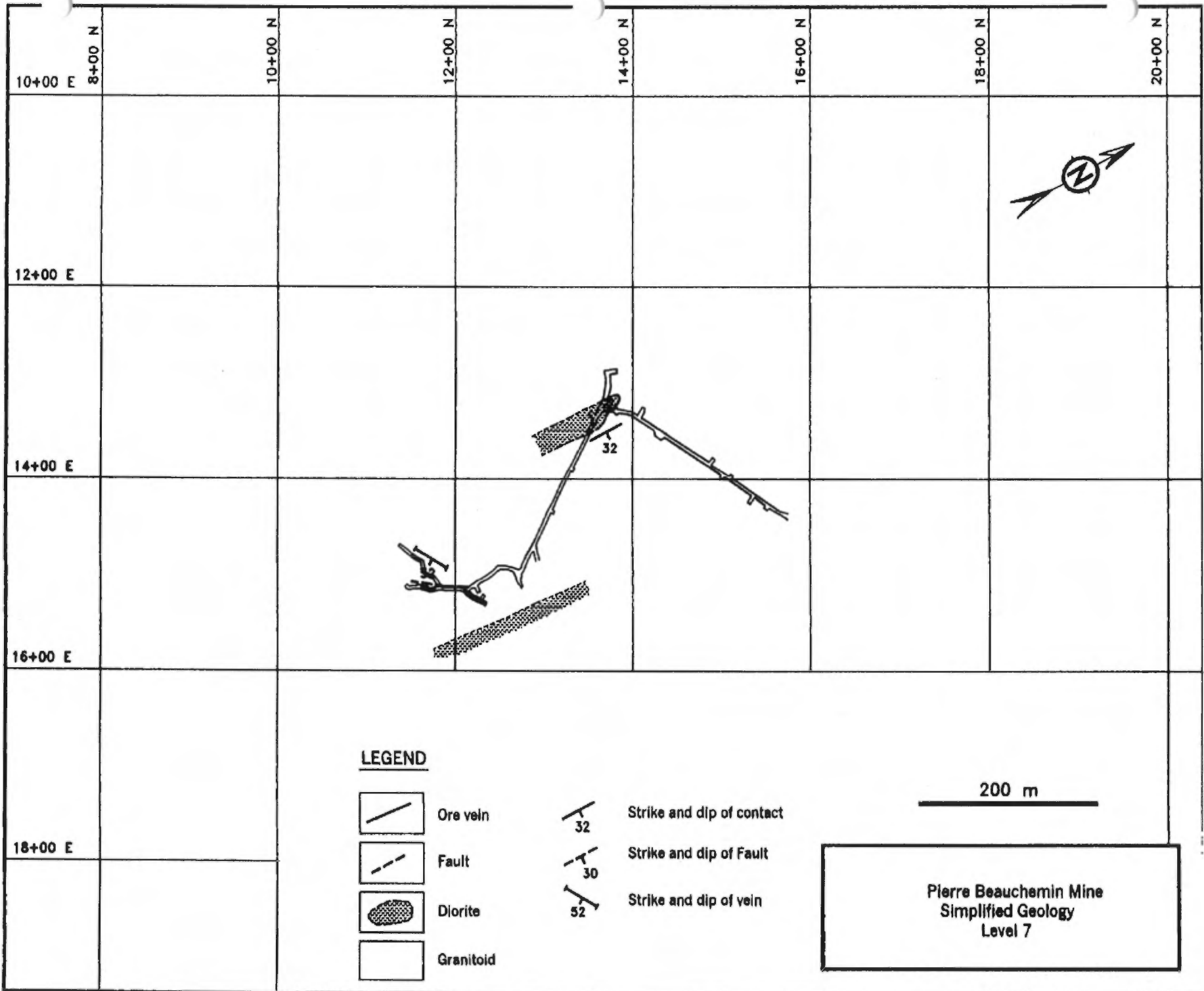
-  Ore vein
-  Fault
-  Diorite
-  Granitoid

-  32 Strike and dip of contact
-  30 Strike and dip of Fault
-  52 Strike and dip of vein

200 m

Pierre Beauchemin Mine
Simplified Geology
Level 5





APPENDIX VI. Location of Pierre Beauchemin Samples

Sample Number	Coordinates		Thin Section
1-1	18+70N	11+38E	
1-3	18+00N	11+81E	
1-4	17+30N	12+04E	
1-5	16+92N	12+15E	
1-6	16+28N	12+08E	X
1-7	15+35N	11+50E	
1-8	10+10N	12+16E	
1-9	10+35N	11+85E	
1-10	11+31N	11+59E	
1-11	11+77N	11+48E	X
1-12	11+77N	11+48E	X
1-13	12+41N	11+41E	
1-14	13+70N	11+67E	
1-X	15+20N	11+60E	X
1-30	15+00N	11+60E	X
2-1	7+63N	13+20E	X
2-2	7+63N	13+20E	X
2-3	7+87N	12+97E	X
2-4	8+35N	12+51E	X
2-5B	9+91N	12+60E	X
2-5H	9+91N	12+60E	X
2-6	13+82N	12+04E	X
2-7	9+82N	12+57E	X
2-8	9+63N	12+60E	X
2-9	12+30N	11+88E	X
2-10	12+34N	11+85E	X
2-11	17+30N	12+40E	X
2-186	18+60N	12+00E	X
2-186A	18+60N	12+00E	X
3-1	19+50N	11+80E	
3-2	19+50N	11+80E	
3-4	14+12N	12+45E	
3-5	13+10N	12+37E	
3-6	12+37N	12+78E	X
3-7	12+37N	12+78E	
3-8	12+37N	12+78E	X
3-9	12+34N	12+78E	
3-10	11+44N	12+56E	
3-11	10+41N	12+92E	
3-12	11+00N	12+67E	
3-13	11+00N	12+67E	
3-14	10+53N	12+96E	
3-15	9+40N	12+74E	
3-16	8+55N	11+85E	
3-17	8+50N	11+56E	

Sample Number	Coordinates		Thin Section
4-0	16+90N	12+80E	X
4-1	16+98N	12+82E	X
4-2	12+20N	13+10E	X
4-3?	8+40N	12+70E	X
4-4	9+50N	13+35E	X
4-5	13+00N	12+70E	X
4-6	11+10N	13+50E	X
4-7	16+60N	12+85E	X
4-8	16+55N	12+55E	X
4-9	14+00N	13+25E	X
4-10	14+50N	13+05E	X
4-11	15+00N	13+00E	X
4-12	15+10N	13+00E	X
4-13	18+70N	12+60E	X
4-15-1	17+80N	12+65E	X
4-15-2	17+80N	12+68E	X
4-135	12+50N	13+40E	X
5-1	10+65N	13+66E	
5-2	10+85N	13+70E	X
5-3	10+94N	13+72E	X
5-4	11+27N	13+73E	
5-5	11+86N	13+80E	
5-6	12+52N	13+87E	
5-7	13+02N	13+88E	X
5-8	13+64N	14+09E	
5-9	14+63N	14+85E	X
5-10	14+91N	13+68E	
5-11	14+91N	13+68E	
5-12	14+29N	13+48E	
5-A			
6-4	11+64N	15+04E	X
6-5	11+58N	14+99E	X
6-6	11+53N	14+94E	X
6-7	11+60N	15+00E	X
6-8	11+78N	15+15E	X
6-9	11+99N	15+33E	X
6-12	10+03N	14+18E	
6-14	10+04N	15+85E	
6-15	10+05N	14+59E	
6-16	11+60N	14+99E	
6-17	11+72N	15+09E	
6-18	12+75N	13+58E	
6-19	16+05N	13+73E	
6-20	16+52N	13+75E	
6-21	15+80N	13+67E	
6-22	15+13N	14+27E	
6-23	18+10N	16+83E	
6-24	18+10N	16+83E	
6-25	18+13N	16+80E	
6-26	18+47N	16+53E	

Sample Number	Coordinates	Thin Section
6-27	18+90N 16+18E	
6-28	18+90N 16+18E	
6-29	18+80N 15+46E	
6-30	18+40N 15+06E	
6-31	9+95N 16+52E	
6-32	9+97N 16+50E	
6-33	10+00N 16+48E	
6-34	10+00N 16+48E	
6-35	10+04N 16+10E	
6-36	10+03N 15+55E	
6-37	10+04N 15+43E	
7-1	12+75N 15+10E	
7-2	12+75N 15+10E	
7-3	new develop.	not on map
7-4	new develop.	not on map
7-5	new develop.	not on map
7-5A		X
7-6	new develop.	not on map
7-7	new develop.	not on map
8-1	13+71N 13+02E	
8-2	13+75N 13+13E	
8-195		X
9-1	13+80N 13+16E	
9-2	13+86N 13+19E	
10-1	13+80N 13+15E	
10-2	13+80N 13+15E	
11-1	13+46N 13+10E	X
11-2	13+67N 13+06E	
85-85-1	drill hole	X
85-85-2	drill hole	X
85-85-3	drill hole	X
85-85-4	drill hole	X
85-85-5	drill hole	X
85-85-6	drill hole	X